HYDRODYNAMIC STUDIES AND MATHEMATICAL MODELING OF FINE COAL FLOTATION

by

Gerald Harvey Luttrell

Dissertation submitted to the Faculty of the
Virginia Polytechnic Institute and State University
in partial fulfillment of the requirements for the degree of

DOCTOR OF PHILOSOPHY

in

Mining and Minerals Engineering

APPROVED:

R. H. Yoon, Chairman

J. R. Lucas, Dept. Head

W. E. Foreman

G. T. Adel

W. W. Wen

September, 1986

Blacksburg, Virginia

HYDRODYNAMIC STUDIES AND MATHEMATICAL MODELING OF FINE COAL FLOTATION

by

Gerald Harvey Luttrell

Committee Chairman: Roe-Hoan Yoon
Mining and Minerals Engineering

(ABSTRACT)

The probability of particle capture by an isolated bubble rising through a suspension of particles has been determined using fundamental principles of fluid mechanics. This analysis has allowed the rate constant for flotation to be evaluated as functions of bubble size, particle size, flotation column diameter, air flow rate and critical film rupture thickness. The last parameter is a measure of the hydrophobicity of the particles to be floated.

Using the theoretically determined rate constant, a population balance model has been developed for the flotation of fine coal in a column. The model is capable of predicting the dynamic response of the flotation column to changes in a wide range of operational conditions. Model simulations have been found to be in reasonable agreement with experiments conducted using a bench-scale column.

ACKNOWLEDGEMENTS

The utmost appreciation is expressed to my advisor, Dr. Roe-Hoan Yoon, for his encouragement, guidance and patience throughout the course of this investigation. Special thanks are also given to Dr. Gregory Adel, "Buddy" Brown, Waverly Hale and Michael Mankosa for their continued interest and invaluable assistance, and to Courtney Young for his help with computer simulations. Sincere gratitude is expressed to the numerous individuals, especially those at the "Plantation", whose support and friendship through the long days and late nights contributed much toward making this work possible.

The author would like to acknowledge the United States Department of Energy for the funding of this project (Grant No. DE-FG22-83PC60806), and the financial support of the Department of Mining and Minerals Engineering at Virginia Tech. Additional gratitude is given to Beth Dillinger and Wayne Slusser for their technical assistance.

My special appreciation is given to my parents for their continued support. Finally, deepest thanks are expressed to my wife, , for the endless confidence, encouragement and patience she has given her part-time husband.

TABLE OF CONTENTS

LIST OF FIGURES

Page

LIST OF TABLES

LIST OF SYMBOLS

A_b = Cross-sectional of a bubble

A_l = Limiting area swept by a rising bubble

B = Stokes correction factor

C = Particle concentration

C_1, C_2 = Constants

D_b = Bubble diameter

D_c = Cross-sectional area of a flotation column

D_p = Particle diameter

F_p = Hydrodynamic pressing force

F_r = Viscous resistance force

g = Acceleration of gravity

h = Total height of a flotation column

H = Separation distance between bubble and particle surfaces

H_c = Critical rupture film thickness between a bubble and particle

H_i = Initial film thickness between a bubble and particle

k = Flotation rate constant

k_a = First order rate constant for bubble-particle attachment

k_e = First order rate constant for particle entrainment

m = Particle mass

M_f = Cumulative mass floated in time period t

M_c = Total mass contained in a flotation cell

n = Order of kinetics

N_t = Total number of particles in a flotation column

P = Probability of particle collection by a bubble

P_a = Probability of adhesion between a bubble and colliding particle

P_c = Probability of collision between a bubble and particle

P_{ci} = Probability of collision calculated for intermediate Reynolds numbers

P_{cp} = Probability of collision calculated for potential flow conditions

P_{cs} = Probability of collision calculated for Stokes flow conditions

P_d = Probability of detachment of a particle from a bubble

P_e = Probability of entrainment

P_i = Probability of interceptional collision

P_g = Probability of gravitational collision

Q = Volumetric gas flow rate

R = Radial coordinate from the center of a bubble

R_b = Bubble radius

Re = Reynolds number

R_1 = Limiting radius at an infinite distance ahead of a rising bubble within which bubble-particle collision occurs

R_1' = Limiting radius at an infinite distance ahead of a rising bubble within which bubble-particle collection occurs

R_p = Particle radius

S_g = Gas density

S_l = Liquid density

St = Stokes number

t = Time

T = Induction time

T_s = Sliding time

U_b = Bubble rise velocity

U_p = Particle settling velocity

U_r = Radial velocity of a fluid element relative to the bubble center

U_{rp} = Radial velocity of a particle relative to the bubble center

U_t = Tangential velocity of fluid element relative to the bubble center

U_{tp} = Tangential velocity of a particle relative to the bubble center

V = Total volume of a flotation column

V_w = Dimensionless wake volume (wake volume/bubble volume)

X = R/Rb

Y = Stream function

Y_i = Stream function for intermediate Reynolds numbers

Y_p = Stream function for potential flow conditions

Y_s = Stream function for Stokes flow conditions

Z = Proportionality constant for determining bubble rise velocities

α = Parameter indicating the deviation from Stokes or potential flow conditions

θ = Cylindrical coordinate from the center of a bubble as measured from vertical

θ_g = Angle measured from vertical over which gravitational deposition of particles may occur

θ_1 = Angle measured from vertical within which a particle must strike a bubble in order to achieve attachment

ρ_l = Liquid density

ρ_p = Particle density

μ = Liquid viscosity

CHAPTER 1

INTRODUCTION

1.1 Preamble

Coal is America's most abundant energy resource. Recent studies by the U.S. Energy Information Administration indicate that the United States possesses 483 billion tons of economically mineable coal. This energy reserve is equivalent to more than two and one half times the known world oil supply. Potential reserves are estimated to be as high as 4 trillion tons. Yet, despite the availability of coal, the U.S. imports approximately 5.4 million barrels of oil per day to meet its energy requirements. Compared to the total U.S. trade picture, imported oil amounts to nearly half of the national trade deficit (Ingersol-Rand, 1984). Therefore, it would be difficult to dispute that increased utilization of the vast U.S. coal reserves would not only help the U.S. move closer toward energy independence, but would also aid in the stabilization of the national economy.

A number of reasons can be given for the preferred use of liquid and gaseous fuels over solid coal. Oil and gas are relatively clean burning, easy to store and transport, and typically offer high conversion efficiencies to mechanical work. Coal, on the other hand, is difficult to handle because of its solid form. Also, run-of-mine coals

generally contain significant quantities of noncombustible, inorganic mineral matter composed primarily of shales, clays, carbonates and iron sulfides. Upon combustion, these impurities leave behind a residue commonly referred to as ash. Unprocessed coals may consist of up to 40% ash by weight. In electrical utilities, economic penalities are associated with the ash content of coal. These include ash disposal costs, higher coal transportation costs, increased plant maintenance costs, and expenses associated with a reduction in plant capacity and availability. For a coal containing 25% ash, these costs are estimated to be approximately $8.00 per ton of coal (Phillips and Cole, 1980).

In addition to ash, coal can contain as much as 10% sulfur. Sulfur may be present in coal as chemically bound organic sulfur, as pyrite and marcasite, and as sulfates. During combustion, sulfur in coal is oxidized to form SO_2, a toxic gas which contributes to respiratory problems and acid rain. In response to the Clean Air Act of 1977, the Environmental Protection Agency has placed strict limits on the amount of SO_2 which can be released to the atmosphere. Removal of sulfur from the utility exhaust by flue gas scrubbing is expensive, both in terms of the initial capital expenditure and operational costs.

Despite these problems, a future increase in coal utilization is almost certain. The 1978 Power Plant and

Industrial Fuel Act prohibits the use of oil in all new utilities. Given the availability of natural gas and the current state of the nuclear power industry, neither of these fuels are as attractive as coal. In addition, the total national energy consumption is expect to increase despite recent improvements in energy conservation. Reports by the United States Department of Energy (DOE) suggest an annual rise in consumption between now and the year 2000 of approximately 1.3 percent. As shown in Figure 1.1, DOE predicts that coal will be called upon to supply an increased percentage of the future energy market (Ingersol-Rand, 1984).

As a result of these developments in the energy industry, coal research organizations have recently devoted much effort to developing cleaner and more convenient burning liquid coal fuels. Synthetic fuels which are produced from coal are technically attractive, but the costs of developing and operating these conversion plants remain prohibitive. Another option which has received increased interest in recent years is the use of pulverized solid coal in the form of a slurry. Coal-water mixture (CWM) fuels have the advantage that they can be used in oil-fired utilities with a minimum of modification to the existing equipment. DOE estimates that approximately 4.8 million barrels of oil per day (about 25% of the total daily

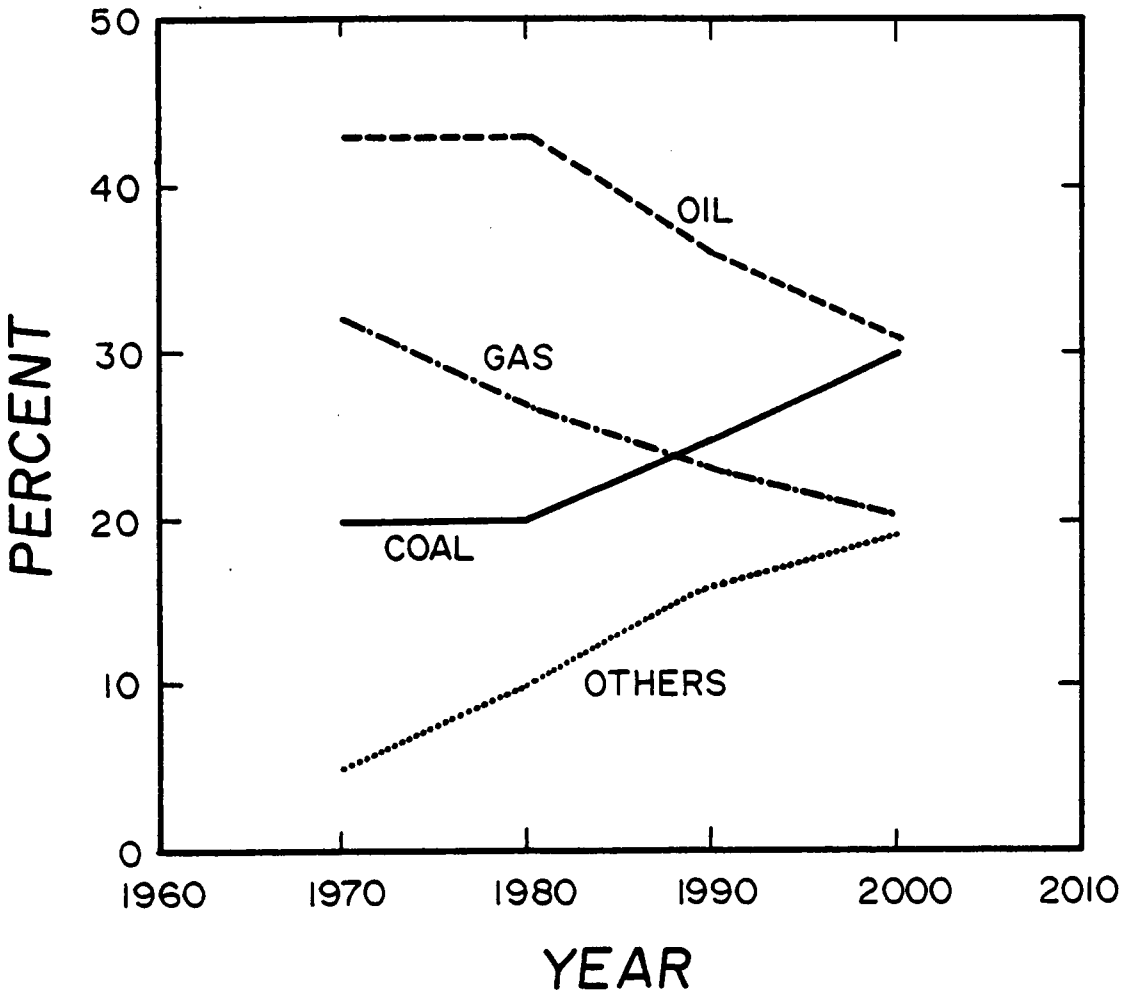

Figure 1.1 Past and predicted consumption of energy in the United States (Ingersol-Rand, 1984).

domestic consumption) can be substituted by CWM's in utility and industrial boilers (Green, 1982). The CWM technology is currently capable of producing stable, low-viscosity suspensions consisting of approximately 70 percent coal and 30 percent water. Cost projections by the Electric Power Research Institute for 1985 suggest that CWM's can be produced for $2.80 to $3.50 per million Btu, whereas oil costs about $4.50 per million Btu (Wright, 1985). Depending on the current price of oil, CWM's may offer a substantial economic advantage.

However, in order to serve as an attractive substitute for fuel oil, the ash and sulfur levels of CWM's must be reduced below those which are currently produced. Although it is the subject of much debate, an ash level of 1 to 4 percent and a sulfur level below 1 percent is believed to be adequate in order to fulfill boiler requirements and meet existing emission standards (Bethell and Sell, 1983).

A number of advanced physical and chemical techniques are currently being investigated as a means for producing coal with a very low level of impurities. While chemical processes show a great deal of potential, particularly with regard to the reduction of sulfur, the expense of chemical cleaning has retarded their development. The treatment cost for producing chemically cleaned coal is estimated to be in the range of $25 to $35 per ton (Boron and Kollrack, 1983). Furthermore, some of the chemical cleaning processes

substantially alter the nature of the coal, making it difficult to burn efficiently in existing boilers. The environmental impact of chemical coal cleaning processes must also be considered since many generate significant quantities of toxic wastes. Physical coal cleaning methods, on the other hand, are considered the least costly in reducing sulfur emissions from the combustion of coal (Hall, 1981). For this reason, much attention is currently being given to the development of advanced physical coal cleaning techniques and the improvement of existing conventional processes.

Since the CWM fuel consists of fine coal suspended in water, it is well suited to cleaning by physical coal beneficiation techniques in that total dewatering and drying are not necessary. However, extensive cleaning is possible only after the coal is pulverized to micron sizes in order to liberate fine impurities. Experimental investigations by Mathieu and Mainwaring (1986) have demonstrated a continuous improvement in the liberation of pyrite during grinding. Their results, shown in Figure 1.2, suggest that complete separation of pyrite can occur only at particle sizes below approximately 10 microns for this particular coal. Washability studies conducted by DOE showed that the Upper Freeport seam coal could be cleaned to 1.5 percent ash at a specific gravity of 1.3 after grinding to below 200 mesh

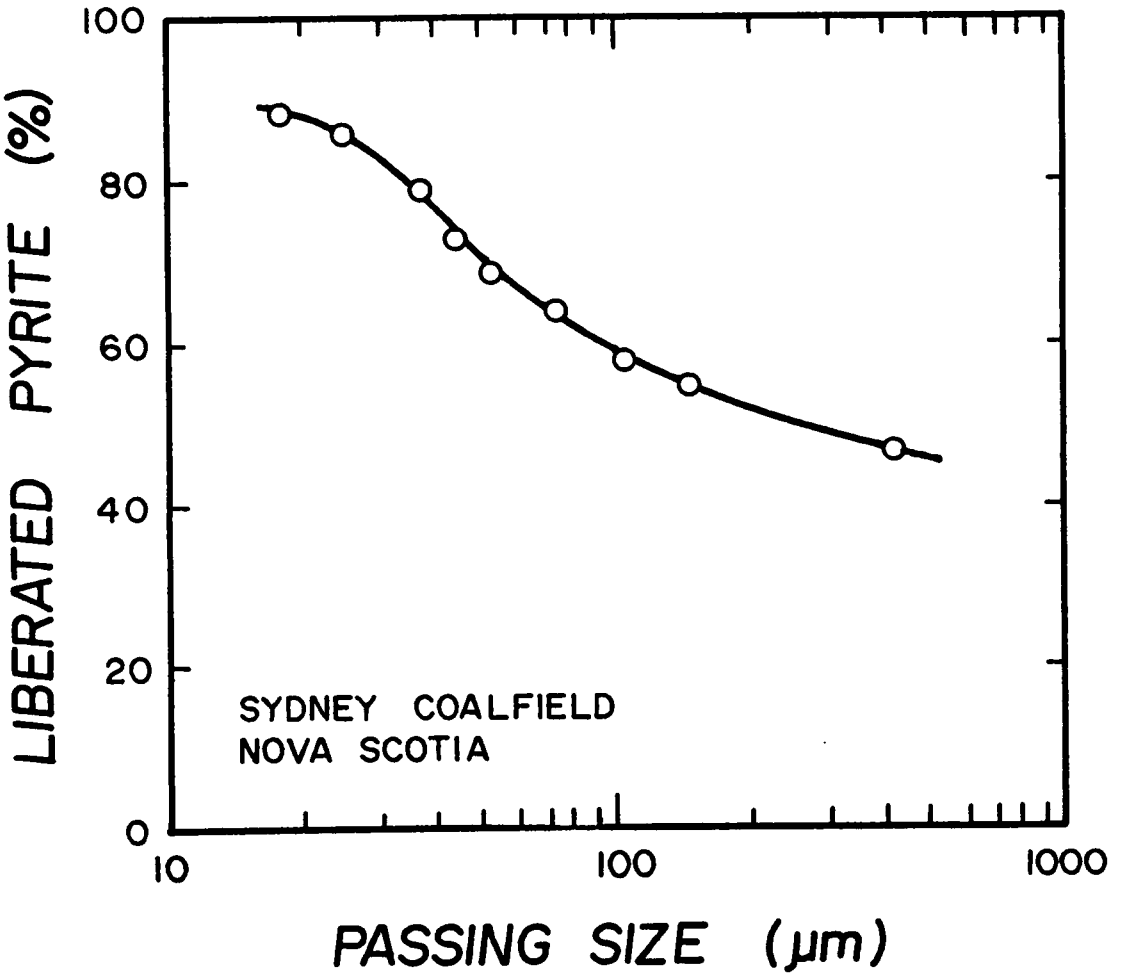

Figure 1.2 Percentage of liberated pyrite versus passing size for coal from the Sydney Coalfield, Nova Scotia (Mathieu and Mainwaring, 1986).

(Holt and Killmeyer, 1984). The Btu recovery was, however, only 39.4 percent. This result suggests that the coal needs to be pulverized to a much finer size if the recovery is to be improved while maintaining the low ash content. Photomicrographs of this coal indicate the presence of a large portion of submicron pyrite particles (Choi, 1986). Finely disseminated, discrete pyrite grains of approximately 1 to 2 microns in diameter are a common occurrence in coal (Thiessen, 1920; Gray, Schapiro and Coe, 1963). If the sulfur content of this coal is to be reduced using physical separation techniques, extremely fine grinding will be required to liberate these pyrite particles. The benefits of fine grinding on the liberation of mineral matter and pyrite are currently being investigated by DOE (Hucko, 1984).

Although several physical coal cleaning processes are available, froth flotation is generally recognized as the best method for beneficiating fine coal (Fourie, 1977). Coal is particularly well suited to separation from hydrophilic gangue using flotation because of its inherent floatability. Froth flotation is the only technology routinely used for cleaning fine coal on a commercial basis. According to one estimate, almost 3 million tons of clean coal are recovered each year by this method (Wright, 1985). In treating micronized particles by flotation, however, the efficiency of the process drops rapidly for very small

particles (Trahar and Warren, 1976; Fuerstenau, 1980). As can be seen in Figure 1.3, an increase in the flotation time rate of coal begins to be observed when the particle diameter falls below approximately 200 microns (Zimmerman and Sun, 1979). In addition, a notable decrease in flotation selectivity occurs when floating very fine coal fractions (Aplan, 1976). The causes for the low flotation rate and poor selectivity must be identified and appropriate measures should be taken to counteract these problems if flotation is to become widely applied as a means for the deep cleaning of coal.

1.2 Research Objectives

The primary objective of the present investigation has been i) to identify the mechanisms responsible for the diminishing effectiveness of froth flotation at finer particle sizes and ii) to propose plausible solutions for overcoming these difficulties. In order to achieve these objectives, an attempt has been made to develop fundamental relationships between the principal operating variables of the process and flotation response. These relationships have been derived by studying each of the elementary flotation subprocesses independently. Examples of these include bubble-particle collision, bubble-particle adhesion, particle entrainment in bubble wakes, etc. An overall

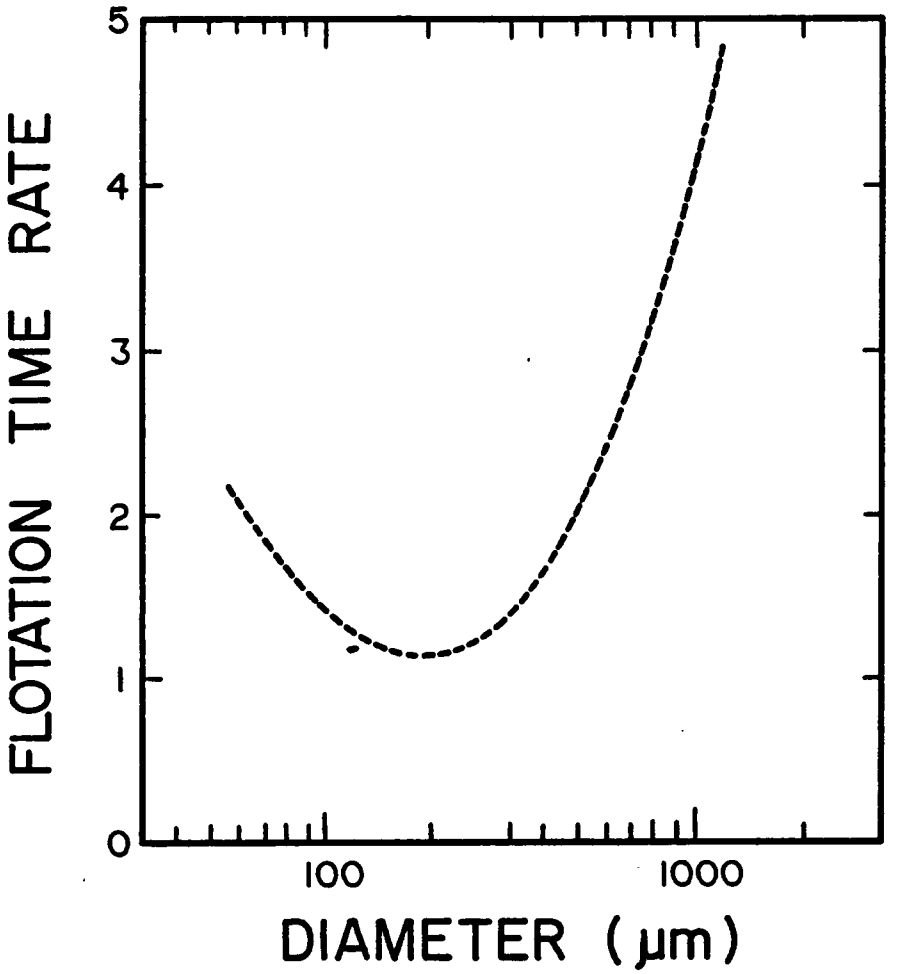

Figure 1.3 Flotation time rate of coal as a function of particle size (Zimmerman and Sun, 1979).

description of flotation response has been evaluated by combining the effects of these subprocesses. The development of flotation models by this methodology has provided insight into the complex phenomena that occur during the flotation of fine particles.

It is hoped that the findings of this investigation will help increase the utilization of flotation as a means for deep-cleaning fine coal, and ultimately lead to an increased utilization of coal as a substitute for oil and gas. In addition, many of the conclusions drawn from this study are applicable to other flotation processes in which a significant fraction of potentially valuable material is lost as fines.

1.3 Organization of this Report

The findings of this investigation have been reported in a series of relatively independent chapters. In Chapter 2, a theoretical model which predicts the probability of collection of small particles by a rising bubble has been developed from an analysis of hydrodynamic interactions. The basic form of the model is similar to that proposed by Sutherland (1948), although several important modifications have been made. The most noteworthy of these is the determination of the probability of particle adhesion using the concept of a critical rupture film thickness.

Experimentally determined values for the probability of collection have been obtained and have been found to correlate well with model predictions. Bubble size has been shown to be a major factor in determining the effectiveness of particle capture by a rising air bubble.

Chapters 3 and 4 respectively address the effect of bubble size on the rate of flotation and on the efficiency of flotation separations. A continuous flotation column has been utilized to experimentally demonstrate the rapid increase in the flotation rate constant as the bubble size is decreased. The selectivity of flotation as a function of bubble size has been studied using a specially designed "frothless" flotation cell. This design permitted a quantitative study of particle entrainment without interference by the froth. From this data, a simple flotation rate constant expression has been derived which incorporates both particle attachment and entrainment phenomena. Several important implications regarding the effectiveness of flotation are discussed in light of this expression.

In Chapter 5, a population balance model has been developed to describe the flotation of fine coal particles in a column. Using the rate expressions derived in the preceding chapters, this model has been used to predict flotation response under a variety of operating conditions

and cell geometries. Since this model is based on first principles, it is useful for the optimization, control and scale-up of column flotation.

CHAPTER 2

BUBBLE-PARTICLE INTERACTIONS IN FLOTATION

2.1 Introduction

Of the various subprocesses which contribute to the overall rate of flotation, none is quite so important as the elementary step of particle capture by a bubble. Despite recent advances, this phenomenon is still not well understood from a quantitative viewpoint. It is this lack of understanding which has largely contributed to the inability of many investigators to predict flotation response from mechanistic-type models. As a result, mineral and coal processing engineers have resorted to empirical models which are valuable in many cases, but which lack the fundamental insight that only phenomenological models provide. There is no doubt that the development of fundamental models for predicting flotation behavior will be greatly limited until a quantitative description for the process of particle capture by a bubble has been clearly developed.

2.2 Literature Review

Prior to the 1930's, research performed in the area of froth flotation was primarily devoted to studies of reagent adsorption and surface wetting phenomena. Many of the

pioneering concepts of flotation surface chemistry were developed during this period. It was not until the following decades that studies began to appear demonstrating the importance of the physical interactions in flotation. Some of the first published reports on this topic include those of Frumkin (1931), Ostwald (1932) and Wark (1933). The early experimental investigations by Bagdanov and Filanovski (1940), and later those of Spedden and Hannan (1948) and Whelan and Brown (1956), provided direct photographic evidence for the important role of physical interactions in flotation. It was the work performed during this period that laid the foundation for our current understanding of the collision and adhesion mechanisms which occur during flotation.

Perhaps the first attempts to quantitatively describe the rate of flotation through physical mechanisms were those performed by Gaudin (1932) and Schuhmann (1942), who considered the probability of collision between particles and bubbles to be a fundamental parameter in determining the rate of flotation. Their analyses were greatly hampered, however, by the lack of detailed information concerning the bubble-particle hydrodynamics. It was not until later that the first analytical relationships between the rate of flotation and hydrodynamics were derived by Sutherland (1948) in his landmark article entitled "Kinetics of the

Flotation Process." In this article, Sutherland assumed that the probability of flotation (P) could be represented by:

$$P = P_c P_a P_d \qquad [2.1]$$

where P_c is the probability of collision between bubbles and particles, P_a is the probability of adhesion after collision and P_d is the probability that subsequent detachment would not occur. According to this expression, P is simply the fraction of particles in the path of a bubble that is actually collected by the bubble. Expressions were then derived for each of these probabilities by examining the theoretical interaction between a single particle and an isolated rising bubble. Sutherland's assumptions of potential streamline flow around the bubble and inertialess particles allowed him to determine these probabilities from hydrodynamic considerations. Regretfully, quantitative predictions from his model do not correlate well with experimental observations. His model was inadequate primarily because of his assumption of inviscid flow past the bubble which is strictly valid only for very high Reynolds numbers. Nonetheless, Sutherland presented a conceptional framework upon which future investigators could build.

The next major contribution toward understanding the physical mechanisms involved in flotation was made by

Derjaguin and Dukhin (1961). They considered the encounter between a particle and bubble to consist of three distinct stages:

i) approach of the particle to the bubble under the influence of hydrodynamic and gravitational forces,
ii) passage though a diffuse electrical field, and
iii) penetration and subsequent rupture of a thin liquid film separating the particle and bubble.

In particular, the approach of Derjaguin and Dukhin was (1961) innovative in that the forces acting in the last stages of attachment were determined by utilizing concepts of colloid chemistry. They postulated that the magnitude of hydrodynamic and gravitational forces relative to those of surface forces (i.e., van der Waals, double layer attraction-repulsion) determined whether the liquid film between a bubble and particle would thin sufficiently to become unstable and rupture. Several related articles followed, most of which were attempts to quantify the model they proposed (Derjaguin et al., 1976a,b; Dukhin and Rulev, 1977; Rulev et al., 1977; Rulev, 1977; Derjaguin and Dukhin, 1979). However, as with the analysis of Sutherland, predictions from their model yielded results which were in many cases contradicted by practical experience. Criticisms of their work included an oversimplified consideration of

hydrodynamics (Jameson et. al, 1977), a mathematical error in their calculations (Flint and Howarth, 1971) and an overestimated significance of the contribution made by the diffuse electrical layer (Lyman, 1974). These criticisms do not, however, diminish the conceptional insight this model provides toward understanding the behavior of a particle as it approaches a bubble.

Since the introduction of the pioneering work by Sutherland (1948) and Derjaguin and Dukhin (1961), a number of investigations have appeared on the topic of physical effects in flotation. The most common is the evaluation of the frequency of particle collision with a bubble. Work of this type requires that the flow patterns around the bubble be well quantified. Because of its importance in a wide range of disciplines, the study of fluid dynamics for a spherical obstruction (such as a raindrop or a bubble) is a classical problem with extensive literature. Unfortunately, review of this literature would be beyond the scope of this work. Particularly detailed in the literature is the case of low Reynolds numbers for which analytical solutions to the Navier-Stokes and continuity equations are possible. In addition, several approximate numerical solutions have been presented for higher Reynolds numbers (Jenson, 1959; Hamielec et al., 1967; Rimon and Cheng, 1969; Michael and Norey, 1969; LeClair, 1970; Pruppacher et al., 1970).

Some of the first applied studies in this area were in

the determination of collision probabilities for dust particles and raindrops (Pearcey and Hill, 1957; Fonda and Herne, 1960; Hocking, 1960; Shafrir and Neiburger, 1964). By extending these concepts, Flint and Howarth (1971) numerically solved the equations of motion for a particle approaching a bubble, and determined values for the probability of collision appropriate for conditions present in froth flotation. Shortly thereafter, Reay and Ratcliff (1973) modified Flint and Howarth's method for determining the probability of collision and derived their own equations applicable for the case of effluent treatment. The primary conclusion of this investigation is that the total probability of collision (P) between bubbles and particles could be expressed as:

$$P = P_i + P_g \qquad [2.2]$$

in which P_i is the probability of interceptional collision and P_g is the probability of gravitational collision. Interceptional collision results when a particle, moving with the streamline flow around a bubble, intercepts the bubble due to the finite dimensions of the particle. Gravitational collision, on the other hand, occurs as a result of the deviation of a particle from the streamline because of its settling velocity. Reay and Ratcliff also showed that probability of gravitational collision could be

described by:

$$P_g = \frac{U_p}{U_p + U_b} \left(1 + \frac{D_p}{D_b} \right)^2 \sin^2\theta_g \qquad [2.3]$$

where θ_g is the angle, as measured from vertical, over which gravitational deposition may occur, and U_p and U_b are the terminal velocities of the particle and bubble, respectively. Values for the probability of interceptional collision were found using a numerical solution technique, from which they determined that:

$$P_i \propto \left(\frac{D_p}{D_b} \right)^2. \qquad [2.4]$$

More recently, an expression for interceptional collision has been reported in the literature by Weber (1981) and Weber and Paddock (1983). In these analyses, the value of the probability of collision was directly determined for low Reynolds numbers by analytical means. The influence of larger Reynolds numbers on the probability of collision was then evaluated from the numerical results of Masliyah (1970) and Woo (1971). A curve-fitting technique was employed to yield a complete expression for interceptional collision:

$$P_i = \frac{3}{2} \left(\frac{D_p}{D_b} \right)^2 \left[1 + \frac{(3/16)\ Re}{1 + 0.249\ Re^{0.56}} \right] \qquad [2.5]$$

in which Re is the Reynolds number of the bubble. Because of the assumptions made in the derivation of Equation [2.5], it is strictly valid only for rigid spheres of $D_p/D_b < 0.1$ and $0 < Re < 300$. Unlike previous studies, this work was the first of its kind to present a single quantitative equation for predicting the probability of collision for a wide range of bubble and particle sizes. However, these investigators made no experimental measurements to support their analysis.

Recognizing the importance of Weber and Paddock's (1983) analysis, Dobby and Finch (1985) have recently developed a flotation model which includes Equation [2.5] for determining the probability of collision. Their model, although conceptionally identical to that initially proposed by Sutherland (1948), has been substantially improved by eliminating the assumption of potential flow. As a result, the predicted values they have obtained are far more realistic. Simulations using the model have resulted in two major observations. First, their results suggest that a peak in the probability of particle capture occurs with particle size. This finding agrees with the experimentally observed optimum in flotation recovery as a function of particle diameter. Secondly, their model suggests that the probability of adhesion for small particles (less than about 10 microns) is very high and is somewhat independent of the

hydrophobic condition of the particle. A direct implication of this finding is that the selective flotation of fine particles is not possible. However, this conclusion would appear contrary to some experimental results where particles of this size have been selectively recovered by flotation (Gaudin et al., 1942; Reynolds, 1956; Lewis and Morris, 1962; Fuerstenau et al., 1970; Kelsall et al., 1974; Sennett and Young, 1979; Yang, 1984).

2.3 Objectives

Although a number of investigations have been performed on the topic of particle capture, a unified solution to the problem has not yet been presented. With the exception of the excellent work presented by Weber and Paddock (1983), few simple expressions are available for the quantitative evaluation of particle capture in a range applicable to flotation. Dobby and Finch (1985) have presented perhaps the best effort of combining the various influences acting on a particle and bubble into a workable model for predicting flotation behavior. However, their analysis appears to contradict experimental data in some cases.

Following the framework presented by Sutherland (1948), the present investigation has attempted to develop a new model which more thoroughly describes the process of particle capture by a rising air bubble. Formulation of the

model has been subjected to a number of guidelines. First, the model development should provide a workable solution to the problem of bubble-particle attachment rather than a strict analytical solution which can be cumbersome and too complex for practical application. Second, the model should be based on parameters that have a physical significance and that can be readily calculated or estimated. Finally, the predictions made by the model should be well supported by experimental observations. The model developed under these constraints should be directly applicable in the areas of simulation, design and scale-up of laboratory and industrial flotation processes.

2.4 Development of a Hydrodynamic Collection Model

2.4.1 Preliminary Model Development

Particle capture by a bubble generally takes place in a complex and highly turbulent environment of the flotation cell. It is possible to assume, however, that as the separation distance between the particle and bubble decreases, conditions will develop which may to some extent be simulated by an unperturbed flow field. This is particularly realistic in the case of pneumatic flotation where no external agitation is employed. From this assumption, it is possible to quantify some of the

fundamental subprocesses occurring in flotation for a number of ideal and simplified cases.

As a plausable starting point, let us consider the case of an isolated bubble rising through a suspension of particles, as shown in Figure 2.1. As the liquid sweeps past the bubble, a flow pattern develops which can be represented by an infinite series of streamlines. Streamlines are defined so that a velocity vector of the fluid at every point on the line is tangent to the streamline at that instant. The arrangement of the streamlines depends on the properties of the respective fluids and geometry of the obstacle placed in the flow field. The streamline flow pattern has a large influence on the trajectory of small particles swept by the bubble. As shown, large particles having sufficient inertia to deviate from the streamlines directly collide with the bubble. These particles become attached if the surface conditions are appropriate. On the other hand, small particles will tend to follow the streamlines and skirt around the bubble without contact. Stokes number (St) which is the ratio of inertial to drag forces, is useful for determining the tendency of a particle to adjust to changes in fluid flow, i.e., the tendency of a particle to follow the streamlines. It may be expressed as:

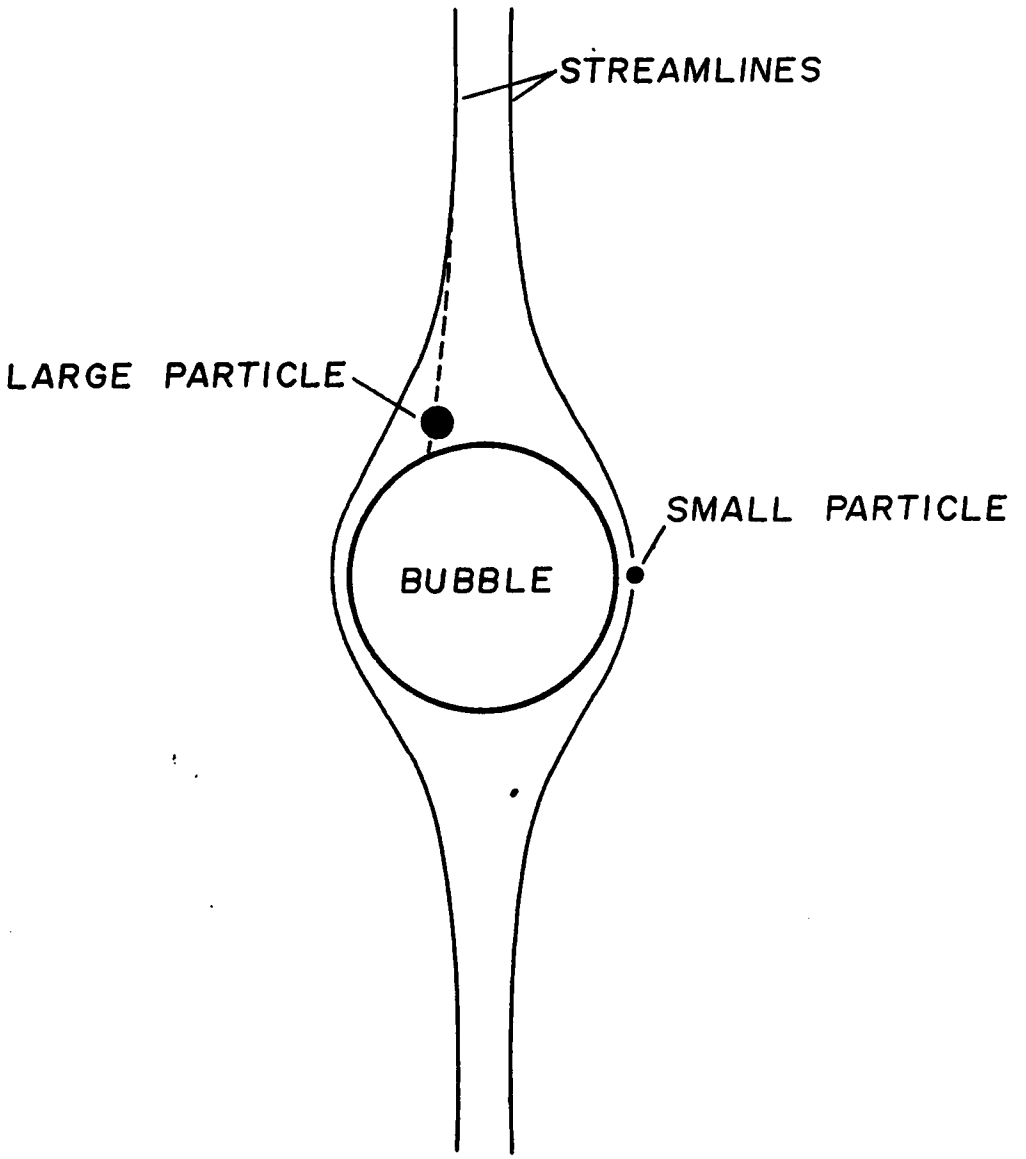

Figure 2.1 Particle trajectories for a large and a small particle in streamline flow around a bubble.

$$St = \frac{1}{9}\frac{\rho_p}{\rho_l}\left(\frac{D_p}{D_b}\right)^2 Re \qquad [2.6]$$

in which D_p and D_b are the respective particle and bubble diameters, and ρ_p and ρ_l are the densities of the particle and liquid, respectively. The Reynolds number of the bubble (Re) is the ratio of inertial to viscous forces and is given by:

$$Re = D_b U_b \rho_l / \mu \qquad [2.7]$$

where U_b is the terminal rise velocity of the bubble and μ the liquid viscosity. As shown, the tendency of a particle to follow a streamline around the bubble depends on both the bubble and particle size. A value of Stokes number less than approximately 0.2 is generally accepted as an indicator that the particle has insufficient inertia to deviate from a streamline. For the case of coal flotation, a plot of Stokes number versus bubble diameter for a range of particle diameters is shown in Figure 2.2. For bubbles of less than 2000 microns in diameter, collisions resulting from inertial impact with the bubble need not be considered for coal particles less than approximately 100 microns in diameter.

2.4.2 Bubble-Particle Collision

If particle inertia can be neglected, it becomes a simple matter to calculate the probability of particle

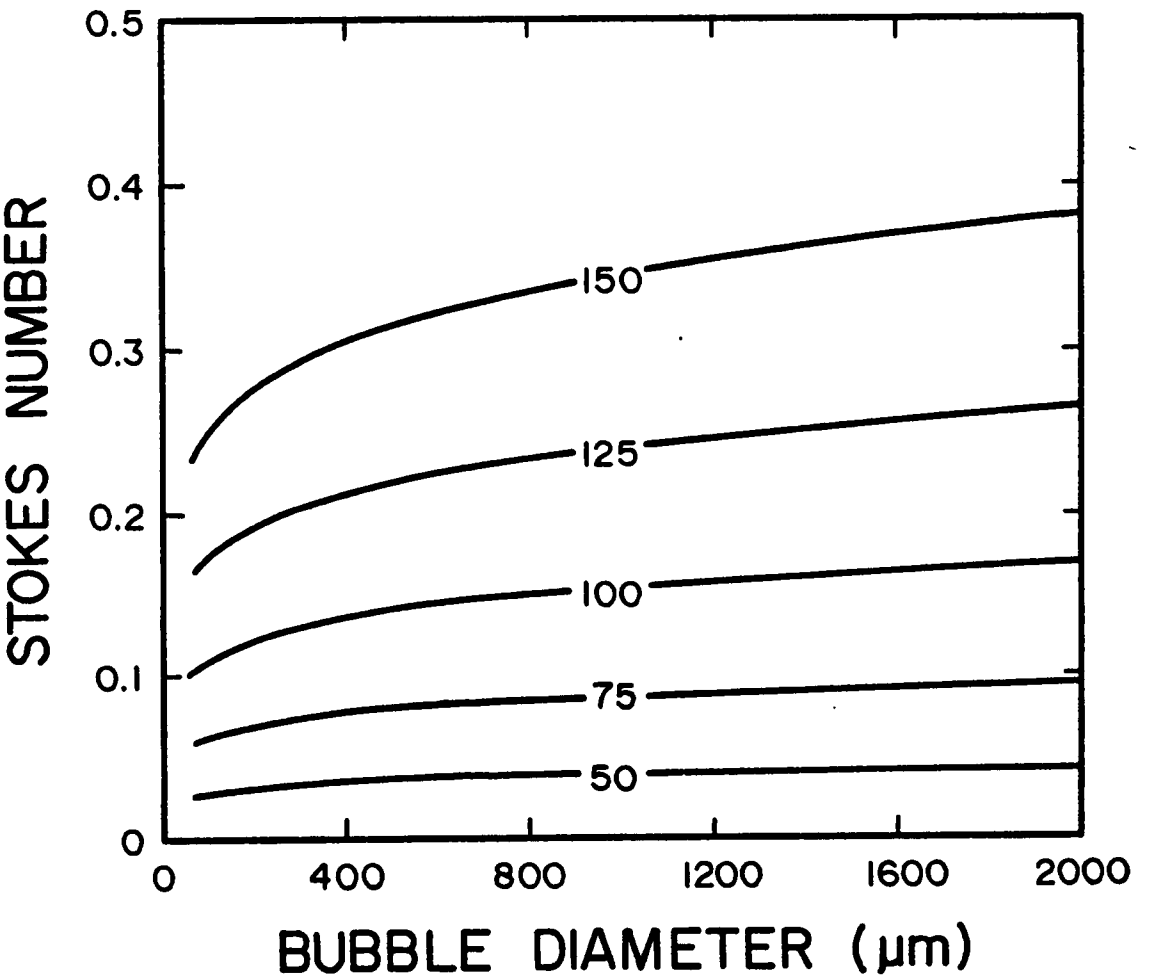

Figure 2.2 Stokes number versus bubble size for particle diameters of 50, 75, 100, 125 and 150 microns.

collision for cases where the streamline pattern is well described. As shown in Figure 2.3, the bubble can be considered stationary with fluid moving past at a velocity equal to the terminal rise velocity of the bubble, but in an opposite direction. A cylindrical coordinate system is assumed through the center of the bubble for mathematical convenience. It is assumed that the bubbles and particles under consideration behave as rigid spheres. This assumption is reasonable for bubbles less than approximately 1200 microns (Clift et al., 1978) and for finely ground particles (Davis, Hansen and Sullivan, 1980).

The trajectory of a particle is considered to be determined by the streamline which passes through its center (Flint and Howarth, 1971). This assumption becomes less valid as the ratio of particle to bubble diameter increases. Since the streamlines come closest to the bubble at its equator, this assumption allows a critical grazing streamline to be defined at a distance of one particle radius from the equator of the bubble. Particles which collide with the bubble must lie within an area described by a limiting radius (R_1) which is determined by the grazing streamline. Those which lie outside this area will sweep past the bubble without having an opportunity for contact. The probability of collision, which is defined as the fraction of particles ahead of the bubble that actually

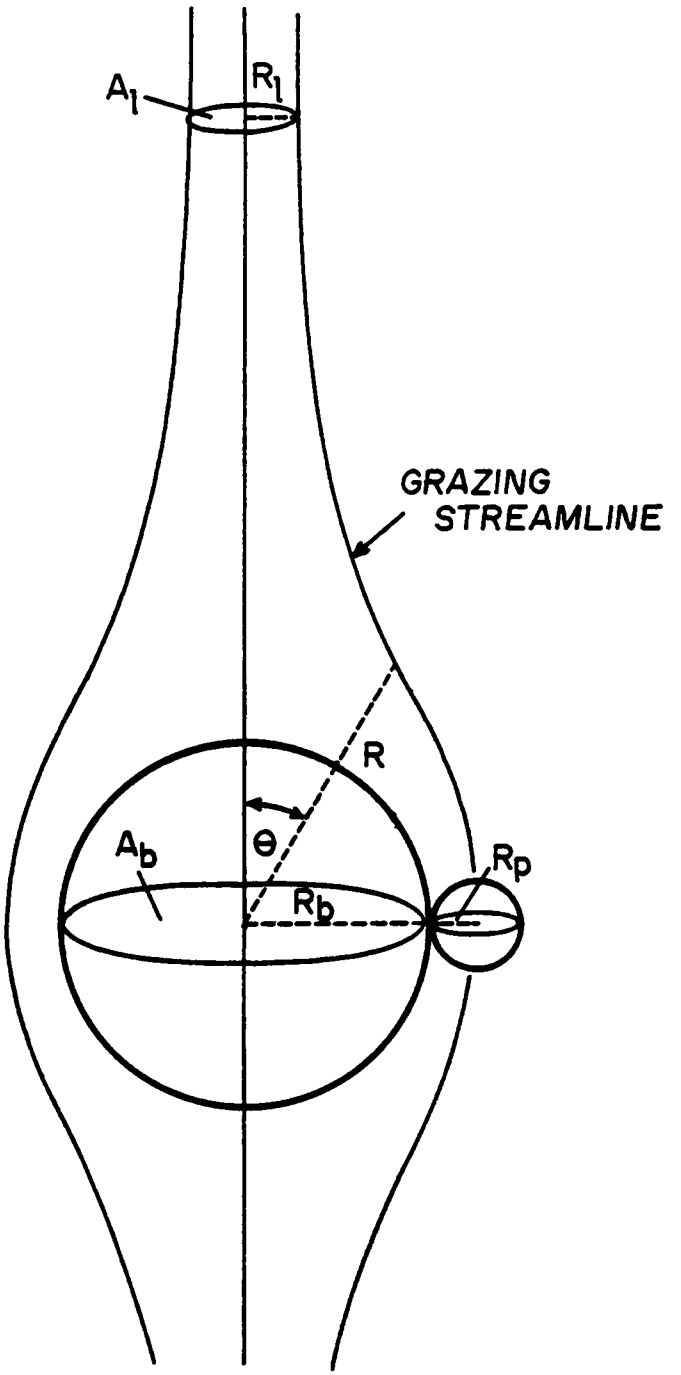

Figure 2.3 Cylindrical coordinate system used to describe the trajectory of a particle moving along a grazing streamline.

collide with the bubble, is determined by the ratio of the area (A_1) inscribed by limiting radius (R_1) to the area (A_b) inscribed by the bubble radius (R_b). Therefore, the probability of collision (P_c) is given as:

$$P_c = \frac{A_1}{A_b} = \left(\frac{R_1}{R_b}\right)^2. \qquad [2.8]$$

The value of R_1 is unknown and must be determined from the mathematical description of the streamline.

a) Stokes Flow Conditions

For cases where Reynolds number is much less than unity, the streamlines are described by the Stokes stream function (Y_s). The stream function may be expressed mathematically as:

$$Y_s = U_b R_b^2 \sin^2\theta \left(\frac{1}{2} X^2 - \frac{3}{4} X + \frac{1}{4X}\right) \qquad [2.9]$$

where $X = R/R_b$ and the cylindrical coordinate values of R and θ are as shown schematically in Figure 2.3. Considering the case far ahead of the bubble, it is possible to show that:

$$\sin\theta = R_1/R. \qquad [2.10]$$

Substitution of Equation [2.10] into Equation [2.9] yields:

$$R_1^2 = 2Y_s/U_b \qquad [2.11]$$

as R approaches infinity. By combining Equations [2.8], [2.9] and [2.11], the probability of particle collision (P_{cs}) for Stokes flow is found to be:

$$P_{cs} = \frac{2Y_s}{U_b R_b^2} = \sin^2\theta \left(X^2 - \frac{3}{2} X + \frac{1}{2X} \right). \qquad [2.12]$$

The limiting case is when the particle just grazes the bubble equator. From the geometry of the system, it can be shown that:

$$R = R_p + R_b \qquad [2.13]$$

$$X = 1 + R_p/R_b \qquad [2.14]$$

$$\theta = 90^o. \qquad [2.15]$$

Substitution of these limiting values into Equation [2.12] yields the well-known expression for P_{cs} as follows:

$$P_{cs} = \frac{3}{2} \left(\frac{R_p}{R_b} \right)^2. \qquad [2.16]$$

This expression demonstrates that the probability of collection for Stokes flow conditions varies with the square of particle size and the inverse square of bubble diameter.

b) Potential Flow Conditions

For the extreme case of very large Reynolds numbers, the potential flow stream function is given by:

$$Y_p = U_b R_b^2 \sin^2\theta \left(\frac{1}{2} X^2 - \frac{1}{2X} \right). \qquad [2.17]$$

The probability of collision for potential flow conditions (P_{cp}) can be determined using the same procedure given for Stokes flow conditions. This analysis yields:

$$P_{cp} = 3 \left(\frac{R_p}{R_b} \right). \qquad [2.18]$$

Therefore, for potential flow conditions, the probability of collision varies linearly with the ratio of R_p/R_b as opposed to a squared relationship for Stokes flow.

c) Intermediate Flow Conditions

The preceding analyses are useful for determining collision probabilities at extremely small and large Reynolds numbers. However, the range of Reynolds numbers encountered for the sizes of bubbles typically employed during flotation fall into a range between 0.2 to 100. As a result, neither of the previous solutions is appropriate for describing the flotation process.

Therefore, a new stream function for intermediate Reynolds numbers (Y_i) has been developed in the present investigation by combining the Stokes (Equation [2.9]) and potential (Equation [2.17]) flow equations. The combined form of this expression is given as:

$$Y_i = U_b R_b^2 \sin^2\theta \left(\frac{1}{2} X^2 - \alpha X - \frac{1}{2X} + \frac{\alpha}{X} \right) \quad [2.19]$$

where α is an unknown parameter which varies between 0 and 3/4. If the value of α is set equal to 0, Equation [2.19] is reduced to Equation [2.17], which is the case for potential flow. Likewise, if α is set equal to 3/4, Equation [2.19] becomes Equation [2.9], which describes the stream function under Stokes flow conditions. Values of α between 0 and 3/4 represent the intermediate cases of Reynolds number.

In order to determine the relationship between α and Re for the intermediate case, streamline patterns around a spherical obstruction have been collected from various investigations for a wide range of Reynolds numbers (Jenson, 1959; Coutanceau, 1968; Masliyah, 1970; Masliyah and Epstein, 1972; Payard and Coutanceau, 1974; Seeley et al., 1975; Van Dyke, 1982). As shown in Figure 2.4, each streamline is uniquely identified by a particular value of R_1. By measuring R_1, Equation [2.11] can be used to determine the stream function if the bubble rise velocity is

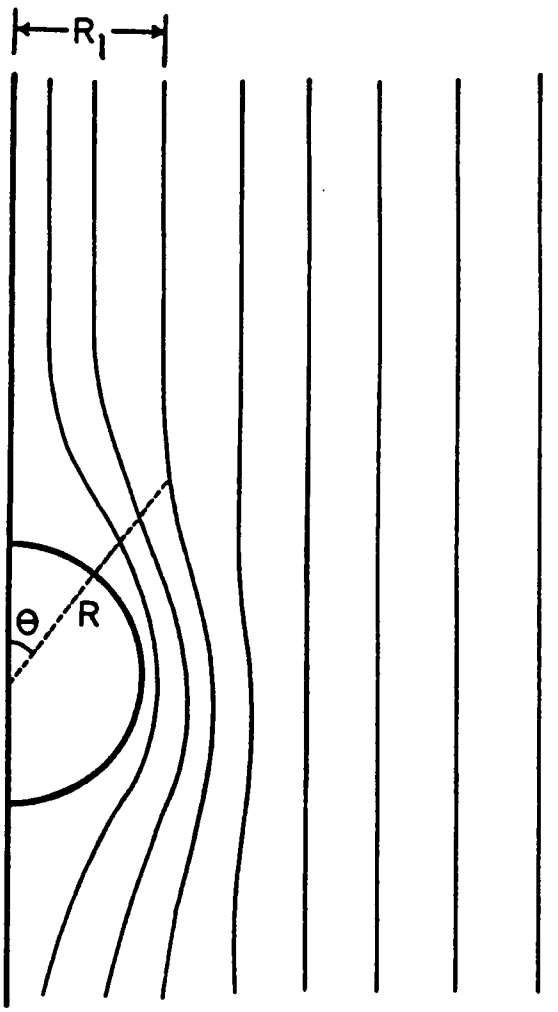

Figure 2.4 Schematic drawing to demonstrate the identification of a particular streamline using the value of R_1.

known. Therefore, for any combination of R and θ, the value of α can be uniquely obtained from Equation [2.19]. Using this technique, the data shown in Figure 2.5 was plotted. The value of α was found to be adequately represented by:

$$\alpha = \frac{3}{4} + \frac{Re^{.72}}{15} [1/X - 1]. \qquad [2.20]$$

Substitution of Equation [2.20] into Equation [2.19] yields the stream function for intermediate flow conditions (Y_i) as:

$$Y_i = Y_s + U_b R_b^2 \sin^2\theta \ \frac{Re^{.72}}{15} \left(\frac{1}{X^2} - \frac{1}{X} + X - 1 \right) \qquad [2.21]$$

For the purpose of comparison, the stream functions for each of the three flow regimes are summarized in Table 2.1.

In Figure 2.6, a comparison has been made between the Stokes and potential stream functions. This has been accomplished by plotting each of the stream functions, made dimensionless by dividing by $U_b R_b^2$, versus the dimensionless radial distance from the bubble surface (R/R_b-1). In addition, the intermediate case was also plotted for several values of Reynolds number. These results show that as the Reynolds number increases there is a smooth shift in the stream function from Stokes flow toward potential flow.

The probability of collision (P_{ci}) for intermediate

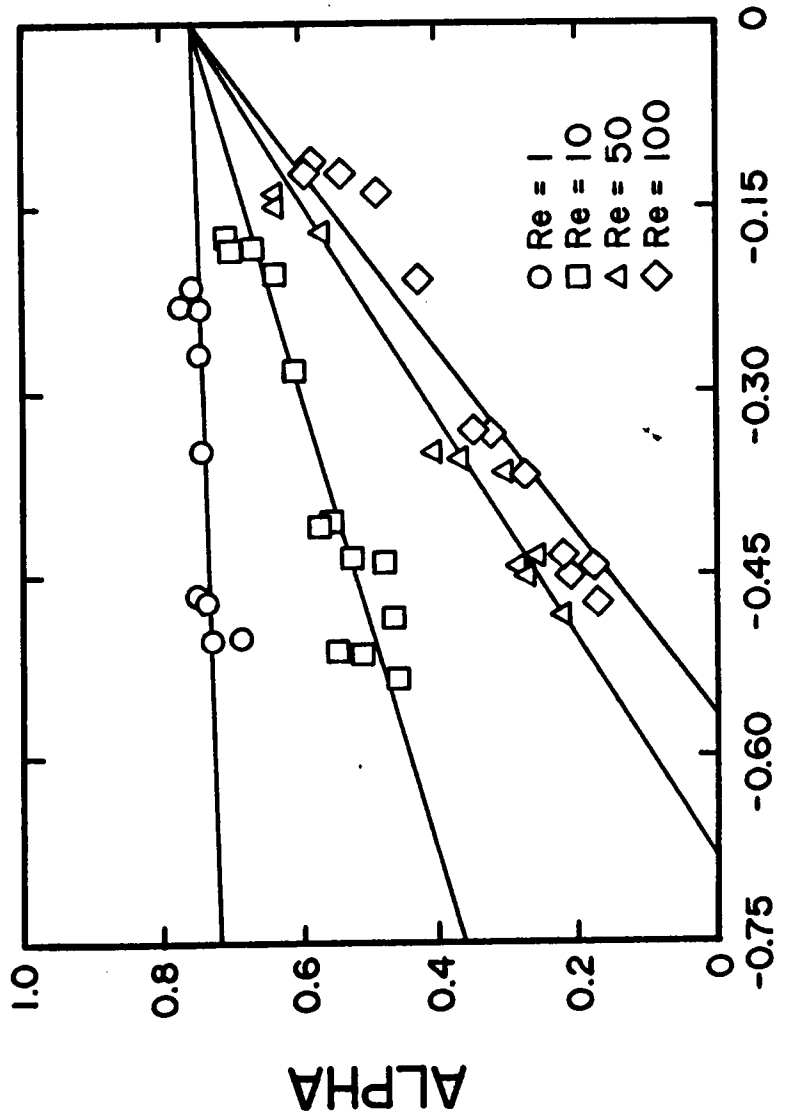

Figure 2.5 Relationship between α and X for a range of Reynolds numbers.

Table 2.1 - Dimensionless Stream Function for Various Ranges of Reynolds Numbers

Case	Dimensionless Stream Function
Small Re	$\left(\frac{1}{2}X^2 - \frac{3}{4}X + \frac{1}{4X}\right)\sin^2\theta$
Large Re	$\left(\frac{1}{2}X^2 - \frac{1}{2X}\right)\sin^2\theta$
Intermediate Re	$\left[\frac{1}{2}X^2 - \frac{3}{4}X + \frac{1}{4X} + \frac{Re^{.72}}{15}\left(\frac{1}{X^2} - \frac{1}{X} + X - 1\right)\right]\sin^2\theta$

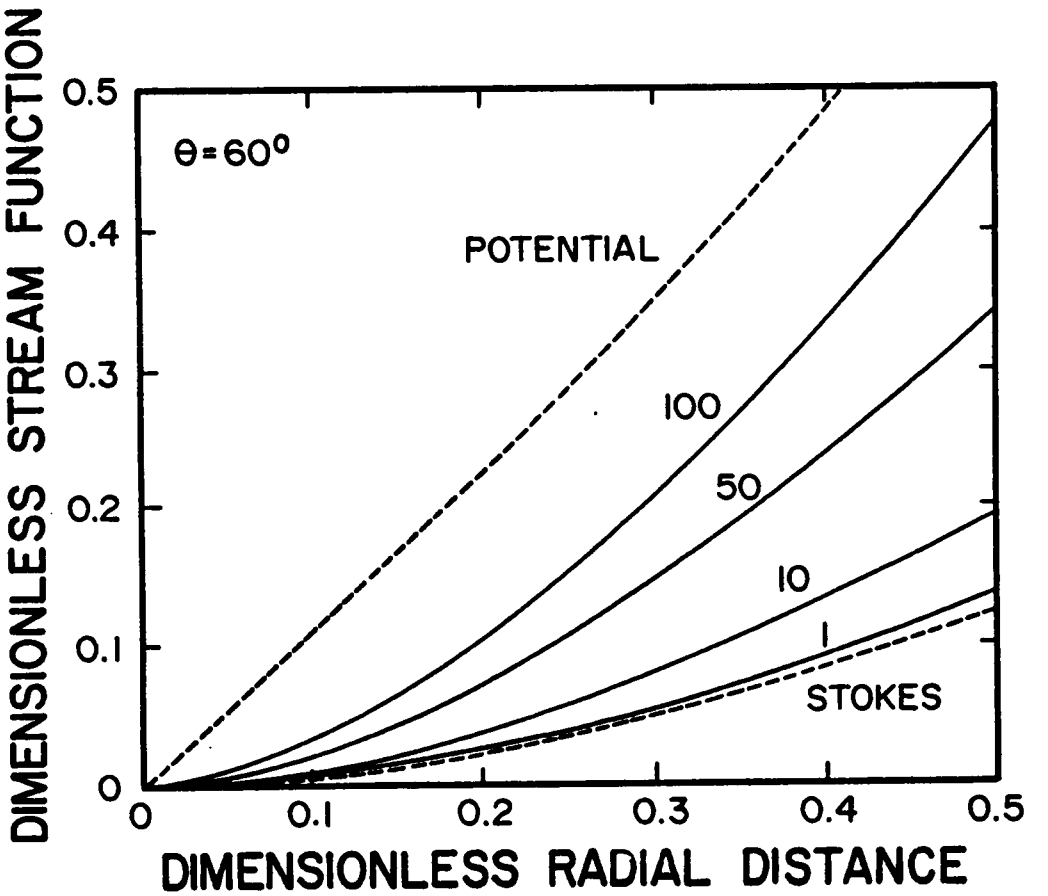

Figure 2.6 Dimensionless stream functions calculated assuming Stokes flow (Re<<1), potential flow (Re>>1), and intermediate flow (Re=1 to 100).

Reynolds numbers can now be determined from the stream function given by Equation [2.21]. Using the same procedure as employed for Stokes and potential flow conditions, it is possible to show that:

$$P_{ci} = \left[\frac{3}{2} + \frac{4Re^{.72}}{15} \right] \left(\frac{R_p}{R_b} \right)^2. \qquad [2.22]$$

Equation [2.22] clearly demonstrates that for the flotation of a given particle size, the probability of collision increases as bubble size decreases.

Figure 2.7 compares the probability of collision calculated for the three flow regimes considered in the present work as a function of bubble diameter. Predictions using Equation [2.5] suggested by Weber and Paddock (1983) are also shown as a dashed line in the figure. As can be observed, there is a very good correlation between Weber and Paddock's predictions and those of the present work. The Stokes flow solution appears to agree with the solutions for the intermediate range only for the case of very small bubbles. The potential flow solution, which was the type of flow considered by Sutherland (1948), does not agree with the intermediate flow case at any bubble size. For example, the probability of collision calculated for a 500 micron bubble and 10 micron particle by the Stokes and potential flow cases are 0.0006 and 0.600, respectively. The value predicted by Equation [2.22] for the intermediate case is

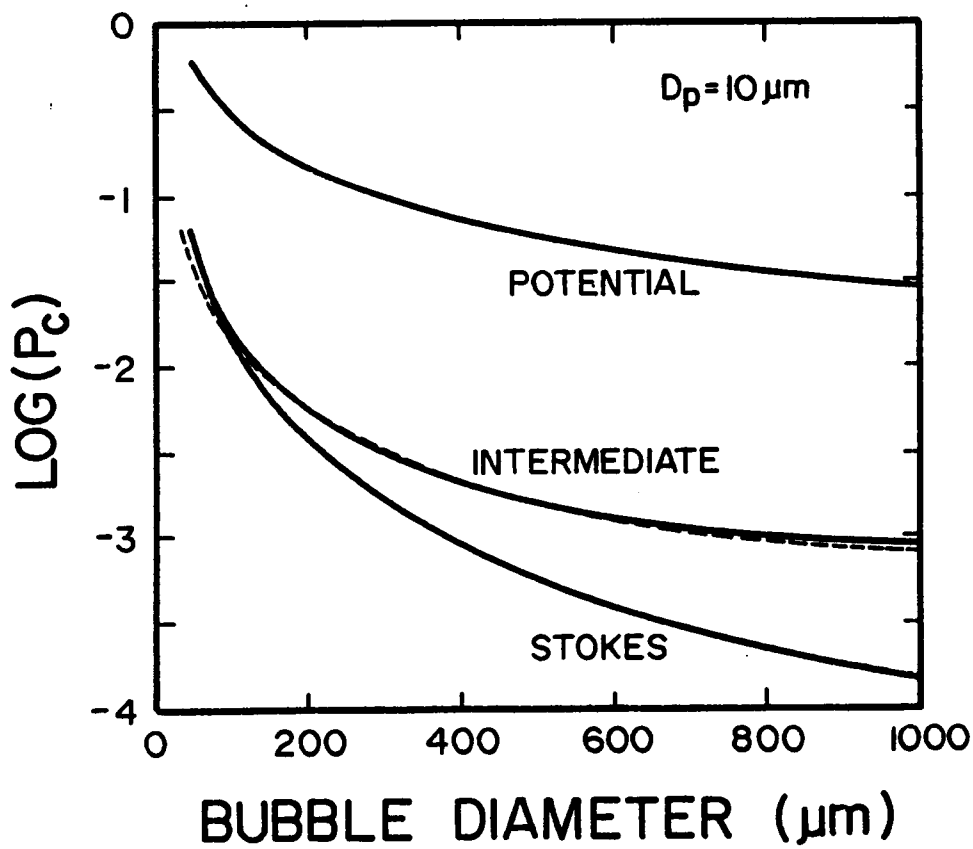

Figure 2.7 Probability of collision calculated assuming Stokes (Eq. 2.16), potential flow (Eq. 2.18) and intermediate flow conditions (—— present work, Eq. 2.22; --- Weber and Paddock, 1983, Eq. 2.5).

0.0017. Table 2.2 summarizes the three expressions for the probability of collision derived for the different flow regimes considered in the present work.

2.4.3 Bubble-Particle Adhesion

a) Relationship Between Adhesion and Induction Time

Not all of the particles which collide with the bubble become attached. Therefore, in addition to the probability of collision term, an adhesion term must also be considered in the particle capture model. Detachment need not be considered for the size of bubbles and particles employed in the present work (Derjaguin and Dukhin, 1979).

When a particle collides with a bubble, it slides over the surface of the bubble for a given period, generally referred to as the "sliding" time. During this period, particle attachment must take place. The sweeping action of a particle over the surface has been experimentally verified by King et al. (1974). A limited number of experimentally measured sliding times have also been reported by Schulze and Gottschalk (1981). The magnitude of the sliding time is determined by the velocity profile of the liquid which is moving the particle across the bubble surface. A particle will attach when it resides on the bubble surface for a period longer than the "induction" time (Sutherland, 1948).

Table 2.2 - Calculated Probability of Collision for Various Ranges of Reynolds Numbers

Case	Probability of Collision
Small Re	$\frac{3}{2}\left(\frac{D_p}{D_b}\right)^2$
Large Re	$3\left(\frac{D_p}{D_b}\right)$
Intermediate Re	$\left[\frac{3}{2} + \frac{4Re^{.72}}{15}\right]\left(\frac{D_p}{D_b}\right)^2$

Induction time is defined as the period of time required for the intervening film between a particle and bubble to thin to a critical thickness where the film spontaneously ruptures and three-phase contact is established. Therefore, the particle must slide a distance over the bubble surface before attachment becomes possible. As shown in Figure 2.8, this distance can be quantified by a limiting angle (θ_1). Particles which collide within this angle reside on the surface of the bubble for a period longer than the induction time and, as a result, become attached. Those particles which collide with the bubble at a point beyond θ_1 do not adhere since their residence time on the bubble surface is shorter than the induction time.

Using this concept, a new limiting radius (R_1') is defined which must be less than that described for the collision process. The overall probability of collection (P) is now described by:

$$P = \left(\frac{R_1'}{R_b}\right)^2. \qquad [2.23]$$

The value of R_1' can be obtained from the expression:

$$R_1'^2 = \frac{2Y_i}{U_b} \qquad [2.24]$$

which is analogous to Equation [2.11]. Upon substituting Equations [2.24] and [2.21] into Equation [2.23], one can

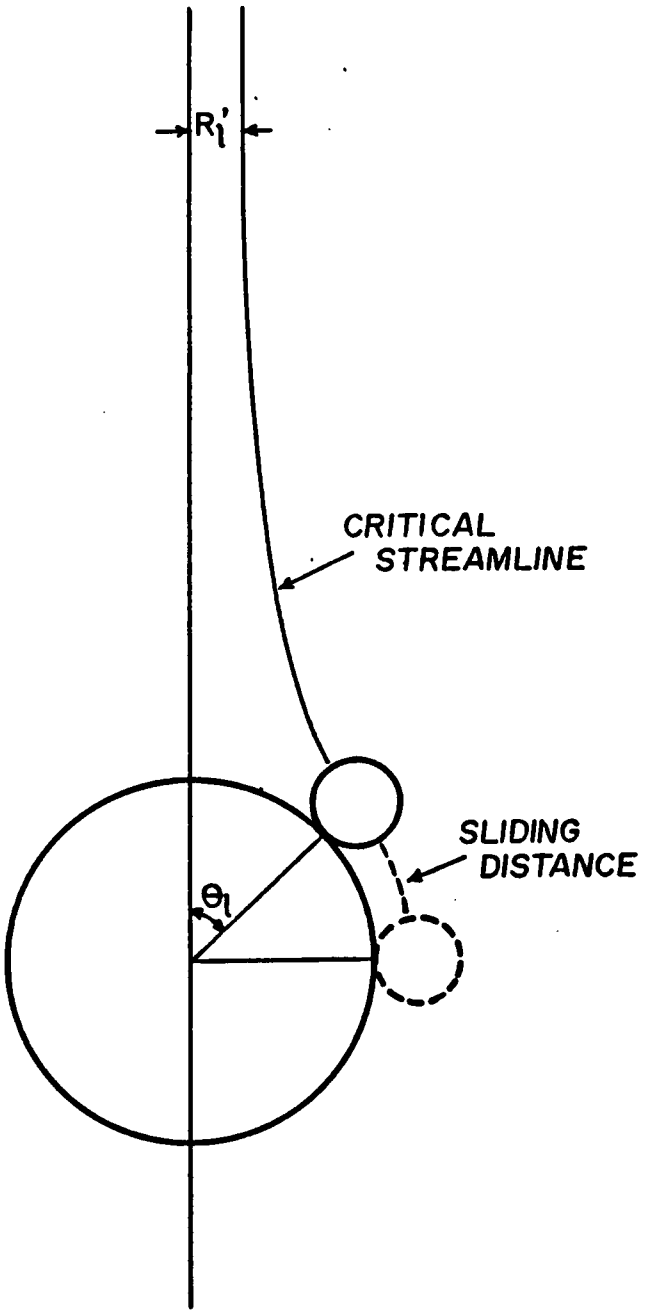

Figure 2.8 Schematic drawing defining the distance that a particle must slide over a bubble surface in order for attachment to be achieved.

obtain P as follows:

$$P = \sin^2\theta \left[X^2 - \frac{3}{2} X + \frac{1}{2X} + \frac{2Re^{\cdot 72}}{15} \left(\frac{1}{X^2} - \frac{1}{X} + X - 1 \right) \right]. \quad [2.25]$$

The limiting values for X and θ required for a particle to have a longer sliding time than induction time are given by:

$$R = R_b + R_p \quad [2.13]$$

$$X = 1 + R_p/R_b \quad [2.14]$$

$$\theta = \theta_1. \quad [2.26]$$

Substituting these expressions into Equation [2.25], the expression for P becomes:

$$P = \left[\frac{3}{2} + \frac{4Re^{\cdot 72}}{15} \right] \left(\frac{R_p}{R_b} \right)^2 \sin^2\theta_1. \quad [2.27]$$

Sutherland (1948) has shown that the probability of collection (P) is the product of the probabilities of collection (P_c), adhesion (P_a) and detachment (P_d). For the flotation of fine particles, P_d is approximately unity (Derjaguin and Dukhin, 1979). Therefore, for fine particle flotation, P is given as:

$$P = P_c P_a. \quad [2.28]$$

The value of P_c for intermediate conditions has been given

previously in Equation [2.22]. As can be observed, this expression represents the first part of Equation [2.27]. Therefore, Equation [2.28] dictates that:

$$P_a = \sin^2\theta_1. \qquad [2.29]$$

It has been determined that Equation [2.29] also represents P_a for the other two flow cases, i.e., Stokes and potential flow conditions.

The value of the limiting angle (θ_1) is determined by the magnitude of the tangential velocity of the particle as it slides over the bubble surface. Since it has been assumed that the velocity of the particle corresponds to that of a streamline passing through its center, the tangential velocity of the streamline (U_t) determines the sliding velocity of the particle. The particle sliding time (T_s) is calculated by dividing the arc length swept, by the sliding velocity of the particle. From this it is possible to show that:

$$T_s = \int_{\theta_1}^{\pi/2} \frac{R_b + R_p}{U_t}\, d\theta. \qquad [2.30]$$

It is well known that for axisymmetric flow around a rigid sphere, the instantaneous tangential velocity of the fluid (U_t) can be determined from the stream function (Y) using the relationship:

$$U_t = \frac{1}{R\sin\Theta} \frac{dY}{dR}. \qquad [2.31]$$

This expression allows a quantitative value for U_t to be derived for any choice of the stream function. Table 2.3 shows the results of these calculations for each of the flow conditions considered in the present work. The particle sliding time can be determined by substituting the appropriate expression for U_t into Equation [2.30], followed by integration. The expressions for U_t may be rearranged to yield Θ_1 as a function of the other variables. The probability of adhesion (P_a) can then be determined by substituting the Θ determined as such into Equation [2.29]. The probability of adhesion is calculated by noting that attachment occurs when the sliding time (T_s) becomes equal to the induction time (T). For intermediate Reynolds numbers, the probability of adhesion derived by this method is given by:

$$P_a = \sin^2\left[2 \arctan \exp\left\{\frac{-(45+8Re^{\cdot 72})U_b T}{15D_b(D_b/D_p+1)}\right\}\right]. \qquad [2.32]$$

The expressions derived from this analysis for each of the flow conditions considered in this investigation are summarized in Table 2.4. Since the expressions for P_a depend on the square of a sine function, the value of P_a will always fall between zero and unity, which are correct

Table 2.3 - Tangential Particle Velocity for Various Ranges of Reynolds Numbers

Case	Tangential Velocity
Small Re	$U_b \sin\theta \left(1 - \frac{3}{4X} - \frac{1}{4X^3} \right)$
Large Re	$U_b \sin\theta \left(1 + \frac{1}{2X^3} \right)$
Intermediate Re	$U_b \sin\theta \left[1 - \frac{3}{4X} - \frac{1}{4X^3} + \frac{Re^{.72}}{15} \left(\frac{1}{X^3} - \frac{2}{X^4} + \frac{1}{X} \right) \right]$

Table 2.4 - Calculated Probability of Adhesion for Various Ranges of Reynolds Numbers

Case	Probability of Adhesion
Small Re	$\sin^2 \left[2 \arctan \exp \left\{ \frac{-3U_b T}{D_b(D_b/D_p+1)} \right\} \right]$
Large Re	$\sin^2 \left[2 \arctan \exp \left\{ \frac{-3U_b T}{D_p+D_b} \right\} \right]$
Intermediate Re	$\sin^2 \left[2 \arctan \exp \left\{ \frac{-(45+8Re^{\cdot 72})U_b T}{15D_b(D_b/D_p+1)} \right\} \right]$

limits for probabilities.

According to Equation [2.32], an increase in the magnitude of the value of induction time results in a lowering of the probability of adhesion. Thus, a less hydrophobic particle, which requires a large T, will have a correspondingly lower probability of becoming attached. An induction time of less than approximately 10 ms is typical for a particle which is strongly floating (Eigeles, 1939). For a 100 micron diameter bubble and 10 micron diameter particle, the value of P_a predicted by Equation [2.32] for a strongly floating particle is 0.999.

With regard to particle diameter, an increased value for P_a is observed as particle diameter becomes smaller. This finding, which is identical to the conclusion drawn by Dobby and Finch (1985), suggests that small particles will tend to become attached more readily than larger particles of the same hydrophobicity.

The effect of bubble diameter on the probability of adhesion is somewhat more complex. Upon first examination, Equation [2.32] suggests that a decrease in bubble size would rapidly decrease P_a because the denominator of the equation is a squared function of bubble diameter. However, as bubble diameter decreases, there is also a tendency for P_a to increase because of a decrease in the values of Re and U_b. As a result of this combined effect, P_a is actually found to decrease very slightly as bubble size is decreased.

In Figure 2.9, the values predicted by Equation [2.32] are plotted against induction time for particle diameters ranging from 5 to 40 microns and for bubble sizes of 100 and 1000 microns. As observed, the results predict that as the value of induction time is decreased, i.e., as the particle becomes more hydrophobic, the probability of adhesion increases. This relationship continues until an induction time of zero is reached, resulting in an adhesion probability of unity. As has been previously reported by Dobby and Finch (1985), the probability of adhesion shows a strong dependency on particle size. For a fixed value of induction time, the probability of adhesion increases as particle size is reduced. This implies that very fine particles, even those which are only weakly hydrophobic, have a high probability of becoming attached.

As dictated by Equation [2.28], the overall probability of collection (P) for small particles is given by the product of the collision and adhesion probabilities. Expressions for P are given in Table 2.5 for each of the flow conditions considered in the present investigation.

If the overall probability of collection for the intermediate Reynolds number case is plotted as a function of bubble diameter, an interesting observation is made. Observe the case shown in Figure 2.10 for a particle diameter of 40 microns. The results have been calculated

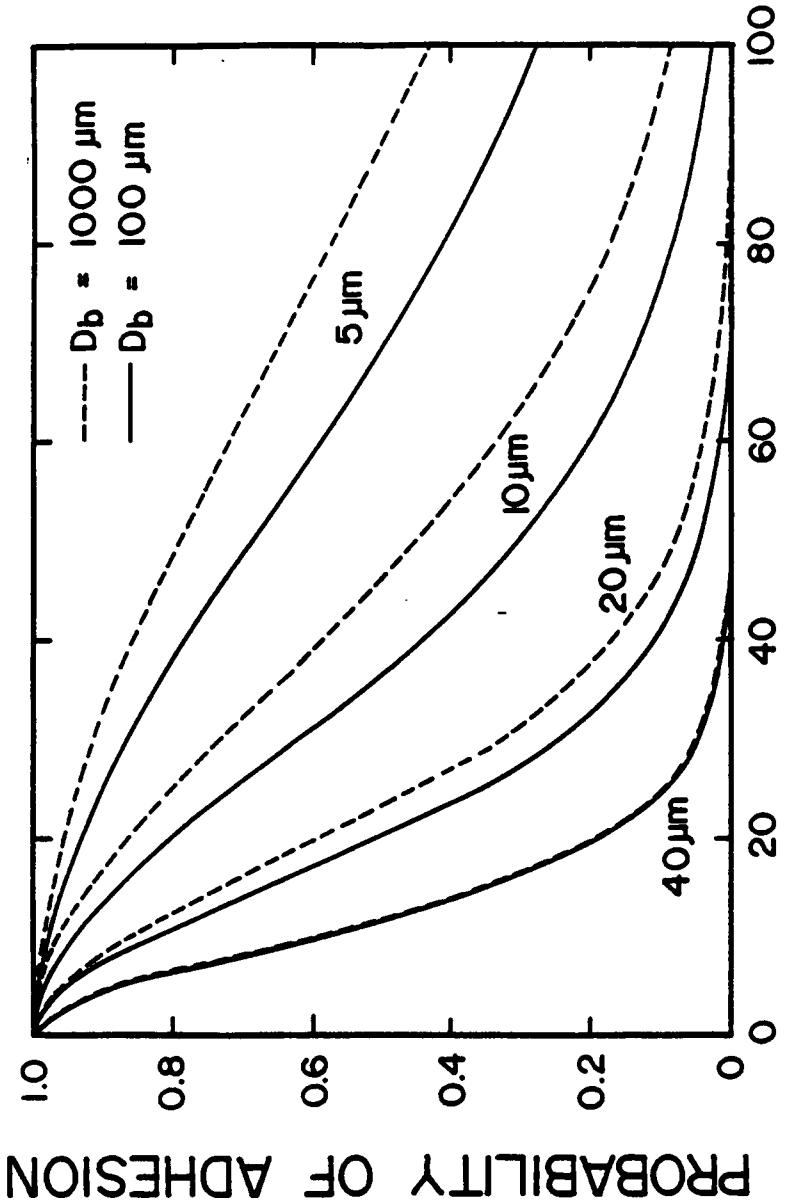

Figure 2.9 Probability of adhesion versus induction time as calculated for two bubble sizes and for particle diameters of 5, 10, 20 and 40 microns.

Table 2.5 - Calculated Probability of Collection for Various Ranges of Reynolds Numbers

Case	Probability of Collection
Small Re	$\frac{3}{2}\left(\frac{D_p}{D_b}\right)^2 \sin^2\left[2 \arctan \exp\left\{\frac{-3U_bT}{D_b(D_b/D_p+1)}\right\}\right]$
Large Re	$3\left(\frac{D_p}{D_b}\right) \sin^2\left[2 \arctan \exp\left\{\frac{-3U_bT}{D_p+D_b}\right\}\right]$
Intermediate Re	$\left[\frac{3}{2} + \frac{4Re^{\cdot 72}}{15}\right]\left(\frac{D_p}{D_b}\right)^2 \sin^2\left[2 \arctan \exp\left\{\frac{-(45+8Re^{\cdot 72})U_bT}{15D_b(D_b/D_p+1)}\right\}\right]$

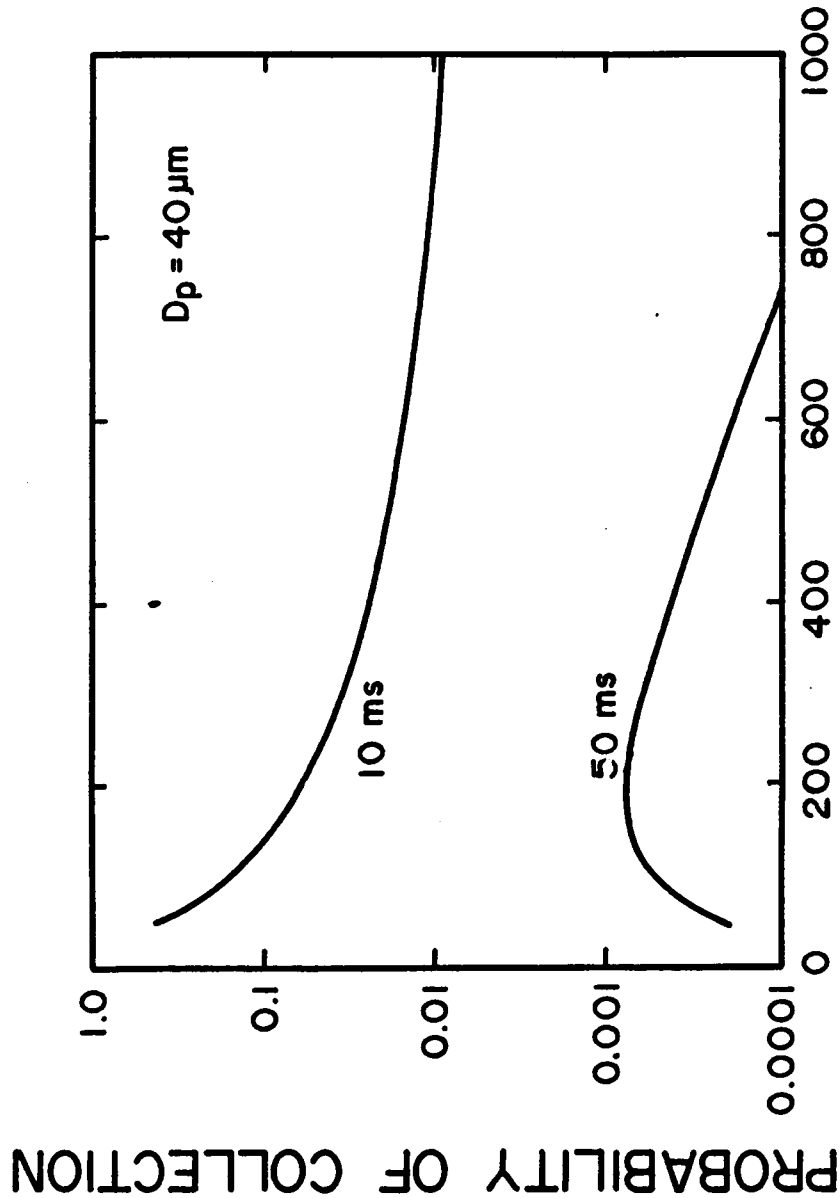

Figure 2.10 Probability of collection as calculated from Eq. 2.28 for particles having 10 ms (weakly hydrophobic) and 50 ms (strongly hydrophobic) induction time values.

for strongly (T = 10 ms) and weakly (T = 50 ms) floating particles. In general, a larger separation distance between the two curves indicates an improvement in selectivity. From this it can be observed that selectivity appears to slowly decrease with bubble size until a bubble diameter of approximately 200 microns is reached. At this point, the two curves become increasingly more separated as bubble size is reduced. In fact, for the case shown, the maximum selectivity occurs when the bubble size is smallest. The change in behavior of the 50 ms curve below a bubble diameter of 200 microns is a result of the opposing influence of the probabilities of collision and adhesion (i.e., as bubble size is reduced, the value of P_c from Equation [2.22] increases while the value of P_a from Equation [2.32] decreases). In contrast, predictions for the probability of collection of 5 micron diameter particles are considerably different. As shown in Figure 2.11, the separation distance between the 10 ms and 50 ms curves is small. This situation would imply that selective separation of these two particles would be difficult. Although the probability of collection increases with decreasing bubble diameter, no improvement in selectivity was observed.

This preceding discussion does not, however, preclude the possibility of selectively recovering fine particles by flotation. The induction time for a hydrophilic particle is yet to be quantified and may in some cases approach infinity

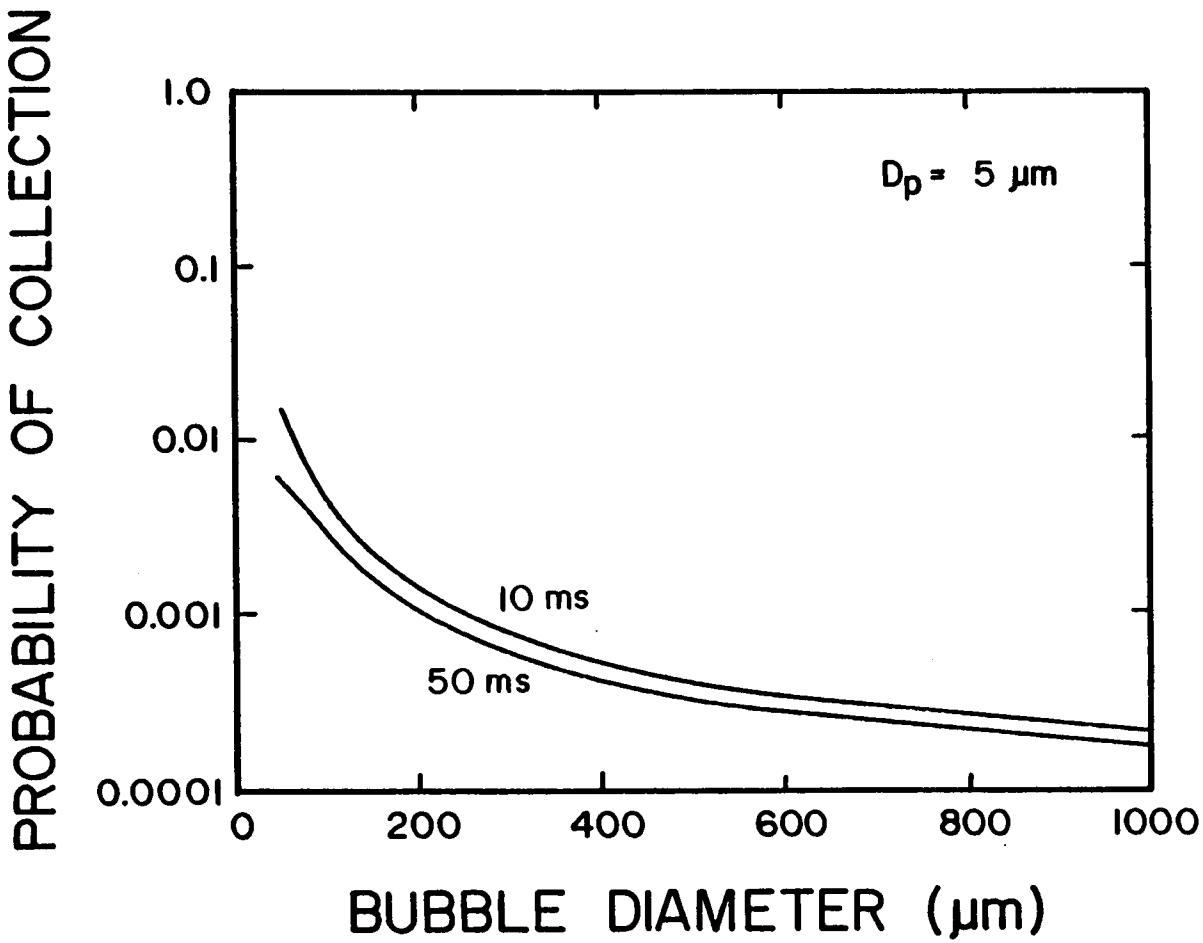

Figure 2.11 Probability of collection as calculated from Eq. 2.28 for particles having 10 ms (weakly hydrophobic) and 50 ms (strongly hydrophobic) induction time values.

for very hydrophilic surfaces. As will be shown later in Chapter 5, the primary problem of fine particle flotation appears to be that of entrainment - not attachment. Futhermore, predictions from this analysis and that of Dobby and Finch (1985) may be in error since induction time has been assumed to be independent of particle size. Experimental studies suggest that induction time may be strongly dependent on particle size (Eigeles and Volova, 1960; Jowett, 1980; Yordan and Yoon, 1985). This possibility is considered in more detail in the following section.

b) A Critical Analysis of Induction Time

One of the major difficulties encountered with the model developed in Section 2.4.2 is in the choice of an appropriate value for the induction time. It has been assumed that the induction time depends only on the hydrophobic nature of the particle and is independent of physical parameters, such as bubble and particle size. Let us examine this assumption more closely.

Consider the case shown in Figure 2.12 of a particle sweeping along a streamline toward a bubble. The separation distance between the bubble and particle is given by H. As H becomes smaller, the viscous thinning resistance of the intervening film begins to inhibit further movement of the

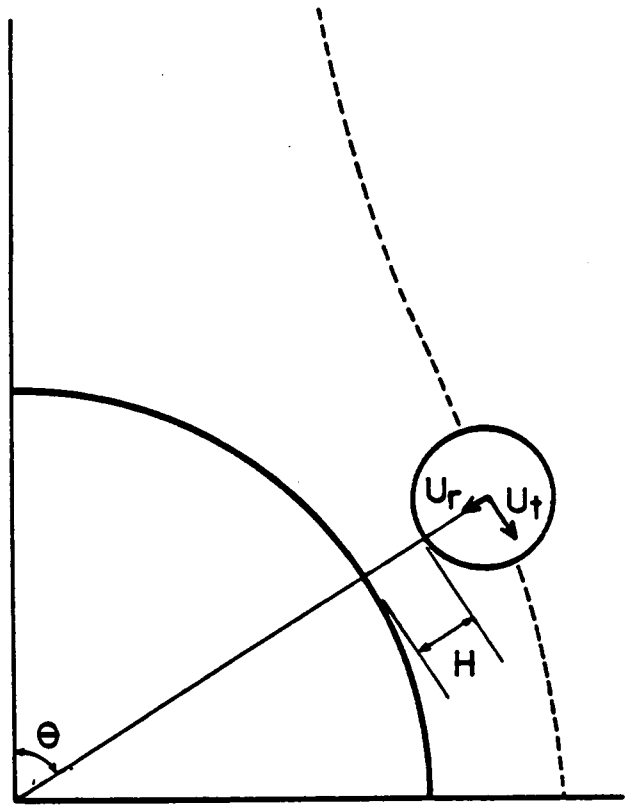

Figure 2.12 Schematic representation of a particle approaching a bubble surface under the influence of streamline flow.

particle toward the bubble. The rate at which the film thins from some initial thickness (H_i) to the critical rupture thickness (H_c) is determined by the radial velocity of the particle (U_{rp}). Therefore, by noting that:

$$dH/dt = U_{rp}, \qquad [2.33]$$

it becomes a simple matter to show that induction time (T) is related to the radial particle velocity by:

$$T = \int_{H_i}^{H_c} \frac{1}{U_{rp}} dH. \qquad [2.34]$$

Thus, induction time can be calculated if U_{rp} is known as a function of H.

According to lubrication theory, the force resisting (F_r) the thinning of the film can be related to U_{rp} by:

$$F_r = 6\pi\mu R_p U_{rp} B \qquad [2.35]$$

in which μ is the liquid viscosity and B is the Stokes correction factor. The magnitude of B increases as the value of H becomes smaller. As expected, F_r increases for smaller separation distances, higher viscosities, larger particles and higher approach velocities.

Dynamic equilibrium requires that the force pressing (F_p) the particle toward the bubble be equal to the resisting force (F_r), i.e., $F_p=F_r$. From this, induction

time can now be determined by solving Equation [2.35] for U_{rp} and substituting the result into Equation [2.34] to yield:

$$T = \int \frac{6\pi\mu R_p B}{F_p} dH. \qquad [2.36]$$

The use of Equation [2.36] for predicting induction time values is the source of much confusion in the literature. Previous investigators have made two erroneous assumptions. First, the value of B generally chosen is:

$$B = R_p/H \qquad [2.37]$$

which was calculated from Reynolds lubrication theory (1886) by Taylor (1925) for the case of a sphere approaching an infinitely flat plate. The second assumption is that the value of F_p is assumed to be constant and given by:

$$F_p = mg \qquad [2.38]$$

in which m is the mass of the approaching particle and g is the acceleration of gravity. By substituting Equations [2.37] and [2.38] into Equation [2.36], integration yields an expression for induction as:

$$T = \frac{6\pi\mu R_p^2}{mg} \ln\frac{H_c}{H_i}. \qquad [2.39]$$

Note that Equation [2.39] suggests a squared power

dependency between induction time and particle size. As shown in Figure 2.13, experimental investigations tend to support the suggestion that induction time increases with increasing particle size. It should be noted, however, that in the experimental induction time measurements, a captive bubble is pressed against a bed of particles with a constant force. Therefore, it is not surprising that the trend predicted by Equation [2.39] is actually observed in these experiments.

The problem with this analysis is that the assumptions which make the derivation possible are not valid for the conditions existing in flotation. It has been shown (Maude, 1961; Brenner, 1964) that the value of B given by Equation [2.37] is valid only as the separation distance between the objects approaches zero. Furthermore, this expression is only valid for the case of a sphere approaching a flat plate. For the case of bubble-particle collision, where a small sphere approaches a larger one, Goren and O'Neill (1971) have shown that the value of B is significantly smaller than that predicted for the case of a flat plate. Figure 2.14 shows a comparison of B predicted by each of these theories. A problem also exists with the determination of the pressing force (F_p). Equation [2.38] can only be employed when the force moving the particle is gravity alone. For the case of fine particle flotation,

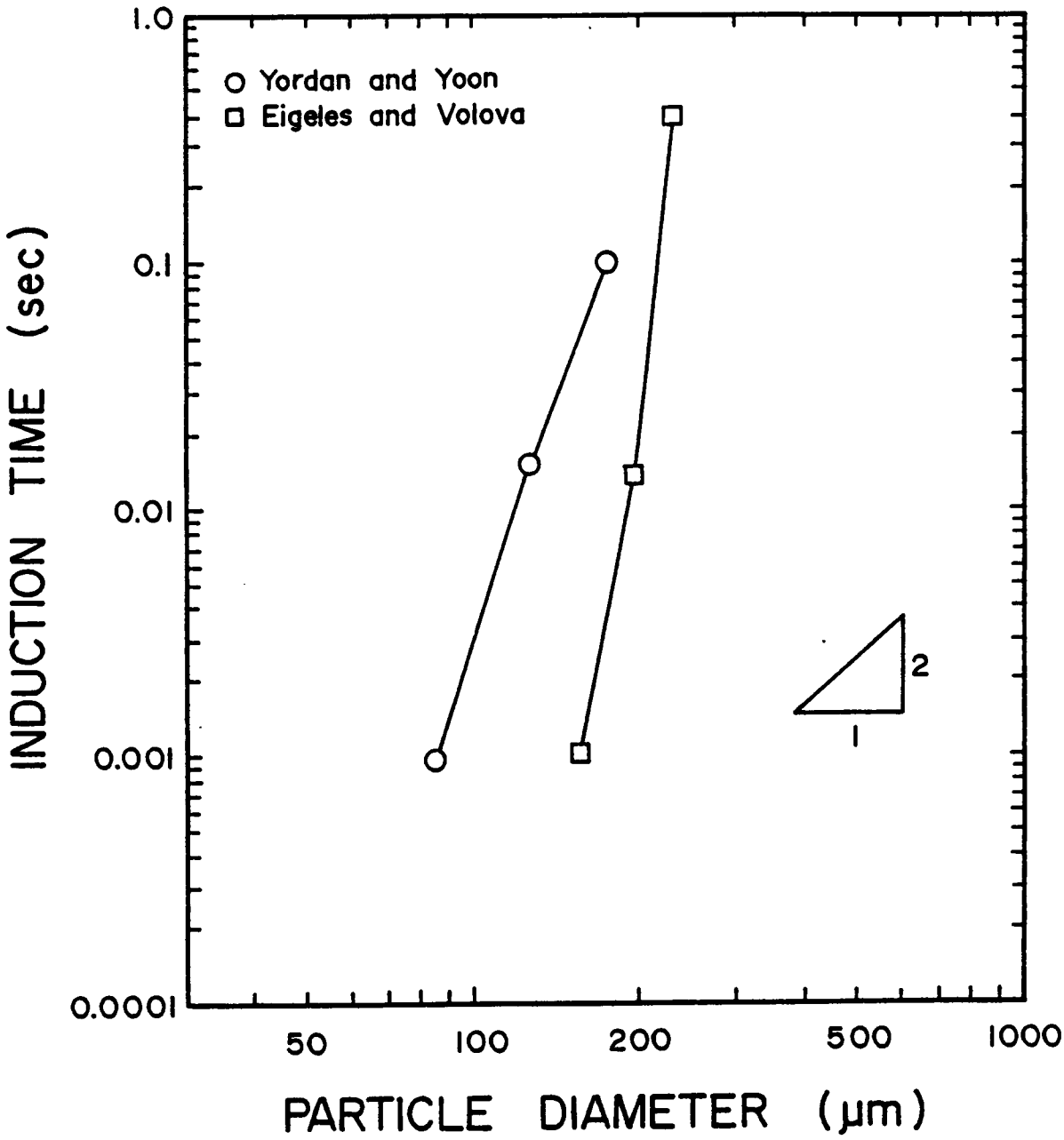

Figure 2.13 Experimentally determined values of induction time as functions of particle diameter.

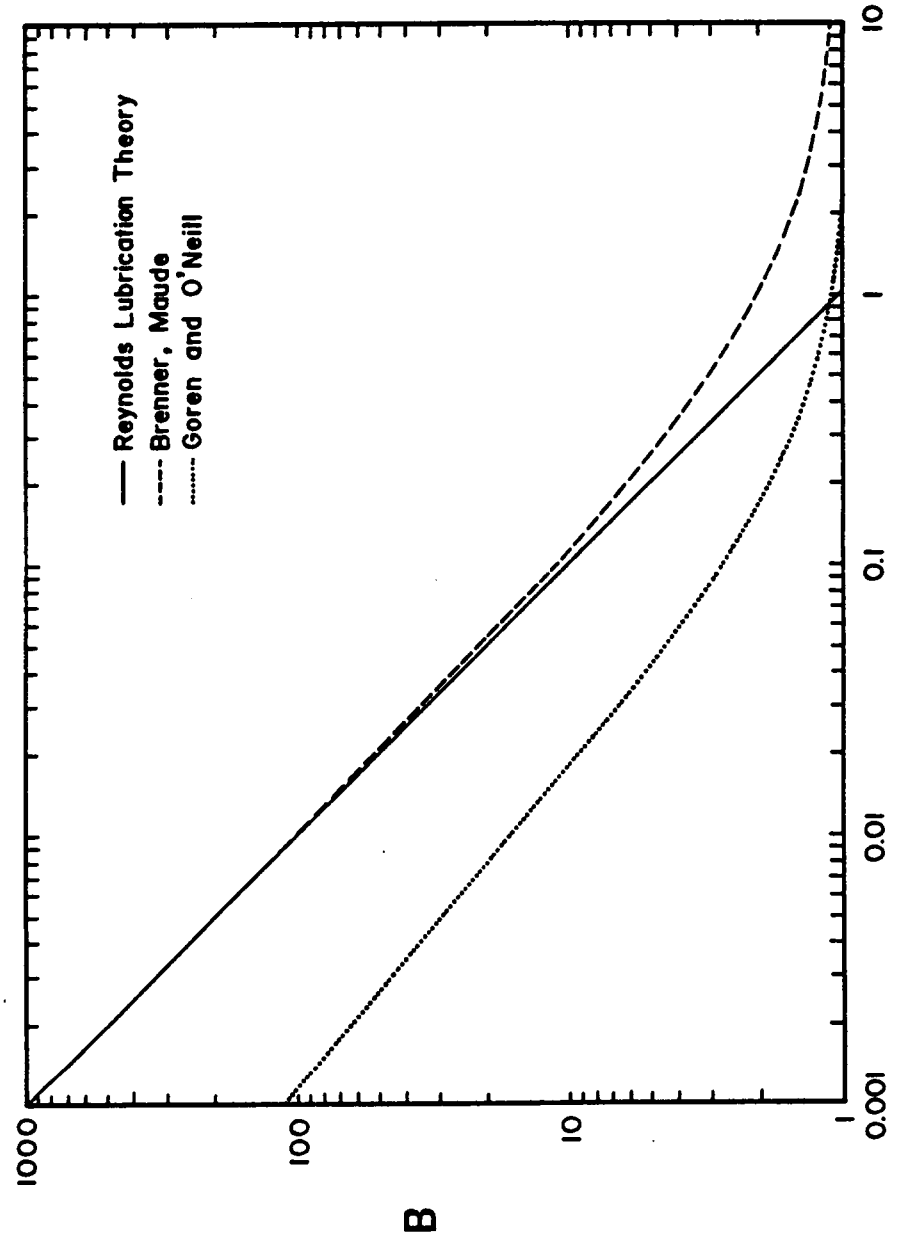

Figure 2.14 Relationship between B and H/R_p determined by various investigators.

hydrodynamic drag is the major force driving the particle towards the bubble, and gravity exerts only a minor influence. Therefore, values obtained by Equation [2.38] are not reasonable estimates of F_p.

In light of the above, let us again consider the situation given in Figure 2.12. At any point, the radial velocity of a streamline (U_r) can be determined from the well-known expression:

$$U_r = \frac{1}{R^2 \sin\theta} \frac{dY}{d\theta}. \qquad [2.40]$$

Expressions for U_r are shown in Table 2.6 for each of the flow conditions considered in the present work. The actual force which presses the particle against the bubble (F_p) is given by the hydrodynamic drag force (F_d). Thus, for a spherical particle, the Stokes drag equation states that:

$$F_p = F_d = 6\pi\mu R_p U_r. \qquad [2.41]$$

Since the value of U_r varies with the position of the particle around the bubble, F_p cannot be considered to be constant. In fact, values calculated from Equation [2.40] indicate that the radial velocity decreases sharply with decreasing distance from the bubble surface. As a result, Equation [2.41] indicates that a larger particle which is sliding around the surface of the bubble will tend to be more strongly pressed against the bubble than will a smaller

Table 2.6 - Radial Particle Velocity for Various Ranges of Reynolds Numbers

Case	Radial Velocity
Small Re	$-U_b \cos\theta \left(1 - \frac{3}{2X} - \frac{1}{2X^3} \right)$
Large Re	$-U_b \cos\theta \left(1 + \frac{1}{X^3} \right)$
Intermediate Re	$-U_b \cos\theta \left[1 - \frac{3}{2X} - \frac{1}{2X^3} + \frac{2Re^{\cdot 72}}{15} \left(\frac{1}{X^4} - \frac{1}{X^3} + \frac{1}{X} - \frac{1}{X^2} \right) \right]$

particle. The attachment of larger particles is enhanced by this effect.

A correct expression for the radial particle velocity must be determined in order to accurately derive an expression for induction time. This is accomplished by recalling that dynamic equilibrium requires that Equations [2.35] and [2.41] be equal. Upon elimination of like terms, the radial velocity of the particle is given by:

$$U_{rp} = U_r/B. \qquad [2.42]$$

According to the results shown in Figure 2.14, B approaches unity when H is large. In this case, the radial velocity of the particle and that of the streamline are the same. However, as H becomes small, the value of B increases sharply. As can be seen in Equation [2.42], the increased value of B causes the particle velocity to become less than that of the surrounding fluid.

Substituting the value of F_p from Equation [2.41] into Equation [2.36] yields:

$$T = \int \frac{B}{U_r}\, dH. \qquad [2.43]$$

This expression clearly demonstrates that induction time is not independent of physical parameters, such as bubble and particle size, as was previously assumed. According to

Equation [2.43], the magnitude of induction time is determined by the product of two opposing effects. As shown in Figure 2.14, the value of B increases as particle size increases. This results in an increase in the induction time value. On the other hand, since U_r increases with increasing particle size, the magnitude of the induction tends to decrease. The net value of induction time is determined by the combined influence of these effects. Unfortunately, in the present work, an acceptable analytical solution to Equation [2.43] could not be found because of algebraic complexity of the equations involved. Numerical integration of this equation was also not possible due to the ambiguity of defining the value of H_i.

Nevertheless, the above analysis provides a great deal of insight toward understanding the concept of induction time. In general, one can consider induction time to be the result of two components. The first component is related to the chemistry or thermodynamics of the system, with H_c being the major parameter. In accordance with Equation [2.43], an increase in hydrophobicity (which increases H_c) decreases the induction time. The second component includes the hydrodynamic terms such as B, U_r and H_i, and is independent of the chemistry of the system. The second component determines the rate at which the film thins, while the first component determines the distance to which the film must thin before rupture occurs. Depending on the circumstances,

either of these components may be the rate limiting step in bubble-particle attachment.

At this time, the utilization of the induction time concept into a quantitative model for determining particle capture is not possible since an analytical expression for induction time cannot be determined.

2.4.4 An Improved Model for Particle Collection

a) Simulation of Particle Trajectory

Considering the difficulties in modeling flotation processes on the basis of induction time as described in the previous sections, a new method for determining the overall probability of particle capture is needed. With this in mind, a numerical simulation technique was developed which allows the trajectory of a particle to be determined as it sweeps past a rising air bubble. Attachment of the particle is assumed to occur when a particle approaches to a distance of H_c from the bubble surface. At this point, the thin liquid film between the bubble and particle instantaneously ruptures and the particle becomes attached.

In order to simulate the particle trajectory, the correct tangential and radial velocities of the particle must be determined. The radial velocity of the particle has been determined by Equation [2.42]. Unlike the radial

components, there are no constraints which resist the movement of the particle in the tangential direction. Therefore, it can be shown that:

$$U_{tp} = U_t \qquad [2.44]$$

in which U_t and U_{tp} are the tangential velocities of the streamline and particle, respectively.

The simulation is performed as follows. Initially, a particle is located at a distance ahead of the bubble where it is not influenced by either the curvature of the streamlines or hydrodynamic resistance. Equations [2.42] and [2.44] can be utilized for evaluating the instantaneous velocity of the particle. The values of U_r and U_t to be substituted are obtained from Equations [2.40] and [2.31]. The use of these velocity expressions require only that the stream function be known for the flow conditions under consideration. The contribution from gravity to the radial and tangential velocity components of the particle have also been considered.

For a small increment in time, the new position of the particle can be estimated by:

$$\theta_{new} = \theta_{old} + U_t \Delta t/R + U_p \sin\theta \qquad [2.45]$$

and,

$$R_{new} = R_{old} + U_r \Delta t/B + U_p \cos\theta \qquad [2.46]$$

where Δt is time interval and U_p the terminal settling

velocity of the particle. The appearance of B in Equation [2.46] comes about because of the hydrodynamic resistance to thinning of the liquid between the bubble and particle. At great distances, the value of B is unity and does not effect the particle trajectory. As the particle approaches the bubble surface, hydrodynamic resistance increases and the radial velocity of the particle is retarded by an amount proportional to the separation distance. Therefore, the resultant trajectory of the particle will tend to be slightly skewed from that of the streamline, as shown in Figure 2.15. The program used to simulate the particle trajectory and to determine the approach distance of the particle to the bubble is contained in Appendix I.

b) Overall Probability of Collection

The criterion for particle attachment is whether or not the particle approaches close enough to the bubble so that the intervening film becomes unstable and ruptures. This critical film thickness has been previously designated as H_c, and is assumed to directly represent the chemistry of the system.

For a given set of conditions, a unique value of R_1 is necessary in order to obtain a closest approach distance which is equivalent to H_c. Therefore, Equation [2.23] can be used to directly relate the probability of collection to

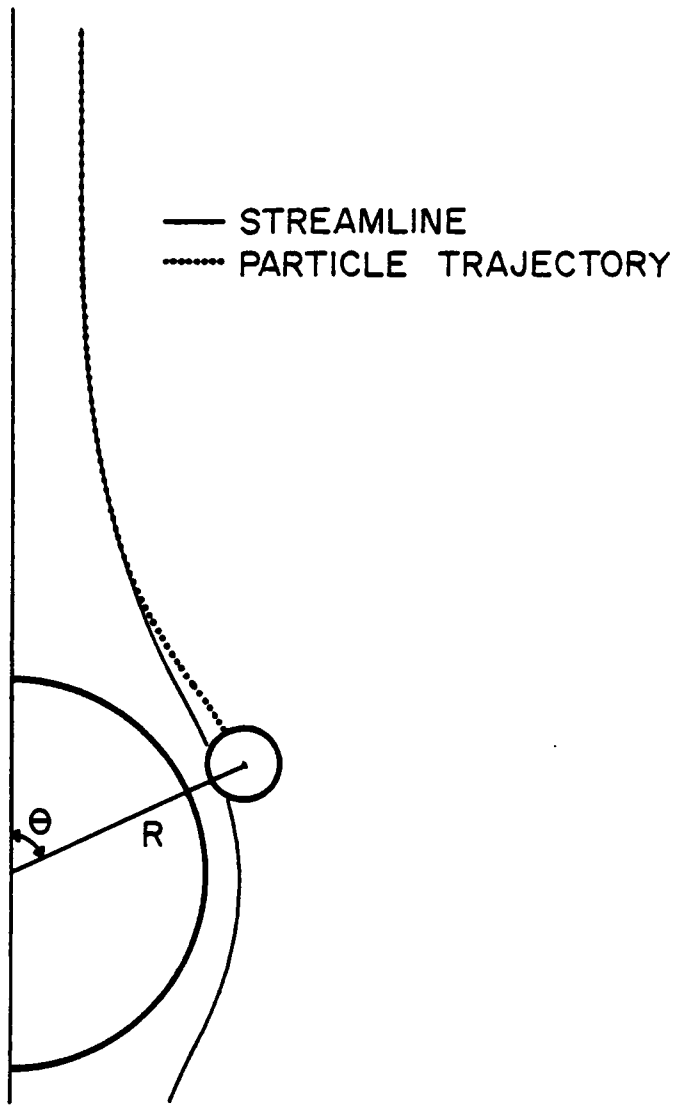

Figure 2.15 Trajectory of a particle moving under the influence of streamline flow and film thinning resistance.

H_c. Figure 2.16 shows the results of such an analysis for a bubble diameter of 100 microns and a range of particle sizes. Therefore, if the critical film thickness, bubble size and particle size are known, this plot can be used to evaluate the probability of collection. A good estimate of H_c for very hydrophobic particles would be between approximately 100 nm and 150 nm (Platikanov, 1964; Shulze and Cichos, 1972; Blake, 1973; Schulze, 1975; Derjaguin and Dukhin, 1979). H_c will increase with increasing hydrophobicity.

This analysis has been repeated for a number of bubble sizes. It was found that the results from these simulations could be normalized with respect to the curves drawn for the 100 micron diameter bubble using the normalization factors plotted in Figure 2.17. Thus, the probability of collection for different bubble sizes can be determined by finding the value of P from Figure 2.16 and multiplying it by the normalization factor given in Figure 2.17.

The main objective of the following section will be to experimentally determine the probability of collection as a function of bubble and particle size, and compare the results with the values predicted by this model.

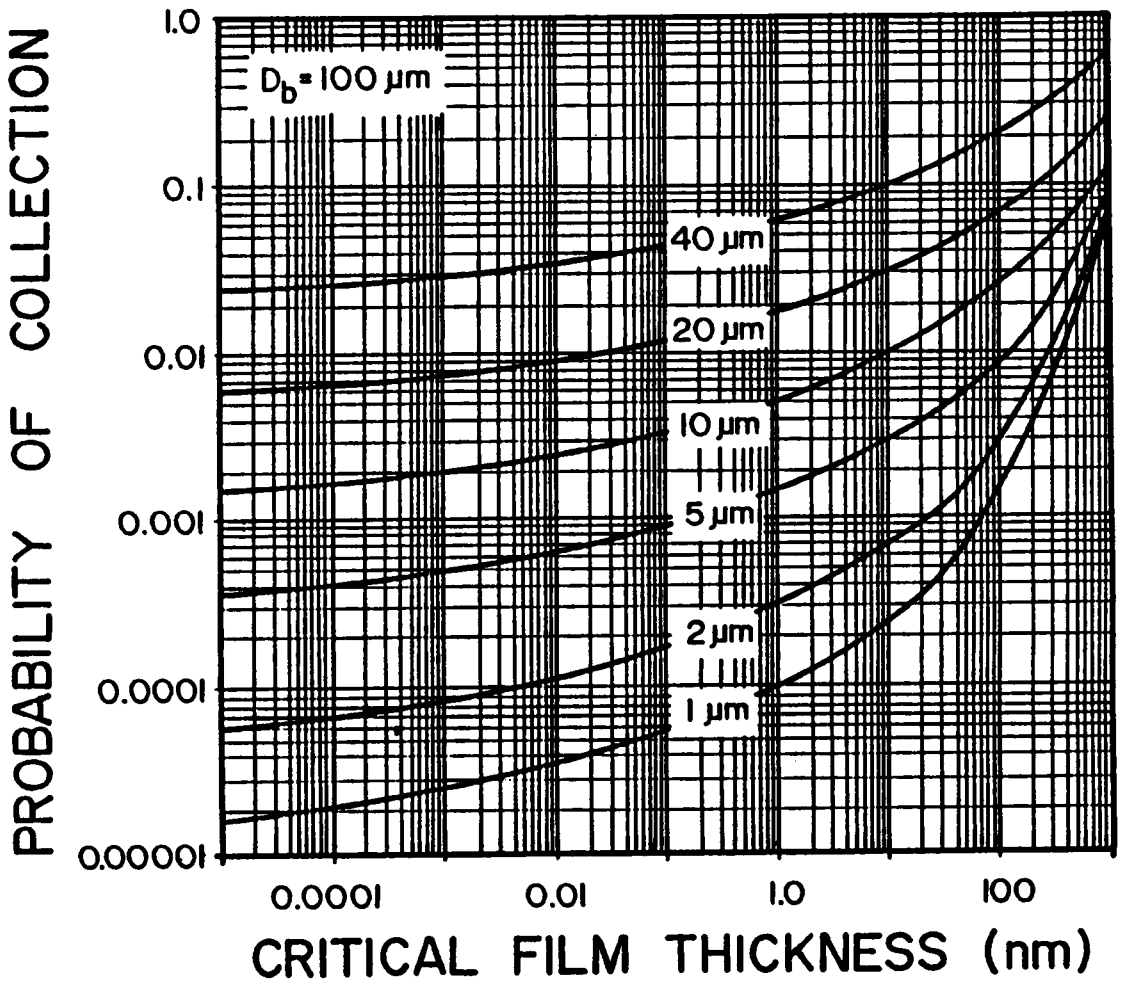

Figure 2.16 Theoretical relationship between P and H_c for a bubble diameter of 100 microns and particle diameters of 1, 2, 5, 10, 20 and 40 microns.

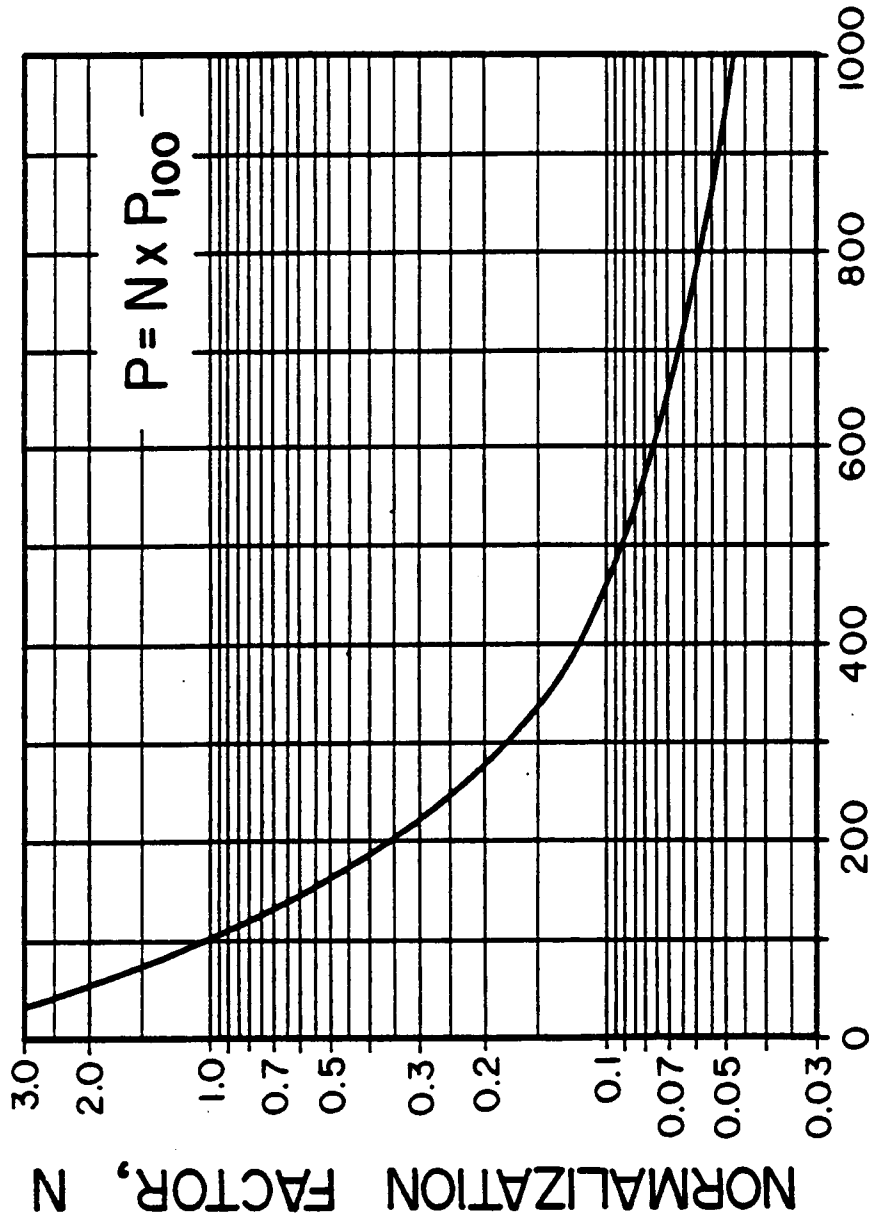

Figure 2.17 Normalization plot for determining the probability of collection at various bubble sizes.

2.5 Experimental

2.5.1 Samples

The probability of collection measurements were performed using coal from the Buller seam in New Zealand. The Buller seam coal contained only 0.13% ash and was very hydrophobic as mined. Samples of different size fractions were prepared by dry-grinding in an agate mortar and pestle, followed by screening or centrifugal sedimentation, depending on the size of particles desired. To minimize oxidation, the samples were stored under a nitrogen atmosphere in air-tight containers at -20^{o}C.

2.5.2 Apparatus and Procedure

The apparatus used for the measurement of the probability of collection is shown in Figure 2.18. It is similar in design to that used by King et al (1974) for the measurement of bubble loading, but the technique of measurement is fundamentally identical to that employed by Anfruns and Kitchener (1976, 1977). In each measurement, a single bubble was injected into a dilute slurry (of approximately 0.2% solids) by means of a small syringe. Ultrasonic agitation coupled with gentle stirring was employed to provide a completely dispersed suspension. The suspension was examined under a microscope to ensure that

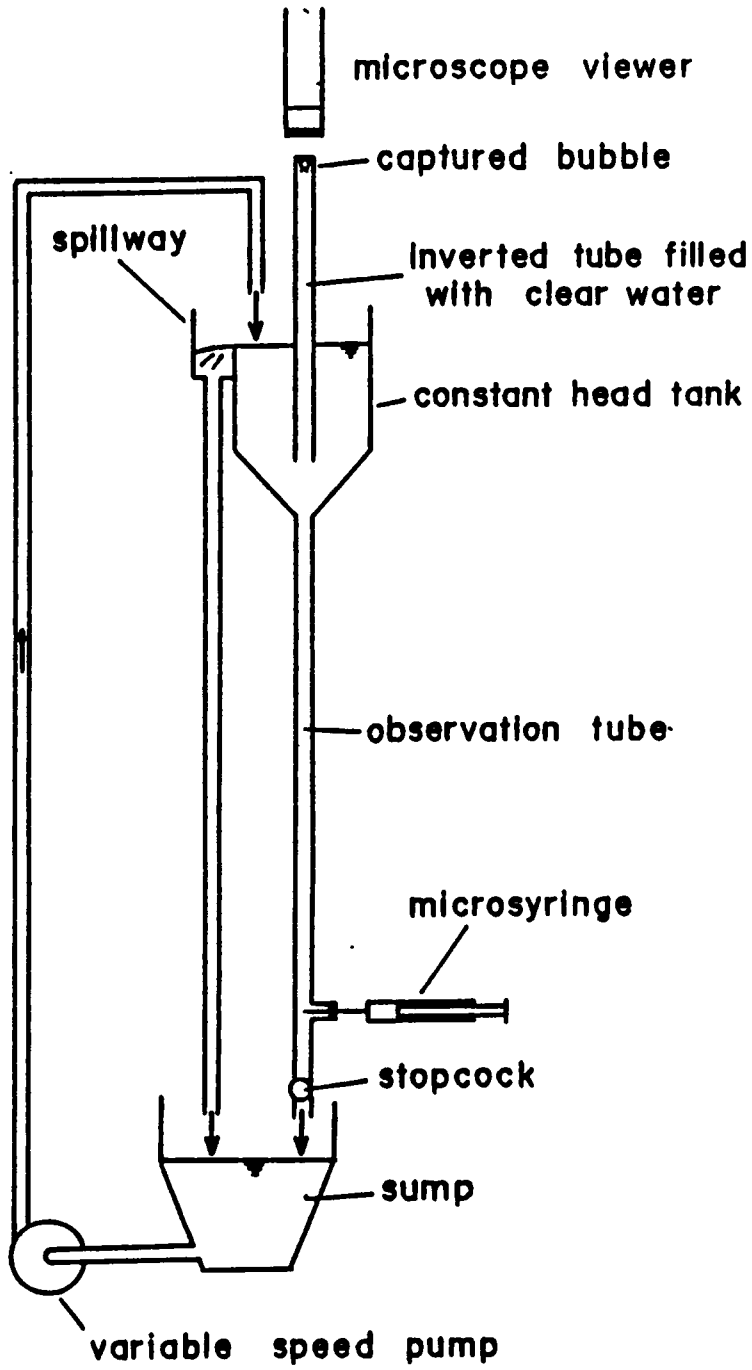

Figure 2.18 Apparatus employed for the measurement of the probability of collection for single bubbles.

only single particles were present. As the bubble was allowed to rise through the observation tube, the downward flow of suspension was adjusted by the two-way stopcock to counterbalance the upward velocity of the bubble. In this manner, the bubble was "trapped" for the desired period of time. By closing the stopcock, the bubble was then allowed to rise into an inverted tube filled with clear water. The number of particles attached to the bubble was determined visually using a microscope viewer. Particles entrained within the wake of the bubble were allowed to settle back down the tube prior to particle counting. The diameter of the bubble was determined by inserting a graduated eyepiece into the microscope. A photograph of a bubble with attached particles as viewed through the microscope is included in Figure 2.19.

The probability of collection (P) was determined by dividing the number of particles collected (N) by the total number of particles that were in the path of the bubble as:

$$P = \frac{4N}{\pi D_b^2 t U_b C} \qquad [2.47]$$

in which D_b is the diameter of the bubble, t the residence time, U_b the velocity of the particle suspension moving past the bubble, and C the number of particles per unit volume of suspension. The value of U_b, which is actually the bubble rise velocity, was determined experimentally by measuring

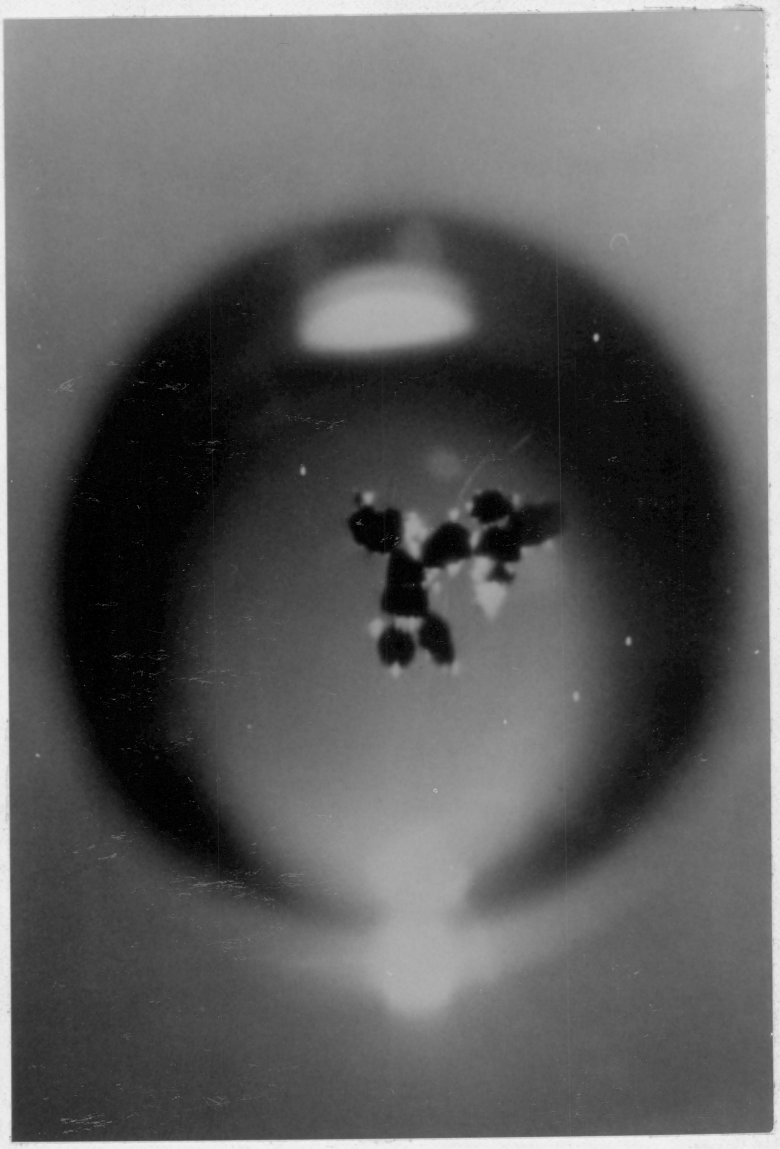

Figure 2.19 Photograph of particles attached to a bubble as seen through the microscope viewer.

the time required for a bubble to rise a given distance in the column. The value of C was determined on the basis of the mean diameter of each narrowly-sized sample.

2.5.3 Results

a) Bubble Rise Velocity

The results of bubble rise velocity measurements are shown in Figure 2.20. For the range of bubble sizes investigated, U_b was found to be well represented by:

$$U_b = Z\ (D_b)^{1.14} \qquad [2.48]$$

where Z is the proportionality constant obtained for a given set of experimental conditions. This equation has the form of the equation of motion for spherical particles settling in the intermediate region between Stokes' and Newton's conditions (McCabe and Smith, 1976).

b) Probability of Collection Measurements

Figure 2.21 shows the results of the probability of collection measurements conducted on the Buller seam coal as a function of bubble size. Experiments have been carried out using samples having 40.1-, 31.0- and 11.4-micron mean sizes. Similar results have been reported previously (Anfruns and Kitchener, 1976), but only for bubble sizes

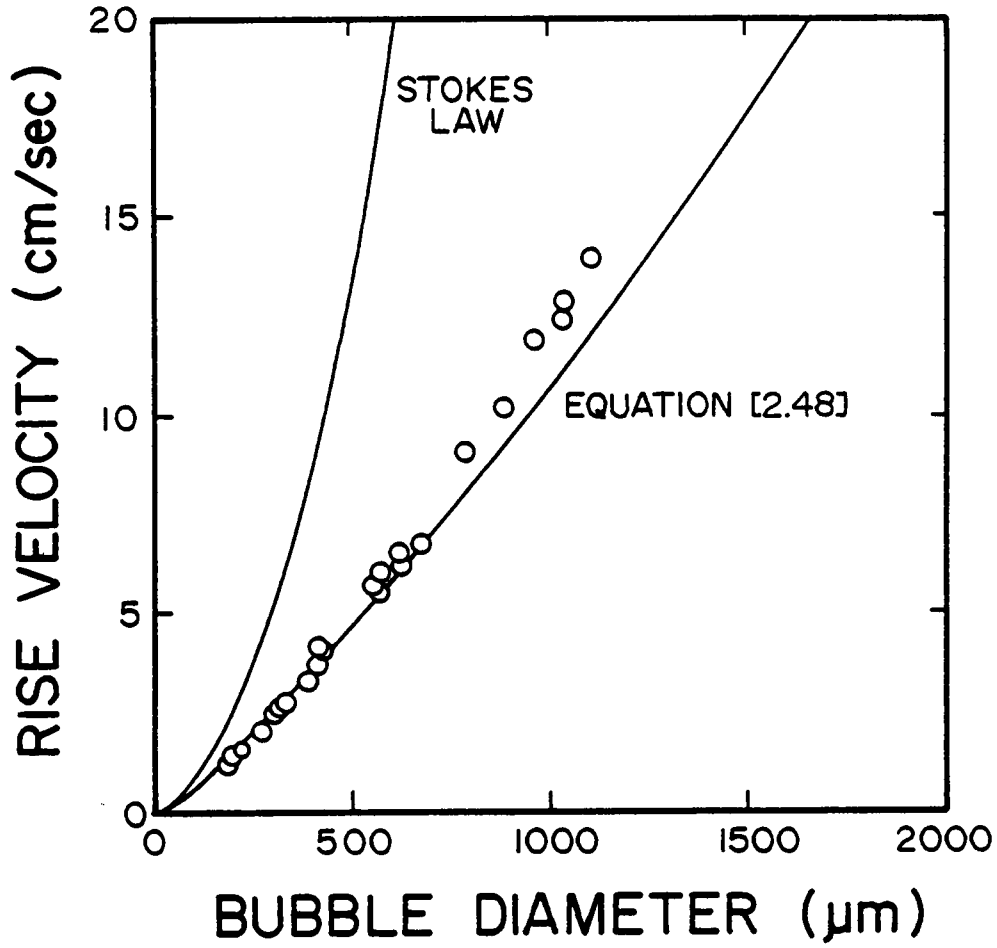

Figure 2.20 Comparison of theoretical and experimental bubble rise velocities as a function of bubble diameter.

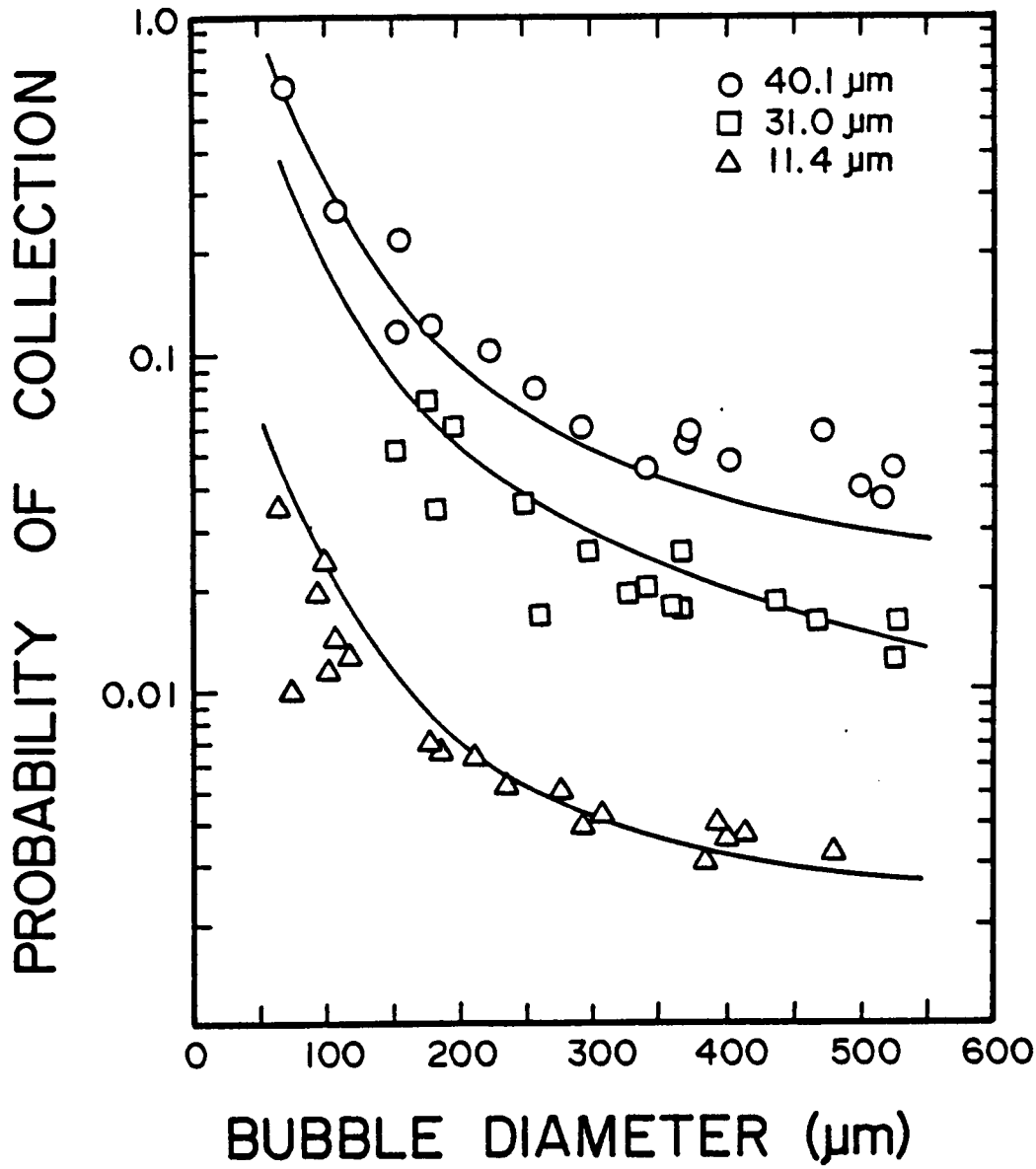

Figure 2.21 Comparison between the theoretical (lines) and experimental (points) probability of collection values determined for the low-ash Buller seam coal as a function of bubble diameter. H_c has been assumed to be 150 nm.

larger than approximately 350 microns in diameter. The solid lines in this figure represent the theoretical probabilities of collection calculated from Figures 2.16 and 2.17 assuming a critical film thickness of 150 nm. A thickness of 150 nm is a good estimate of H_c for very hydrophobic surfaces (Derjaguin and Dukhin, 1979).

The experimental results show a dramatic increase in the probability of particle collection as bubble diameter is reduced. The correlation between the theoretical and experimental results is very good, although slightly more deviation is seen for the larger particle sizes. This slight discrepancy may be due to the deviation of larger particles from the streamlines because of inertia. This possibility would be in accordance with Figure 2.2, which shows that the deviation of a particle from a streamline increases with increasing particle and bubble diameters.

2.6 Discussion

The analysis performed in the present work has allowed the probability of collection (P) to be calculated from a fundamental analysis of the hydrodynamic interaction between a bubble and particle in flotation. As shown in Figure 2.16, the magnitude of P increases with H_c. This implies that the collection of particles is increased by increasing the hydrophobicity. It is common practice to employ higher

collector dosages when floating finer particles. The reason typically given for this action is that the increased surface area of the fine particles adsorbs more collector. However, as predicted by Figure 2.16, smaller particles must be made significantly more hydrophobic in order to achieve the same probability of collection observed for larger particles. Therefore, the fact that higher reagent levels are required to float finer particles may also be a result of the hydrodynamics of the system.

Another interesting observation is made when analyzing the effect of bubble size on the probability of collection. Figure 2.22 shows the predicted value of P versus H_c for two different bubble sizes. As shown, the values of P for the 100 micron diameter bubble are greater than those of the 1000 micron bubble for the particle size range considered. The importance of this comparison is that an adequate degree of floatability can be achieved with fine particles by simply decreasing the bubble size. From this comparison, one can see that fine particle flotation can be improved by simply decreasing the bubble size rather than by adding more reagents.

2.7 Summary and Conclusions

1) An expression for the stream function has been developed for intermediate values of Reynolds numbers. This

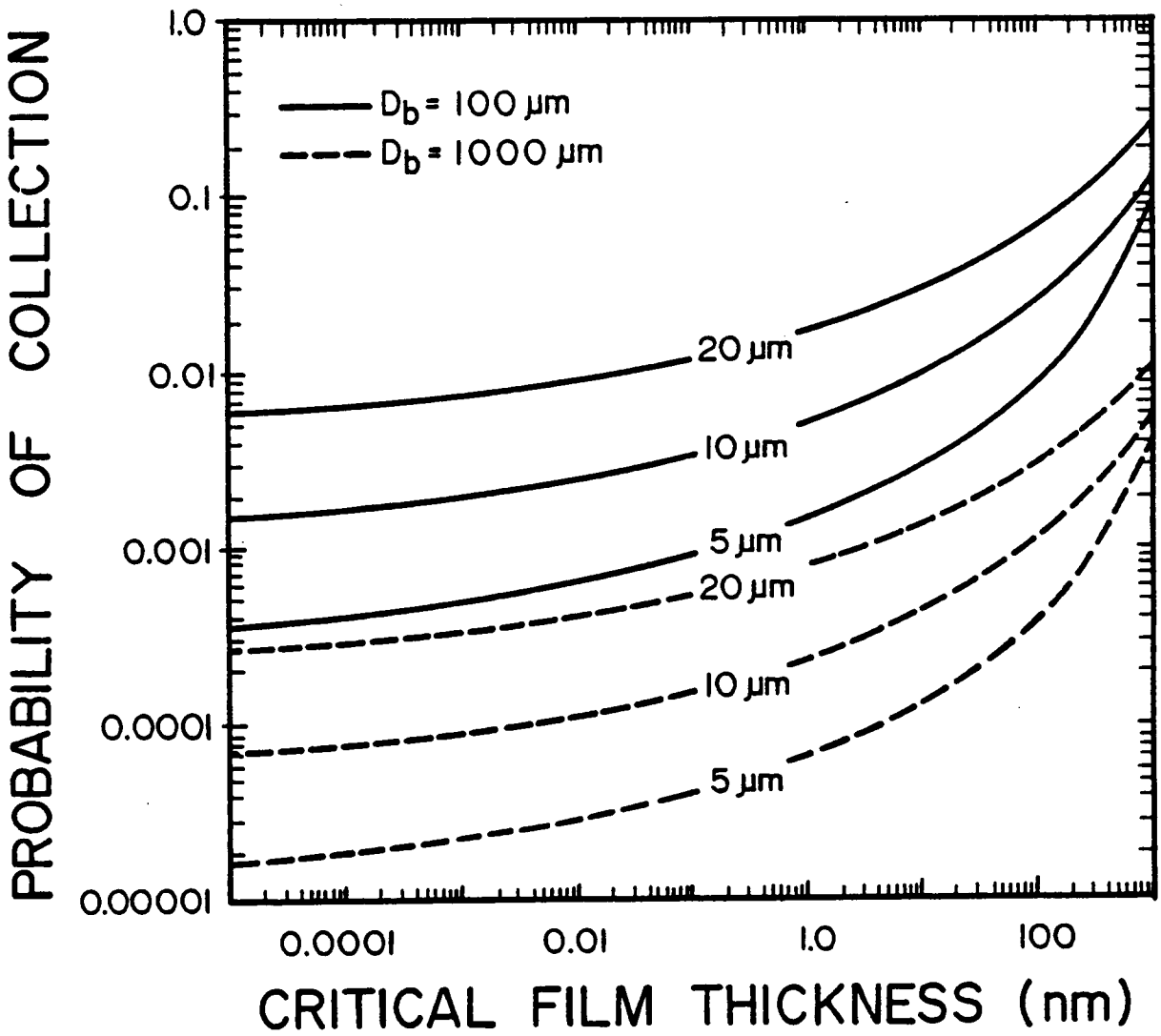

Figure 2.22 Effect of bubble size on the relationship between P and H_c for particle diameters of 5, 10 and 20 microns.

expression is appropriate for the sizes of bubbles typically observed in flotation.

2) Using the intermediate stream function, an analytical expression has been derived for the probability of collision (P_c) between a particle and bubble. The expression predicts that the magnitude of P_c increases dramatically as bubble size is reduced. This finding suggests that an excellent method for increasing the efficiency of fine particle flotation would be to decrease the bubble diameter.

3) Using the intermediate stream function, an analytical expression for the probability of adhesion (P_a) has been derived by assuming that adhesion occurs when sliding time exceeds the induction time. In order to use this expression, one must assume that induction time is independent of physical parameters (such as bubble size, particle size, etc.). Regretfully, evidence obtained in the present work suggests that this assumption is not valid for the case of fine particle flotation.

4) Because of the problems involved in determining induction time, a numerical simulation of the particle trajectory was employed to determine a relationship between the critical rupture thickness (H_c) and the probability of collection (P). This analysis shows that

P increases with increasing particle size, decreasing bubble size and increasing hydrophobicity.

5) Experimental measurements of the probability of collection (P) were performed using very hydrophobic, narrowly-sized coal particles. These values were found to correlate well with predictions made using the numerical simulation technique. Both the theoretical and experimental data suggest a rapid increase in the probability of collection (P) with decreasing bubble size.

CHAPTER 3

KINETICS OF FINE PARTICLE FLOTATION

3.1 Introduction

In the early years of coal preparation, little attention was given to the recovery of fine coal. Particles too fine to be successfully treated by gravity processes were simply discarded. However, in the past few decades, mining mechanization has increased the proportion of fine coal arriving at the processing plant from the mine. Combined with the substantial increases in the cost of coal production, economics now dictate that fine coal be recovered. As a result, virtually all new coal processing plants incorporate a flotation circuit into their basic flowsheet to collect this material.

Besides the economic incentives, environmental considerations have also increased the demand for fine coal cleaning. As shown in Figure 3.1 the United States Department of Energy has concluded that the availability of low sulfur coal may be substantially increased by processing coal at finer sizes (Hucko, 1984). In fact, a number of advanced coal flotation processes have been proposed in which the entire tonnage of feed coal is finely ground in order to liberate mineral matter associated with the coal (Singh, 1982; Keller, 1982; Burgess et al., 1983; Yoon et

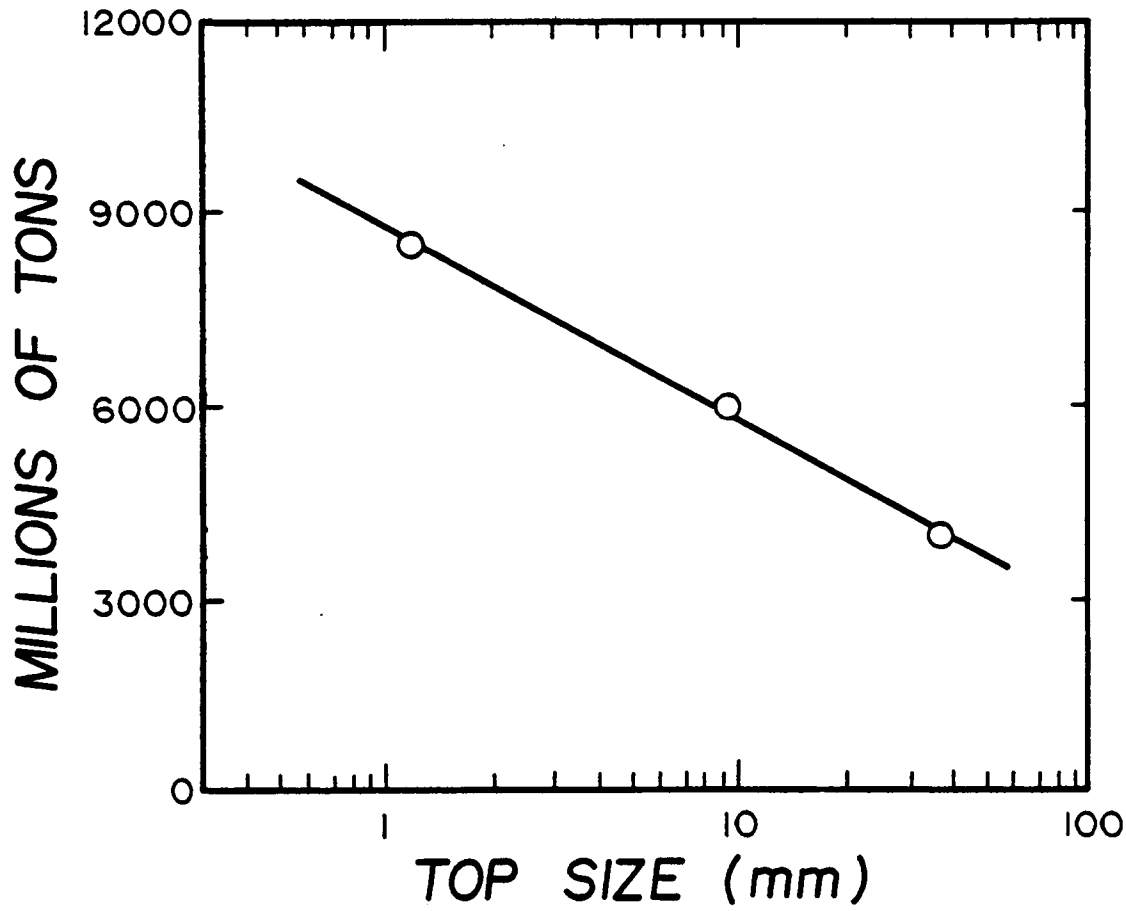

Figure 3.1 Increase in the availability of <0.85% sulfur coal as a function of top size (U. S. Bureau of Mines).

al., 1984). There appears to be little doubt that methods for improving fine coal processing will become one of the major areas of research for some years to come.

The most widely accepted method for treating fine coal is froth flotation. As shown in Figure 3.2, flotation is the only major commercial coal cleaning device currently capable of processing coal which is finer than approximately 200 mesh (Green, 1982). Since coal is inherently hydrophobic, it is ideally suited for separation by flotation. However, the efficiency of coal flotation falls sharply for coarse and very fine particle sizes, with an optimum particle diameter observed at approximately 200 microns (Zimmerman and Sun, 1979). Therefore, some modifications must be made if flotation is to be effective in treating very fine coal fractions.

3.2 Literature Review

A number of studies have been published on the effect of particle size in flotation. Recent reviews are available which present an excellent overview of much of the work performed in this area (Trahar and Warren, 1976; Jameson et al., 1977). In nearly all cases, a continuous decrease in the recovery of material occurs as particle size is decreased. Studies suggest that this behavior is typical for particles down to near colloidal sizes (Kihlstedt, 1968;

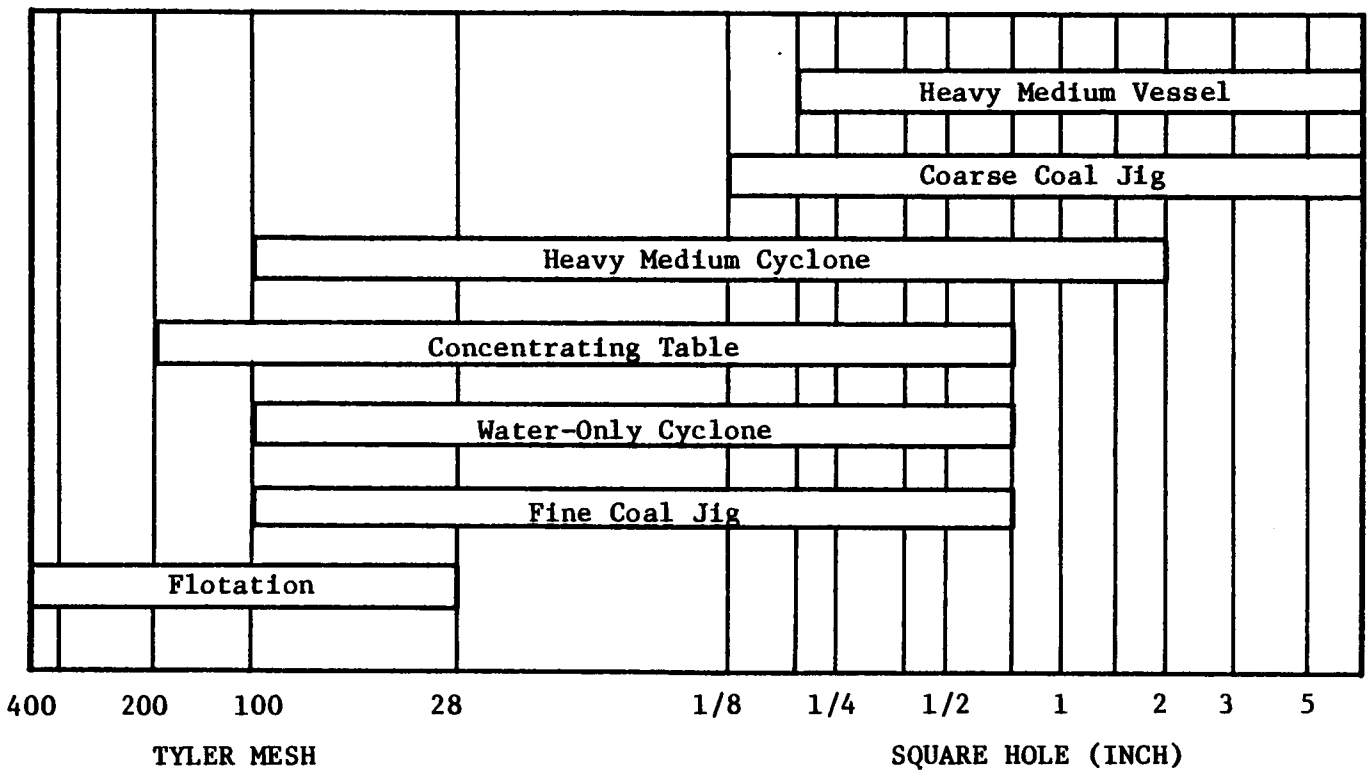

Figure 3.2 Size range of applicability for various conventional processing techniques used in the industrial processing of coal (Green, 1982).

Kelsall et al., 1974).

The best method of analyzing the flotation response of particles of different sizes is to measure the rate of flotation for each size fraction. The first detailed description of flotation as a rate process is attributed to Garcia (1935), who concluded that the concentration of floatable material (C) remaining in a flotation cell is depleted exponentially with time (t). In differential form, this relationship is given as:

$$dC/dt = -k\ C \qquad [3.1]$$

in which k is the rate constant for the process. This equation bears a formal analogy to many processes in chemical engineering which have been studied quite extensively (Smith, 1956). The flotation rate constant has been found to decrease sharply with particle size. Experimental studies by Tomlinson and Fleming (1963) suggest that the flotation rate constant is related to particle diameter (D_p) by the expression:

$$k = q\ D_p^{\,n} \qquad [3.2]$$

in which q is a constant for a particular mineral and n varies between 1 and 2. This relationship has been verified experimentally in bench-scale and microflotation experiments (Trahar, 1981; Collins and Jameson, 1976; Reay and Ratcliff, 1975).

The decreasing flotation rate constant with particle size can be related to the basic mechanisms of the interaction between bubbles and particles, as described in Chapter 2. For large particles, inertial impaction with the bubble plays a very important role in particle capture (Levich, 1960). Because of their small mass, small particles lack sufficient inertia to resist the tendency to follow the streamlines of the fluid around the bubble. As a result, small particles are swept past the bubble without an opportunity to make direct contact (Sutherland, 1948). Therefore, the frequency of collision is reduced by the reduction in particle size.

The problem associated with decreased collection of fine particles may potentially be resolved by either increasing the effective size of the particles through the formation of flocs or aggregates or by inducing hydrodynamic conditions which encourage bubble-particle encounters (Fuerstenau, 1980). A limited number of studies are available regarding the effect of aggregation or flocculation in a flotation cell (Morris, 1952; DeVivo and Karger, 1970; Yousef et al., 1971). Most of the studies indicate an improvement in the recovery of the very fine particles, but flotation selectivity may be limited due to gangue entrapment in the flocs (Warren, 1985).

Several articles have been published which deal with

methods for improving the collision frequency of bubbles with particles. Some of the methods investigated include ultrasonically enhanced flotation (Nicols et al., 1986), dissolved air flotation (Kitchener and Gochin, 1980) and microbubble flotation (Yoon, 1982). Flotation in a ultrasonic field is a relatively new concept, and little data is available. Dissolved air flotation is an attempt to eliminate the need for a bubble-particle collision step by preferentially nucleating bubbles on hydrophobic surfaces (Gochin and Solari, 1983). However, the application of this process has been limited to water purification processes, and may not be efficient in the processing of mineral and coal fines because of a lack of selectivity. Microbubble flotation utilizes micron sized bubbles which are more efficient in collecting fine particles. The possibility of improving fine particle flotation by reducing bubble size is examined more closely in the following paragraphs.

The amount of data regarding bubble size distributions in flotation cells is surprisingly small. Typically, most bubbles in froth flotation are in the range of 400 to 2500 microns in diameter, with an average of approximately 800 microns (Bogdanov, 1947; Klassen and Mokrousov, 1963). In conventional flotation cells, bubble size is determined primarily by frother concentration (Bennet, 1958), impeller speed and air flow rate (Kawecki et al., 1967).

Despite the lack of conclusive data, there is a

continued growth of evidence, both experimental and theoretical, which indicates that the use of small bubbles should improve the recovery of fine particles in flotation. The experimental results of DeVivo and Karger (1970) show very clearly that smaller bubbles produce higher recoveries in the case of ultrafine kaolin and montmorillonite flotation. In the case of coal, Bennett et al. (1958) established the relationship between the flotation rate constant (k) and bubble diameter (D_b) as:

$$k \propto \frac{1}{D_b^{(3-n)}}, \qquad [3.3]$$

in which n was found to vary between 0.5 and 1. Brown (1962, 1965) has also concluded that, for a given air flow rate, the rate of coal flotation can be substantially increased by reducing bubble size and increasing the number of bubbles. More recently, Yoon (1982) has advocated using microbubbles (D_b < 100 microns) for the cleaning of ultrafine coal. This suggestion is supported by hydrodynamic analyses which indicate that the rate of particle capture can be substantially improved using smaller bubbles (Flint and Howarth, 1971; Reay and Ratcliff, 1975; Anfruns and Kitchener, 1977; Weber and Paddock, 1983). Recoveries and separation efficiences approaching that of oil agglomeration have been claimed by this process.

3.3 Objectives

Since it is likely that flotation will be called upon to treat finer and finer particles, investigations into methods for improving the effectiveness of flotation in the very fine size ranges are tremendously important. A good deal of evidence has been given to suggest that smaller bubbles can be more effective in treating fine coal. Therefore, the primary objective of the present work has been to determine more precisely the role of bubble size in flotation. As a means to achieve this goal, a simplistic model of the flotation process has been considered. From the model, expressions for the flotation rate constant have been determined which demonstrate the relationship between flotation response and bubble size. These expressions should prove useful in the development of predictive models of the flotation process.

It is hoped that the findings of this investigation will help instigate the use of fine air bubbles for the beneficiation of fine coal by flotation, and that flotation will continue to become more widely utilized as a means for producing clean coal.

3.4 Experimental

3.4.1 Coal Sample

For the kinetic studies, a run-of-mine Elkhorn seam coal containing 15.5% ash was used. Flotation feed was prepared by crushing the coal to -1/4 inch and splitting it into 500 gram lots. The samples thus prepared were stored in a freezer at -20°C in an attempt to minimize surface oxidation prior to grinding.

3.4.2 Experimental Apparatus and Procedure

Figure 3.3 shows the apparatus used for the flotation kinetics experiments. Prior to flotation, a representative sample of 100 grams of the coal was ground to -100 mesh, and was then wet-ground at 40 percent solids in a 13.3 cm diameter stirred ball mill for 15 minutes. The mean particle size of the mill product was determined to be 4.8 microns by means of a Particle Data Elzone 80 XY particle size analyzer. Once pulverized, the sample was diluted to 5 percent solids in the feed/conditioning tank and conditioned with 1.5 kg/ton of kerosene for 15 minutes. The hydrocarbon collector was added as a 0.4 percent emulsion prepared by ultrasonic agitation. A volume of Dowfroth M-150 was then added to the slurry just before flotation so that the pulp contained 4×10^{-4} moles/l of the frother.

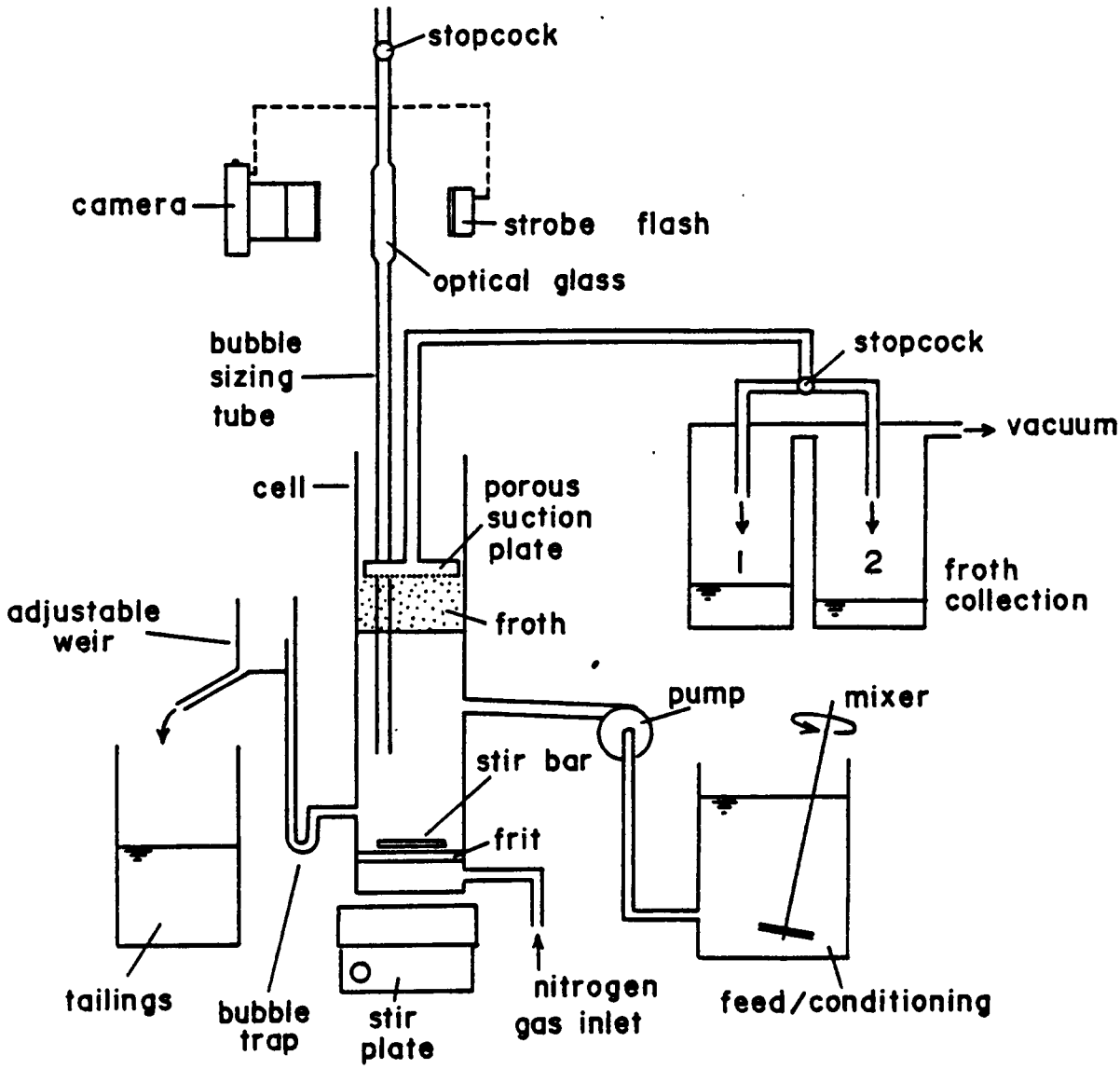

Figure 3.3 Schematic drawing of the flotation apparatus used for the determination of flotation rate constants.

The conditioned coal slurry was then pumped at 90 ml/min to the glass flotation cell (4.3 cm diameter). The pulp level was maintained at a constant level of 9 cm by means of an adjustable weir. Flotation commenced when nitrogen gas was introduced at 100 cm^3/min through the glass frit at the bottom of the cell. Frits having three different porosities (40-60 micron coarse, 10-15 micron medium and 4-5.5 micron fine) were used to generate a range of bubble sizes. The froth formed on top of the pulp was removed by means of a porous suction plate and initially collected in container 1. When steady state was reached, the froth product was collected in container 2 for a desired period of time (usually 1 minute). The froth depth was kept constant at 1 cm in all the experiments.

The bubble size measurement was accomplished by lowering a glass tube filled with a frother solution (4 x 10^{-4} moles/l) into the pulp through a small hole in the suction plate. To prevent the frother solution from flowing into the cell, a stopcock on the glass tube was closed. As the bubbles rose through the tube and passed between two flat optical glass plates, photographs were taken using a 35 mm camera equipped with a strobe flash. The bubble sizes were then measured directly from the photographs after calibration against a micrometer. This procedure provided a means of in situ bubble size measurement. The bubble size distributions were generally found to be rather narrow,

which allowed the bubble diameters to be represented by single mean values.

The flotation rate constant was determined using the first order rate equation:

$$\frac{dM_c}{dt} = -k\ M_c, \qquad [3.4]$$

in which M_c is the mass of floatable material in the cell at time t and k is the rate constant. It was verified that the flotation of this coal displayed first order behavior under the experimental conditions employed. Equation [3.4] can be rewritten as:

$$k = \frac{M_{f2} - M_{f1}}{M_c(t_2-t_1)}, \qquad [3.5]$$

in which M_{f1} is the material floated in time t_1 and M_{f2} is the material floated in time t_2. In calculating k, (M_{f2} - M_{f1}) was the weight of coal collected in container 2 during the period of t_2-t_1, and M_c was determined by measuring the total mass of coal in the cell at steady state.

In order to perform experiments over a wider range of bubble sizes, a second flotation column equipped with interchangeable frits was constructed. During the entire series of tests, five different frits of varying pore sizes were used to generate bubbles. These tests were performed

in a batch mode in which the froth product was collected for 2 minutes. With the exception of operating in a batch mode, the experimental conditions were otherwise identical to those of the continuous tests.

3.5 Results

3.5.1 Effect of Bubble Size on Flotation Rate

In view of the drastically increasing values of the probability of collection with decreasing bubble size as shown in Chapter 2, one should expect a corresponding increase in flotation rate. Figure 3.4 indeed shows that the rate constant (k) increases substantially with decreasing bubble size for the continuous flotation of the Elkhorn seam coal containing 15.5% ash. According to these data, the flotation rate constant appears to vary as the inverse square of bubble diameter. Note that two series of duplicate experiments have been conducted in order to test the reproducibility of the flotation procedure. Excellent reproducibility was observed, most likely due to the elimination of operator bias with this technique.

The results of the batch experiments, shown in Figure 3.5, also demonstrate a similar trend. As bubble size is decreased, the coal recovery steadily increases as the bubble diameter decreases from 1450 microns to 75 microns. The increased recovery of coal is a direct result of the

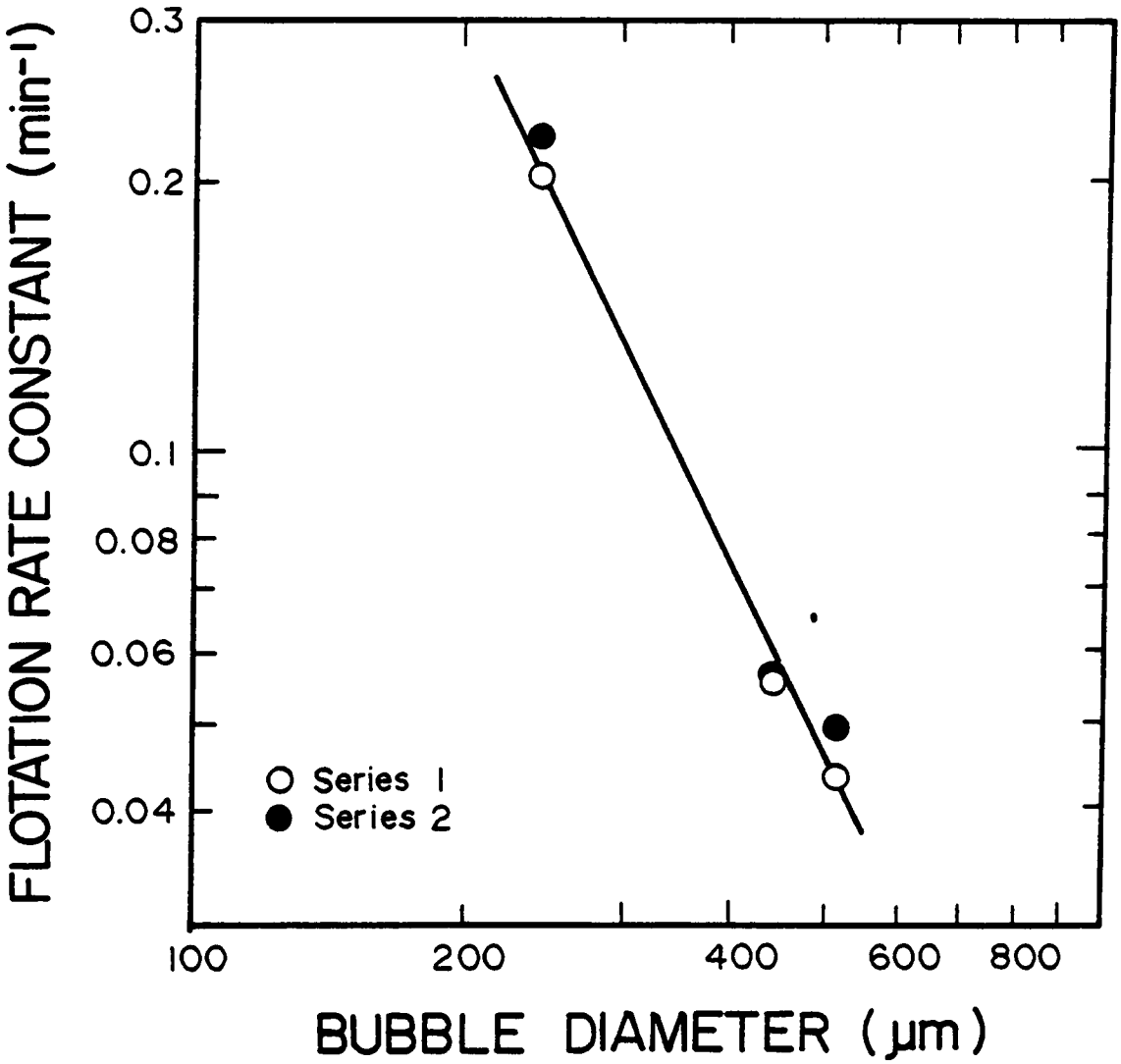

Figure 3.4 Flotation rate constant versus bubble diameter for two sets of continuous flotation tests conducted using the Elkhorn seam coal.

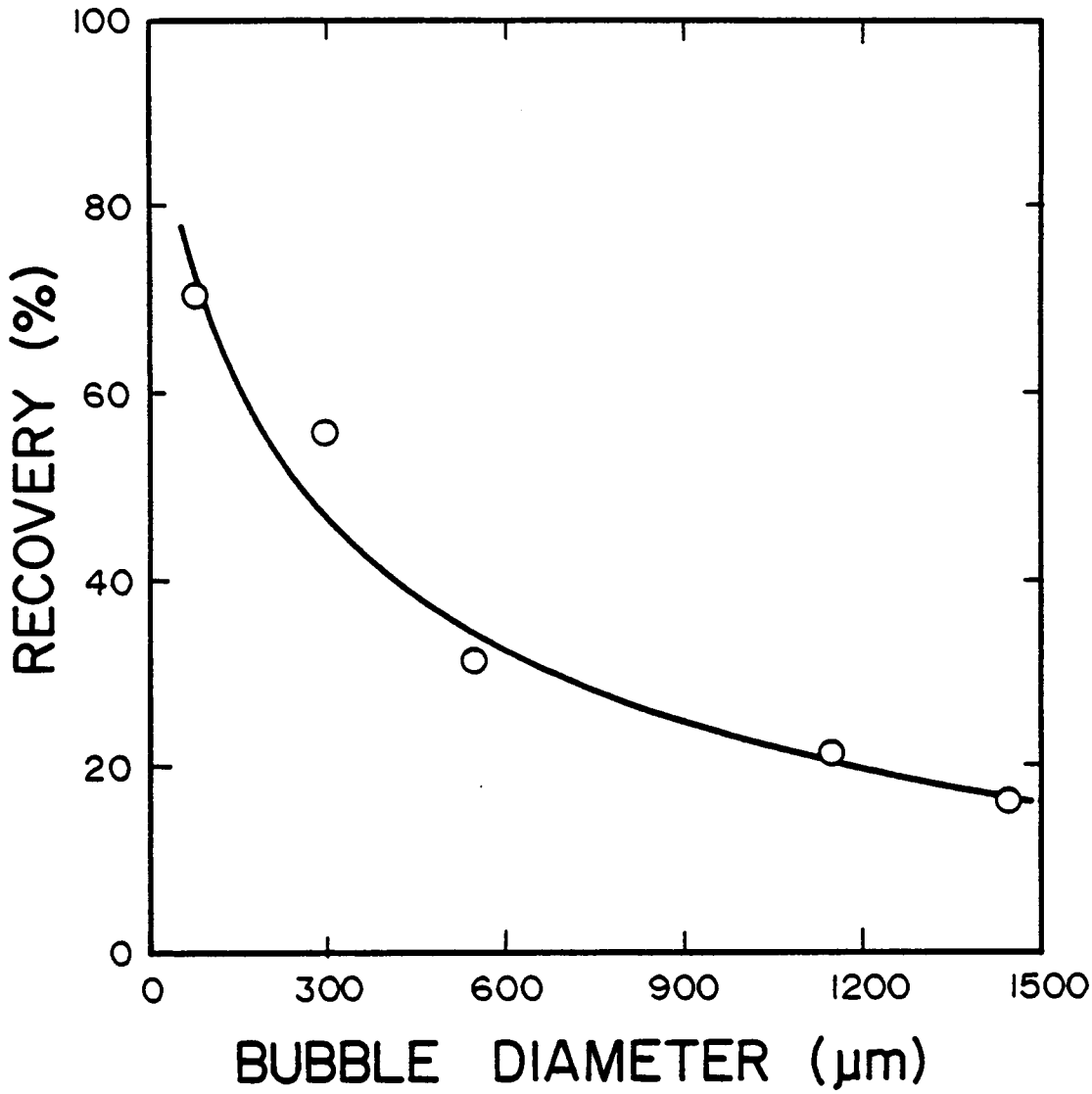

Figure 3.5 Flotation recovery versus bubble diameter for the batch flotation of the Elkhorn seam coal.

increasing flotation rate constant with decreasing bubble size.

3.5.2 Effect of Bubble Size on Product Ash

As shown in Figure 3.6, a rather unexpected result is obtained in the continuous flotation experiments regarding the relationship between the product ash content and bubble size. The ash content is shown to decrease with decreasing bubble size until a bubble diameter of approximately 400 microns is reached, and then increases again with a further decrease in bubble size. Although the changes in the ash content are small, a definite trend can be observed and is within the limits of experimental reproducibility. As shown in Figure 3.7, the same trend is also shown for the batch flotation experiments. A possible explanation for this behavior follows.

It is generally recognized that the primary mechanism responsible for the recovery of fine gangue particles is its entrainment with water (Johnson et al., 1974; Lynch et al., 1981; Trahar, 1981). In most cases, a linear relationship is observed between the recovery rate of water and recovery rate of nonfloatable gangue. As shown in Figure 3.4, a decrease in bubble size results in an increase in the recovery rate of coal. If one assumes that the recovery rate of water (or gangue) is constant, then a decrease in

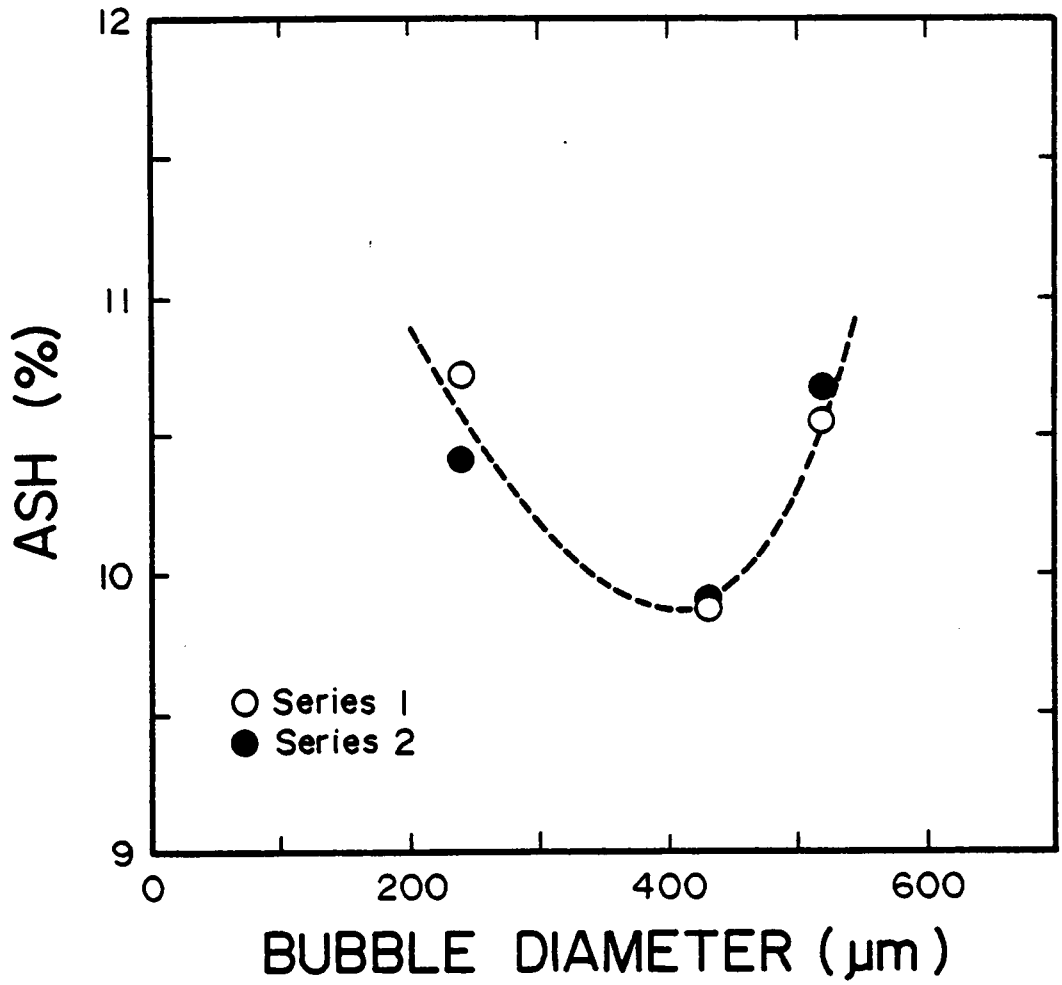

Figure 3.6 Product ash content versus bubble diameter for two sets of continuous flotation tests conducted using the Elkhorn seam coal.

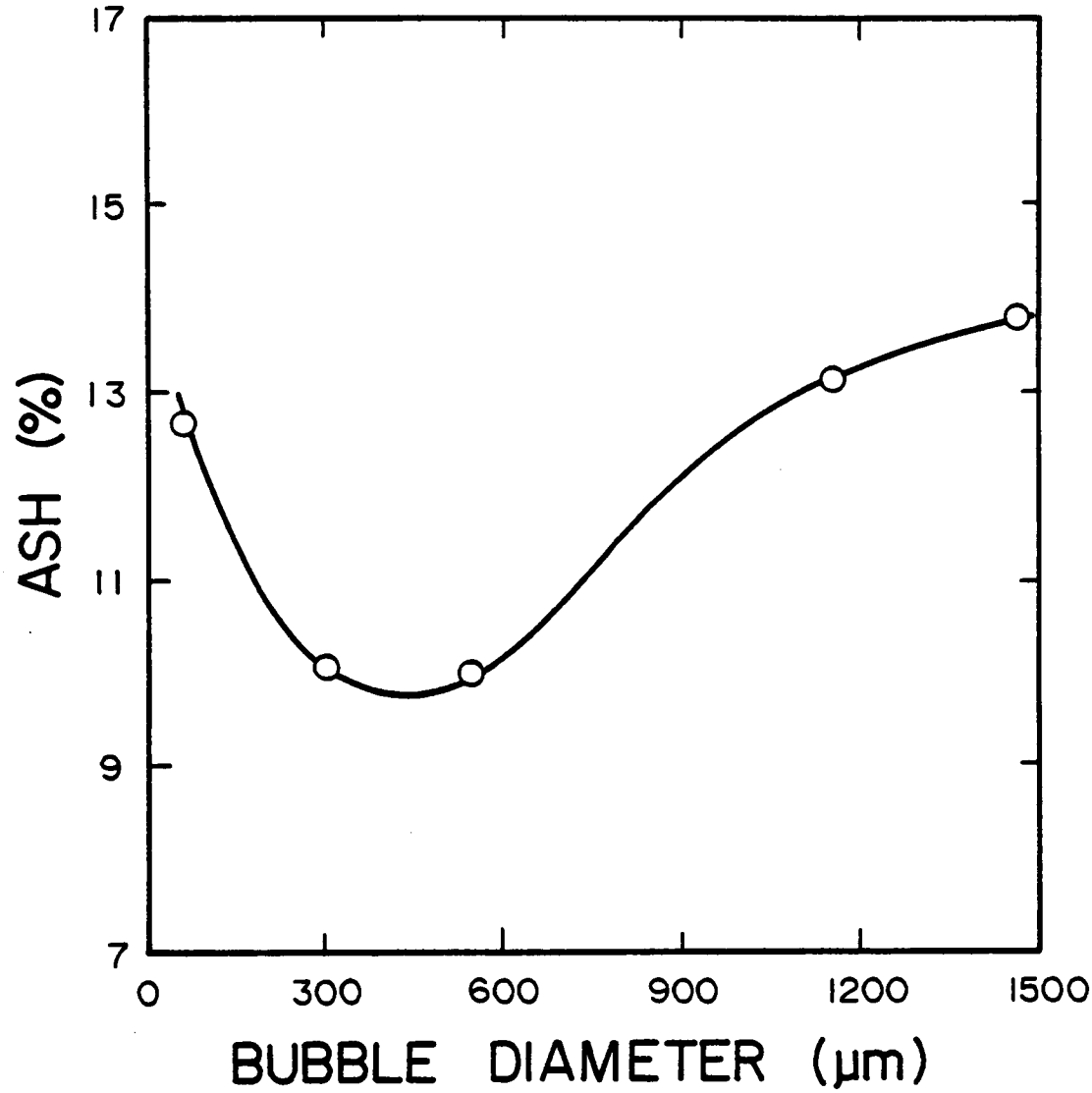

Figure 3.7 Product ash content versus bubble diameter for the batch flotation of the Elkhorn seam coal.

bubble size results in an increased recovery of coal to that of the ash. This explains the decrease in the product ash content with decreaseing bubble size observed in Figures 3.6 and 3.7 down to a bubble size of approximately 400 microns.

However, the results shown in Figure 3.8 suggest that the water recovery rate is not constant and, instead, increases quite sharply as bubble size is decreased. This finding agrees with theoretical predictions regarding the effect of bubble size on water content in a foam (Hartland and Barber, 1974; Steiner et al., 1977). Since the recovery of ash is directly proportional to the recovery of water, the product ash content should increase with decreasing bubble size.

The total percentage of ash in the product is controlled by two factors, i.e., the increase in coal recovery due to decreased bubble size and the increase in water recovery. This relationship is hypothetically represented in Figure 3.9. Since these processes act in an opposing fashion, a minimum in the ash content should be observed when plotted as a function of bubble size.

Although further experiments are necessary, the data presented in Figures 3.6 and 3.7 suggest that there may be a critical bubble size below which some provisions have to be made to deal with the increased water recovery and resultant ash entrainment problem. Possible techniques for solving

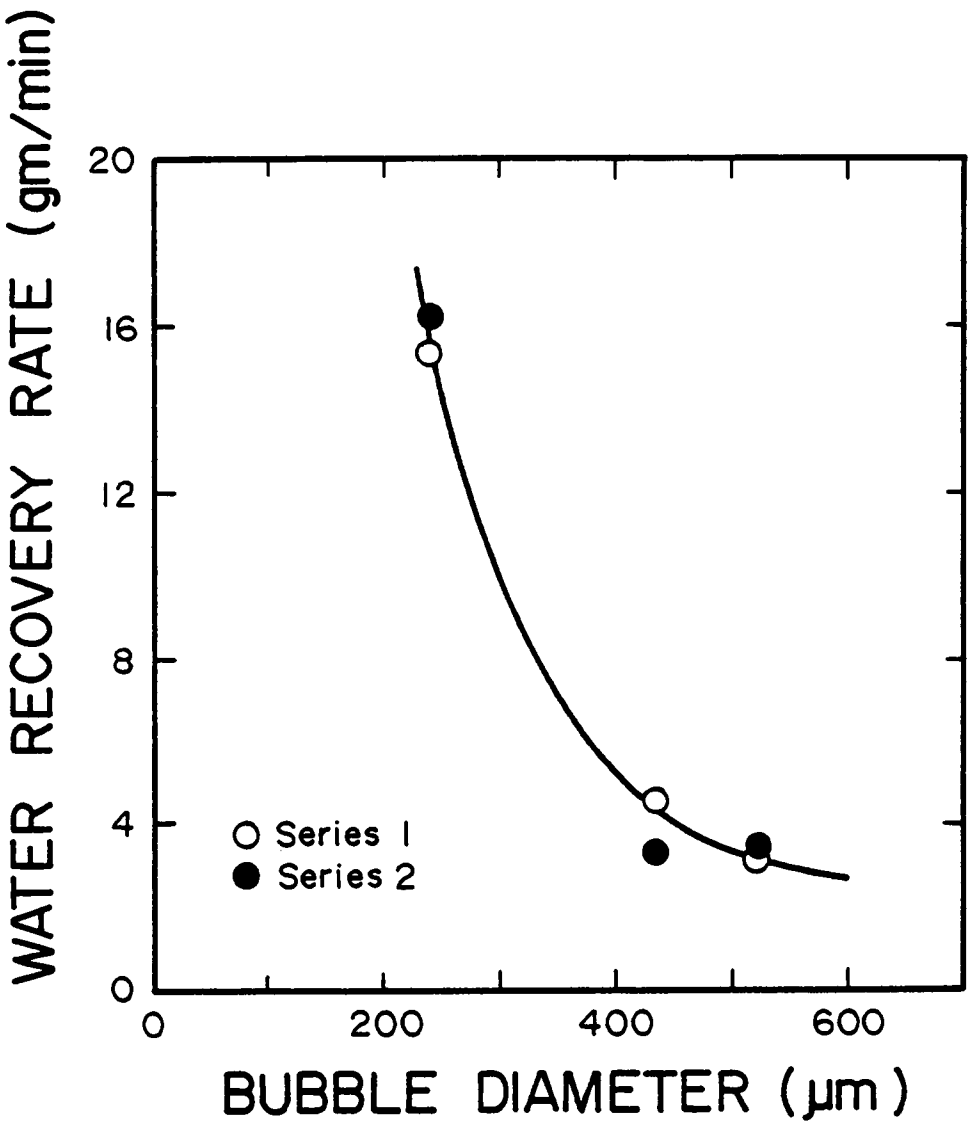

Figure 3.8 Water recovery rate versus bubble diameter for two identical series of continuous flotation experiments conducted using the Elkhorn seam coal.

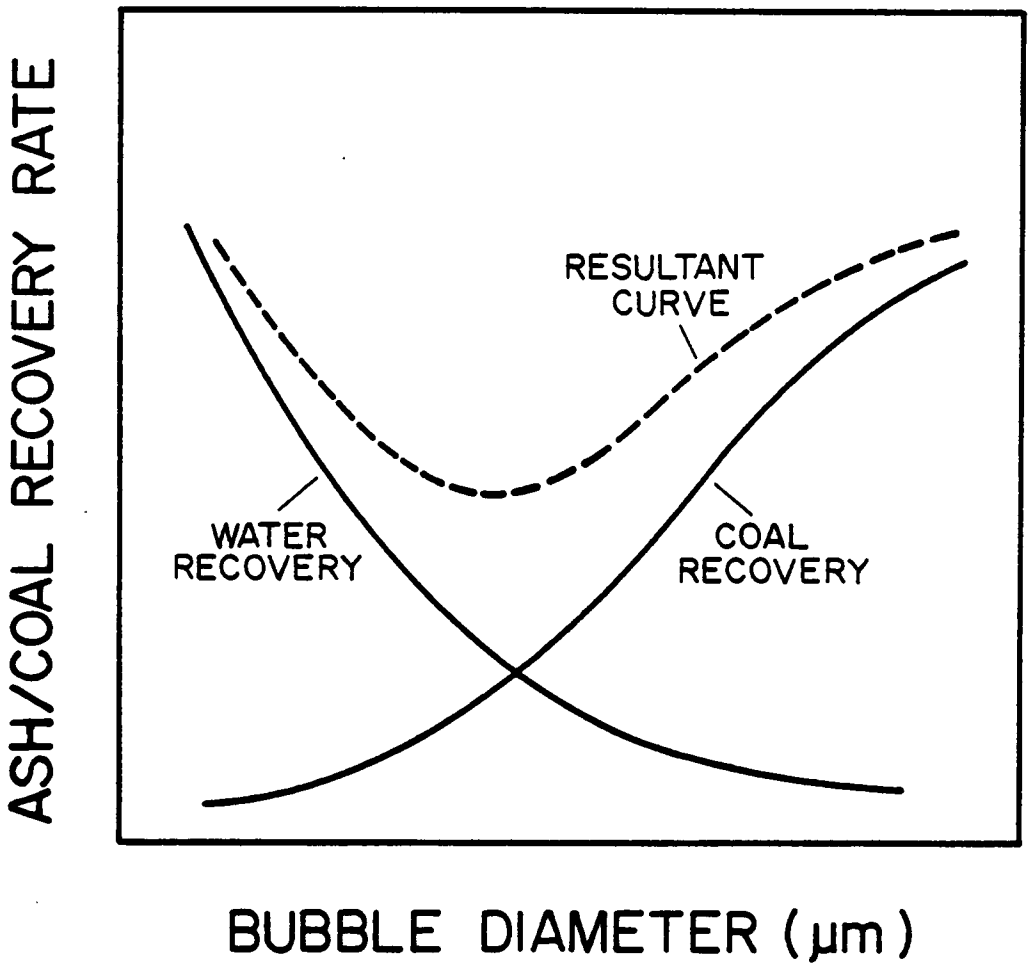

Figure 3.9 Hypothetical relationship between the ash/coal recovery rate and bubble diameter.

this problem could include the use of a water spray on the froth during flotation (Klassen et al., 1956, 1957; Miller, 1969) or a counter-current stream of wash water in the flotation column (Boutin and Wheeler, 1967).

3.6 Discussion

3.6.1 Simple Flotation Rate Model

The results obtained in the present work clearly demonstrate the benefits of using smaller air bubbles for floating finer particles. It is quite reasonable to assume, from the previous experimental and theoretical results given in Chapter 2, that the improvement is associated with the increased probability of collection with decreasing bubble size. A direct consequence of the increased probability of collection is, of course, a corresponding increase in the flotation rate constant, as demonstrated in Figure 3.4.

It is of interest to compare the experimentally determined k values with those that can be predicted from hydrodynamic considerations. One can readily derive a relationship between the bubble diameter (D_b) and the flotation rate constant (k) by considering the passage of a bubble through a slurry. The number of particles removed per bubble can be expressed as:

$$N_p = \frac{P\pi {D_b}^2 h}{4} \frac{N_t}{V_c}, \qquad [3.6]$$

where P is the probability of collection, h is the cell height, N_t is the number of particles in the cell, and V_c is the volume of the cell. The number of bubbles passing through the cell per unit time is given by:

$$N_b = \frac{Q}{\pi D_b^3/6}, \qquad [3.7]$$

where Q is the volumetric flow rate of air. Multiplying Equations [3.6] and [3.7], and substituting

$$V_c = \pi {D_c}^2 h/4 \qquad [3.8]$$

for a cylindrical flotation cell with a diameter of D_c, the number of particles removed per unit time is given by:

$$-\frac{dN_t}{dt} = \frac{6PQ}{\pi D_b {D_c}^2} N_t, \qquad [3.9]$$

This equation shows that flotation is a first-order process with its rate constant given by:

$$k = \frac{6PQ}{\pi D_b {D_c}^2}. \qquad [3.10]$$

It is interesting to note that for a given gas flow rate (Q) the value of k increases substantially as D_c decreases,

which may be a reason for the improved recoveries observed in column-type flotation cells (Narasimhan et al., 1972).

In Chapter 2, the value of the probability of collection (P) was determined to be a function of bubble and particle sizes. The effect of hydrophobicity on the value of P was represented by the critical rupture thickness of the intervening film (H_c). It can be assumed, however, that the value of P for very hydrophobic particles can be adequately approximated by the value of the probability of collision (P_c). It has been shown in Chapter 2 that P_c can be expressed as:

$$P_c = \left[\frac{3}{2} + \frac{4Re^{.72}}{15} \right] \left(\frac{D_p}{D_b} \right)^2 , \qquad [3.11]$$

in which Re is the Reynolds number of the bubble and D_p is the particle diameter. Therefore, by substituting Equation [3.11] for P in Equation [3.10], one can derive an expression for k as:

$$k = \frac{C_1}{D_b{}^3} \left(1 + C_2 D_b{}^{1.54} \right) \qquad [3.12]$$

in which C_1 and C_2 are constants for a given set of experimental conditions. The expressions for these constants are:

$$C_1 = \frac{9Q}{\pi} \left(\frac{D_p}{D_c}\right)^2 \qquad [3.13]$$

and,

$$C_2 = \frac{[gS_1(S_1-S_g)]^{.51}}{21.73\mu^{1.03}}, \qquad [3.14]$$

in which g is the acceleration of gravity, μ is the liquid viscosity, and S_1 and S_g are the densities of the liquid and gas, respectively. As shown, C_1 is a function of controllable variables such as gas flow rate, cell geometry and, to some extent, particle size. In contrast, C_2 is a function of physical constants which cannot normally be controlled. The first term in Equation [3.12] is simply the flotation rate constant calculated for collision probabilities under the condition of Stokes flow. The second term of Equation [3.12] reflects the correction to the probability of collision due to finite values of Reynolds number.

Equation [3.12] suggests that as bubble size is increased, k should approach zero. Conversely, as the bubble size is decreased, k should approach a limiting value of C_1/D_b^3. This relationship is shown in Figure 3.10, in which both the experimentally determined k values for the Elkhorn seam coal and the theoretical values predicted by Equation [3.12] are given. As shown, the experimental k

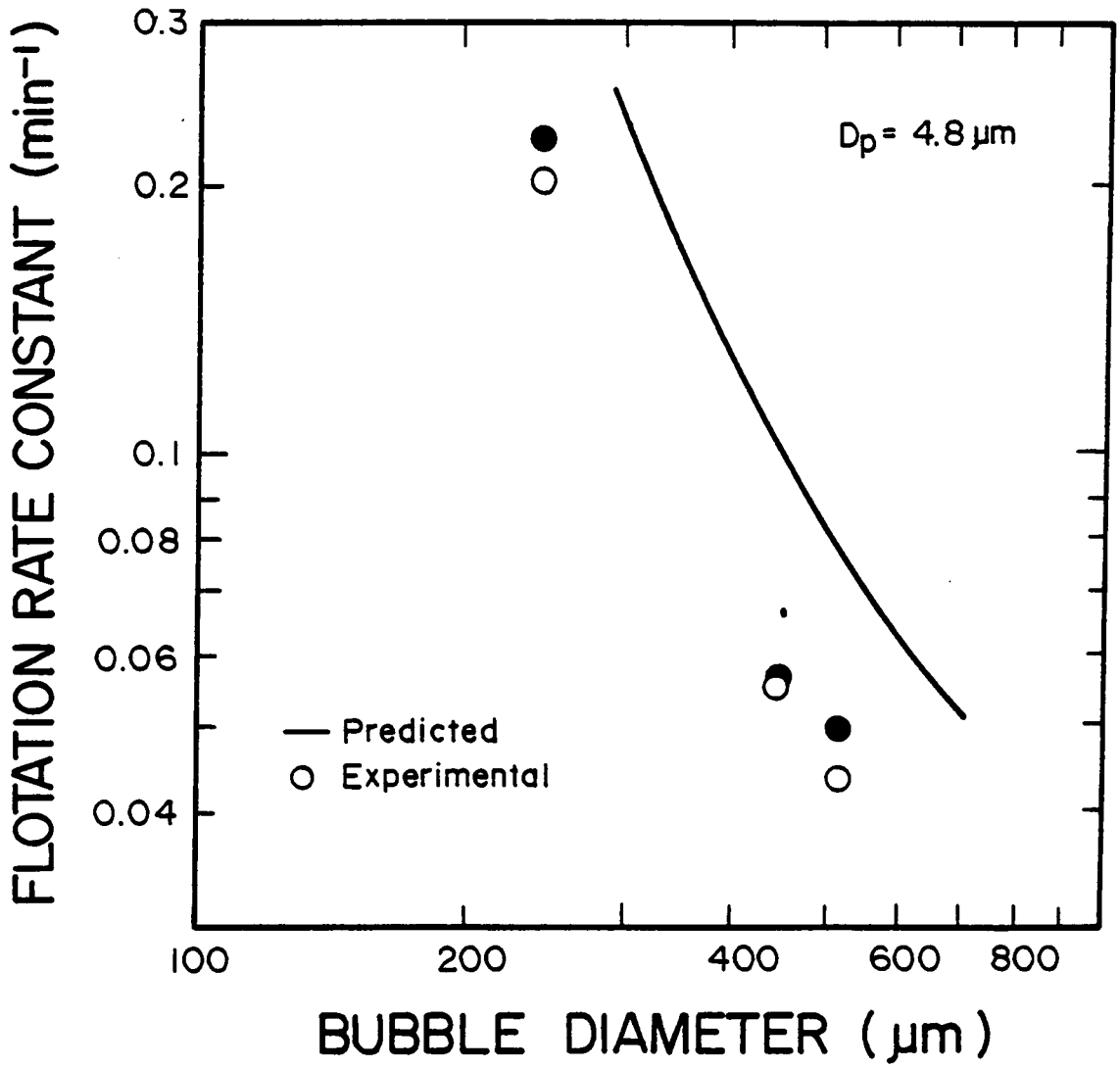

Figure 3.10 Comparison of experimentally determined flotation rate constants and theoretical values predicted assuming $P=P_c$.

values are significantly lower than the predicted values. However, the slopes of the plots, representing the power relationship between k and D_b, are comparable throughout the bubble size range studied. Many investigators have expressed the power relationship using the general formula:

$$k \propto \frac{1}{D_b^{\,m}}, \qquad [3.15]$$

where m is generally assumed to be independent of D_b. However, by taking the first derivative of the logarithm of Equation [3.12], it can be shown that the slope (m) of a log-log plot of k versus D_b is given by:

$$m = 1.54 \frac{y}{1 + y} - 3 \qquad [3.16]$$

where,

$$y = C_2 D_b^{\,1.54}. \qquad [3.17]$$

Equation [3.16] demonstrates that the power relationship varies with D_b. Reay and Ratcliff (1975) determined that m = -2.9 for the flotation of quartz particles using bubbles less than 100 microns in diameter. This value is comparable to that of m = -2.8 calculated from Equation [3.16]. Bennett et al. (1958) carried out conventional coal flotation experiments to obtain the value of m = (3-n), where n ranges from 0.5 to 1.0 for bubble

diameters in the 300-450 micron range. From Equation [3.16], the values of m calculated for bubble sizes of 300 and 450 microns are -2.3 and -2.0, respectively. Therefore, it appears that this equation is reasonably accurate in predicting the power relationship between k and D_b. Equation [3.16] also suggests that in order to take advantage of the highest value of m (indicating the largest increase in k with D_b) bubbles of less than approximately 100 microns in diameter must be used. This bubble size is approximately an order of magnitude smaller than the average size of bubbles utilized in conventional flotation equipment.

As has already been noted, the magnitude of the predicted k values are substantially higher than those determined experimentally. This discrepancy is most likely caused by the coal not being sufficiently hydrophobic. As a result, the assumption made in deriving Equation [3.12] was not valid, i.e., P cannot be approximated by P_c for this particular coal. The lower hydrophobicity of the coal may be partly attributed to its high ash content of 15.5%.

In order to obtain an adequate fit between the theoretical and experimental k values, an appropriate value for the probability of collection must be chosen which reflects the lower hydrophobicity of the coal. Once the appropriate value of P has been chosen, Equation [3.10] can

then be utilized to determine k. The variation of P with hydrophobicity can be determined using the data given previously in Chapter 2 (Figures 2.16 and 2.17). Using a trial-and-error approach, an appropriate critical film thickness (H_c) was chosen in such a way that the predicted k values closely approximated the experimental values. A comparison between the experimental data and predictions using an H_c value of 10 nm is shown in Figure 3.11.

3.7 Summary and Conclusions

1) It has been found that the use of small air bubbles for fine coal flotation results in a substantial increase in flotation rate. This improvement can be attributed to the increase in the probability of collision with decreasing bubble size.

2) A simple hydrodynamic model based on bubble-particle collision probabilities has been developed to predict the flotation rate constant (k) of a very hydrophobic coal as a function of bubble size, flotation cell geometry, air flow rate and particle size.

3) The experimental k values determined in the present work using a coal sample containing 15.5% ash are substantially lower than those predicted by the model. This discrepancy has been attributed to the relatively

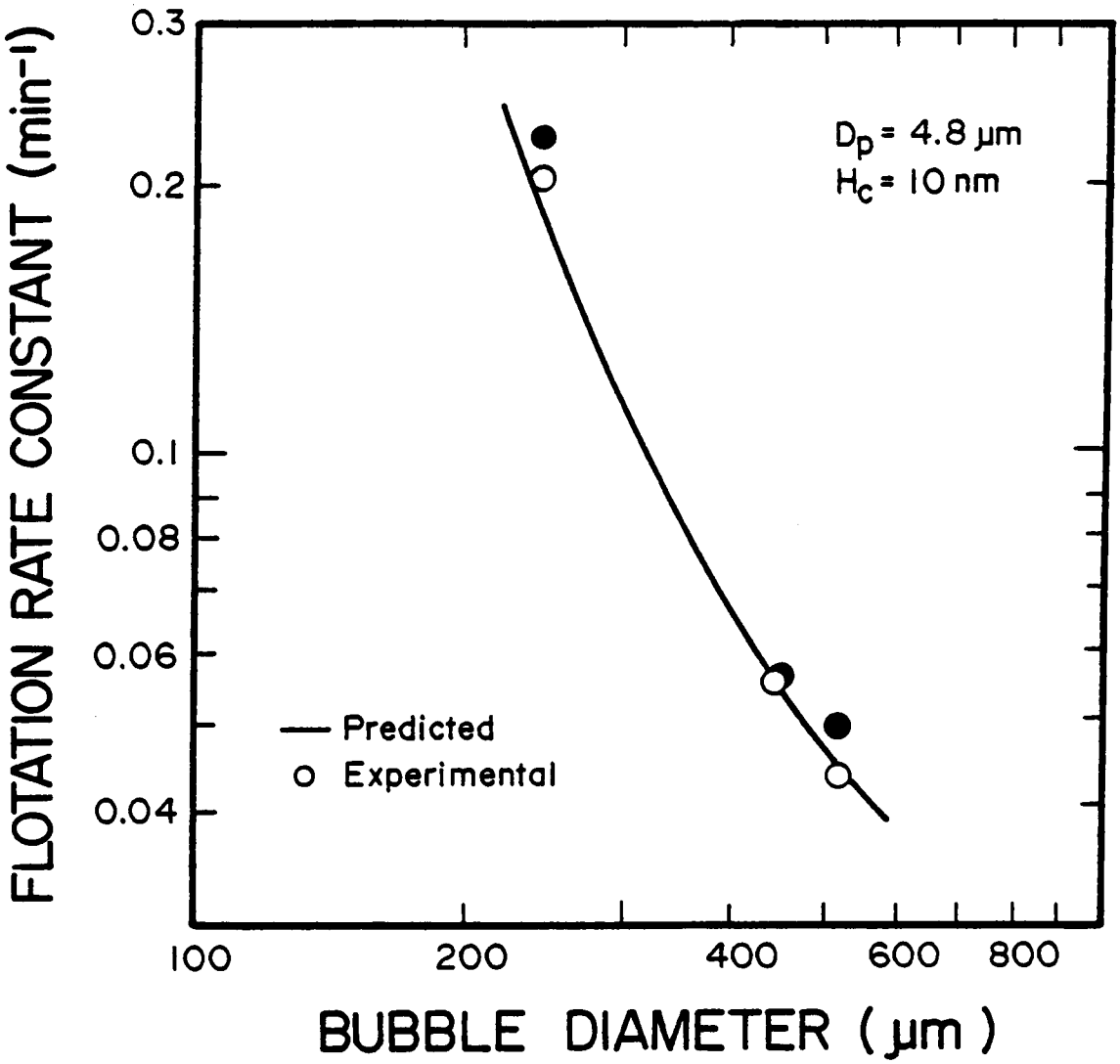

Figure 3.11 Comparison of the experimentally determined flotation rate constants and the theoretical values predicted assuming H_c=10 nm.

low hydrophobicity of the coal used in the present work, which results in a probability of adhesion less than unity. Nevertheless, the proposed model has been successful in predicting the power relationship between the flotation rate constant (k) and bubble size (D_b).

4) There are indications that when using bubble sizes that are too small, the increase in the flotation rate is associated with an increased water recovery rate, which results in increased ash entrainment and decreased separation efficiency. Possibilities of minimizing this problem have been briefly discussed.

CHAPTER 4

FLOTATION SELECTIVITY

4.1 Introduction

In recent years, more attention has been given to the selective flotation of fine particles. While flotation remains the most appropriate means of treating fine particles, the efficiency of the process drops quite substantially for ultrafine particles (<10 microns). The reduced efficiency is manifested not only as a reduction in recovery, but also a loss in flotation selectivity (Hornsby and Leja, 1982).

The loss of recovery at fine sizes is generally attributed to the fact that air bubbles generated in conventional flotation machines are too large to capture small particles (Flint and Howarth, 1971; Reay and Ratcliff, 1973; Collins and Jameson, 1976; Anfruns and Kitchener, 1977). Recent investigations have shown that the use of smaller air bubbles in fine coal flotation results in a substantial increase in flotation recovery (Yoon and Miller, 1981; Bahr et al., 1982; Yoon, 1982; Halsey et al., 1982; Yoon et al., 1984; Luttrell et al., 1985). On the other hand, a thorough understanding of the reasons for the decrease in the selectivity when floating very small particles is yet to be fully established.

4.2 Literature Review

One of the first studies regarding the effect of particle size on flotation selectivity was made by Gaudin (1931), who identified the important distinction between product grade and selectivity. He noted that since incomplete liberation greatly affects product grade, selectivity should be determined only from the flotation behavior of free particles. As a result of his experimental studies, he concluded that, in general, an optimum particle size exists for maximum grade, but selectivity decreases continuously with decreasing particle size.

The findings of Gaudin have been verified for the flotation of most materials, although the mechanisms responsible for the decreased selectivity are still a subject of considerable debate. The major causes of poor selectivity for fine particles have been generally attributed to i) surface energy effects, ii) froth stabilization and iii) entrainment (Fuerstenau, 1980; Warren, 1984).

Because of the increased number of exposed surface features, fine particles display a higher specific surface energy than coarse particles of the same material (Adamson, 1976). As a result, there may be a tendency for reagents to adsorb on fine particles nonspecifically. Problems

associated with the nonspecific adsorption include increased collector consumption and the flotation of undesired particles (Fuerstenau, 1980).

Froth characteristics are also known to affect flotation selectivity. In some cases, the stability of the flotation froth is the controlling factor which determines the effectiveness of separation (Livshitz and Dudenkov, 1957; Lovell, 1976). Sutherland and Wark (1955) have noted that the presence of hydrophobic fine particles increases the stability of three-phase froths, whereas Livshitz and Dudenkov (1965) found these particles to be disruptive to froth stability. Fine hydrophilic particles appear to have little or no effect on froth stability (Livshitz and Dudenkov, 1965). The influence of particle size, shape and hydrophobic nature on flotation selectivity is of much importance, but is not yet understood.

The principal mechanism responsible for determining selectivity is that of fine gangue entrainment (Johnson, McKee and Lynch, 1974; Lynch et al., 1981; Trahar, 1981). The desired mode of particle recovery in flotation is the attachment of particles to bubbles, and subsequent levitation of the particle-laden bubbles into the froth. Attachment is a selective process with the degree of selectivity being determined by the surface characteristics of the particles and bubbles. On the other hand, a second

mode of recovery, which is commonly termed entrainment, also contributes to the overall recovery. Particles which enter the base of the froth in the water films between bubbles will either return to the pulp by drainage or be recovered with the water in the final froth product. The entrainment is nonselective and adversely affects flotation efficiency. The extent of entrainment depends strongly on particle size as larger particles drain more easily from the froth than smaller ones. For silicious gangue, the effect of entrainment is essentially negligible for particle sizes greater than approximately 30 microns (Johnson, McKee and Lynch, 1974).

A number of methods have been suggested for improving the selectivity of fine particle flotation (Trahar and Warren, 1981; Fuerstenau, 1980; Trahar, 1981; Warren, 1984). Most of the improvements come about as the result of i) an increase in the effective size of particles by selective aggregation or ii) an increase in the attachment of fine particles to bubbles through the use of chemisorbing collectors which are highly selective. In certain cases, much success has been achieved using these techniques.

Recently, some attention has also been given to the possibility of using small bubbles as a means of improving the selectivity of fine particle flotation. Although some evidence suggests that the use of small bubbles will improve the recovery of fine particles, there is little or no

published information concerning the effect of bubble size on selectivity. Waste treatment engineers have long realized the importance of using small bubbles in flotation. However, since they are concerned only with the total removal of suspended solids, studies performed by this group provide no data regarding the effects of small bubbles on selectivity.

In a comparison made between vacuum flotation and conventional flotation, Klassen and Meshcheriakov (1958) obtained results showing an increased selectivity with the former, which may suggest that selectivity improves with decreasing bubble size. Evidence has also been shown by Yoon (1982; 1984a,b) that coal flotation carried out using microbubbles of less than 100 microns in diameter is more selective than the conventional process using larger bubbles. However, the mechanisms responsible for the improved selectivity have not been identified.

4.3 Objectives

The main objective of this investigation has been to study the effect of bubble size on flotation selectivity. The selectivity of flotation has been determined experimentally as a function of bubble size using a mixture of essentially pure coal and quartz. The results of the experiments have been correlated with the entrainment of

particles in the turbulent wake behind the bubbles. This correlation has led to the development of a rate constant model incorporating flotation due to adhesion and to entrainment.

4.4 Experimental

4.4.1 Samples

Samples used for determining the collection probability and flotation rate included coal from the Buller seam in New Zealand and Brazilian rock quartz obtained from Ward's Scientific Company. Samples of various sizes were prepared by dry-grinding in an agate mortar and pestle, followed by wet-screening or centrifugal sedimentation to produce narrow size fractions. The Buller seam coal contained only 0.13% ash and was very hydrophobic as mined. To minimize oxidation, coal samples were stored in air-tight containers at -20°C.

4.4.2 Experimental Apparatus and Procedure

a) Probability of Collection Measurements

The probability of collection (P), defined as the fraction of particles in the path of a bubble that is actually collected by the bubble, was determined for both

coal and quartz by counting the number of particles collected by an individual bubble as it rose through a suspension of known particle concentration. The apparatus and procedure for this measurement are described in detail in Chapter 2 (Section 2.5.2).

b) Frothless Flotation Experiments

The flotation rates were determined using a specially designed "frothless" flotation cell shown in Figure 4.1. By eliminating the effect of the froth, it was possible to study the phenomena that occur only within the pulp. The cell (2.2 cm diameter) was fed a 2% solids mixture of particles and water held by vacuum in a sealed container. To prevent the settling of particles, the suspension was agitated by a magnetic stir bar. The feed rate of particles entering the cell was precisely controlled at 2.5 ml/min by injecting a controlled volume of air into the container by means of a syringe pump. The feed entered the cell at approximately 8.0 cm below the surface of the liquid. The liquid level was held constant by an adjustable weir. The attachment of particles to bubbles took place in the region between the tip of the feed funnel and the point of bubble generation. In order to produce small bubbles, the frother concentration in the pulp was maintained at a concentration of 5×10^{-4} moles/l Dowfroth M-150 in all experiments.

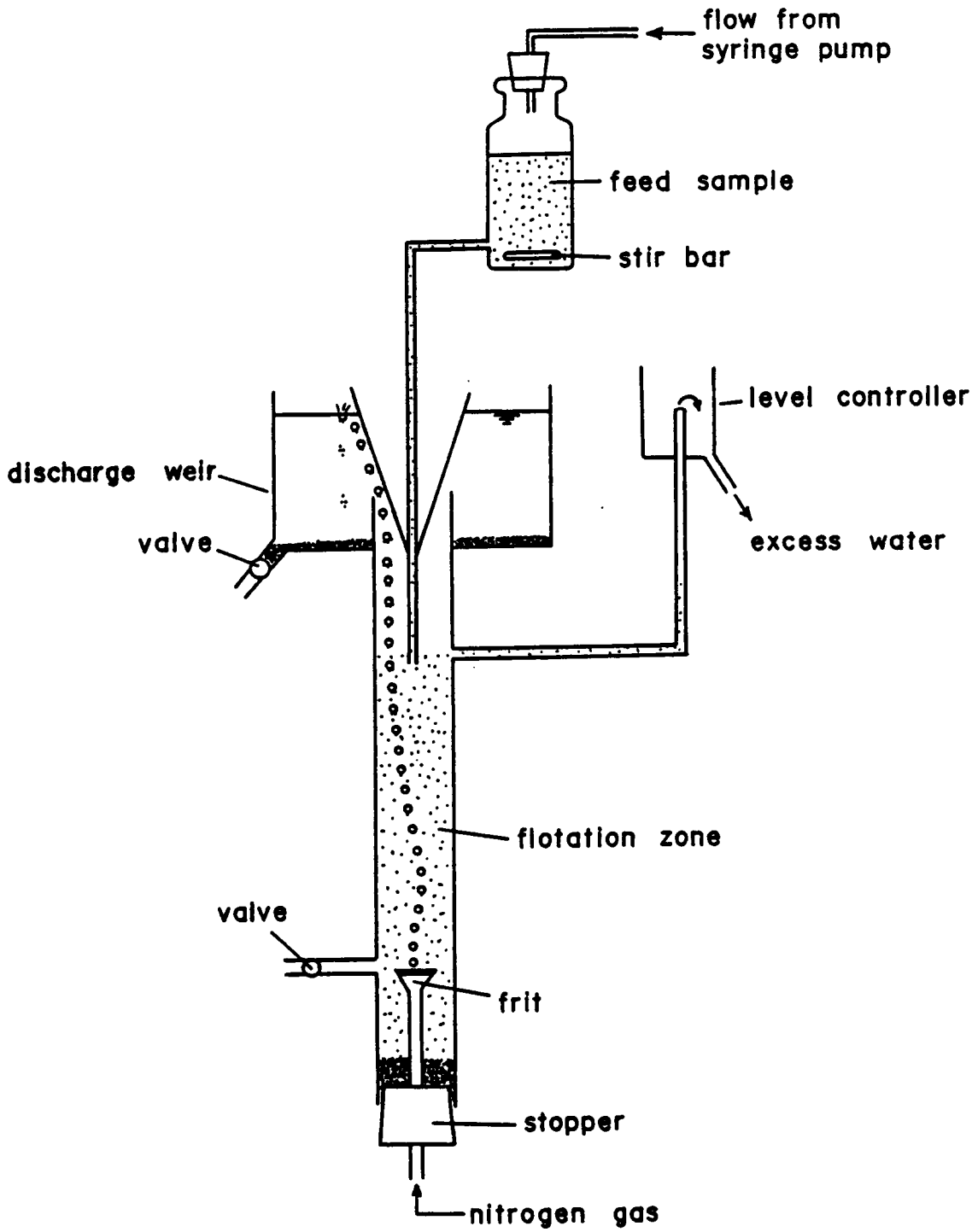

Figure 4.1 Apparatus employed for the frothless flotation experiments.

Bubbles of various sizes were produced by forcing nitrogen gas at a rate of 10 ml/min through glass frits of five different pore sizes (6, 15, 38, 60, and 85 microns). As bubbles rose through the cell, they first passed through the particle suspension between the feed inlet and the air sparger and became loaded with particles. After passing the feed inlet point, the particle-laden bubbles entered a clear, quiescent zone in the column. The bubbles carrying the particles were deflected to the sides of the cell by a funnel. Upon reaching the surface of the liquid the bubbles burst and discharged their particle load into the collection basin. After experimentally verifying the first order nature of the flotation process under the conditions employed, flotation rate constants were determined using the same procedure described in Chapter 3 (Section 3.4.2).

Since the suspension was dilute, it was possible to directly photograph the bubbles as they passed through the flotation cell. Bubble diameters were measured from the photographs after calibration against a micrometer. Bubble size distributions were generally found to be narrow, which allowed the bubble diameters to be represented by single mean values.

c) Turbulent Wake Measurement

As a means of investigating a possible mechanism for

particle entrainment, the turbulent wake formed behind a rising bubble was measured using the apparatus shown in Figure 4.2. The wake formed behind bubbles of various sizes was simulated by suspending a teflon sphere in a downward flow of water. The flow rate was adjusted by means of a valve to obtain Reynold's numbers ranging from 0 to 400. An organic dye solution, fed through the body support of the sphere, entered the boundary layer through a hole at the top of the sphere and was carried by the flow to form an outline of the wake. Wake dimensions were then determined directly from photographs in the same manner as discussed previously for bubble size measurements.

4.5 Results

4.5.1 Probability of Collection Measurements

The probability of collection obtained as a function of bubble size for the Buller seam coal and the Brazilian rock quartz is shown in Figure 4.3. The mean particle diameter for both materials was approximately 31 microns, and the measurement was made using a mixture containing equal amounts of coal and quartz by number. Because of the large color difference between coal and quartz, they were easily distinguished when attached to a bubble. This figure supports the previous data (Figure 2.21) showing a drastic increase in the probability of collection as bubble diameter

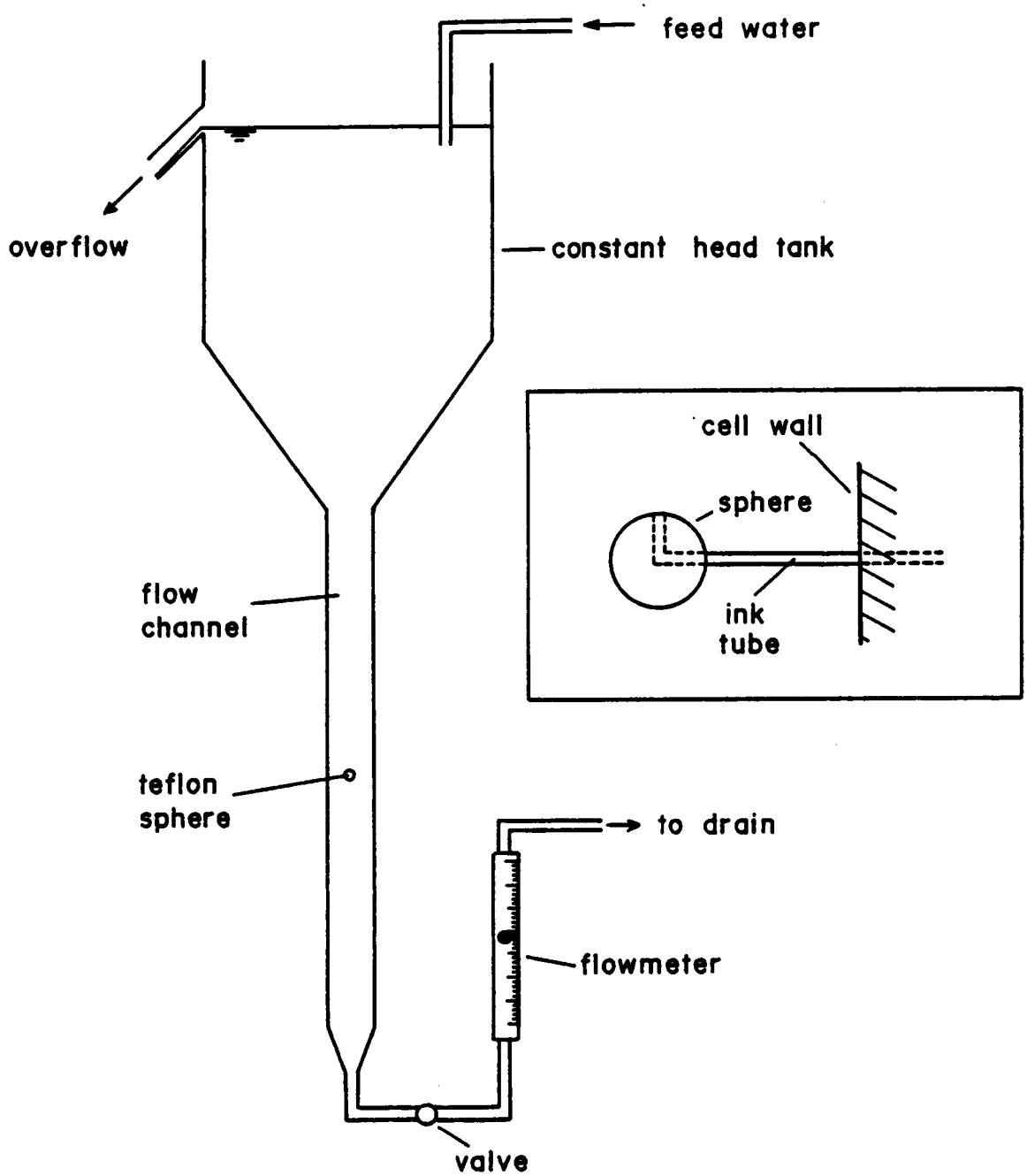

Figure 4.2 Device employed for the measurement of turbulent wake geometry.

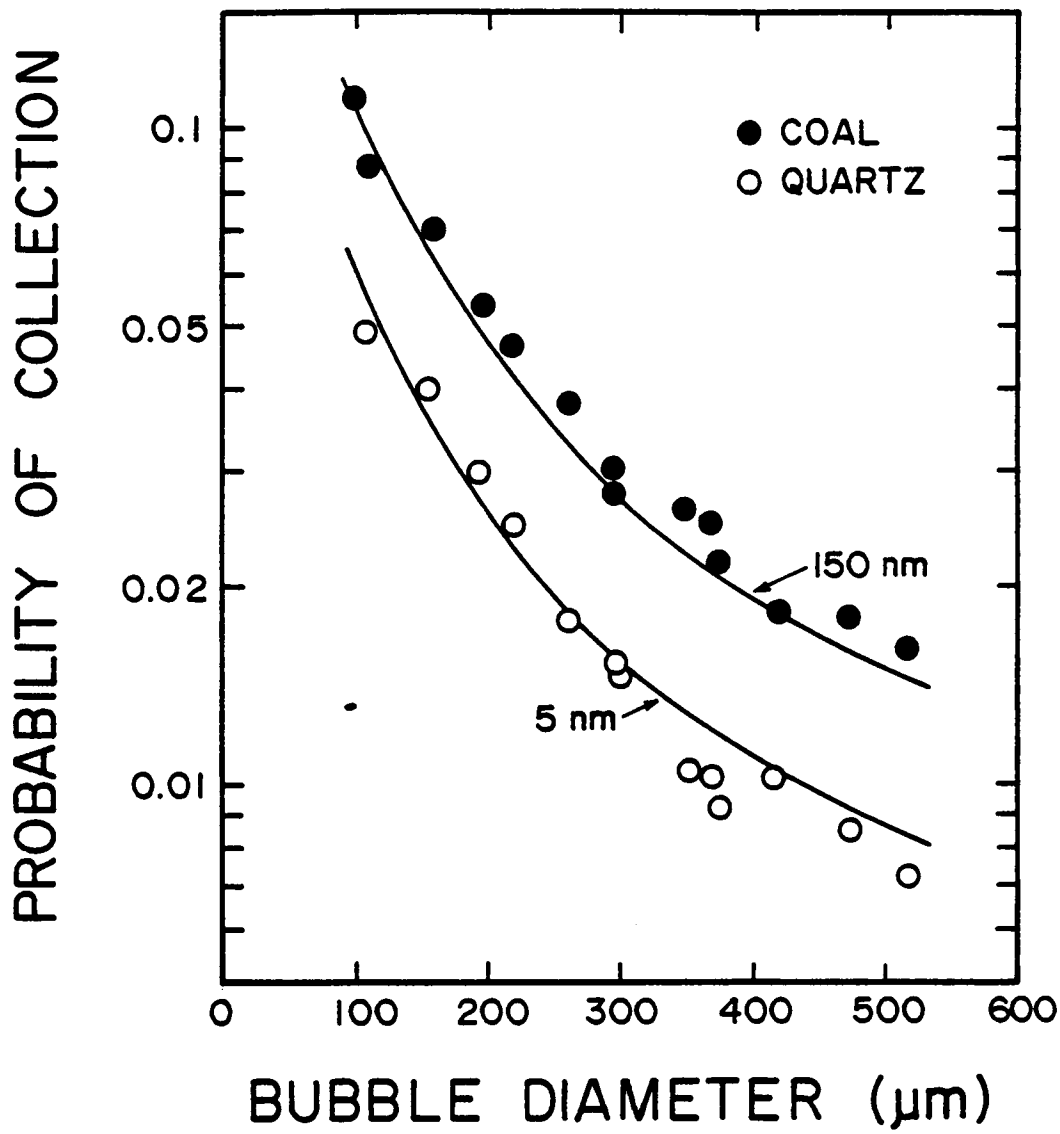

Figure 4.3 Probability of collection versus bubble size for 31-micron diameter coal (H_c=150 nm) and quartz (H_c=5 nm) particles.

is reduced. Note that the trends are the same for both coal and quartz, although the probability of collection of quartz is approximately half that of coal. The fact that a hydrophilic material such as quartz exhibits a non-zero collection probability may be explained by the possibility that fine particles may have long sliding times along the surface of a bubble during the collision process. If the sliding time exceeds the induction time (defined as the minimum time required for bubble particle adhesion), the particle will be collected by the bubble. This mechanism has been previously discussed in detail in Chapter 2 (Section 2.4.2).

Also plotted in Figure 4.3 are theoretical curves (solid lines) for the probability of collection using the procedure formulated in Chapter 2 (Section 2.4.4). For coal particles, a very good fit between the experimental and theoretical values was obtained by choosing a critical rupture film thickness of 150 nm. This is a typical value for very hydrophobic materials. A much smaller critical rupture film thickness (5 nm) was required to obtain an adequate fit for the quartz particles. The smaller magnitude of the critical rupture thickness for the quartz is a direct consequence of its low hydrophobicity.

4.5.2 Effect of Bubble and Particle Size on Flotation Rate

As was clearly demonstrated in Chapter 3 (Section 3.5.1), a direct result of decreasing bubble size is an increase in flotation rate. As shown in Figure 4.4, the same trend is observed for the frothless flotation experiments. It is also shown that the rate constant decreases substantually with decreasing particle size. In general, the increase in flotation rate constant follows the trend observed in the plot of collection probability (P) versus bubble diameter (D_b) shown previously in Chapter 2 (Figure 2.21). However, the results presented in Figure 4.4 show that the flotation rate constants for the 6.6- and 16.4-micron particles begins to increase slightly at D_b values above approximately 500 microns. This discrepancy suggests that a mechanism other than the collision-adhesion process may be reponsible for the increased flotation rate of fine particles at larger bubble sizes. A likely candidate is the mechanism involving entrainment of particles within the bubble wake. As pointed out in Chapter 2 (Section 2.5.2), this mechanism is not detected in the probability of collection measurements, but may play a significant role in flotation.

4.5.3 Effect of Bubble Size on Wake Formation

Since the wake behind a rising bubble may affect both

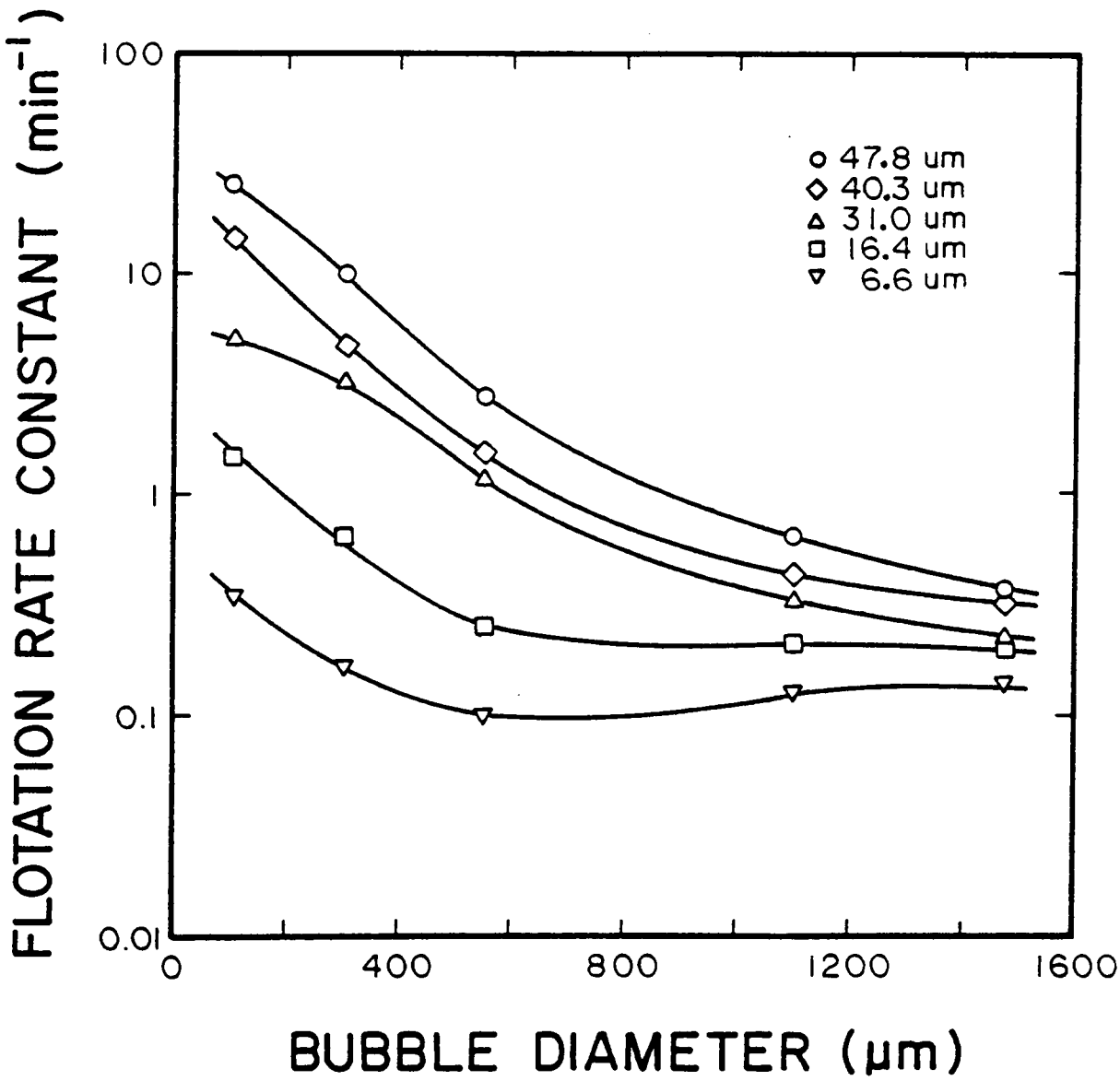

Figure 4.4 Effect of particle diameter on the relationship between the flotation rate constant and bubble diameter for the flotation of the low-ash Buller seam coal.

the recovery and selectivity of fine particle flotation, a series of experiments was performed to gain better insight into the phenomenon of wake formation. Figure 4.5 shows the outline of wakes formed behind a rigid sphere for various Reynolds number values determined using the apparatus previously described. The size of the turbulent wake present for various bubble sizes is given in Figure 4.6, where the dimensionless wake length, given as the ratio of wake length to bubble diameter, is plotted against the bubble size. The results show that bubbles less than approximately 300 microns in diameter carry no wake while larger bubbles exhibit a substantial wake which increases with increasing bubble size.

4.5.4 Effect of Bubble Wake on Selectivity

The influence of entrainment is illustrated in Figure 4.7, where the ratio of coal to quartz recovery rate (a measure of selectivity) is plotted against bubble diameter. This ratio was determined from experiments conducted in the frothless flotation cell on an equal mixture by number of coal and quartz particles of the same size. Since an equal number of particles was employed, recovery rate ratios greater than one indicate a preferential flotation of coal, while a ratio of one indicates no selectivity. The range of mean particle diameters tested varied from 47.8- to 6.6-

a) Re = 8.3
b) Re = 31.2
c) Re = 43.8
d) Re = 105
e) Re = 125
f) Re = 206
g) Re = 401

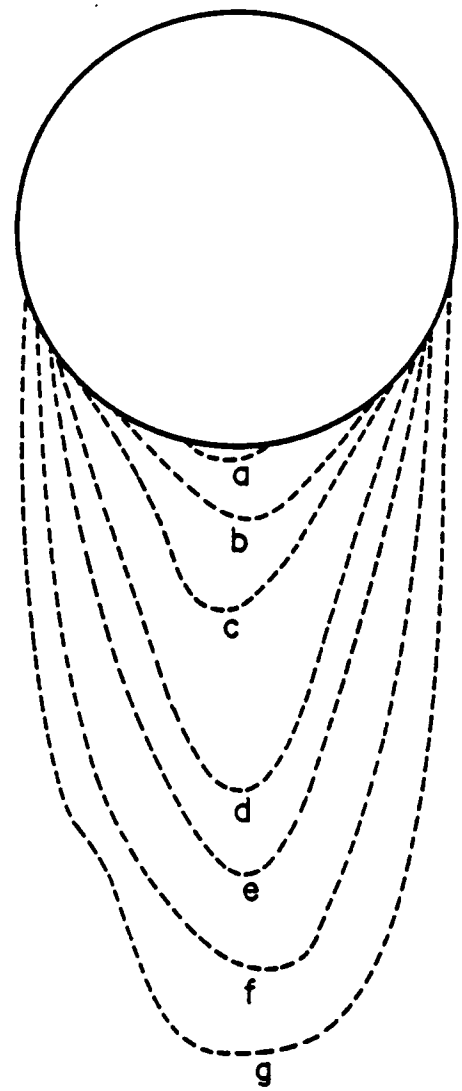

Figure 4.5 Wake geometry for various Reynolds number values.

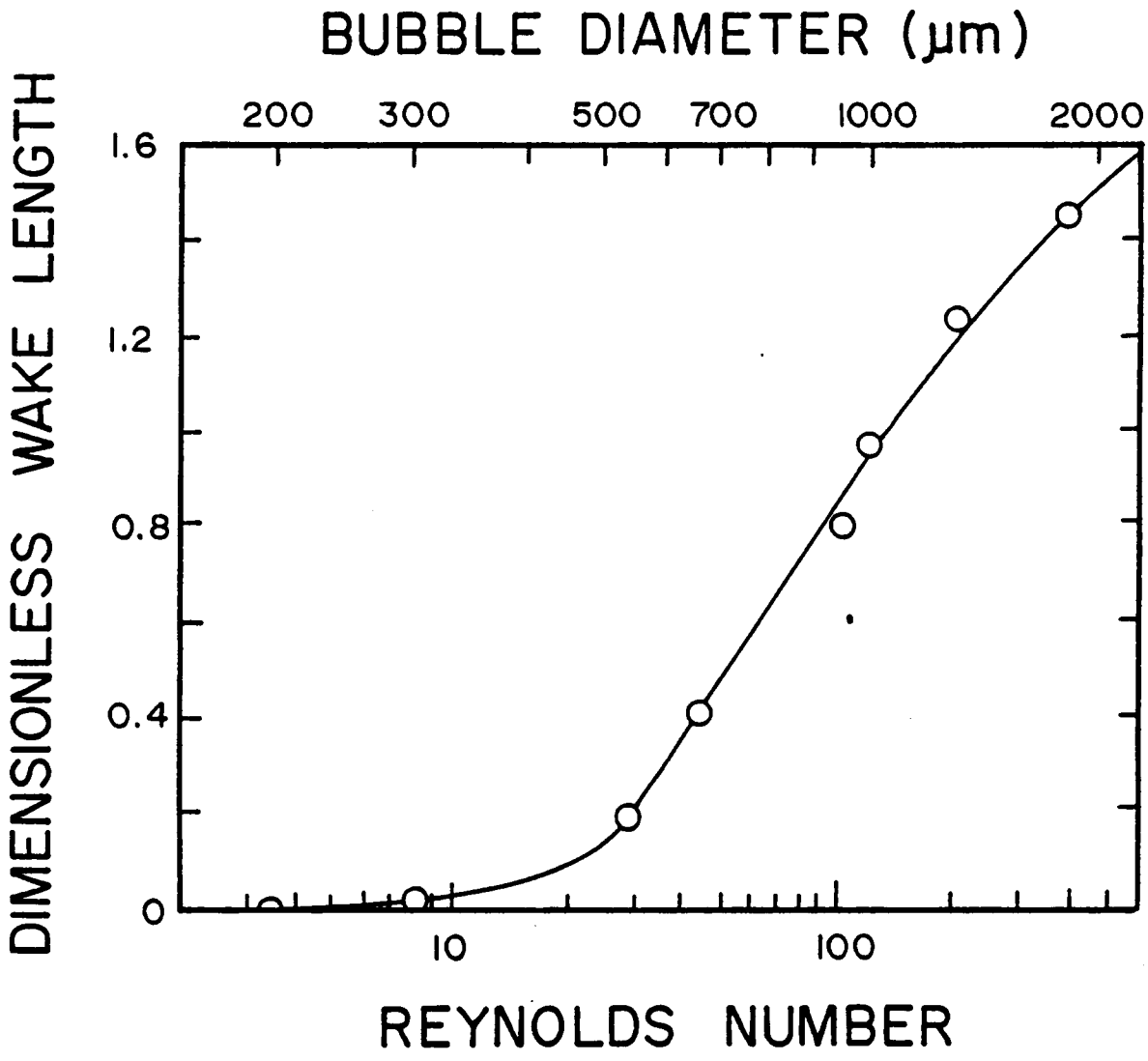

Figure 4.6 Variation in the dimensionless wake length (wake length/bubble diameter) as a function of bubble diameter.

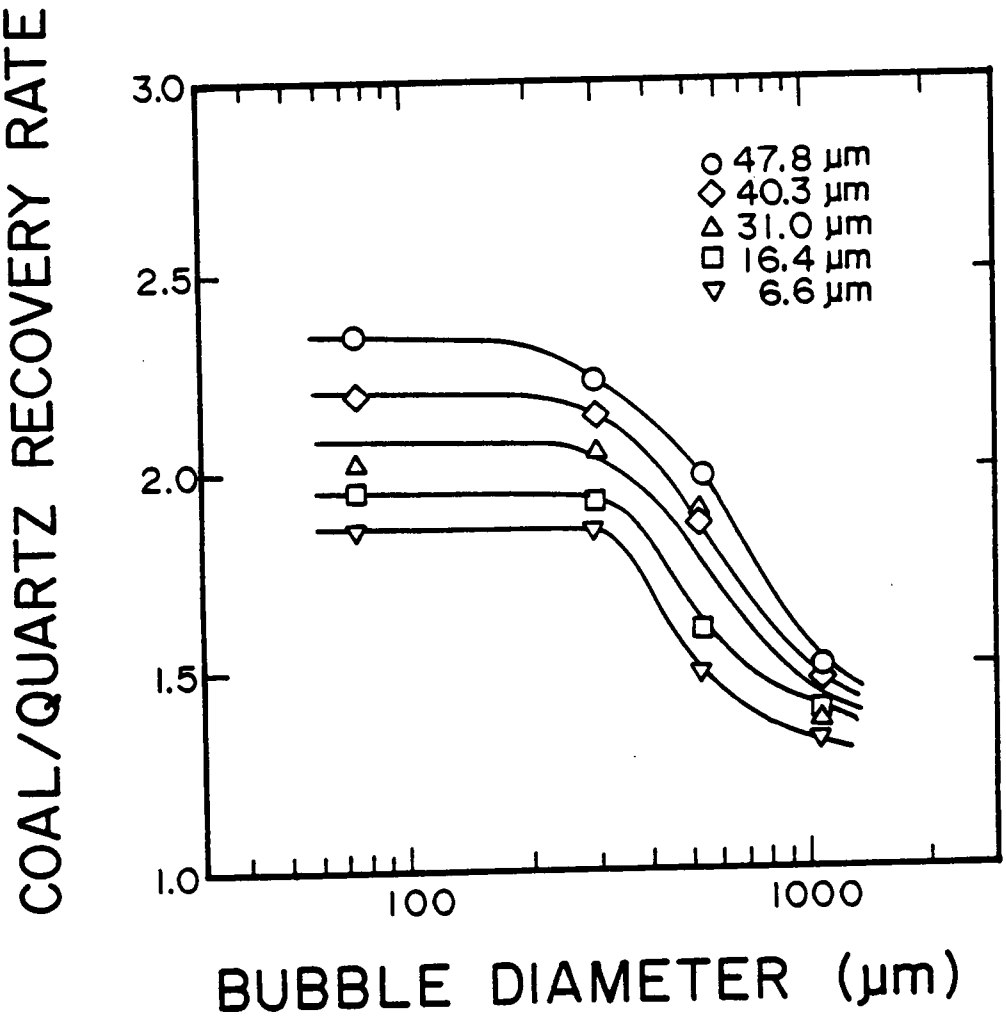

Figure 4.7 Effect of particle diameter on the coal/quartz recovery rate ratio as a function of bubble diameter.

microns.

As shown, selectivity is clearly much better for fine bubbles than for large bubbles. For bubbles smaller than approximately 300 microns, the point at which the turbulent wake disappears, little change in selectivity is seen as a function of bubble size. On the other hand, selectivity drops rapidly for bubbles greater than 300 microns as the turbulent wake volume increases. The selectivity also decreases with decreasing particle size, which may be attributed to the indiscriminate flotation of fine particles owing to their long sliding times as has already been discussed in Chapter 2 (Section 2.4.2).

When experiments are carried out without involving entrainment, as in the case of collection probability measurements, the decrease in selectivity with increasing bubble size should not be observed. This is illustrated in Figure 4.8, where the data presented previously in Figure 4.3 are replotted to show the ratio of collection probabilities for coal and quartz as a function of bubble diameter. As shown, the selectivity does not seem to change with bubble size in this case.

The fundamental information presented here suggests that the use of smaller bubbles should improve the flotation of coal through a reduction in the entrainment of ash particles.

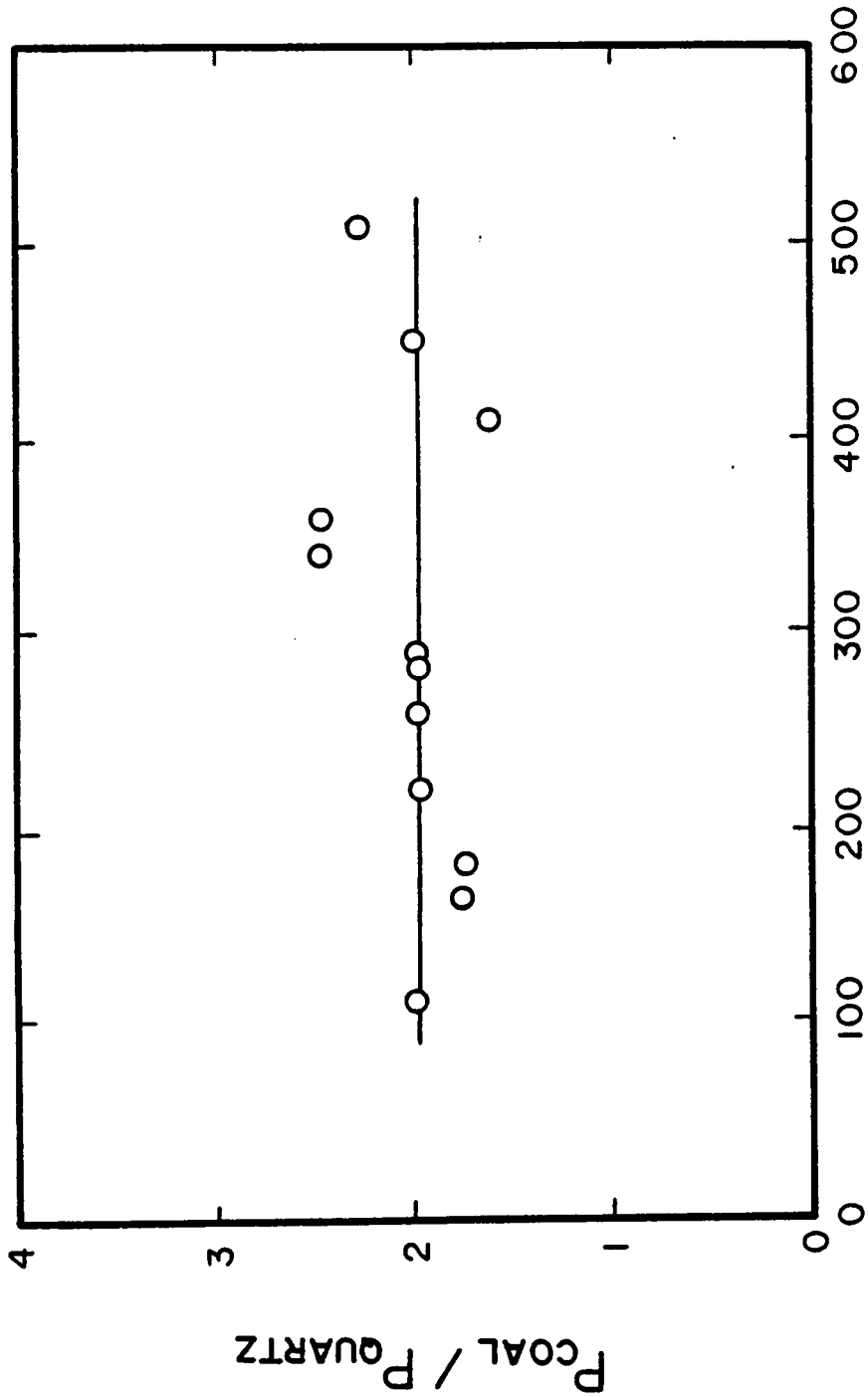

Figure 4.8 Coal/quartz collection probability ratio as a function of bubble size for 31 micron diameter particles.

4.6 Discussion

4.6.1 Attachment/Entrainment Flotation Model

The benefits of using small air bubbles for the flotation of fine particles have been clearly demonstrated by the results presented in the foregoing sections. The probability of collection (P) is seen to increase dramatically as bubble size decreases, giving rise to a corresponding increase in the flotation rate constant. It has been shown, however, that when the bubble size is greater than approximately 300 microns, the flotation rate constants for smaller particles are significantly larger than can be expected from the bubble-particle collision and adhesion process alone (Figure 4.4). It has also been shown that the selectivity of coal flotation begins to deteriorate at bubble sizes above 300-400 microns (Figure 4.7). Furthermore, the wake measurements have shown a sudden increase in the turbulent wake volume at bubbles sizes greater than 300 microns (Figure 4.6). Thus, particles may be removed from the pulp by entrainment in the turbulent wake behind the rising bubbles, making the selective flotation of fine particles using large bubbles difficult.

The magnitude of the entrainment effect on the rate of flotation can be determined quantitatively by considering that flotation occurs via adhesion and entrainment

processes. One can then sub-divide the overall flotation rate constant (k) into two components:

$$k = k_a + k_e \qquad [4.1]$$

where k_a and k_e are the flotation rate constants due to adhesion and entrainment, respectively.

a) Rate Constant for Bubble-Particle Attachment

In Section 3.6.1, it has been shown that the flotation rate constant (k_a) for very hydrophobic particles can be described by:

$$k_a = \frac{C_1}{D_b^3}\left(1 + C_2 Db^{1.54}\right) \qquad [3.12]$$

where C_1 and C_2 are given by Equations [3.13] and [3.14], respectively. The values of k_a obtained from Equation [3.12] are shown in Figure 4.9 with the experimental rate constants determined in the frothless flotation cell.

For particle sizes greater than 30 microns, the theoretical predictions are found to fit the experimental data reasonably well. Since the theoretical predictions are based purely on the particle collision process, this correlation indicates that there is little entrainment taking place when floating relatively large particles. For particle sizes below 30 microns, however, the predicted rate

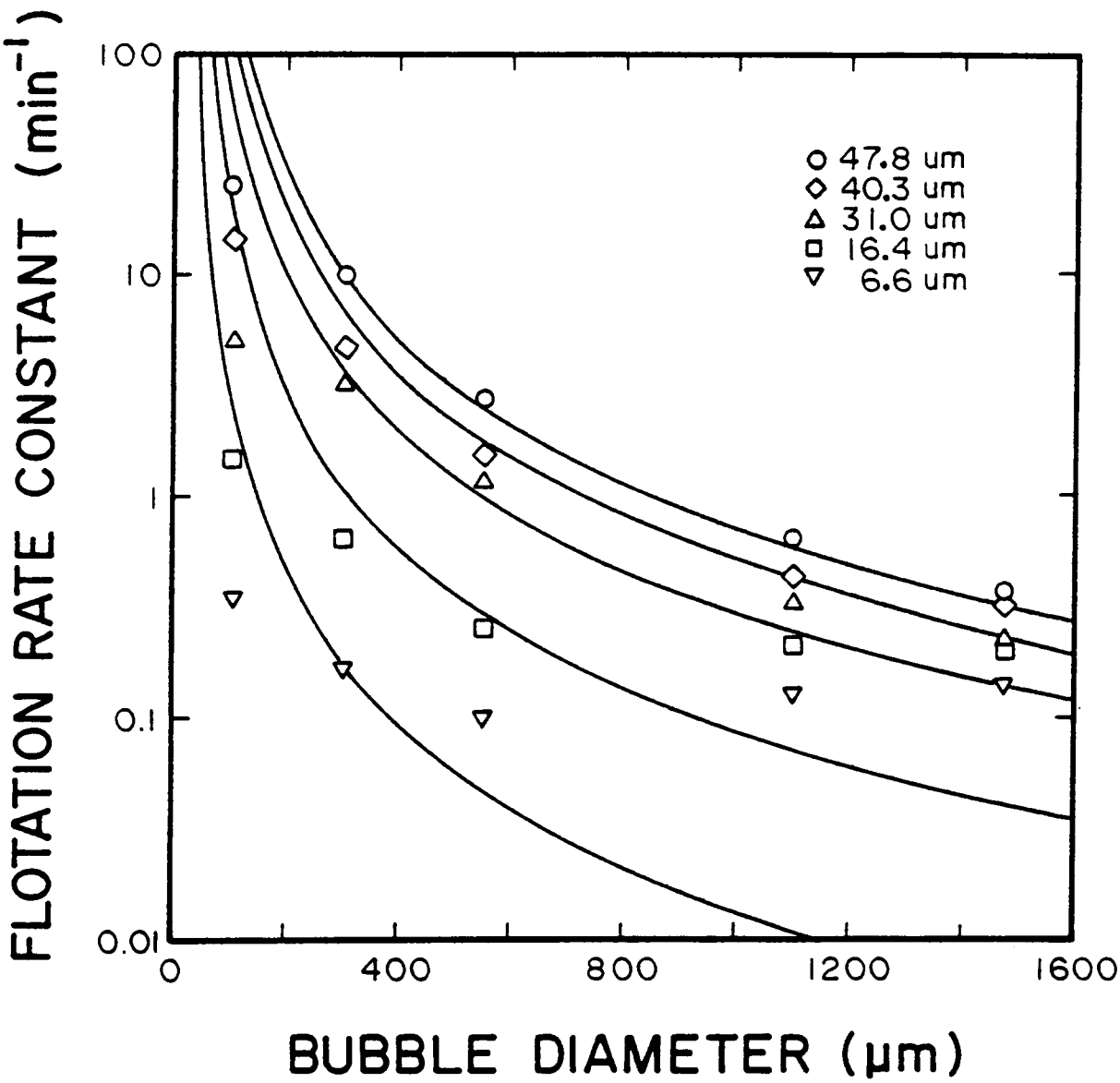

Figure 4.9 Comparison of the experimental flotation rate constants and model predictions assuming $P=P_c$ for various particle diameters.

constants are much lower than the experimental values. Note further that this discrepancy increases as bubble size increases, indicating that entrainment in the turbulent wake becomes much more significant with increasing bubble size. The rate constants predicted by Equation [4.5] are also found to deviate from the experimental data when the bubble sizes are very small. In this case, the predicted values are higher than the experimental values, which may indicate that the assumption that $P=P_c$ may not be valid for these very small bubbles.

b) Rate Constant for Particle Entrainment

A rate constant due to entrainment (k_e) can be derived by considering the probability of entrainment (P_e). The number of particles recovered by entrainment per unit time is then expressed by:

$$N = P_e Q V_w \frac{N_t}{V_c}, \qquad [4.2]$$

where V_w is the dimensionless wake volume (defined as the ratio of the wake volume to the bubble volume), V_c is the cell volume, and N_t is the total number of particles in the cell. Dividing Equation [4.2] by the total number of particles in the cell, and considering a cylindrical cell with height h and diameter D_c, k_e is represented by:

$$k_e = \frac{4P_e Q V_w}{\pi D_c^2 h}. \qquad [4.3]$$

Equations [3.12] and [4.3] can now be substituted into Equation [4.1] to obtain the overall rate constant (k) as follows:

$$k = \frac{Q}{\pi D_c^2} \left[\frac{6P}{D_b} + \frac{4P_e V_w}{h} \right]. \qquad [4.4]$$

If P is replaced by P_c from Equation [2.22], as has been done in deriving Equation [3.12], the values of k obtained from Equation [4.4] represent cases for the flotation of very hydrophobic particles. If the probability of entrainment (P_e) is known, the theoretical k values can be obtained from Equation [4.4]. However, since these values are not known, the experimental rate constants have been substituted for k, and P_e has been back-calculated in order to obtain a best fit to the data. The solid lines in Figure 4.10 represent Equation [4.4] determined as such, and Figure 4.11 shows the back-calculated P_e values. As shown, particle entrainment increases significantly with decreasing particle size.

In the frothless flotation experiments, the bubbles carrying particles must pass through a clear liquid zone (Figure 4.1). As a result, some of the particles entrained

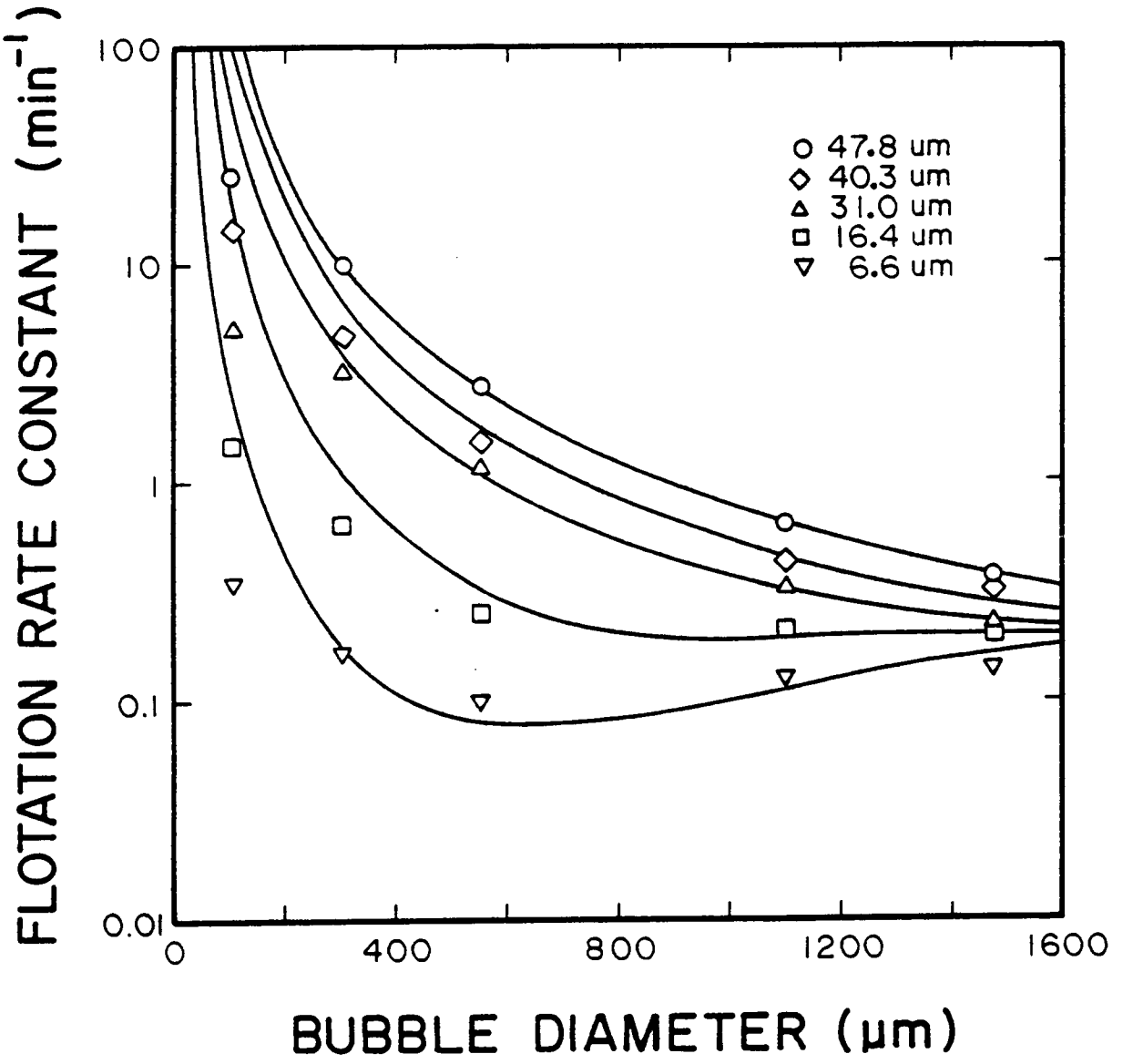

Figure 4.10 Comparison of the experimental flotation rate constants and model predictions based on particle collision and wake entrainment phenomena.

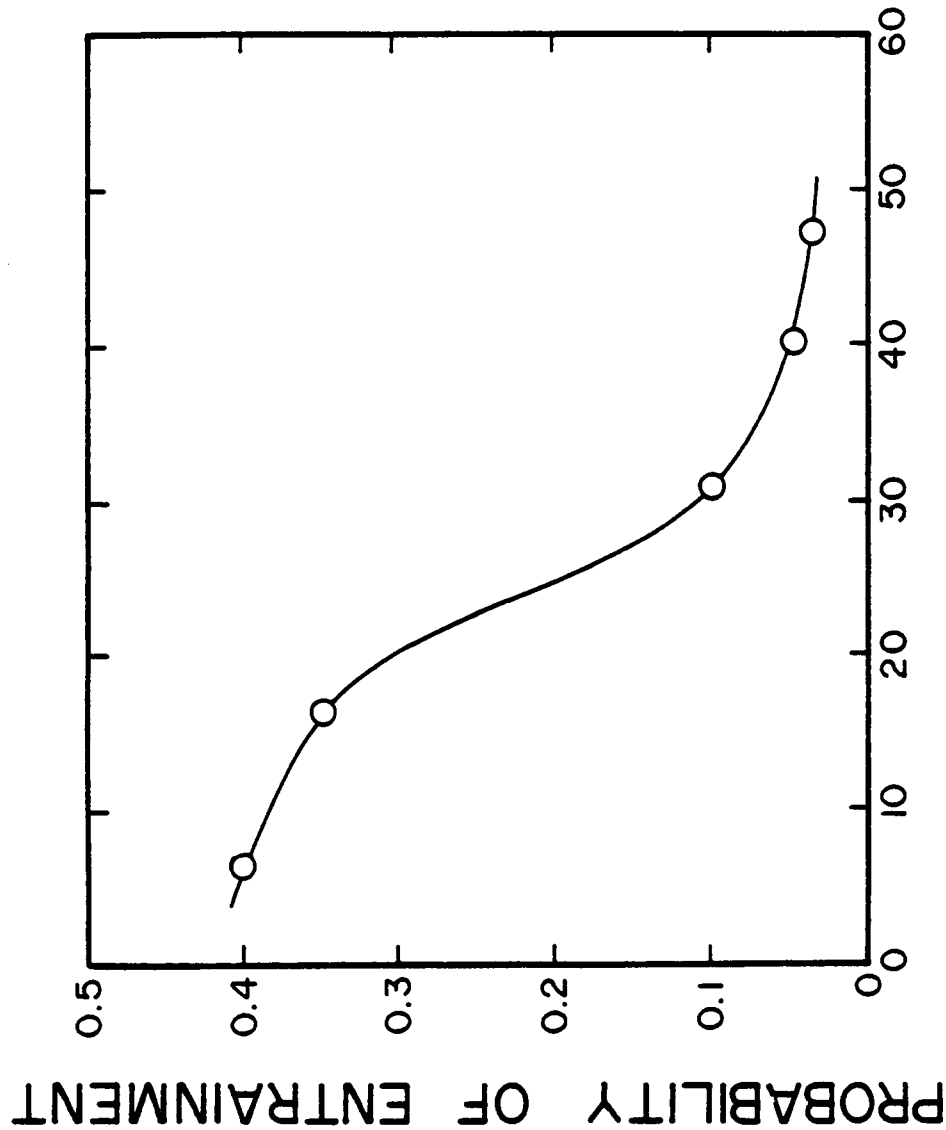

Figure 4.11 Probability of entrainment versus particle size for a clear liquid height of 6 cm.

in the wake may be lost while passing through this zone. Therefore, the values of P_e shown in Figure 4.11 may be lower than those that would have been obtained without the clear liquid zone. In order to account for the particles which were lost in the clear water zone, additional flotation experiments were carried out in which the height of the clear water zone was varied. Using the procedure described previously, values for P_e were determined as a function of the height of the clear liquid zone. The results of these tests, plotted in Figure 4.12, allow the magnitude of P_e to be determined at zero clear liquid height by extrapolation. The findings of this exercise are shown in Figure 4.13. The results indicate that the entrainment of particles increases sharply with decreasing particle size. The particle size at which P_e takes a sharp rise corresponds to approximately 30 microns. This value agrees well with the particle size at which entrainment becomes a problem in actual flotation practice (Johnson, McKee and Lynch, 1974). In light of the very high correlation over a wide range of bubble sizes, it appears that the value of P_e is independent of bubble size. In short, the size of the bubble determines whether or not wake entrainment occurs, while the size of the particle determines the extent of entrainment, i.e., the magnitude of P_e.

The first term in Equation [4.4] represents the contribution to flotation recovery due to attachment and the

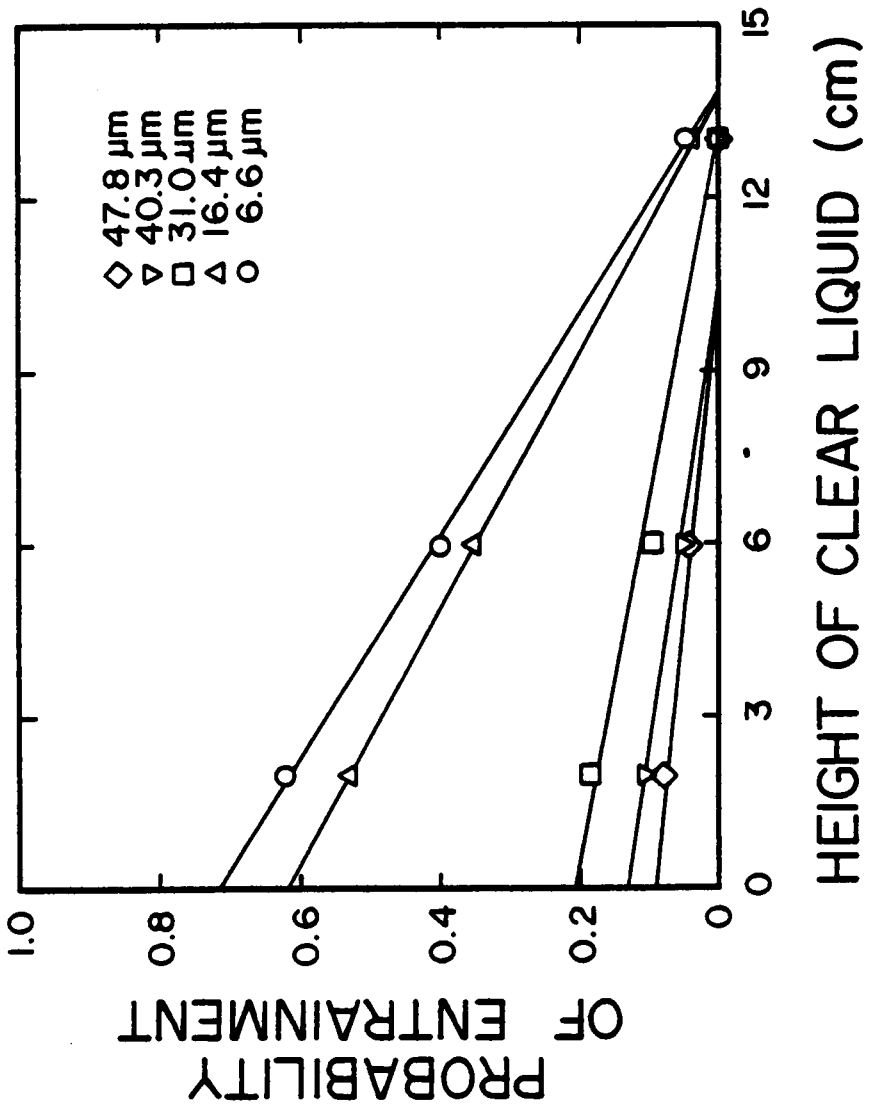

Figure 4.12 Probability of entrainment versus clear liquid height for various particle diameters.

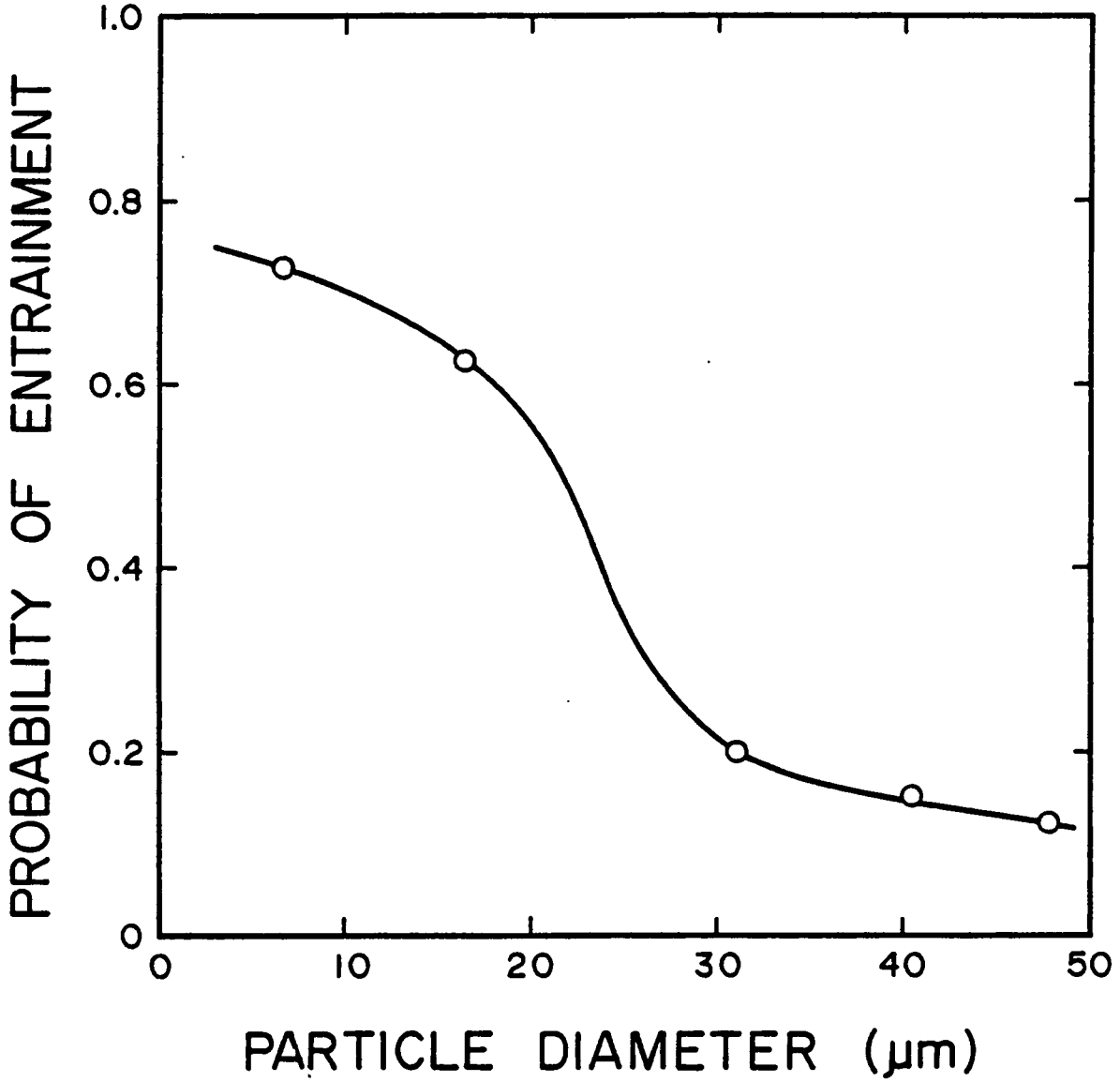

Figure 4.13 Probability of entrainment determined by extrapolation to a clear liquid height of zero as a function of particle size.

second term represents that due to entrainment. A close examination of this equation suggests valuable information for improving fine particle flotation. For example, a decrease in bubble size alone can bring about an increase in k while minimizing the entrainment problem. Equation [4.4] also suggests that by increasing the cell height (h) one can reduce the entrainment problem without affecting the recovery due to the attachment. These analyses strongly suggest the benefits of processing fine coal in a column-type flotation cell using very small bubbles.

4.7 Summary and Conclusions

1) The findings of the present work clearly demonstrate that recovery increases with decreasing bubble size. This improvement is a direct result of the improved hydrodynamic conditions which are more conducive to bubble-particle collision.

2) The use of small air bubbles in the flotation of fine coal has been shown to improve flotation selectivity. Evidence has been shown which suggests that the formation of a turbulent wake behind a rising air bubble may partly contribute to fine particle entrainment. Bubbles less than approximately 300 microns in diameter carry no wake in which particles can be entrained

indiscriminately, and hence an improvement in selectivity is noted for bubbles smaller than this critical size.

3) A flotation rate constant model has been developed considering that flotation occurs via particle collision-adhesion and entrainment processes. This model has been successful in predicting the rate constants determined experimentally in the frothless flotation column. Furthermore, the probability of entrainment, determined from this model, increases with decreasing particle size, but is independent of bubble size.

4) The flotation rate model developed in the present work suggests that decreasing the bubble size or increasing the cell height should result in improved recovery and selectivity for fine particle flotation.

CHAPTER 5

A POPULATION BALANCE MODEL FOR THE FLOTATION OF FINE COAL IN A COLUMN

5.1 Introduction

Froth flotation is a process commonly employed for the selective separation of valuable minerals and coal from unwanted gangue. Because of its operational simplicity and relatively low unit cost, flotation is the most versatile and widely accepted method for treating fine particles. It has been estimated that over two billion tons of ores are treated annually by froth flotation (Leja, 1982).

Although the process of flotation is conceptually very simple, the fundamental principles governing flotation response are extremely complex and are, at present, not completely understood. Rapid advances in flotation theory have been hampered by the large number of process variables which determine flotation response, and the intricate interdependency which exists between them. Rose (1946) has identified over 100 such variables, most of which were found to be interdependent.

In flotation, process variables may be roughly classified as either chemical or physical in nature. Chemical interactions are determined by the surface characteristics of the materials to be separated and the reagent additions. Physical interactions are, to a large

degree, controlled by the particular characteristics of the flotation machine employed.

In past decades, most of the progress made in flotation technology can be largely attributed to advances in the theory of flotation chemistry. On the other hand, physical improvements in flotation have generally come about only through trial-and-error approaches. More recently, increased attention has been given to the development of process type models which can be used to predetermine flotation response. An accurate process model allows the investigator the flexibility to examine process variables independently so that the effects of changes in these variables can be adequately assessed.

5.2 Literature Review

5.2.1 Flotation Machines

Since the introduction of flotation early this century, numerous flotation cell designs have been proposed. Several review articles have recently been published which offer an excellent overview of much of the progress made in this area (Harris, 1976; Tyurnikova and Naumov, 1981; Young, 1982). Presently, there are about 40 designs of flotation cells in use worldwide (Leja, 1982). Of these designs, four major categories of flotation cells can be identified:

mechanical, pneumatic, froth separators and column.

Mechanical flotation devices are by far the most commonly employed type of flotation machine. The primary distinguishing feature of this cell is a mechanically driven impeller which disperses air bubbles and agitates the flotation pulp. Current design trends are toward the development of large mechanical flotation cells (up to 2000 cubic feet) for the processing of large quantities of low grade ores and increased utilization of automatic control systems. Pneumatic cells differ from mechanical flotation machines in that compressed air is utilized for agitating the pulp. Flotation machines of this type are rare, and are offered for sale only in the Soviet Union (Young, 1982). This situation may change, however, with recent development in the United States by the Diester corporation of a pneumatic flotation column (Zipperian and Christophersen, 1985). Froth separators, developed in the Soviet Union (Malinovskii et al., 1973), are unique in that the incoming feed is introduced on the surface of the froth bed instead of into the flotation pulp. This arrangement provides excellent conditions for the flotation of coarse particles, but is not well suited for the treatment of fine particles which are easily entrained in the froth layer.

Perhaps the most exciting development in flotation cell technology has been the relatively recent emergence of column flotation machines. Originally invented in 1961 by

Canadians Boutin and Tremblay, flotation columns are just beginning to gain industrial acceptance. The major advantage of column flotation is the ability to upgrade material in a single stage that would otherwise require multiple cleaning stages for mechanical or pneumatic devices.

The flotation column consists of a long vertical tube into which feed slurry is pumped at some point between the froth layer and air inlet. Particles which enter with the feed flow down the column and encounter a stream of bubbles rising in the opposite direction. The countercurrent flows of pulp and air promote efficient bubble-particle contacts and hence enhance the recovery of hydrophobic particles. The feature which distinguishes the flotation column from other pneumatic cells is a cleaning zone located between the feed inlet and froth layer. From the top of this zone, a downward flowing stream of wash water is introduced. The wash water stream is designed to elutriate away gangue particles which have become entrained between the particle laden air bubbles. The reduction in the mechanical carryover of gangue and improved efficiency for particle capture make the column ideal for treating very fine particles.

Because of its unique design, the column has a low initial capital investment as well as low operational and

maintenance costs. When directly compared to mechanical flotation, column flotation has been found to provide superior results for the cleaning of copper ore (Anon., 1963), uranium ore (Honeywell, 1967), molybdenum (Mathieu, 1972), graphite (Narasimhan, Rao and Chowdhury, 1972) and coal (Halvorsen, 1979; Moon, 1982).

The first full-scale testing of the column was performed late in 1963 at the Opemiska copper mines in Canada, an affiliate of the Falconbridge Nickel group (Anon, 1965). During testing, a number of problems were discovered with the single 3-foot diameter column. The most serious problem was that the porous diffuser used to inject air into the column became plugged after only a few days of use. This prevented continous operation of the column. In addition, the metallurgical results obtained with the column were poorer than expected. This problem was determined to be a result of the increased level of turbulence observed in the 3-foot diameter column. After evaluating the problems, a redesigned, 18-inch square column was taken to Opemiska in June of 1965 (Wheeler, 1966; Boutin and Wheeler, 1967a,b). Problems with the plugging of the air diffuser were solved through the use of porous bubble tubes which could be replaced without shutting down the column. Metallurgical performance was also greatly improved by the smaller design of the column which minimized internal turbulence. For the same amount of throughput, the column was found to occupy

only about 10% of the floor space required by mechanical flotation machines.

Although acceptance of the column by industry has been slow, recent successful applications are expected to result in a rapid rise in column utilization. The Gaspe Division of the Noranda Mines, Quebec, have replaced 13 stages of mechanical cells with 2 columns in their molybdenite cleaning circuit (Coffin, 1982). The installation of the columns has been deemed a complete success, and improved fines recovery and higher grade concentrates have been achieved. At least a half dozen other producers in British Columbia have utilized columns for copper and molybdenum cleaning (Dobby and Finch, 1986). Another column which has found commercial application is the Leeds-Norton flotation machine used primarily for cleaning coal (Adorjan et al., 1982).

Since column flotation machines are a recent development, relatively little data is available concerning their operational behavior and methods for scale-up. This lack of information has largely contributed to the slow acceptance of columns into industry. In order to alleviate this problem, an attempt has been made in the present work to develop a dynamic model of column flotation. The following sections describe the formulation of this model.

5.2.2 Flotation Modeling

The primary purpose of a flotation model is the prediction of product recovery and grade. An appropriate model can be used for equipment design, scale-up, process control and optimization. In addition, models provide an excellent tool for developing a clearer understanding of the fundamental process of flotation.

In the literature, three major categories of flotation models can be identified: empirical, probabilistic and kinetic. Empirical models are useful for predicting the response of a well defined process between the limits of previously obtained experimental data. Simple statistical correlations are common in this type of model (Mular, 1971; 1972). Empirical models are typically easy to develop, but cannot be used beyond the limits of the experimental data base and yield little information regarding the fundamental mechanisms of the process.

Probabilistic models of flotation attempt to describe flotation by quantifying the probability of occurrence of a series of fundamental events (e.g., collision, adhesion, detachment, etc.). The overall success of flotation is then determined by the product of each of these probabilities. Of the various flotation models, probabilistic models are the most theoretical in nature and provide a great deal of conceptual information. Models of this type have been

successfully employed to explain the decline in flotation efficiency observed at very fine particle sizes (Gaudin, 1932; Schuhmann, 1942; Sutherland, 1948). In addition, simple forms of these models have been applied as a means of analyzing flotation circuit performance (Kelsall et al., 1960, 1961, 1971; Davis, 1964). Widespread use of probabilistic models has been hampered by a limited understanding of the fundamental events occurring during flotation. For this reason, most literature deals with the kinetic modeling of flotation.

Kinetic models of flotation have been developed despite a lack of complete theoretical justification for their basic form. Models of this type have evolved primarily as a result of analogy to chemical kinetics (Garcia, 1935). In the development of a kinetic flotation model, particle recovery is considered to take place as the result of one or more elementary subprocesses. Some of the subprocesses commonly considered include bubble-particle attachment, bubble transport, froth transport and froth drainage. Unlike probabilistic models, kinetic models do not attempt to determine the fundamental mechanisms responsible for the occurrence of a particular flotation subprocess. Rather, kinetic modeling uses general rate equations to specify the rate at which material is transferred through the flotation cell. The constants used in the general rate equation are typically determined by means of experimental

investigations.

An example of one of the most simple forms of a kinetic flotation model is:

$$\frac{dC}{dt} = - k\ C^n \qquad [5.1]$$

where k is the rate constant, n is the order of the kinetics (commonly n=1), C is the concentration of floatable particles in the pulp and t is time. Because of the inclusion of time as a modeling parameter, kinetic models are easily employed for simulating dynamic conditions.

One of the first dynamic simulations of flotation which utilized Equation [5.1] was performed by Arbiter and Harris (1962). These investigators discussed how particle properties and operational conditions would affect flotation response through changes in the values of k and n. The basic concept presented by Arbiter and Harris has been utilized in a number of other investigations, though in some cases with extensive modification (Bull, 1966; Harris and Rimmer, 1966; Harris, 1978). Noting that not all particles possess identical flotation characteristics, Kelsall (1961) demonstrated that floatable particles could be divided into two classes with fast and slow flotation rate constants. This concept was later expanded by Imaizumi and Inoue (1966) who developed the notion of a continuous distribution of

flotation rate constants.

The first detailed investigation which quantitatively utilized separate kinetic representations for each flotation subprocess was accomplished by Mika and Fuerstenau (1969). In this model, the pulp and froth phases were considered independently. Particles were considered to exist either freely or attached to air bubbles in each of the two phases. The rate of transfer of particles between free and attached states was quantified by rate constants, whereas the transfer of particles between the froth and pulp was determined by material flows. The concentration of particles, free and attached, was determined by simultaneously solving mass balances around each phase. A similar model, developed with an emphasis toward process control, has been presented by Bascur and Herbst (1982).

Given the proper selection of flotation rate constants, the above models provide some degree of capability for process simulation. In most cases, the value of the flotation rate constant must be determined through extensive experimental testing if accurate predictions of flotation response are to be made. Ideally, the magnitude of the rate constant should be evaluated theoretically from a mechanistic approach to offer a large degree of direct predictability. This condition requires that each of the flotation subprocesses be well described in mathematical terms.

5.3 Objectives

Given the growing interest in column flotation, the development of an accurate model for simulation and scale-up purposes would be very useful. Because of the turbulent nature of mechanical flotation cells, they are difficult to study and to simulate from a mechanistic point of view. The fundamental phenomena of bubble-particle attachment and the transfer of particles and bubbles through the flotation pulp are, at best, poorly quantified for these machines. On the contrary, the well defined hydrodynamic behavior and quiescent nature of the flotation column is well suited to mathematical simulation.

The objective of the present work has been the development of a population balance model which describes the process of flotation in a column. Because of its novel design, the column has been modeled through the quantitative description of distinct sections along the length of the column. Each section has been identified by its unique flow characteristics. Unlike most kinetic models, the rate expressions used in the model have been based on first principles. Because the emphasis of the present work is coal, the specific development of the model has dealt primarily with coal flotation. The completed model is capable of predicting clean coal recovery, ash recovery, and

ash percent in reject and clean coal for a variety of operating conditions and cell dimensions. The model should be applicable to other mineral systems with only slight modification. It is hoped that the model will shed additional light toward understanding the process of column flotation, particularly with regard to advanced cleaning of fine coal.

5.4 Modeling of Column Flotation

5.4.1 Population Balance Models

All coal processing operations are characterized by the fact that they contain at least one particulate phase dispersed in a continuous phase. In grinding, for example, the coal represents the dispersed phase and the water represents the continuous phase. In flotation, two particulate phases are present: coal particles and air bubbles. The number of particles and the number of air bubbles present in the system each represent a population. Therefore, if it is possible to quantify how the population changes with time and space, a number balance can be written to mathematically describe a given process. This number balance is known as a population balance model.

Population balance models provide a convenient framework for modeling almost any processing operation;

however, they do require that information be specified on the basis of number. Since a number balance is not very practical for representing the large populations encountered in processing operations, a conversion must be made to mass or volume. Fortunately, a population balance can be readily converted to mass or volume by applying information on particle size, shape or specific gravity. As a result, population balance models for particulate processes are most commonly seen as mass balance or volume balance models.

5.4.2 Model Development for Column Flotation

Provided that bubbles and feed coal are evenly distributed across the column cross-section, a column flotation cell can be represented as a plug-flow device. In modeling the flotation column, the approach used in the present work has been to model the flow pattern in the column using a series of sections along the column length. A new section has been created wherever flow conditions change. In the model, six sections have been established: reject, lower, feed, upper, transition and froth. These sections are shown schematically in Figure 5.1.

Each section of the column may be represented by one or more completely mixed zones. The transition, feed and reject sections of the column have each been represented by one completely mixed zone. The number of completely mixed

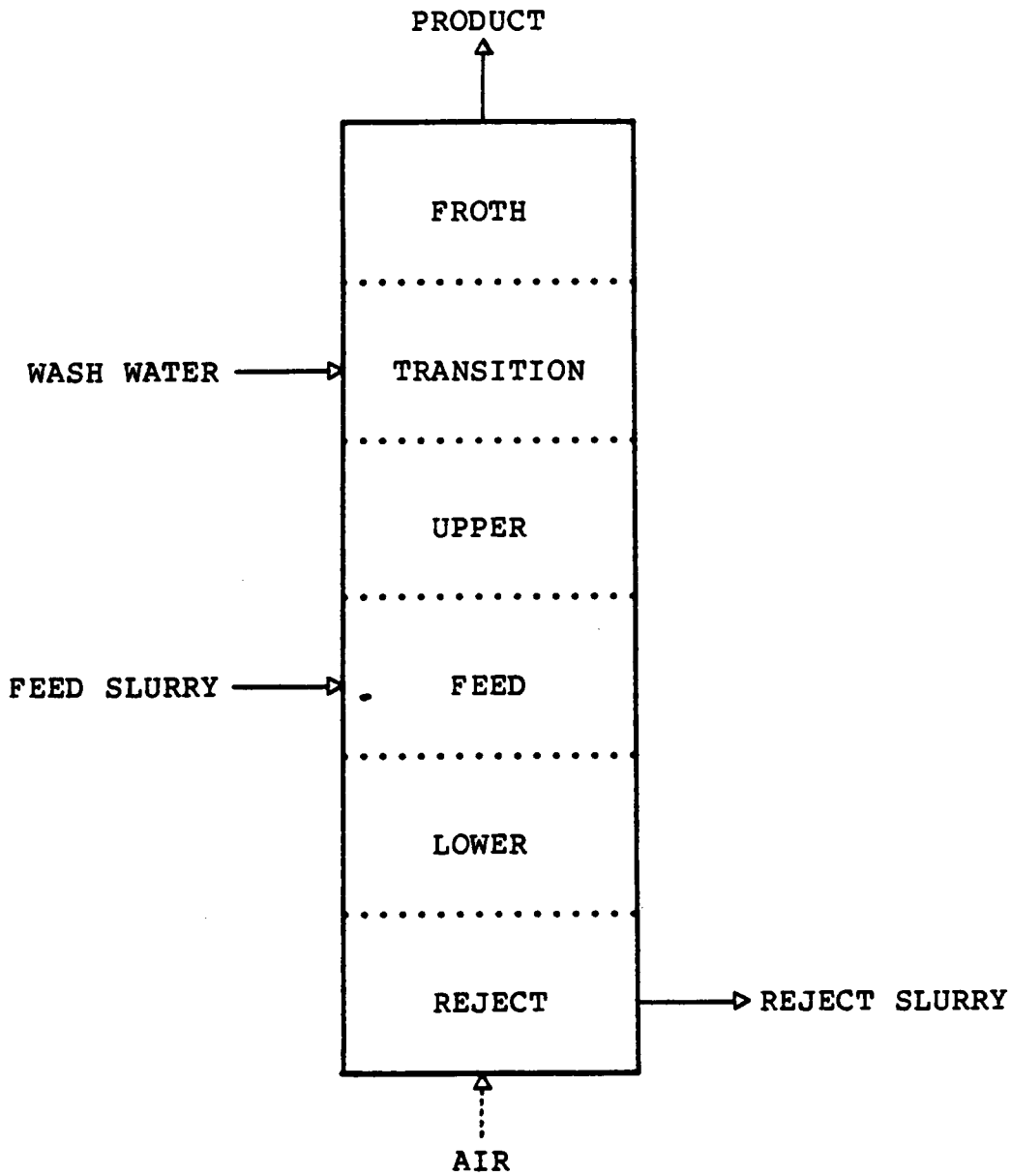

Figure 5.1 Schematic representation of the sections along the height of a flotation column with distinct flow characteristics.

zones contained in the other sections of the column has been varied and depends on the physical height of column. As a result, the minimum number of zones contained in the column is limited to six.

Model equations are written for each completely mixed zone in each section by applying a mass or volume balance around the zone. The volume (or mass) balance around each zone consists of two types of terms: transport and rate. As shown in Figure 5.2, four possible transport terms are possible for a given zone. The quantity $\dot{V}_{d,i+1}$ represents the downward volumetric flow of material from the zone directly above (i+1) into the zone under consideration (i). Similiarly, $\dot{V}_{u,i-1}$ represents the upward volumetric flow of material into the zone (i) from the zone directly below (i-1). The values of $\dot{V}_{d,i}$ and $\dot{V}_{u,i}$ represent the volumetric flows from the zone (i) to the zones directly above (i+1) and below (i-1), respectively. Transport terms are used to describe the movement of bubbles or particles due to volumetric flows, settling or rising velocities and entrainment. Rate terms take the basic form of Equation [5.1] and, as such, the transfer of material is quantified by a rate constants (i.e., k_{in} or k_{out} for the case shown in Figure 5.2). Rate terms represent disappearance from or appearance into a zone due to phenomenon such as bubble-particle attachment.

The rate of change, or accumulation, of mass or volume

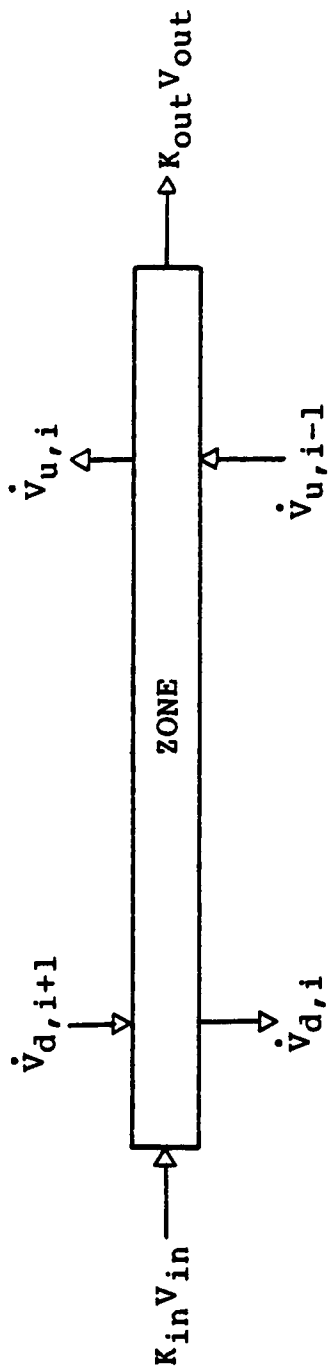

Figure 5.2 Generalized zone within a flotation column.

in a zone is simply represented by the difference of input and output terms due to rate and transport. Quantitatively, this balance may be given as:

$$\text{Accumulation} = \text{Input} - \text{Output} + \text{Generation}. \qquad [5.2]$$

For the general case shown in Figure 5.2, substitution of appropriate terms yields:

$$\frac{dV_i}{dt} = [V_{d,i+1}+V_{u,i-1}]-[V_{u,i}+V_{d,i}]+[k_{in}V_{in}-k_{out}V_{out}]. \qquad [5.3]$$

Steady state conditions are achieved when the rate of change becomes equal to zero.

The balance given by Equation [5.3] can be applied to each particulate phase present in the flotation column, resulting in the complete model for the process. In this case, three distinct particulate phases have been identified, including air, free solids, and solids attached to air bubbles. Particulate solids may be further classified as either coal or ash, with each requiring separate consideration. In the present work, particles have been assumed to be perfectly liberated. For very finely ground particles, this is a reasonable assumption in many cases. Modification of the model to include a third class of incompletely liberated particles is possible.

In order to implement Equation [5.3], the appropriate

rate expressions and flow rates in the column must be established. The following discussion describes this procedure for each phase in the column. For convenience, a complete list of parameter nomenclature is given in Table 5.1.

a) Volumetric Flow Balance

The schematic shown in Figure 5.3 illustrates the relationship between the volumetric flows passing through each zone of the column. Unlike the particulate and gas phases to be shown later, the balance of flows around any of the zones was considered to always be at steady state. This assumption dictates that each of the three phases, (gas, liquid and solid) be incompressible. This assumption is valid for the solid and liquid phases, although the gas phase is subject to some degree of compressibility. Calculations have shown that the effect of compressibility is negligible for the column geometries employed in the present work.

In order to determine the internal flow rates within the column, each of the external flows must be evaluated. Upon performing a total volumetric flow rate balance around the entire column, the steady state assumption requires that:

$$Q_W + Q_F + Q_G = Q_P + Q_T \qquad [5.4]$$

Table 5.1 - Nomenclature for the Column Population Balance Model

A = Cross-sectional area of the flotation column
$C_{f,i}$ = Concentration of free particles in zone i
$C_{a,i}$ = Concentration of attached particles in zone i
C_F = Concentration of free particles in the feed
D_b = Bubble diameter
E_i = Fractional air content in the ith zone
E_F = Fractional air content of the froth
f = Average froth film thickness
k_a = Rate constant for bubble/particle attachment
$M_{a,i}$ = Mass of particles attached to bubbles in zone i
$M_{f,i}$ = Mass of free particles in zone i
Q_P = Total volumetric flow rate reporting to product
Q_T = Total volumetric flow rate reporting to reject
Q_F = Total volumetric flow rate of feed pulp
Q_G = Total volumetric flow rate of feed air
Q_W = Total wash water flow rate
Qd_i = Downward flow rate of pulp from zone i
Qu_i = Upward flow rate of pulp from zone i into zone i+1
Qm_i = Internal flow rate representing column mixing
Qb_i = Internal bubble flow rate
U_b = Bubble rise velocity
U_p = Particle settling velocity
V_z = Volume of a zone within the column
t = Time

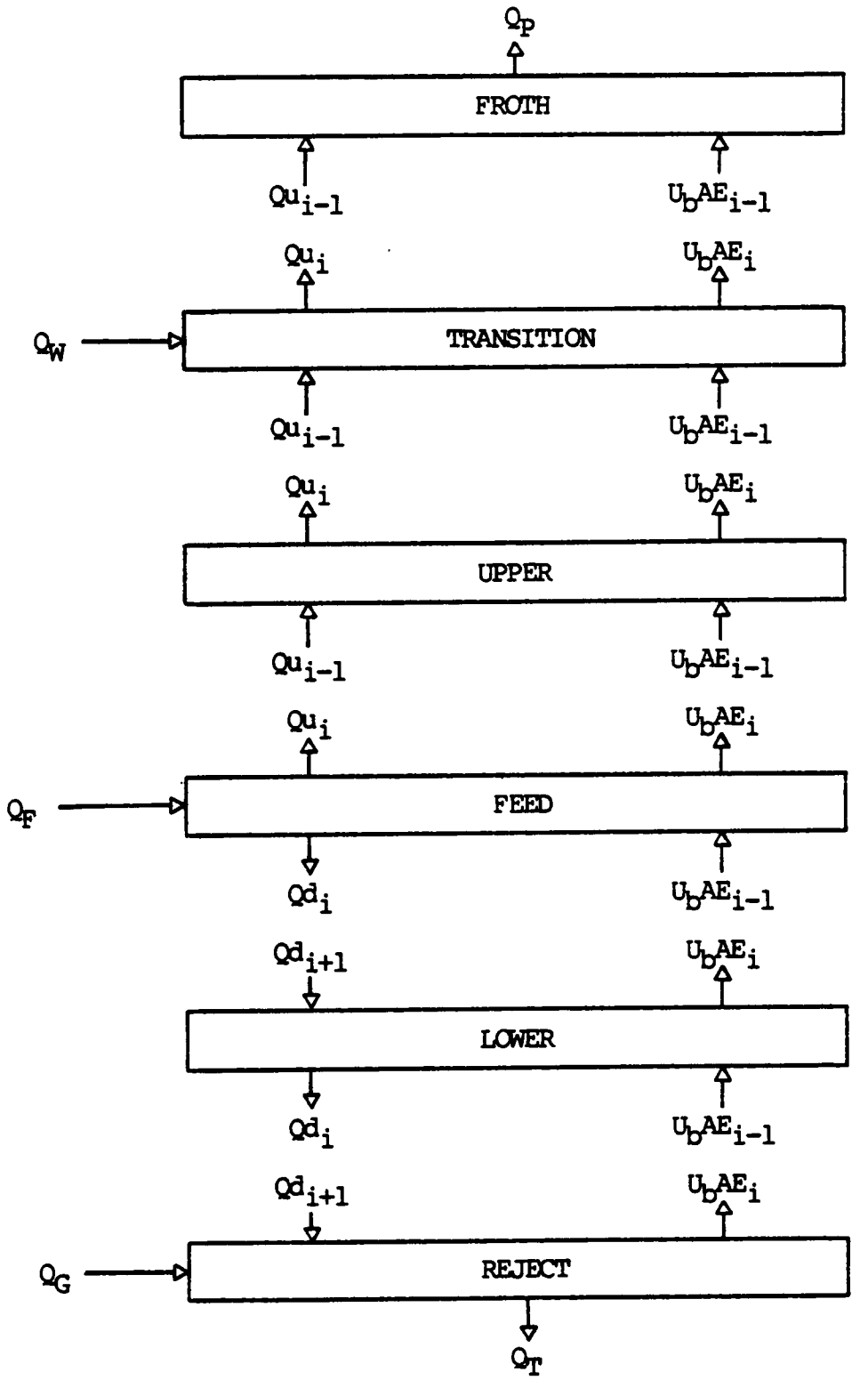

Figure 5.3 Schematic representation of the volumetric flow balance for the column.

The values of Q_W, Q_F and Q_G are input parameters, and are known quantities. The values of Q_P and Q_T are unknown and must be calculated from a second independent equation. The second equation may be obtained by performing a total volumetric flow balance for air around the column. From such an analysis, it is possible to show that:

$$Q_P E_F = Q_G - Q_T E_i, \qquad [5.5]$$

where E_F and E_i (i=1) are the fractional air contents of the froth and reject zones, respectively. At present, the value of E_F has been obtained using a technique suggested by Bascur and Herbst (1982). In this approach, each bubble is considered to carry into the froth a "sheath" of liquid, the thickness of which is determined by surface tension and superficial gas velocity (Hartland and Barber, 1974). From a simple geometric analysis, it can be shown that:

$$E_F = \frac{D_b^3}{D_b^3 + 6D_b^2F + 12D_bF^2 + 8F^3}, \qquad [5.6]$$

where F is equal to the average thickness of the liquid sheath and D_b is the mean bubble diameter. Thus, by estimating the value of F, Equations [5.4], [5.5] and [5.6] yield unique expressions for Q_P and Q_T as functions of E_i.

Once the external flows have been determined, the internal flows within the column are easily determined.

Consider the volumetric flow balance around the reject zone of the column. Using the steady state assumption, it can be shown that the internal flow rate (Q_{di+1}) for the reject zone is:

$$Q_{di+1} = Q_T - Q_G + U_b A E_i. \qquad [5.7]$$

As shown previously in Section 2.5.3, the bubble rise velocity, U_b, can be represented by:

$$U_b = Z(D_b)^{1.14}, \qquad [2.48]$$

where Z is an experimentally determined proportionality constant. For the sizes of bubbles used in the present work, the value of Z was experimentally determined to be 148. This value closely corresponds to that reported by McCabe and Smith (1976). The value of the cross-sectional area of the column (A) is determined by the particular geometry of the column.

Other internal flow rates along the length of the column can be obtained using the methodology utilized in deriving Equation [5.7]. The results of such an analysis have been summarized in Table 5.2. In each of these expressions, all parameters except for the fractional air content (E_i) are known. E_i values are determined independently in the analysis which follows.

Table 5.2 - Volumetric Flow Balance Equations

Froth:	$Q_P = Qu_{i-1} + U_b A E_{i-1}$
Transition:	$Qu_i = Qu_{i-1} + U_b A(E_{i-1}-E_i) + Q_W$
Upper:	$Qu_i = Qu_{i-1} + U_b A(E_{i-1}-E_i)$
Feed:	$Qu_i = Q_F - Qd_i + U_b A(E_{i-1}-E_i)$
Lower:	$Qd_{i+1} = Qd_i + U_b A(E_i-E_{i-1})$
Reject:	$Qd_{i+1} = Q_T + U_b A E_i - Q_G$
	$Q_T = Q_F + Q_G + Q_L - Q_P$

b) Air Phase

The following assumptions are used in the construction of the air phase model:

i) The size of air bubbles in the system can be represented by a single mean diameter.

ii) The rise velocity of bubbles is not significantly changed due to the attachment of particles.

iii) The coalescence of bubbles can be neglected.

The terms necessary to describe the air volume balance between zones are shown schematically in Figure 5.4. In order to utilize the volumetric balance given in Equation [5.3], the transport and rate terms for each zone must be obtained. As an example of this development, consider the reject zone given at the bottom of Figure 5.4.

The net change in the air content with time is determined by the difference of the volume of air per unit time entering the zone and the volume of air per unit time leaving the zone. The volumetric flow of air which enters the zone consists of the air feed rate (Q_G) and the air carried into the zone from above by the downward flow of pulp in the column ($Q_T E_{i+1}$). Flows leaving the zone include the volume flow of air to reject ($Q_T E_i$) and the flow due to the bouyancy of the bubbles ($U_b A E_i$). Each of these volumetric flows can be converted to fractional air content

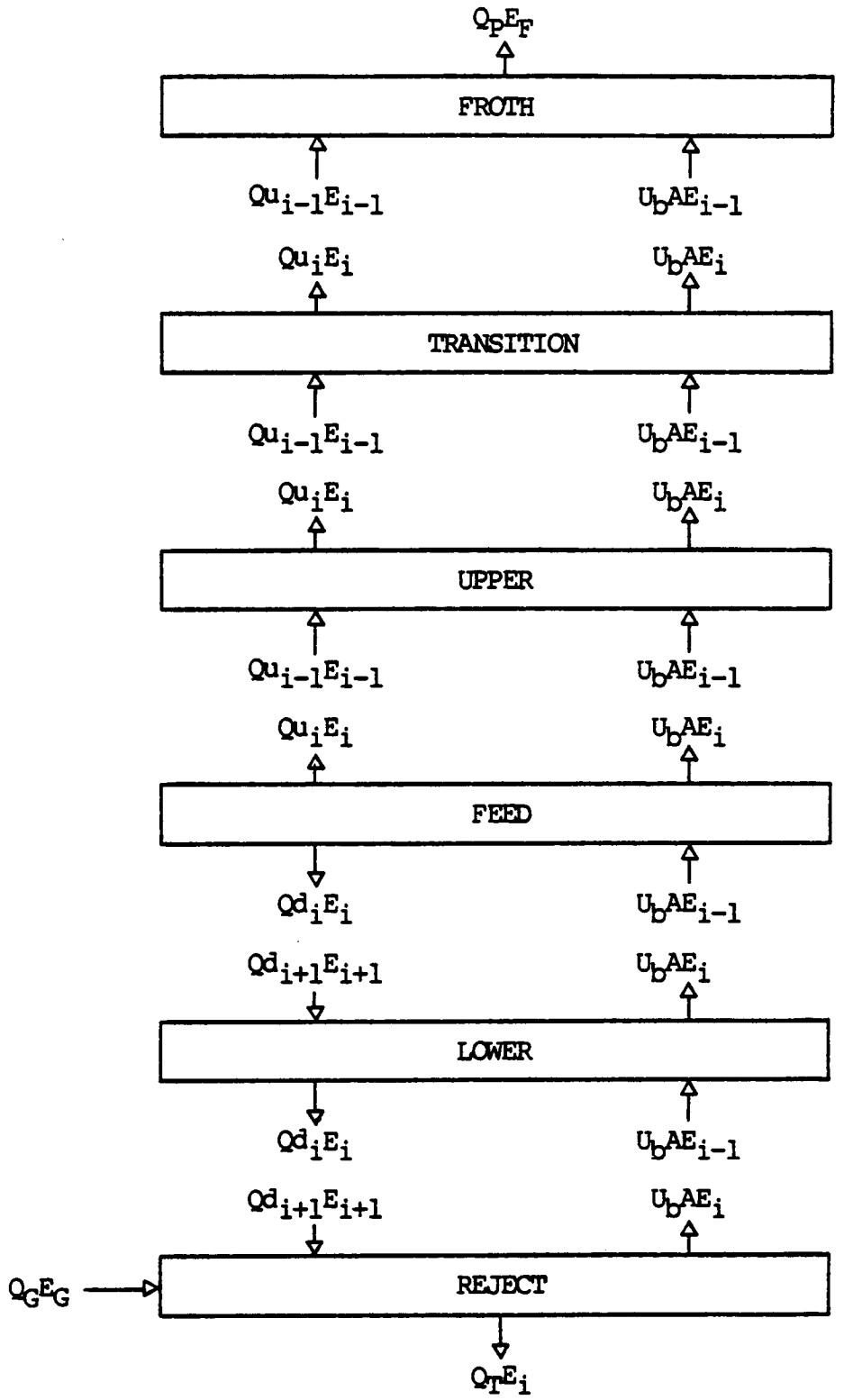

Figure 5.4 Schematic representation of the air balance for the column.

by dividing by the total volume of the zone. Using the analysis given in the development of Equation [5.3], it is possible to show that:

$$\frac{dE_i}{dt} = [(Q_G E_G + Qd_{i+1} E_{i+1})/V_z] - [((Q_T + U_b A) E_i)/V_z] \qquad [5.8]$$

which provides an expression for the change in the fractional air content in the reject zone with time. Volumetric balance equations for the other zones can be derived in the same manner. The expressions obtained by this analysis are given in Table 5.3.

For each of the equations given in Table 5.3, all parameters have previously been determined except for the fractional air content of each zone (E_i). The values of E_i can be evaluated by means of a simultaneous numerical solution to the resultant set of differential equations. In the present work, the Euler method was employed.

c) Free Solids Phase

The assumptions used in the construction of the free solids phase model are:

i) The particle size distribution can be represented by a single mean particle diameter.

ii) Particles of coal (or ash) are equally floatable, nonagglomerating and fully liberated.

Table 5.3 - Population Balance Equations for Air

Froth:	$dE_i/dt = [(Qu_{i-1}+U_bA)E_{i-1} - Q_PE_F]/V_z$
Transition:	$dE_i/dt = [(Qu_{i-1}+U_bA)E_{i-1} - (Qu_i+U_bA)E_i]/V_z$
Upper:	$dE_i/dt = [(Qu_{i-1}+U_bA)E_{i-1} - (Qu_i+U_bA)E_i]/V_z$
Feed:	$dE_i/dt = [U_bAE_{i-1} - (Qu_i+Qd_i+U_bA)E_i]/V_z$
Lower:	$dE_i/dt = [U_bAE_{i-1} + Qd_{i+1}E_{i+1} - (Qd_i+U_bA)E_i]/V_z$
Reject:	$dE_i/dt = [Q_GE_G + Qd_{i+1}E_{i+1} - (Q_T+U_bA)E_i]/V_z$

iii) The settling velocity of a particle can be represented using Stokes equation.

iv) Maximum bubble loading is never exceeded.

v) Particle detachment is negligible.

As with the air phase, it is possible to determine the the rate of change of free particles in a zone using rate and transport terms. Figure 5.5 is a schematic representation of the terms considered for the free solids contained in each zone. For solids, the preferred convention is to represent particles in units of mass. For this reason, a mass flow balance has been chosen in preference to the volumetric balance previously employed.

As a specific example, once again examine the balance of terms around the reject zone. The mass rate of free particles entering the reject zone from above includes particles transported by the downflow of liquid ($Qd_{i+1}C_{f,i+1}$) and particles entering the zone by sedimentation ($U_pAC_{f,i+1}$). Particles may also exit the zone to the tailings stream by liquid transport ($Q_TC_{f,i}$) and sedimentation ($U_pAC_{f,i}$). In addition to the transport terms, a rate term ($k_aM_{f,i}$) must also be considered for the free particles which are lost from this phase by bubble-particle attachment. The rate constant of attachment (k_a) has been derived from the first principles of bubble-particle attachment in Chapter 3 (Section 3.6.1).

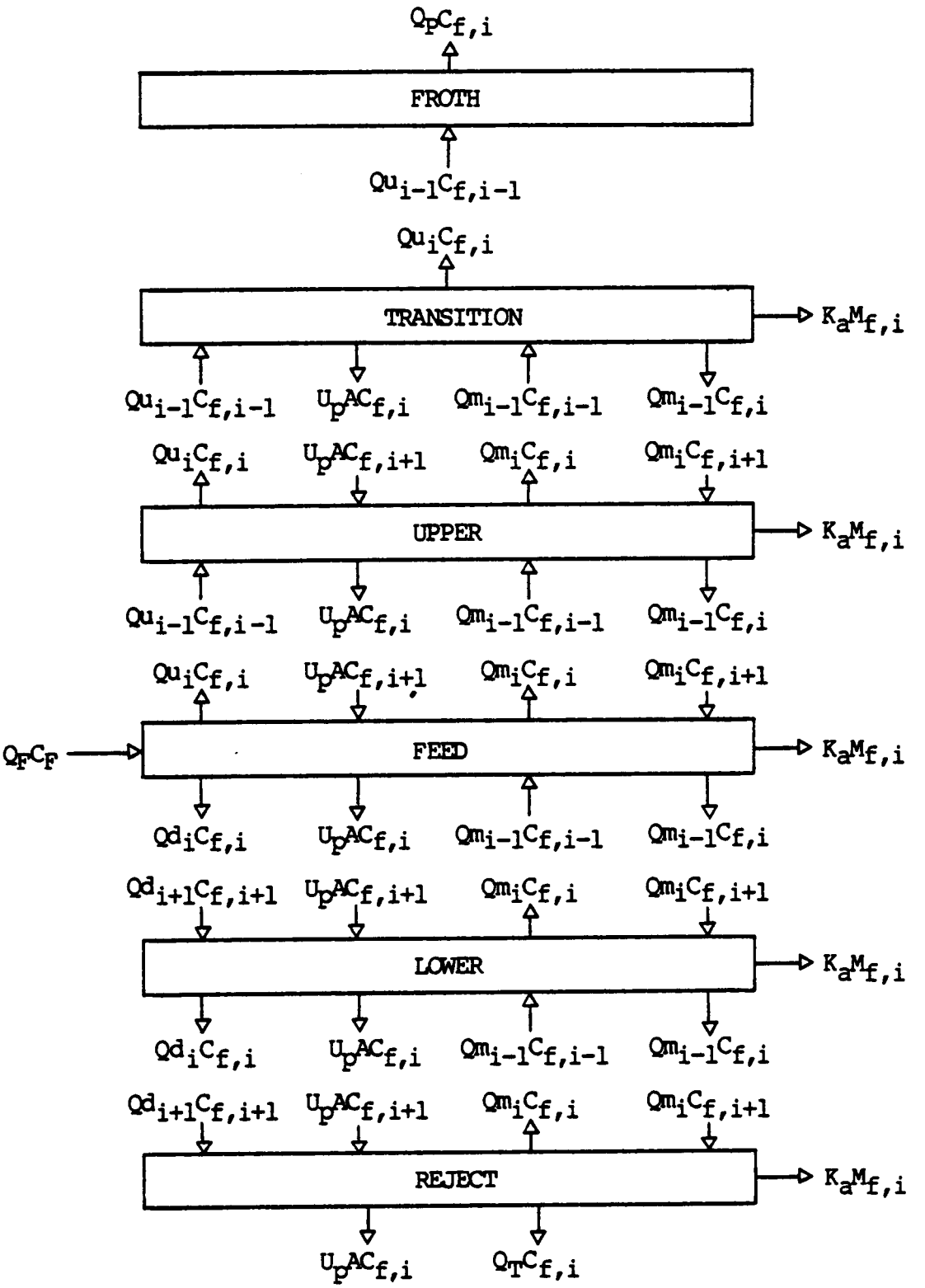

Figure 5.5 Schematic representation of the free solids balance for the column.

When air bubbles are initially introduced during flotation, a strong circulation pattern is developed which disrupts the desired plug-flow behavior of the column, i.e., the column becomes mixed. The extent of mixing appears to depend primarily on the superficial gas velocity, column diameter, gas hold-up, bubble diameter and liquid viscosity (Kato et al., 1972; Joshi and Shah, 1981). Two equal, but opposite, liquid flows develop as a result of the circulation, one upward through the center of the column and a second down along the outside walls of the column. In the present work, the effective liquid flow rate for either of these flows has been represented by Qm. For quantitative purposes, Qm has been made a function of the volumetric flow rate of bubbles passing through a zone (Qb) by the expression:

$$Qm = (M+V_w)Qb, \qquad [5.9]$$

in which V_w is the dimensionless wake volume of the bubble and M is an empirically determined factor used to describe other contributions to mixing.

Because of the circulation within the column, two additional transport terms have been considered in the mass flow balance example of the reject zone. In the model, mixing has been simulated by having a flow of Qm simultaneously enter and exit at the interface of each zone.

The net volumetric flow between zones resulting from this action is zero. However, the net difference between the mass flow of free particles which leave the zone ($Qm_iC_{f,i}$) and the free particles which enter the zone ($Qm_iC_{f,i+1}$) can be substantial. According to Equation [5.9], if the quantity of ($M+V_w$) is zero, the column will behave as plug-flow. On the other hand, a very large value of ($M+V_w$) would result in having the column perfectly mixed. As will be shown later in Section 5.7.1, the effectiveness of the column depends on its ability to remain plug-flow.

The rate of change of free solids in any zone is determined as in the derivation of Equation [5.3] (i.e., accumulation equals the sum of input, output and generation terms). Particle concentrations have been converted to mass by substitution, i.e., $C_{f,i} = M_{f,i}/V_z$. For the reject zone, this procedure yields:

$$\frac{dM_{f,i}}{dt} = [(Qd_{i+1}+U_pA+Qm_i)/V_z]M_{f,i+1} - [(Q_T+U_pA+Qm_i)/V_z-k_a]M_{f,i} \qquad [5.10]$$

A similar procedure has been performed for each of the other zones, the results of which have been given in Table 5.4. Each of these expressions can be solved numerically in conjunction with the air and flow balances previously obtained. This analysis provides a means of determining the total mass flow rate of free solids (coal or ash) leaving

Table 5.4 - Population Balance Equations for Free Solids

Froth:	$dM_{f,i}/dt = [Qu_{i-1}M_{f,i-1} - Q_P M_{f,i}]/V_z$
Transition:	$dM_{f,i}/dt = [(Qu_{i-1}+Qm_{i-1})M_{f,i-1} - (Qm_{i-1}+U_pA+Qu_i)M_{f,i}]/V_z - k_aM_{f,i}$
Upper:	$dM_{f,i}/dt = [(Qu_{i-1}+Qm_{i-1})M_{f,i-1} + (Qm_i+U_pA)M_{f,i+1} - (Qm_{i-1}+U_pA+Qu_i+Qm_i)M_{f,i}]/V_z - k_aM_{f,i}$
Feed:	$dM_{f,i}/dt = Q_FC_F + [Qm_{i-1}M_{f,i-1} + (Qm_i+U_pA)M_{f,i+1} - (Qd_i+U_pA+Qm_{i-1}+Qu_i+Qm_i)M_{f,i}]/V_z - k_aM_{f,i}$
Lower:	$dM_{f,i}/dt = [Qm_{i-1}M_{f,i-1} + (Qd_{i+1}+U_pA+Qm_i)M_{f,i+1} - (Qd_i+U_pA+Qm_{i-1}+Qm_i)M_{f,i}]/V_z - k_aM_{f,i}$
Reject:	$dM_{f,i}/dt = [(Qd_{i+1}+U_pA+Qm_i)M_{f,i+1} - (Q_T+U_pA+Qm_i)M_{f,i}]/V_z - k_aM_{f,i}$

the column as either product or reject, as well as the mass hold-up of solids within any zone in the column.

d) Attached Solids Phase

The same assumptions used in the two other phases are utilized to determine the mass flows of attached particles. As shown in Figure 5.6, the schematic representing the transport between zones of particles attached to bubbles is similar to that of the air balance (Figure 5.4). This is logical since the bubble-particle aggregates are assumed to behave exactly as do free bubbles.

As an example, again consider the balance of terms around the reject zone. The mass flow of attached particles leaving the reject zone consists of those carried out by the tailings flow ($Q_T C_{a,i}$) and those carried upward by the bubbles ($U_b A C_{a,i}$). Attached particles enter the zone either by the downward flow of pulp in the column ($Qd_{i+1} C_{a,i+1}$) or by bubble-particle attachment ($k_a M_{f,i}$). A balance of terms around the reject zone yields:

$$\frac{dM_{a,i}}{dt} = k_a M_{f,i} + [Qd_{i+1} M_{a,i+1} - (Q_T + U_b A) M_{a,i}]/V_z. \qquad [5.11]$$

Expressions for the other zones are given in Table 5.5.

As before, these differential equations can be solved numerically with the air and free solids phases. From the

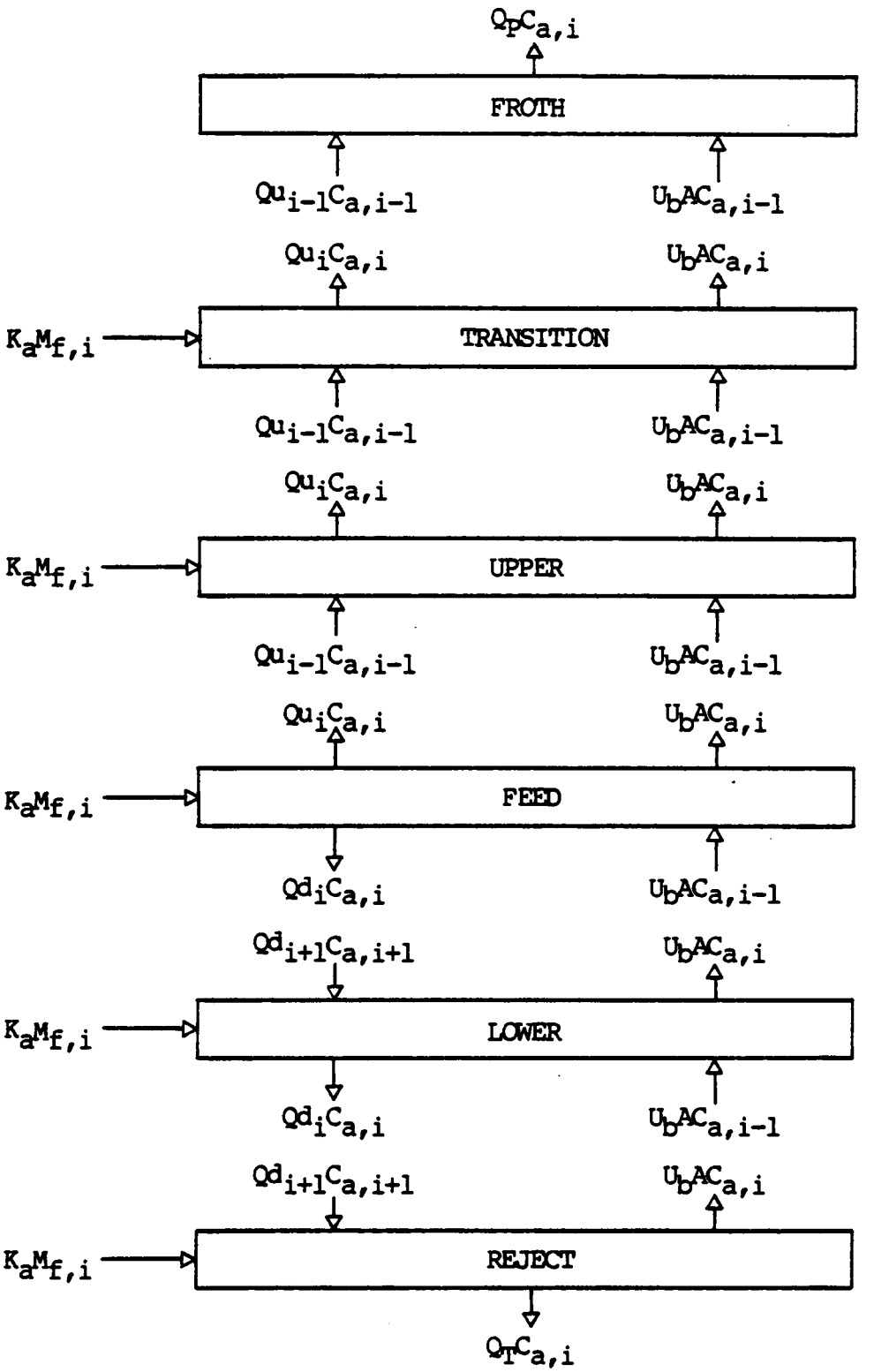

Figure 5.6 Schematic representation of the attached solids balance for the column.

Table 5.5 - Population Balance Equations for Attached Solids

Froth:	$dM_{a,i}/dt = [(Qu_{i-1}+U_bA)M_{a,i-1} - Q_pM_{a,i}]/V_z$
Transition:	$dM_{a,i}/dt = k_aM_{f,i} + [(Qu_{i-1}+U_bA)M_{a,i-1} - (Qu_i+U_bA)M_{a,i}]/V_z$
Upper:	$dM_{a,i}/dt = k_aM_{f,i} + [(Qu_{i-1}+U_bA)M_{a,i-1} - (Qu_i+U_bA)M_{a,i}]/V_z$
Feed:	$dM_{a,i}/dt = k_aM_{f,i} + [U_bAM_{a,i-1} - (Qu_i+Qd_i+U_bA)M_{a,i}]/V_z$
Lower:	$dM_{a,i}/dt = k_aM_{f,i} + [U_bAM_{a,i-1} + Qd_{i+1}M_{a,i+1} - (Qd_i+U_bA)M_{a,i}]/V_z$
Reject:	$dM_{a,i}/dt = k_aM_{f,i} + [Qd_{i+1}M_{a,i+1} - (Q_T+U_bA)M_{a,i}]/V_z$

solution of these equations, the mass flow rate of attached particles leaving the column can be calculated. The total mass flow of coal is determined by the summation of the mass of free and attached coal particles reporting to either the product or reject streams. Combining this solution with a similar analysis for the ash allows both the recovery and grade of the the product and reject streams to be calculated. Other values, such as the percent solids of the product and reject streams, air and liquid flow rates, etc., can also be determined.

Since the population balance model is developed as a function of column geometry and various operating parameters, it can be used for scale-up. The fact that the model is based on the first principles of bubble-particle attachment allows scale-up with no upper limit, provided that a uniform flow of liquid and an even distribution of particles and bubbles are maintained within a given column.

5.5 **Experimental**

Validation of the model was performed using a continuous, laboratory-scale flotation column. A schematic representation of the plexiglas column with appropriate dimensions is shown in Figure 5.7. Tests were performed using a Taggart seam coal sample (36.4% ash) which had been finely pulverized in a stirred ball mill at 40% solids. The

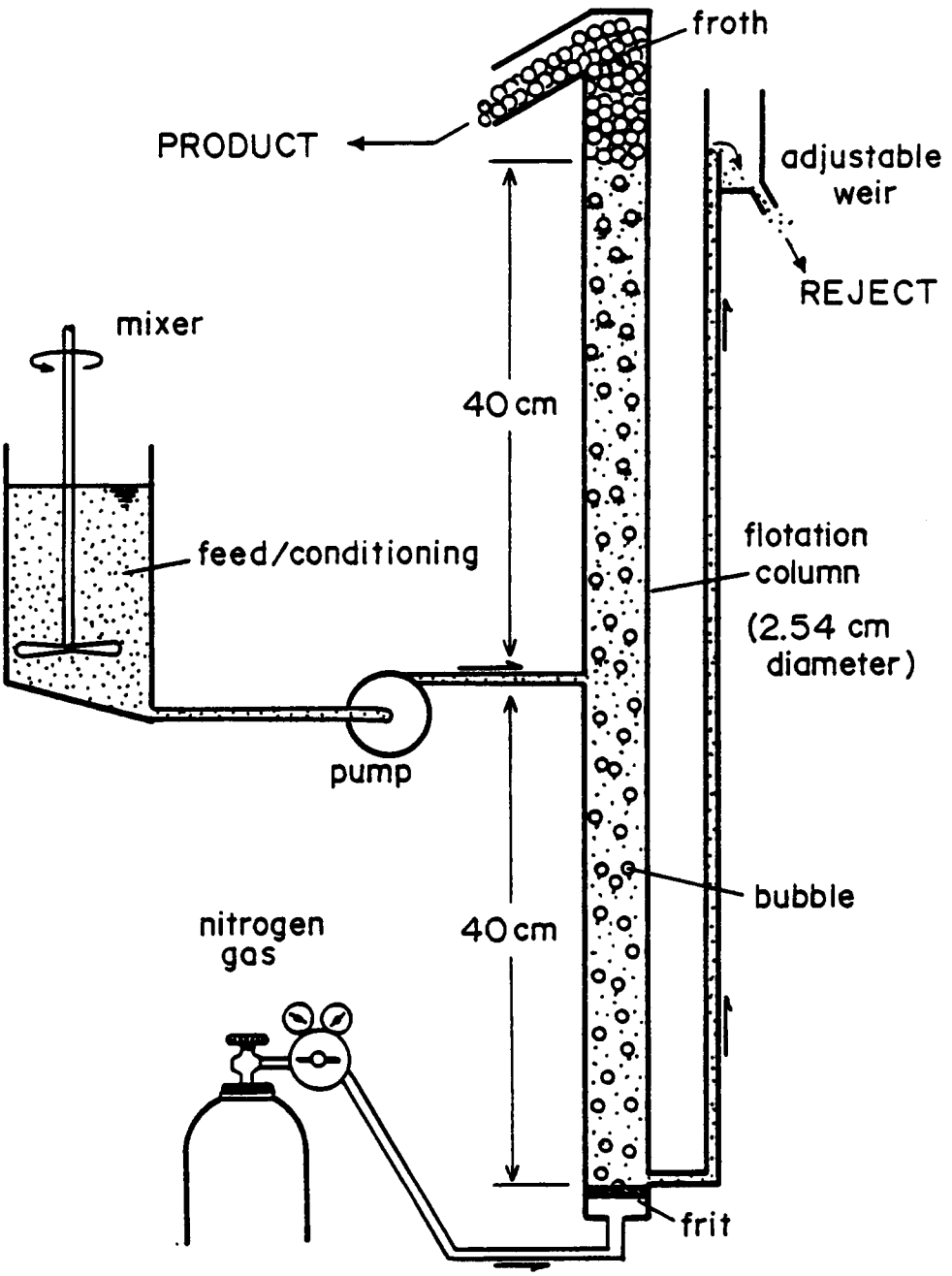

Figure 5.7 Schematic representation of the apparatus employed in the column flotation tests.

mean particle size determined by an Elzone 80-XY particle size analyzer was 5.5 microns. The ground coal slurry was diluted to 5.3% solids in a conditioning tank and fed to the column at 78 ml/min of slurry. A volume of Dowfroth M-150 was added to the feed slurry prior to conditioning to obtain a frother concentration of 4×10^{-4} M. Bubbles were generated using a porous frit (10-15 microns) through which nitrogen gas was passed at a flow rate of 100 ml/min. Bubble size was measured using the photographic technique described in Chapter 3 (Section 3.4.2).

A fixed volume of the froth was taken near the end of the experiment and was used to determine the percentage of solids, liquid and air contained in the froth. From these values, the average thickness of the water film in the froth was back-calculated from Equation [5.6]. The value obtained by this method was found to be 4.9 microns.

Since the model is capable of predicting dynamic behavior, tests were conducted by taking timed samples of the product and reject streams during the course of one hour. The weight of water, solids and percent ash were determined for each sample.

5.6 Results

5.6.1 Estimation of Unknown Parameters

The column simulator program, which is written in

IBM Basic, is included in Appendix II. A step-by-step description of the operation of the program and a sample test run are included in Appendix III. The input data required to run a simulation includes:

i) Bubble and particle diameters
ii) Coal and ash collection probabilities
iii) Air, slurry and wash-water feed rates
iv) Feed coal ash percent
v) Feed slurry percent solids
vi) Average film thickness in froth
vii) Flotation cell geometry
viii) Mixing factor.

If it is assumed that the primary recovery mechanism of ash is by entrainment (i.e., attachment of ash to bubbles is negligible), the only unknown parameters are the probability of collection for the coal and the column mixing factor.

The probability of collection for the coal was determined by trial-and-error. This was accomplished by plotting the steady state values of recovery and ash obtained from simulations as a function of the probability of collection of the coal (Figure 5.8). In this case, the variation in the probability of collection is used as a measure of the hydrophobicity of the coal. The simulated data suggests that as the hydrophobicity of the coal and,

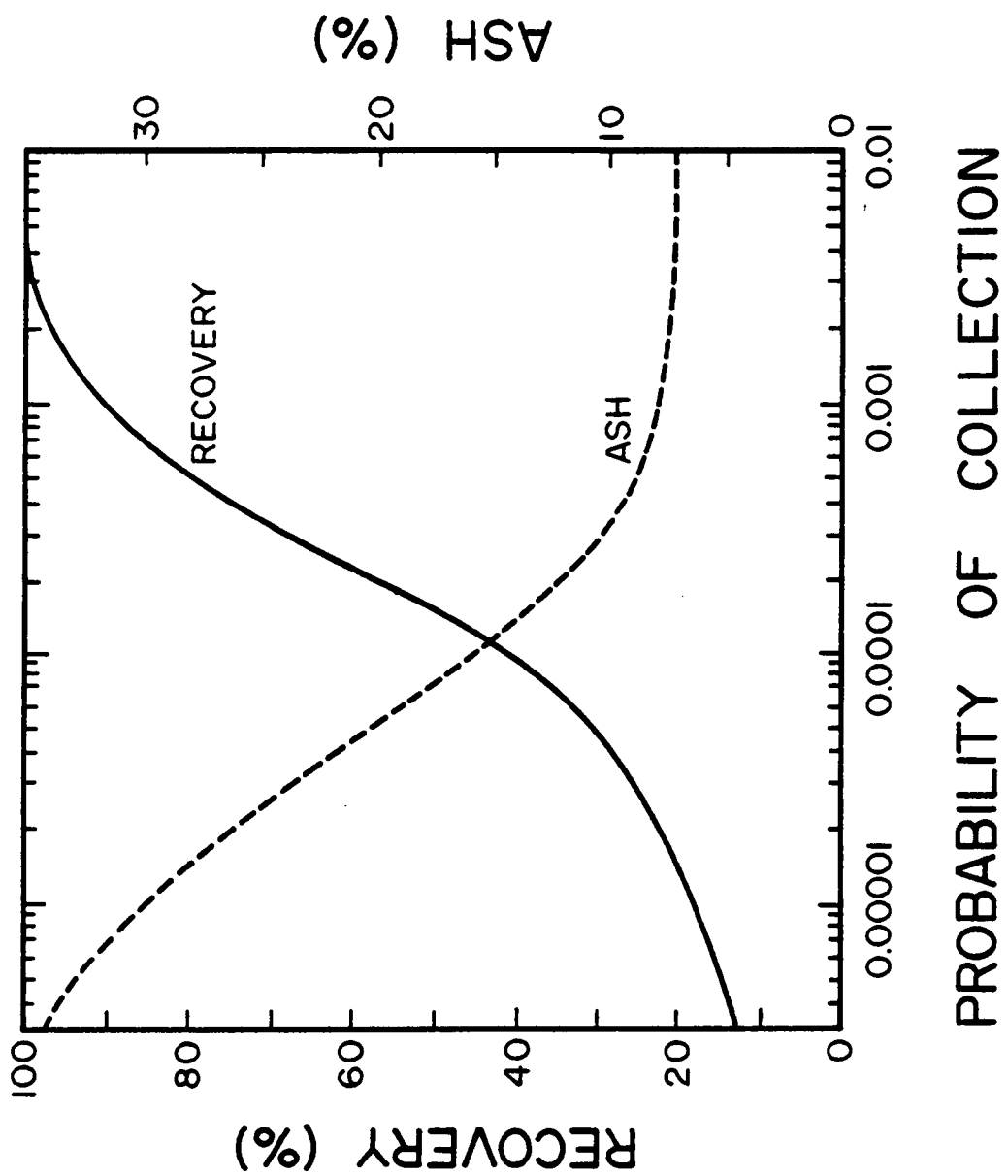

Figure 5.8 Simulated recovery and product ash as a function of the probability of collection.

hence, the probability of collection increases, the recovery of coal and ash rejection steadily increases. At a probability value of approximately 0.001, the recovery begins to reach a maximum value and the product ash levels off at about 7%. For the froth film thickness specified (which dictates the rate of water recovery), the simulation suggests that this is the minimum content of ash which can be achieved without taking steps to reduce the problem of fine particle entrainment. The use of 0.00028 as the value of the probability of collection in the simulation gave the recovery and product ash values which are close to the experimental values (i.e., the simulation gave a product recovery of 65.4% and 10.8% ash, while the experimental values are 64% and 10.4%, respectively). The fact that both the recovery and ash content can be predicted by the same value of P may be taken to prove the validity of the model.

The next step required is to determine the mixing factor (M). A mixing factor of 0 would indicate plug-flow through the column, whereas a very high value would correspond to perfectly mixed conditions. Figure 5.9 shows the simulated recovery of coal versus time as functions of different mixing factors. The recovery of coal reaches steady state very quickly, usually within the first few minutes. The degree of mixing appears to have little effect on the overall recovery of coal.

However, as shown in Figure 5.10, the degree of mixing

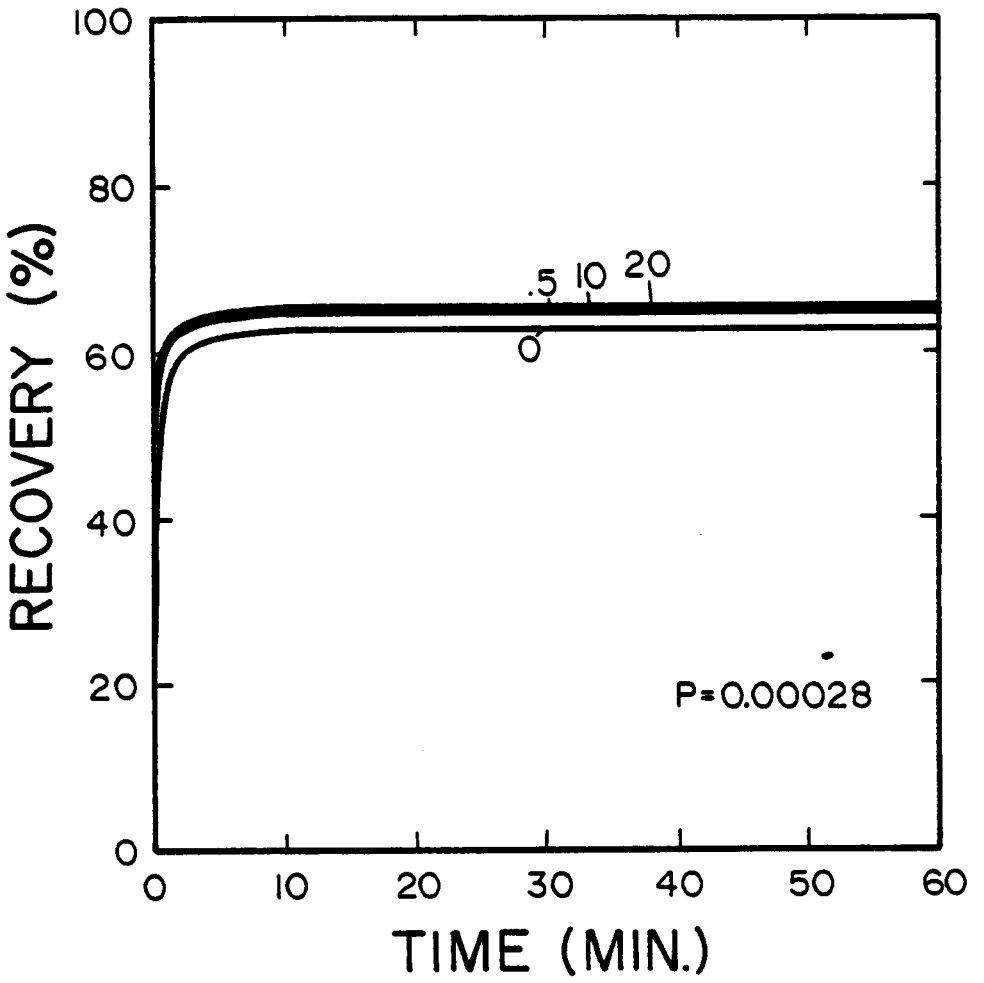

Figure 5.9 Dynamic simulation of recovery for a range of mixing intensities assuming P=0.00028.

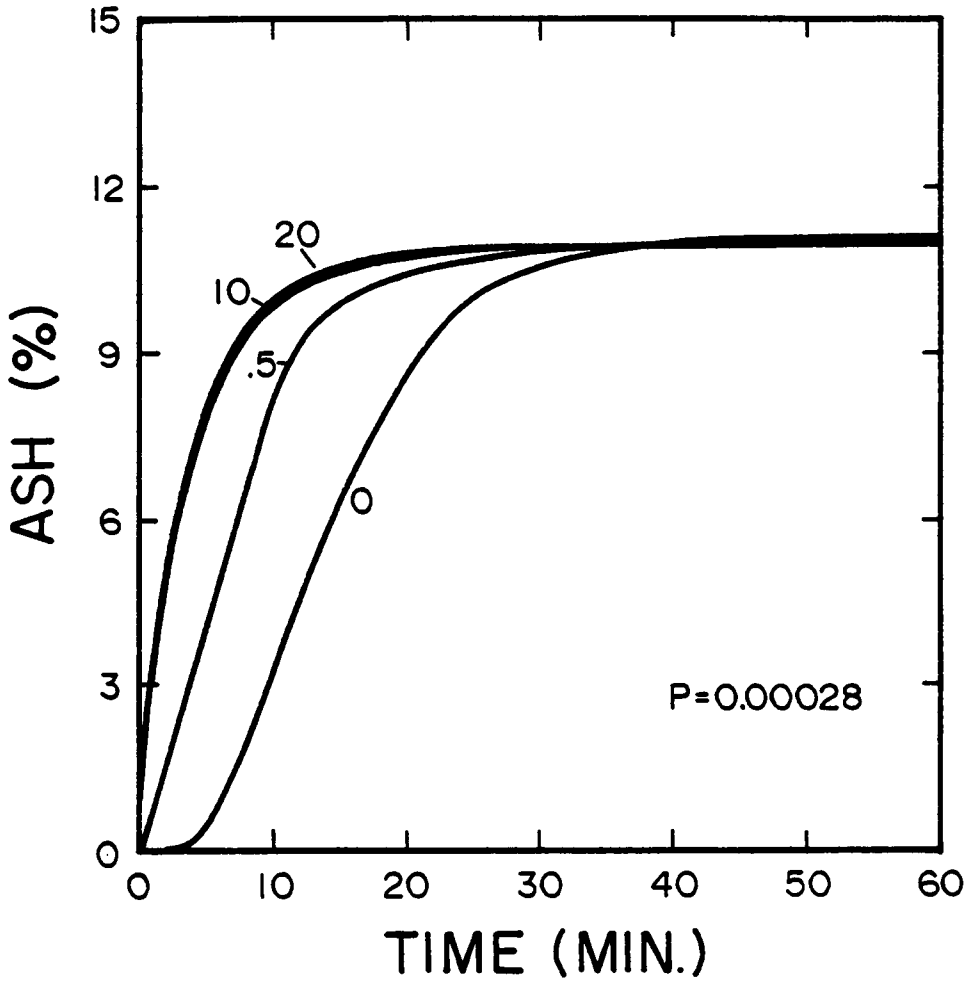

Figure 5.10 Dynamic simulation of product ash for a range of mixing intensities assuming P=0.00028.

in the column has a great effect on the dynamic behavior of the product ash. When highly mixed, the ash content in the product requires nearly 15 minutes to reach steady state. When operating under plug-flow conditions, nearly 40 minutes of operation are required before achieving steady state. A mixing factor of approximately 0.5 was required to fit the experimentally obtained ash values as a function of time. This suggests that the column was operating between plug-flow and well-mixed conditions. It is also interesting to note that the simulated results suggest that the same steady state value of ash is obtained regardless of the intensity of mixing. This finding is important since it allows the steady state recovery and ash values to be predicted without knowledge of the intensity of column mixing.

5.6.2 Comparison of Experimental Data and Model Predictions

After determining the necessary parameters (P and M) for the model, a series of simulations were performed for comparison against the experimental data. Figure 5.11 shows both the simulated (solid line) and experimental (points) recovery of coal as a function of flotation time. The predictions from the simulator correlate reasonably with the experimental results. As shown in Figure 5.12, the change in the product ash content with time is also well represented by the simulator.

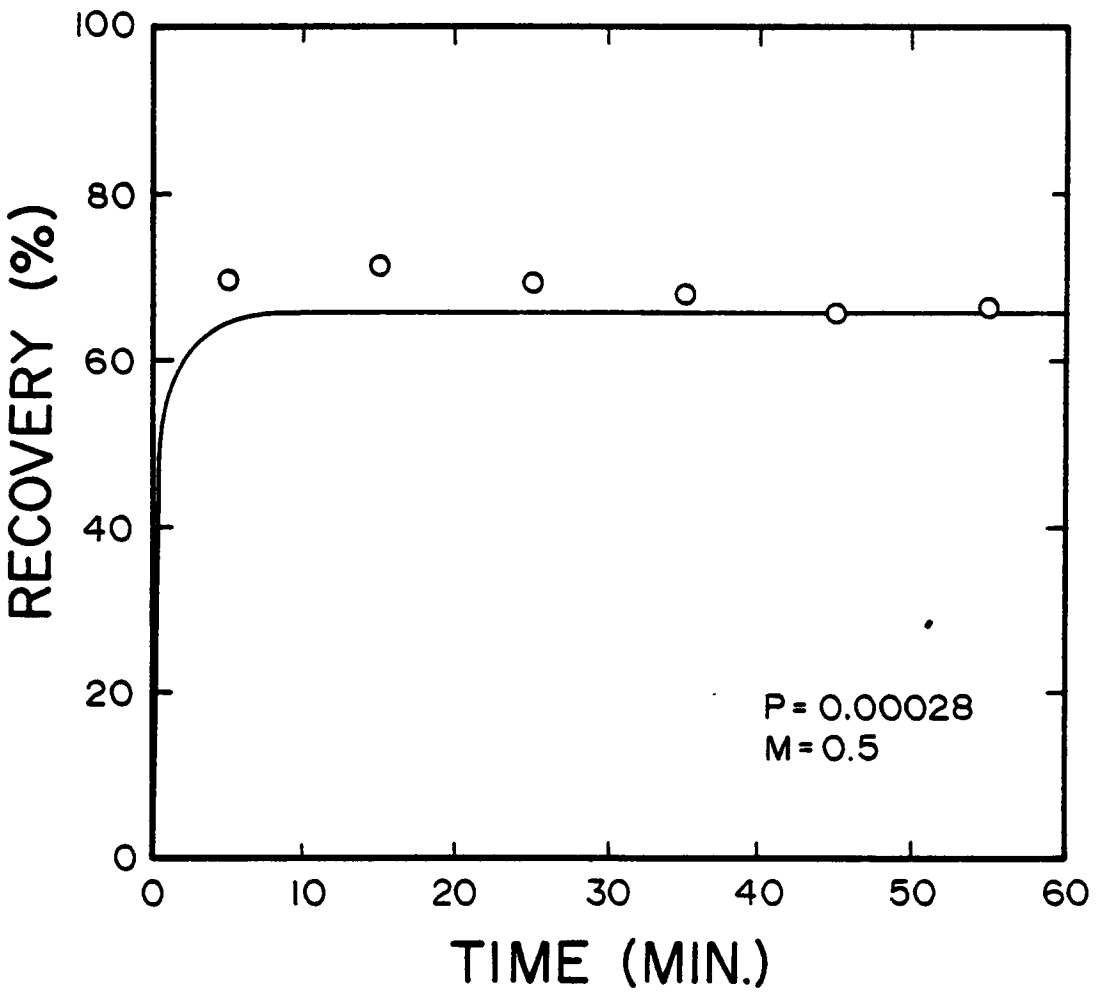

Figure 5.11 Comparison of the experimental (points) and simulated (solid line) recovery as a function of time.

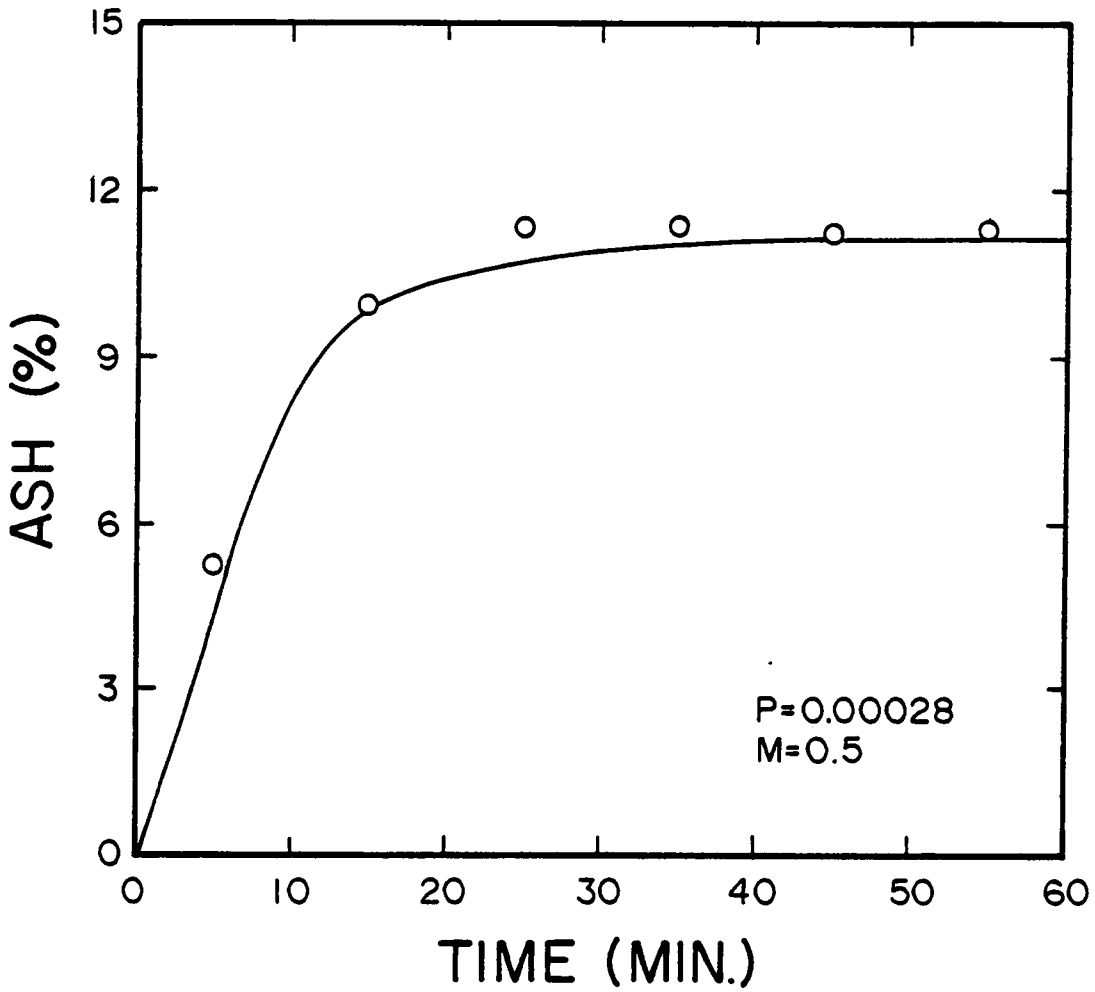

Figure 5.12 Comparison of experimental (points) and simulated (solid line) product ash as a function of time.

In addition to recovery and ash, the model can be used to predict the percent solids of each of the product streams. The percent solids recovered in the product as a function of time is shown in Figure 5.13. Although the steady state values predicted by the simulator are in reasonably close agreement with the experimental data, the dynamic values differ substantially. As shown in Figure 5.14, the major cause for the difference between the experimental and predicted values is the high water recovery obtained during the first half of the flotation experiment. A possible explanation for this behavior is the influence of solids on the froth. As the experiment proceeds, a higher concentration of solids appears in the froth which may adversely affect the froth stability, resulting in an increase in froth drainage. The loss of frother by adsorption on the coal may also partly account for this result. Nevertheless, the steady state prediction of percent solids is quite good, most likely due to the fact that the froth film thickness used in the simulator was determined during this period of the experiment. A much improved dynamic fit should be possible if froth film thickness measurements were made during the entire length of the flotation test.

The major contributor to the recovery of fine ash particles is entrainment. As a result, it has been found in

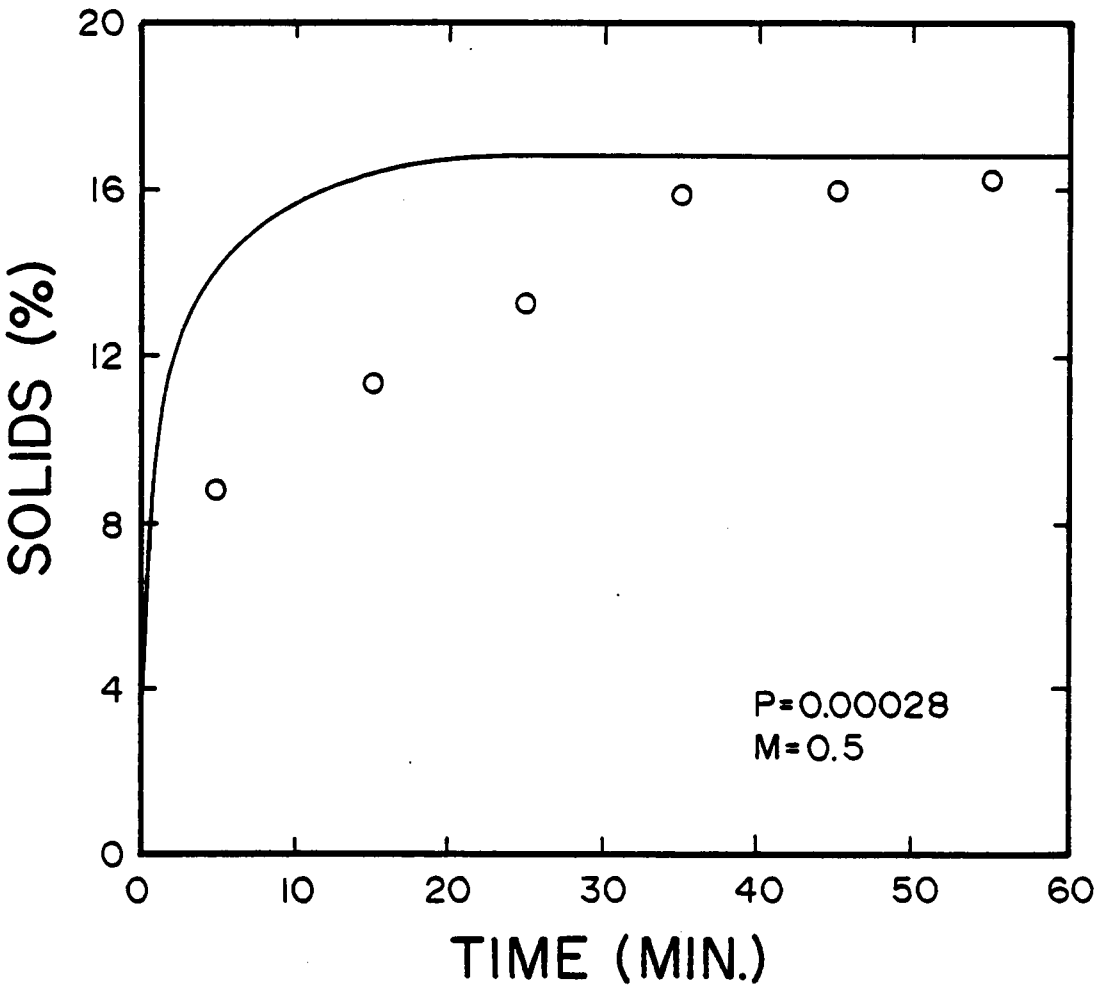

Figure 5.13 Comparison of experimental (points) and simulated (solid line) product percent solids as a function of time.

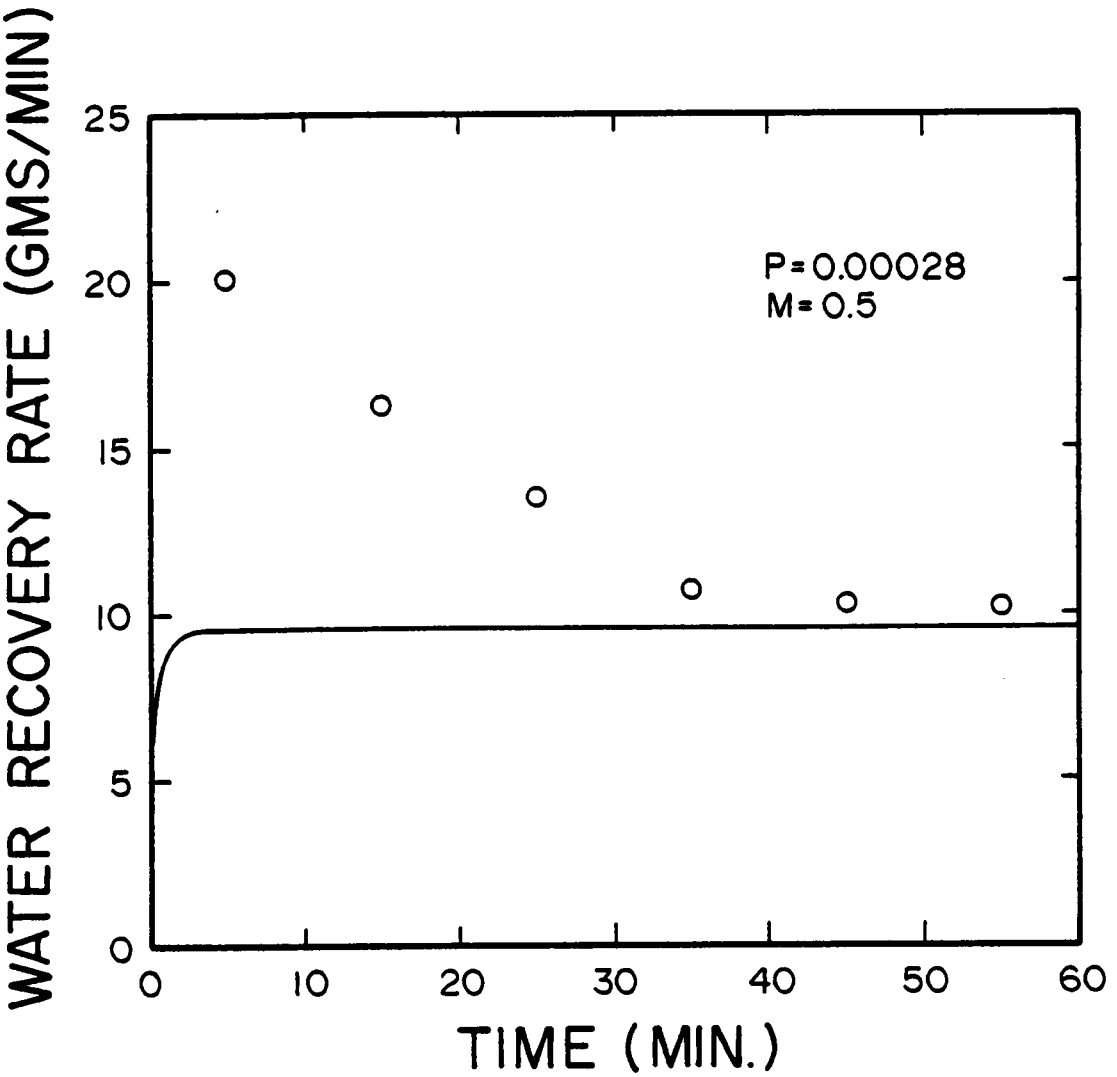

Figure 5.14 Comparison of experimental (points) and simulated (solid line) product water recovery rate as a function of time.

many cases that the recovery rate of ash is directly related to the recovery rate of water in the product. A correlation of this type is shown in Figure 5.15 where hypothetical lines have been drawn through the data obtained at various time increments. In essence, the slope of each of these lines indicates the concentration of ash per unit of water contained within the column. The concentration increases with time, and eventually reaches a steady value for times greater than about 35 minutes. In Figure 5.16, a similar plot has been made for the coal. The recovery rate of coal at zero water recovery indicates the amount of coal recovery purely by bubble-particle attachment. For the data shown, this value corresponds to approximately 1.56 gms/min. The slope of this line also indicates the concentration of coal in the cell, and suggests that steady state is reached much more quickly for coal.

5.7 **Discussion**

Although the model has been tested against a limited amount of data, the results obtained in the present work suggest that the model is successful in predicting the flotation of fine particles in a column. The major advantage of the model is to be able to independently examine the influence of operational parameters on the performance of the flotation column. Several important

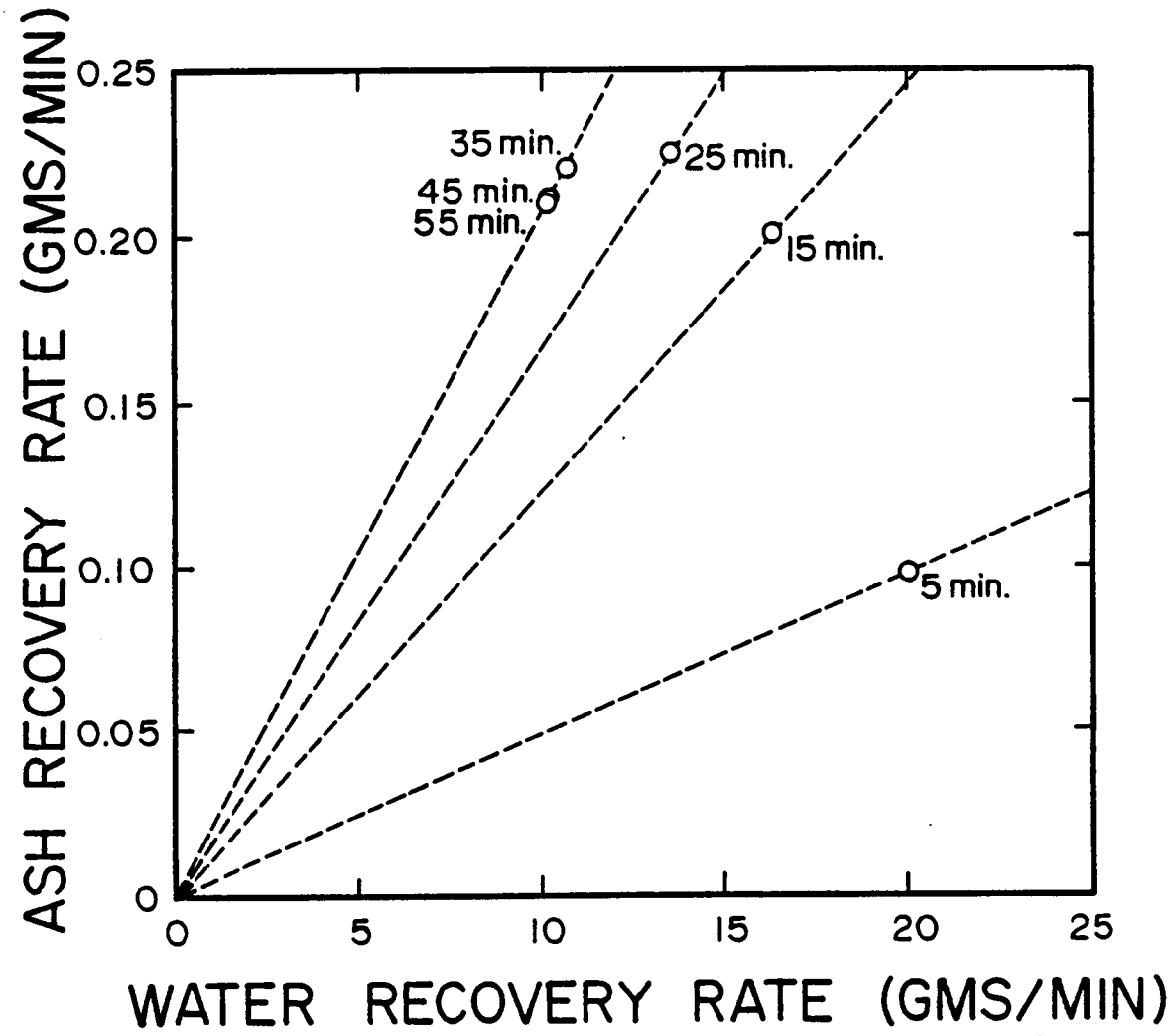

Figure 5.15 Variation in the ash recovery rate versus water recovery rate as a function of time.

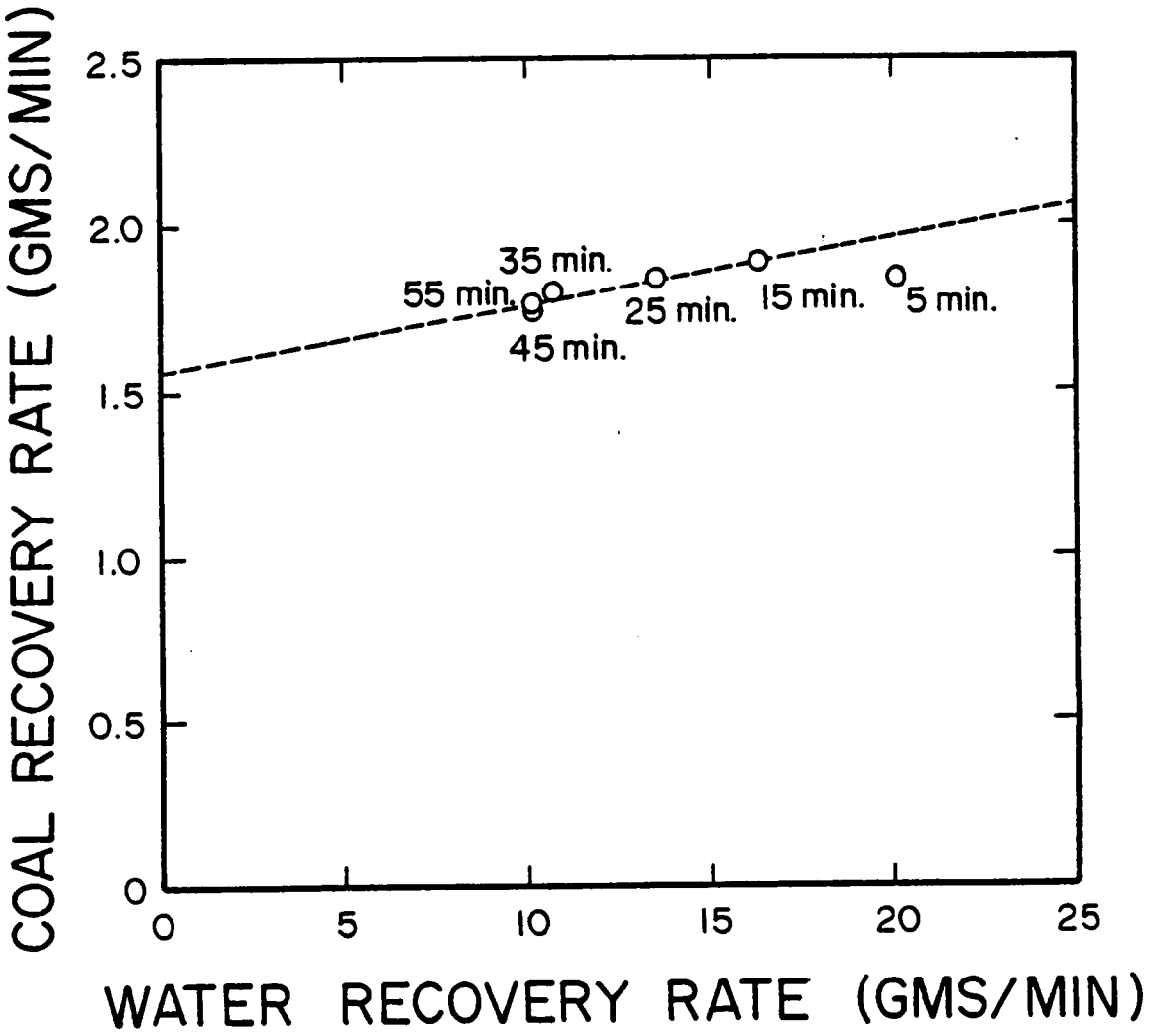

Figure 5.16 Variation in the coal recovery rate versus water recovery rate as a function of time.

parameters are examined in further detail in the following discussion.

5.7.1 Model Predictions

a) Effect of Hydrophobicity

In the present work, the critical rupture film thickness (H_c) has been taken as the measure of the hydrophobicity of the coal to be floated. Since the value of H_c is not known, however, the simulation was carried out by assuming values of P. The results given in Figure 5.8 shown that both the recovery and ash content change profoundly with P. Since the results shown in Figure 5.8 have been obtained using identical bubble and particle sizes, changes in P essentially reflect changes in H_c. Therefore, increasing the hydrophobicity is shown to increase both the recovery and ash rejection, althought the extent of ash rejection is limited by entrainment.

b) Effect of Feed Percent Solids

As shown in Figure 5.17, the model predicts no change in the recovery of coal or ash rejection by changing the percent solids of the feed slurry. Coal flotation experiments conducted as a function of percent solids have, however, in some cases resulted in a significant change in

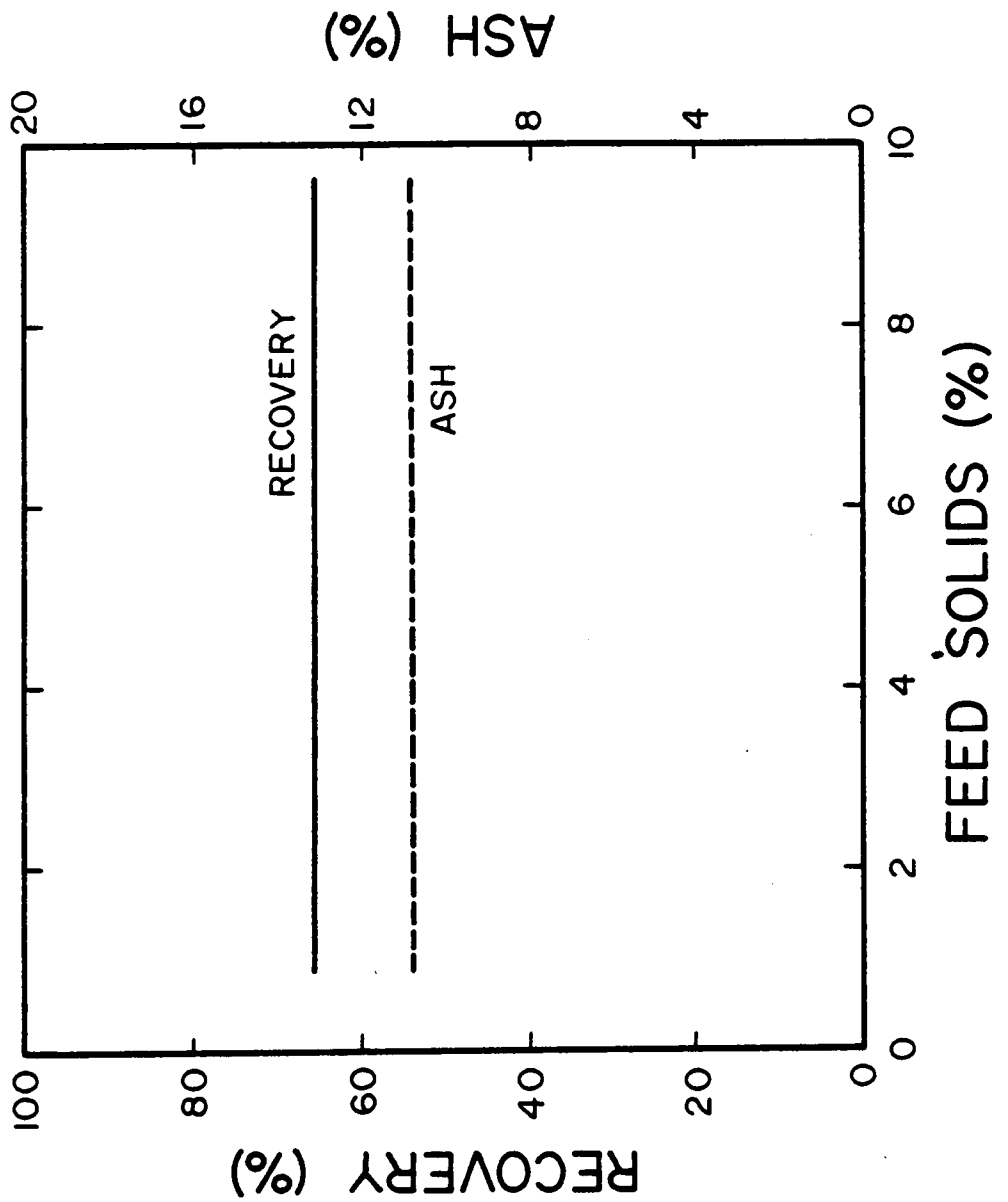

Figure 5.17 Simulated effect of feed percent solids on the product recovery and ash.

the product ash content (Keyser, 1986). The reason for this difference may be attributed to the interdependence of variables in flotation. In the model, a change in percent solids has no influence on the other operational parameters. On the other hand, changing the percent solids during experimental testing may substantially alter the flotation conditions such as reagent concentrations.

c) Effect of Air Flow Rate

It is well known that the recovery of particles can be increased by using a higher flow rate of air through the flotation cell. However, this procedure also tends to result in a higher product ash content. Figure 5.18 shows the results of simulations in which the air flow rate has been increased while maintaining all other factors constant. The observed improvement in recovery is caused by an increase in the number of bubbles available for collision in the cell. For a fixed froth film thickness, the increased number of bubbles also results in a rapid rise in water recovery which increases the flow of entrained ash into the product. Therefore, as expected, increasing the air flow increases recovery, but adversely affects the product ash content.

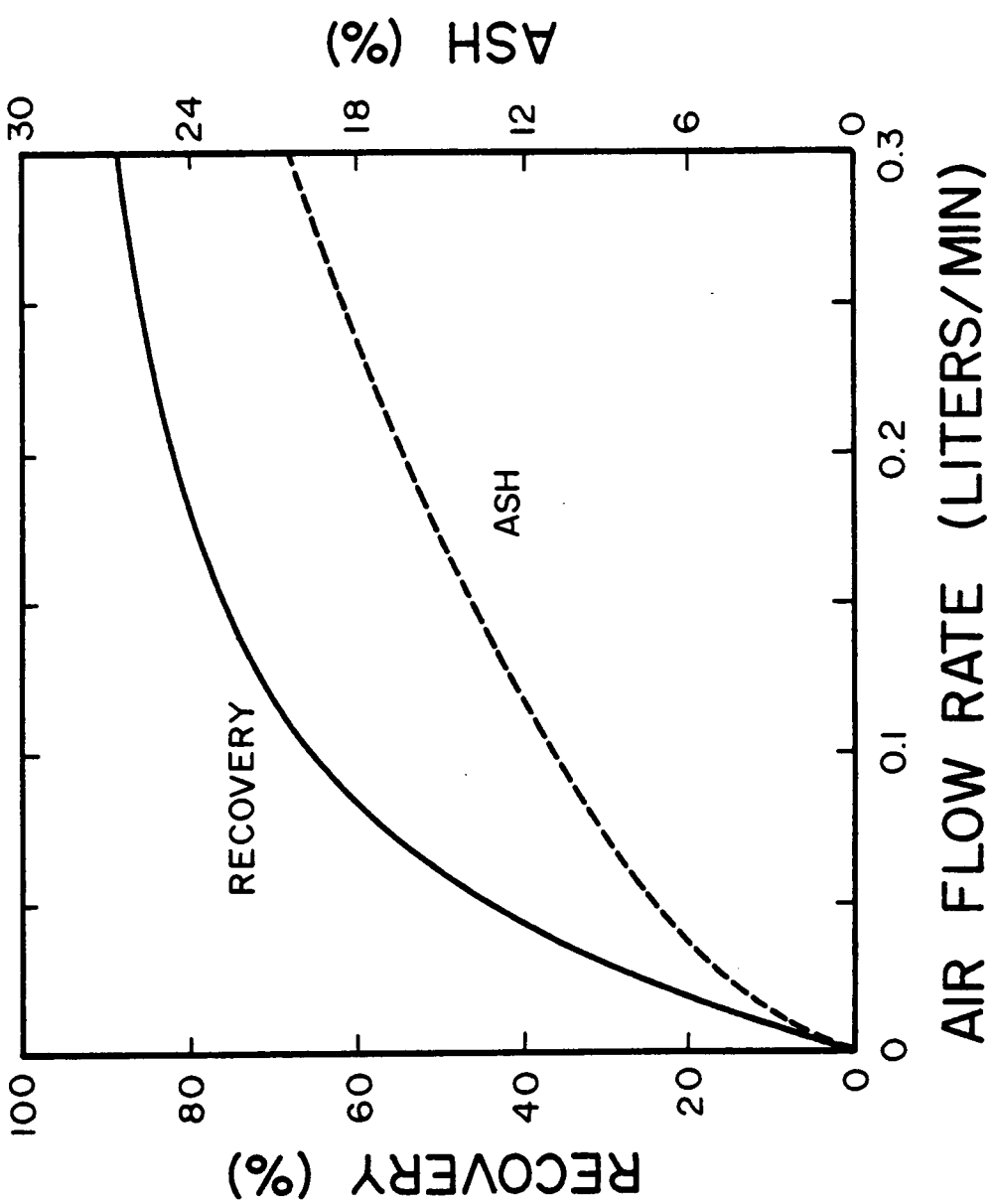

Figure 5.18 Simulated effect of air flow rate on the product recovery and ash.

d) Effect of Bubble Size

A great deal of interest has been shown lately regarding the effect of bubble size on the recovery of fine particles. In Chapters 2 and 3, theoretical and experimental results show that the recovery of coal increases rapidly with decreasing bubble size. In addition, evidence has been presented to suggest that selectivity also increases with decreasing bubble size. In order to more closely examine the effect of bubble size on flotation response, a series of model simulations was carried out as a function of bubble diameter. The appropriate values of the probability of collection for each bubble size were determined using the theoretical data given in Figure 2.17.

The simulated results shown in Figure 5.19 demonstrate the dramatic increase in coal recovery as bubble size is reduced. This trend occurs as a result of the increasing probability of collection of coal with decreasing bubble size. It is shown that the ash content of the product also decreases with decreasing bubble size until a bubble diameter of approximately 250 microns is reached. Below this bubble size, the ash content tends to increase with decreasing bubble size. This phenomenon has previously been discussed in Chapter 3 (Section 3.5.2), and has been explained by the combined effects of increasing water recovery and increasing coal recovery with decreasing bubble

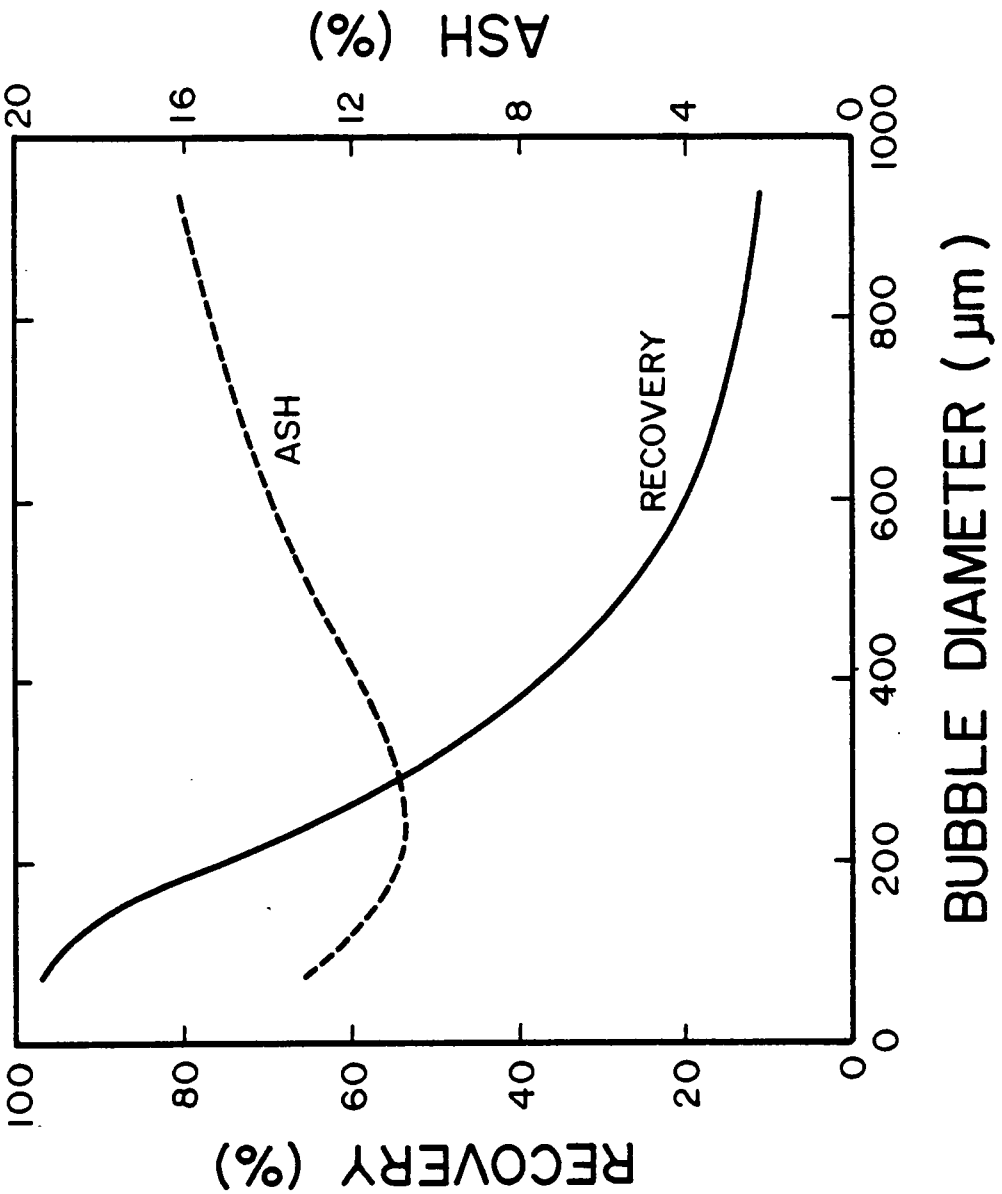

Figure 5.19 Simulated effect of bubble diameter on the product recovery and ash.

size.

e) Effect of Froth Film Thickness

Figure 5.20 shows the effect of changing the value of the froth film thickness on the recovery and ash content. As the froth becomes dryer (the froth film thickness decreases) the proportion of feed water reporting to the product is reduced. A direct result of the decrease in the water recovery rate is a corresponding decrease in the rate of recovery of entrained ash. Thus, the ash content of the product decreases with decreasing froth film thickness. Since coal and ash can both be entrained into the froth, a decrease in coal recovery is also observed as the froth film thickness is decreased.

f) Effect of Column Height

A significant parameter in the design of a column flotation machine is the height of the column. In order to study the effects of column height more closely, a series of simulations was run in which the total height of the column was varied. During the simulations, the feed point to the cell was maintained at a fixed distance from the top of the column. The results of the simulations (Figure 5.21) demonstrate the dramatic influence that column height has on the overall performance of the flotation column. The

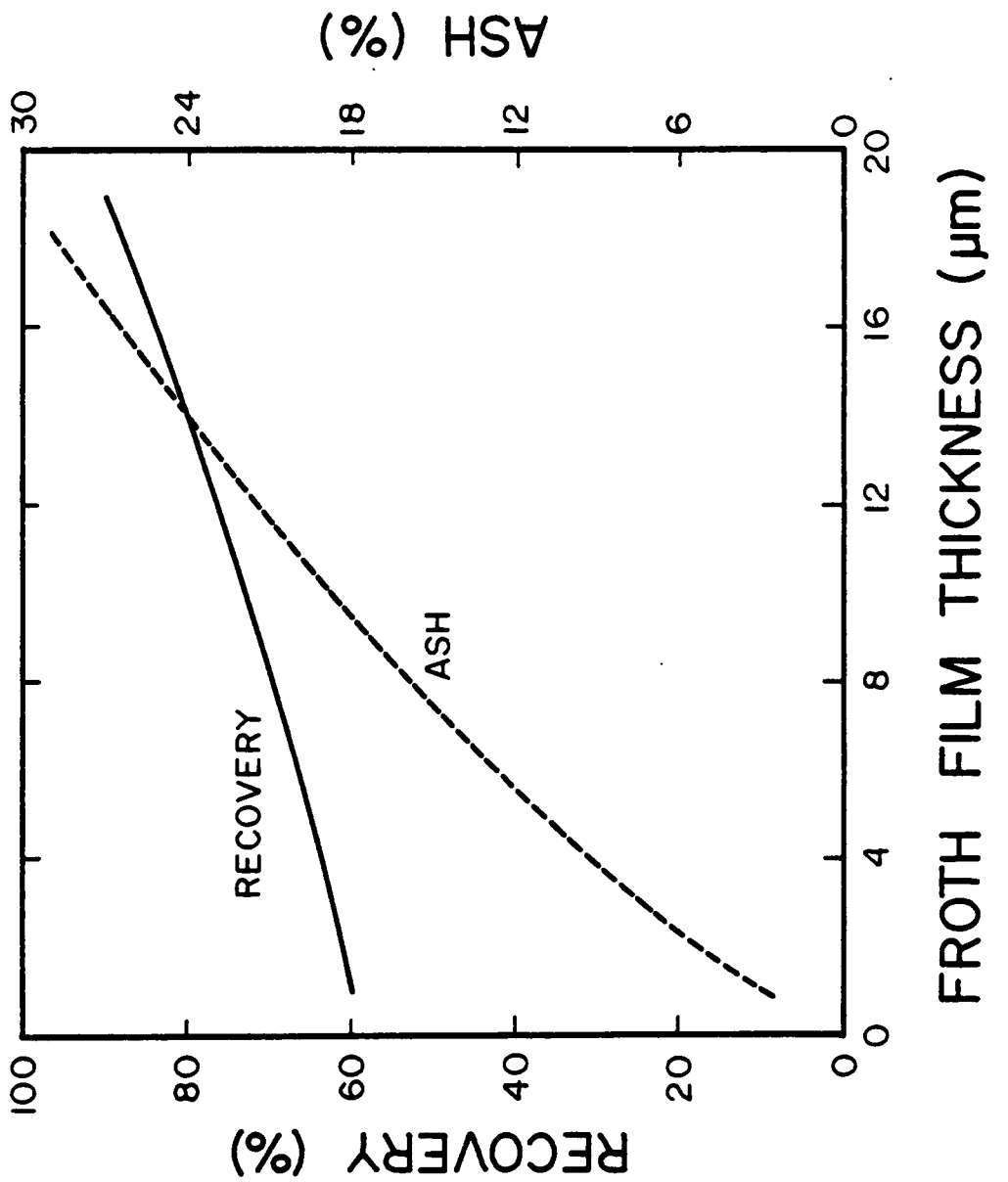

Figure 5.20 Simulated effect of froth film thickness on the product recovery and ash.

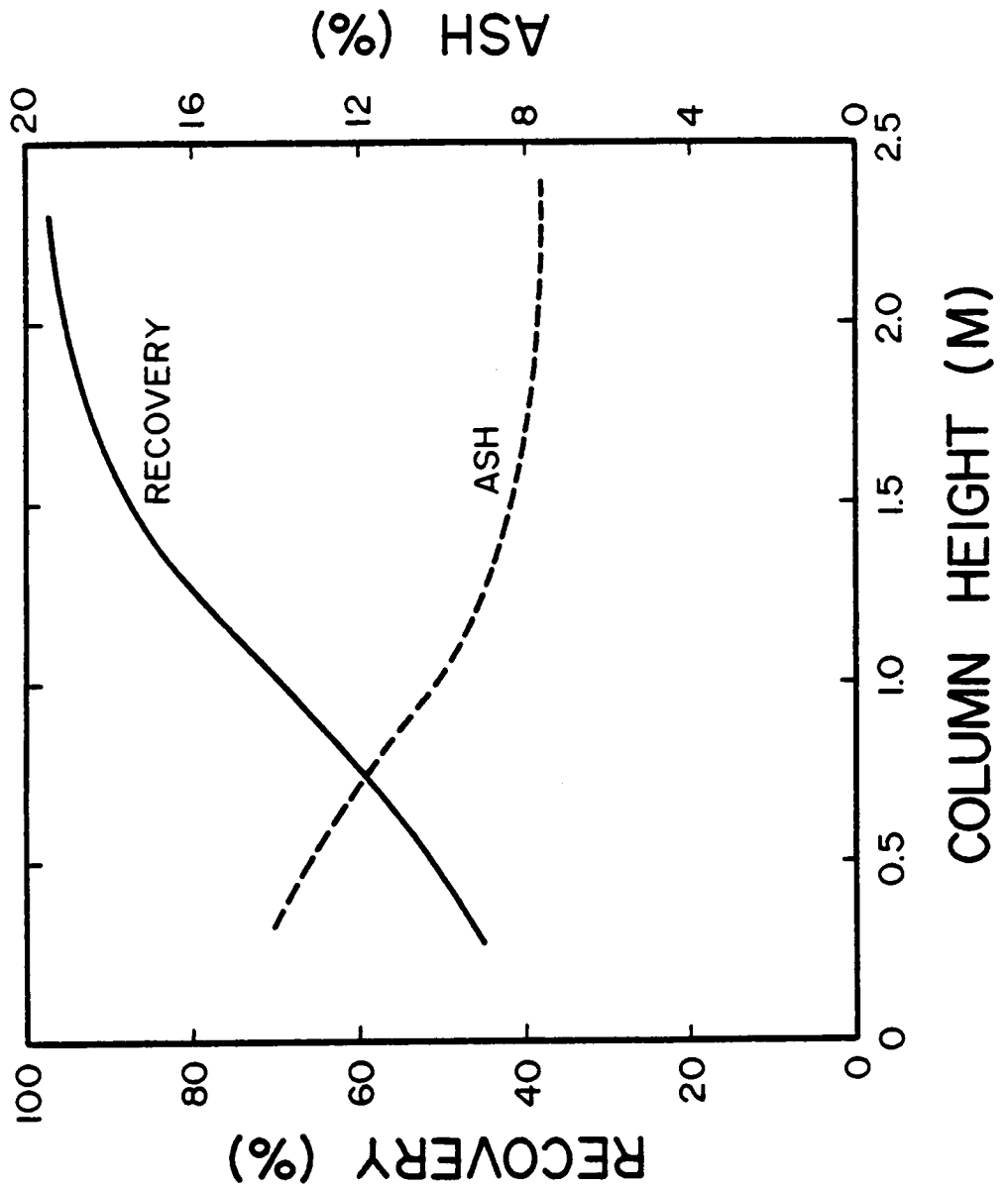

Figure 5.21 Simulated effect of column height on the product recovery and ash.

observed behavior is explained as follows. As the column height is increased, the retention time of paticles is increased correspondingly for a given feed rate. Since recovery is a function of particle retention time, the longer column results in a higher recovery. The drop in the ash content as column height is increased is due to the increase in the recovery rate of coal for a fixed recovery rate of ash. For the column studied in the present work, a column height of at least 2 meters should have been employed in order to achieve the best possible results. Note however, that as with previous examples, improvements in the product ash content begin to diminish upon reaching the maximum recovery of the coal. Once again, the extent of ash rejection is limited by entrainment.

g) Effect of Wash Water

One of the primary advantages claimed by the creators of the column flotation machine is the ability to prevent the entrainment of fine gangue particles by using a counter flow of wash water. Figure 5.22 shows the results of two sets of simulations in which this possibility has been investigated. In the first series of simulations, the normal mixing level (M=0.5) has been employed. As shown, the wash water has a dramatic effect on the product ash content, essentially eliminating ash recovery at flows

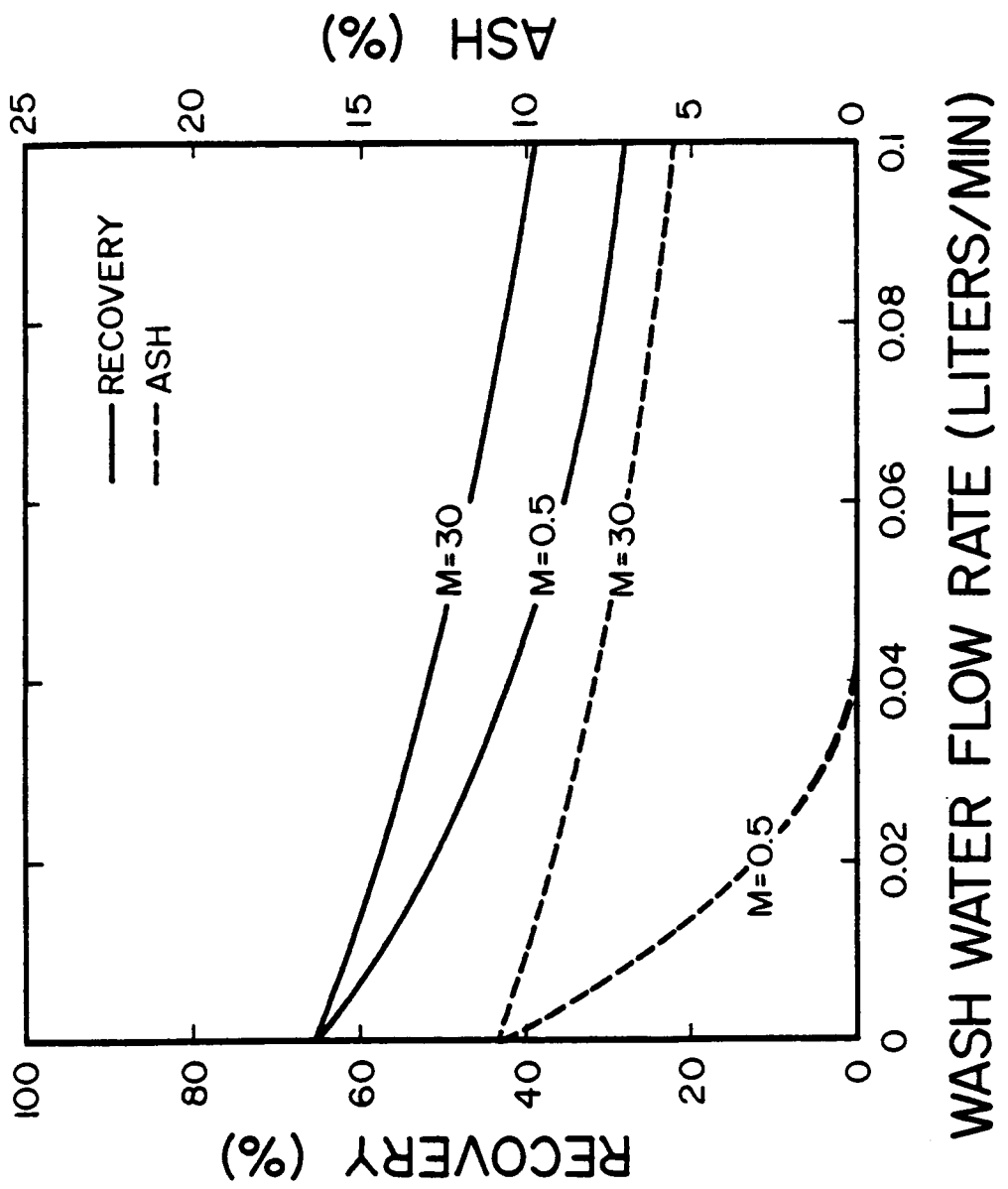

Figure 5.22 Simulated effect of wash water flow rate on the product recovery and ash for high (M=30) and low (M=0.5) mixing intensities.

greater than about 0.04 liters/min. However, a significant drop in the recovery of coal also occurs. Two reasons can be cited for the decrease in coal recovery. First, since both free coal and free ash particles can be entrained, there is a significant loss of free coal particles when entrainment is prevented. Secondly, the higher downward flow of wash water decreases the effective residence time of particles in the column. Furthermore, the increased flow of water tends to increase the percentage of bubbles which are washed out the bottom of the column in the reject stream.

A second series of simulations were performed under identical conditions, only for a higher degree of mixing (M=30). As shown in Figure 5.22, the increased intensity of mixing decreased the effectiveness of the wash water stream with only a minimal decrease in the ash rejection. Since a significant portion of free particles are still recovered by entrainment, the effect of the wash water on the coal recovery was not as large.

5.7.2 **Optimum Column Design**

According to the results of simulations, a number of important conclusions can be drawn regarding the design and operation of column flotation machines. The responses predicted by the simulator for changes in the various operating parameters are summarized in Table 5.6. The

Table 5.6 - Effect of Increasing Various Process Variables on the Recovery and Product Ash

Manipulated Variable	Recovery	Product Ash
Hydrophobicity	Large (+)	Large (-)
Percent Solids	(0)	(0)
Air Flow Rate	Large (+)	Large (+)
Bubble Diameter	Large (-)	Small (+)
Froth Film Thickness	Small (+)	Large (+)
Column Height	Large (+)	Large (-)
Wash Water	Small (-)	Large (-)

results suggest that the variables which have the greatest potential for improving recovery are hydrophobicity, air flow rate, bubble size and column height. On the other hand, the variables having the largest influence on ash rejection are hydrophobicity, bubble size, column height and wash water addition.

The results shown in Figure 5.8 demonstrate that in order to obtain the best possible recovery, the hydrophobicity of the coal should be as high as possible. This justifies the use of collectors such as kerosene for coal flotation. However, the extent of increase in hydrophobicity is limited. In most cases, other methods will be required in order to obtain high recoveries.

The simulation results show that a decrease in bubble size yields both an increase in coal recovery and improved ash rejection. However, the ash rejection reaches a maximum at approximately 250 microns for the specific example given in the present work. Below the optimum, a further decrease in bubble size results in a slight increase in the ash entrainment brought on by a higher recovery rate of water. Although this finding suggests that the best results would be obtained at this optimum bubble size, the benefits derived from the increase in recovery obtained with very small bubbles are much greater than the small increase in ash below this bubble size. Without using small bubbles,

the height of the column necessary to obtain high recoveries of very fine particles would most likely be prohibitive. For example, if the same height to diameter ratio were maintained for a 1 meter diameter column as that required to obtain the best results with the 2.54 cm column, a column height of nearly 100 meters would be required. Furthermore, the real advantage of using small bubbles may be found in the fact that the degree of mixing can be reduced. As shown in Figure 5.22, the wash water becomes less effective as the column becomes more mixed. The use of small bubbles creates conditions closer to plug flow, which is an essential requirement for the column to operate efficiently.

Once the maximum possible recovery has been achieved, improvements in the product grade can only come by preventing the entrainment of fine particles into the froth. With the exception of wash water addition (Figure 5.22), the simulation results suggest that all other methods studied have an ash rejection level which is limited by entrainment. Therefore, it is suggested that sufficient wash water be added to the column to prevent entrainment, while bubble size and column length be used to maximize coal recovery. If wash water is to be effective, the column must be operated as close to plug-flow conditions as possible. The introduction of baffles along the length of the column may help inhibit mixing, and is suggested as a possible area for further study.

5.8 Summary and Conclusions

1) A population balance model has been developed which allows predictions to be made with regard to the influence of operational parameters and column design on flotation performance.

2) Unlike previous attempts at modeling flotation processes, the model developed in the present work is based on first principles of bubble-particle attachment. As a result, the model is well suited for scale-up and process optimization.

3) One of the major advantages of the model is its ability to independently examine the effect of individual operational parameters on flotation response, a difficult or impossible task in experimental testing. As such, the model provides an excellent tool for gaining additional insight into the characteristic behavior of the column.

4) A method was presented for determining from experimental data the two unknown parameters in the model, i.e., the probability of collection (P) for coal and the mixing factor (M). Using these values, the model simulations were found to agree well with experimental results

obtained using a 2.54 cm diameter flotation column.

5) Some of the parameters investigated in the present work include coal hydrophobicity, feed percent solids, gas flow rate, bubble size, froth film thickness, column height and wash water addition. Optimum performance appears to be possible by using sufficient wash water to prevent entrainment, while smaller bubbles and increased column height are used to obtain high recoveries.

Chapter 6

SUMMARY

The results of the present investigation may be summarized as follows:

1. Using a stream function developed in the present work, an analytical expression has been derived for the probability of collision (P_c) between a particle and bubble for Reynolds numbers appropriate in flotation. The expression demonstrates that the inefficiency of fine particle flotation is a direct consequence of the low value of P_c for small particles. According to the expression, the most effective method for improving the effectiveness of fine particle flotation is by reducing the size of bubbles used during flotation.

2. In addition to P_c, the stream function developed in the present work has allowed the probability of adhesion (P_a) to be calculated from induction time (T). The expression indicates that the value of P_a rapidly increases with decreasing particle size, and is relatively independent of the hydrophobic condition of the particle. This finding suggests that the selective flotation of fine particles would be very difficult. However, the expression for P_a was derived assuming that T is independent of physical parameters, such as bubble

and particle size. A theoretical evaluation of induction time has found the contrary to be true, which makes the conclusions drawn by this analysis ambiguous.

3. Because of the problems involved with the determination of P_a using the concept of induction time, a new model has been developed in which the probability of collection (P) is shown to be a function of the critical rupture thickness (H_c) of the intervening film between the particle and bubble. This relationship has been derived by numerically simulating the trajectory of a particle around a bubble and determining the closest approach distance between them. This model shows that P increases with increasing particle size, decreasing bubble size, and increasing H_c (which is a measure of the hydrophobicity of the particle). Values of P determined experimentally were found to correlate well with predictions from this model.

4. A simple model of the flotation process has been developed using the probability of collection evaluated from first principle concepts. For very hydrophobic particles, an expression for the first-order flotation rate constant has been derived by assuming that the probability of collection (P) can be approximated by the probability of collision (P_c). This analysis suggests that the flotation rate constant increases exponentially

with increasing particle size and decreasing bubble size, the exponent changing with Reynolds number (Re). The proposed model has been successful in predicting the power relationship between the flotation rate constant (k) and bubble size.

5. Another expression for flotation rate has been derived by considering the entrainment of particles within the turbulent wake behind a rising bubble. This expression suggests that flotation selectivity can be improved by decreasing the bubble size and increasing column height.

6. Flotation experiments conducted in the present work demonstrate that smaller bubbles improve both the recovery and selectivity of fine particle flotation. The improved recovery is a result of the increased probability of collision for small bubbles, whereas the improved selectivity is a result of the lower degree of turbulence and increased rate of attachment of hydrophobic particles to small bubbles. However, when using bubble sizes that are too small, selectivity tends to be reduced, which is probably due to increased water recovery associated with the increased surface area of smaller bubbles.

7. Using the theoretical expression for the flotation rate constant, a population balance model has been developed

to describe the flotation of fine particles in a column. Because the model has been developed using first principles, it should prove to be useful in scale-up, simulation, optimization and process control. Based on this model, a computer simulator has been developed. The simulator has been used to study the effects of various operational parameters on flotation response. Simulation results suggest that optimum column performance can be achieved by using sufficient wash water to prevent fine particle entrainment, while smaller bubbles and taller columns are used to maintain an adequate level of recovery. Model predictions have been found to be in reasonable agreement with experimental results obtained using a laboratory scale flotation column.

Chapter 7

RECOMMENDATIONS FOR FURTHER STUDY

From the information gathered in the present work, further investigation into the following areas is suggested.

1. The importance of the froth phase in the determination of the final product grade has been known for some time (Watson and Grainger-Allen, 1974; Cutting and Devenish, 1975). The secondary concentration of particles brought on by bubble coalescence and the entrainment of fine particles in the lamella between bubbles can have a drastic influence on flotation performance. However, little research has been performed in the last two decades to analyze and quantify these phenomena. An investigation to determine froth behavior as functions of particle size, particle hydrophobicity, reagent addition, temperature, etc., should prove to be informative. The population balance model presented in the present work may be improved by incorporating a more realistic description of the froth into the model.

2. According to the results of the present work, the use of smaller bubbles during flotation can improve the efficiency of floating fine particles. The factor having the greatest influence on bubble size is frother concentration (Miagkova, 1956; Bennett et al., 1958).

However, increasing the concentration of frother also increases the film thickness of liquid surrounding bubbles in the froth (Waksmundzki et al., 1972). As shown in the present work, an increased film thickness results in an increased water recovery and decreased product grade. Thus, the development of techniques for the generation of small bubbles without using high surfactant concentrations would be desirable.

3. Because the critical rupture thickness of the thin film between a bubble and particle is the parameter which directly controls flotation recovery and selectivity, fundamental studies directed toward improving the understanding of this phenomena would be valuable. One area particularly lacking research is the development of general methods for the estimation of the critical rupture thickness from the principles of surface chemistry.

4. Simulations performed using the column population balance model have shown the importance of entrainment in fine particle flotation. Additional studies directed toward quantifying the fluid flow characteristics within the flotation cell would be useful for design, optimization and scale-up of industrial flotation columns. In particular, the influence of column height, diameter, gas flow rate, bubble size, etc., on the

internal mixing behavior of the column would be beneficial.

5. Since the effectiveness of flotation continuously decreases with decreasing particle size, excessive grinding should be avoided. For this reason, studies regarding the liberation characteristics of ash and sulfur bearing minerals should be considered as a means of directly determining the extent of grinding necessary and for estimating cleaning potential of various coals.

6. Should extensive grinding be required, one method of improving flotation recovery and selectivity would be to increase the effective size of particles by techniques of coagulation/flocculation. Theoretical studies of this phenomena may be possible using the concepts of DLVO theory.

REFERENCES

Adamson, A.W., 1976. Physical Chemistry of Surfaces, 3rd Ed., Wiley-Interscience, New York, N.Y., pp. 698.

Adorjan, L.A., 1982. "Mineral Processing," Mining Annual Review, p. 239.

Anfruns, J.P. and Kitchener, J.A., 1976. "The Absolute Rate of Capture of Single Particles by Single Bubbles," in Flotation, A.M. Gaudin Memorial Volume, Vol. 2, (M.C. Fuerstenau, ed.), AIME, New York, N.Y., p. 625.

Anfruns, J.P. and Kitchener, J.A., 1977. "The Rate of Capture of Small Particles in Flotation," Trans. Inst. Mining & Metall., Vol. 86, Section C., p. C9.

Anon., 1963. "The Flotation Column," Canadian Mining Journal, August, 1963.

Anon., 1966. "Flotation Column Due for Mill Scale Tests," Engrg. Mining J., Vol. 166, No. 1, p.76.

Aplan, F.F., 1976. "Coal Flotation," in Flotation, Vol. 2, (M.C. Fuerstenau, ed.), AIME, New York, N.Y., p. 1235.

Arbiter, N. and Harris, C.C., 1962. "Flotation Kinetics," in Froth Flotation, 50th Anniversary Volume, p. 215.

Bahr, A., Ludke, H. and Mehrhoff, F.-W., 1982. "The Development and Introduction of a New Coal Flotation Cell," Proceedings, XIV International Mineral Processing Congress, October 17-23, Toronto, Canada.

Bascur, O.A. and Herbst, J.A., 1982. "Dynamic Modeling of a Flotation Cell with a View Toward Automatic Control," Proceedings, XIV Inter. Mineral Processing Congress, Toronto, Canada, October 17-23.

Bennett, A.J.R., Chapman, W.R. and Dell, C.C. 1958. "Studies in Froth Flotation of Coal," Proceedings, Third International Coal Preparation Congress, Brussels-Leige, June, Paper E2.

Bethell, P.J. and Sell, F.R., 1983. "The Availability of Very Low Ash Coal for Coal-Based Fuels," Proceedings, Fifth International Symposium on Coal Slurry Combustion and Technology, Tampa, FL, April 25-27, 1983, p. 238.

Blake, T.D., 1973. "Current Problems in the Theory of Froth Flotation," Proceedings, Joint Meeting on Bubbles and Foams, Symposium of the Varfahrenst. Gesell. in VDI, Nuremberg; Chemical Engineer, Vol. 182, p. 117.

Bogdanov, O.S., 1947. Non-Ferrous Metals, Moscow, No. 2, p. 662.

Bogdanov, O.S. and Filanovskij, M.S., 1940. "Adhesion of Mineral Particles to Air Bubbles," J. Phys. Chem. USSR, Vol. 14, No. 2, p. 244.

Boron, D.J. and Kollrack, R., 1983. "Prospects for Chemical Coal Cleaning," Proceedings, 1983 Society of Mining Engineers Fall Meeting, Salt Lake City, Utah, Oct. 19-21, 1983.

Boutin, P. and Wheeler, D.A., 1967a. "Column Flotation Development Using an 18 Inch Pilot Unit," Can. Mining J., Vol 94, p. 101.

Boutin, P. and Wheeler, D.A., 1967b. "Column Flotation," World Mining, Vol. 67, p. 50.

Brenner, H., 1964. Chemical Engrg. Sci., Vol. 19, p. 703.

Brown, D.J., 1962. "Coal Flotation," in Froth Flotation, 50th Anniver. Vol., (D.W. Fuerstenau, ed.), AIME, New York, N.Y., p. 518.

Brown, D.J., 1965. "A Photographic Study of Froth Flotation," Fuel Soc. J., Vol 16, p. 22.

Bull, W.R., 1966. "Rate of Flotation of Mineral Particles in Sulfide Ores," Proceedings, Australian Inst. Min. Metall., Vol 254, p. 69.

Burgess, L.E., McGarry, P.E., Herman, D.E. and Koppelman, L.N., 1983. "The AFT Beneficiation System," Presentation, 5th Inter. Symp. on Coal Slurry Combustion and Technology, April 25-27, Tampa, FL.

Choi, W.Z., 1986. Personal Communication. Department of Mining & Minerals Engineering, Virginia Polytechnic Institute and State University, Blacksburg, Virginia, 24061.

Cliff, R.C., Grace, J.R. and Weber, M.E., 1978. Bubbles, Drops and Particles, Academic Press, New York, N.Y., p. 27.

Coffin, V.L., 1982. "Column Flotation at Mines Gaspe," Proceedings, XIV International Mineral Processing Congress, October 17-23, Toronto, Canada.

Collins, G.L. and Jameson, G.J., 1976. "Experiments on the Flotation of Fine Particles - The Influence of Particle Size and Charge," Chem. Engrg. Sci., 31, p. 985.

Coutanceau, M., 1968. "Mouvement Uniforme D'une Sphere dans L'axe D'un Cylindre Contenant un Liquide Visqueux," J. de Mecanique, Vol. 7, No. 1, p. 4.

Cutting, G.W. and Devenish, M., 1975. "A Steady-State Model of Flotation Froth Structures, Proceedings, Annual Meeting Amer. Inst. Mining Engrs., New York, N.Y., Preprint No. 75-B-56.

Davis, E.G., Hansen, J.P. and Sullivan, G.V., 1980. "Attrition Microgrinding," in Fine Particles Processing, Vol. 1, (P. Somasundaran, ed.), Amer. Inst. Mining Engrs., New York, N.Y., p. 74.

Davis, W.J.W., 1964. "The Development of a Mathematical Model of the Lead Flotation Circuit at the Zinc Corporation Limited," Trans. Aust. Inst. Mining & Metall., Vol 212, p. 61.

Derjaguin, B.V. and Dukhin, S.S., 1961. "Theory of Flotation of Small and Medium Size Particles," Trans. Inst. Mining & Metall., Vol. 70, p. 221.

Deryagin, B.V., Dukhin, S.S. and Rulev, N.N., 1976. "Importance of the Hydrodynamic Interaction in the Flotation of Fine Particles," Inst. Colloid & Water Chem., USSR, Vol. 38, No. 2, p. 227.

Deryagin, B.V., Dukhin, S.S., Rulev, N.N. and Semenov, V.P., 1976. "Influence of Bubble Surface Blocking on the Hydrodynamic Interaction With Paticles in the Elementary Act of Flotation," Inst. Colloid & Water Chem., USSR, Vol. 38, No. 2, p. 233.

Deryagin, B.V. and Dukhin, S.S., 1979. "Kinetic Theory of the Flotation of Fine Particles," Proceedings, 13th International Mineral Processing Congress, (J. Laskowski, ed.), Warsaw, June 4-9, 1979, p. 21.

De Vivo, D.G. and Karger, B.L., 1970. "Studies in the Flotation of Colloidal Particulates: Effects of Aggregation in the Flotation Process," Separ. Sci., Vol. 5, p. 145.

Dobby, G.S. and Finch, J.A., 1985. "Particle Size Dependence in Flotation Derived from a Fundamental Model of the Capture Process," 114th Annual Meeting of SME-AIME, New York, Preprint No. 85-124, 10 pp.

Dobby, G.S. and Finch, J.A., 1986. "Flotation Column Scale-up and Modelling," Can. Inst. Mining Bulletin, Vol 79, No. 889, p. 89.

Dukhin, S.S. and Rulev, N.N., 1977. "Hydrodynamic Interaction Between a Solid Spherical Particle and a Bubble in the Elementary Act of Flotation," Colloid Science, USSR, Vol. 39, No. 2, p. 231.

Eigeles, M.A. and Volova, M.L., 1960. "Kinetic Investigation of Effect of Contact Time, Temperature and Surface Condition on the Adhesion of Bubbles to Mineral Surfaces," Proceedings, 5th Inter. Mineral Processing Congress, Inst. Mining & Metall., London, p. 271.

Flint, L.R. and Howarth, W.J., 1971. "The Collision Efficiency of Small Particles with Spherical Air Bubbles," Chem. Engrg. Sci., 26, p. 1155.

Fonda, A. and Herne, H., 1957. U.K. National Coal Board, , Mining Research Establishment, Report No. 2068.

Frumkin, A., 1931. "O Javlenijach Smacivanija i Prilipanija puxyr'kov," Z. Fix. Chimii, Vol. 12, p. 337.

Fuerstenau, D.W., 1980. "Fine Particle Flotation," in Fine Particle Processing, Vol. 1, (P. Somasundaran, ed.), Amer. Inst. Mining Engrs., New York, N.Y., p. 669.

Fuerstenau, D.W., Harper, R.W. and Miller, J.W., 1970. "Hydroximate Versus Fatty Acid Flotation of Iron Oxide," Trans. Amer. Inst. Mining Engrs., Vol. 247, p. 69.

Fuorie, P.J.E., 1977. "Beneficiation of Fine Coal in the Republic of South Africa, Proceedings, 3rd Symposium on Coal Preparation, Louisville, KY, Oct. 1977, p. 96.

Garcia, Z.H., 1935. "Flotation Recovery is an Exponential Function of Time," Bol. Soc. Mac. Min., Santiago, Vol. 47, p. 83.

Gaudin, A.M., Groh, J.O. and Henderson, H.B., 1931. "Effect of Particle Size on Flotation," Amer. Inst. Mining Engrs., Tech Publ., Vol. 414, p. 3.

Gaudin, A.M., 1932. Flotation, McGraw Hill Book Company, New York, N.Y.

Gaudin, A.M., Schuhmann, R. and Schlechten, A.W., 1942. "Flotation Kinetics, II. The Effect of Size on the Behavior of Galena Particles," J. Phys. Chem., Vol. 46, p. 902.

Gochin, R.J. and Solari, J.A., 1983. "Dissolved Air Flotation for Recovery of Fine Cassiterite," Trans. Inst. Mining Metall., Vol. 92.

Goren, S.L. and O'Neill, M.E., 1971. "On the Hydrodynamic Resistance to a Particle of a Dilute Suspension when in the Neighborhood of a Large Obstacle," Chem. Engrg. Sci., Vol. 26, p. 325.

Gray, R.J., Schapiro, N., and Coe, G.D., 1963. "Distribution and Forms of Sulfur in a High-Volatile Pittsburgh Seam Coal," Trans. Soc Mining Engrs, Vol. 226, p. 113.

Green, P., 1982. "Chemical Cleaning Makes Super-Coal," Coal Age, Vol. 87, No. 4, April, p. 80.

Hall, E.H., et al., 1981. "Use of Coal Cleaning for Compliance with SO_2 Emission Regulations," U.S. Environmental Protection Agency R&D Project Summary, EPA-600/S7-81-146, Oct. 1981.

Halsey, G.S., Yoon, R.H., and Sebba, F., 1982. "Cleaning of Fine Coal by Flotation Using Colloidal Gas Aphrons," Proceedings, Technical Program, International Powder and Bulk Solids Handling and Processing, Rosemont, Illinois, May, 1982, p. 67.

Halvorsen, W.J., 1979. "New Developments in Froth Flotation in U.S.A.," Aufbereitungs - Technik., Vol 5, p. 243.

Hamielic, A.E., Hoffman, T.W. and Ross, L.L., 1967. J. Amer. Inst. Chem. Engrg., Vol. 13, p. 212.

Hardy, W. and Bircumshaw, I., 1925. "Boundary Lubrication - Plane Surfaces and the Limitation of Amonton's Law," Proceedings, Royal Society, Vol. A108, p. 1-27.

Harris, C.C., 1976. "Flotation Machines," in Flotation, A. M. Gaudin Memorial Volume, Amer. Inst. Mining Engrs., New York, p. 753.

Harris, C.C., 1978. "Multiphase Models of Flotation Machine Behaviour," Intern. J. Miner. Processing, Vol 5, p. 107.

Harris, C.C. and Rimmer, H.W., 1966. "Study of a Two-Phase Model of the Flotation Process," Trans. Inst. Mining & Metall., Sect. C, Vol. 75, p. C153.

Hartland, S. and Barber, A. D., 1974. "A Model for a Cellular Foam," Trans. Inst. Chem. Engrs., Vol. 52, p. 43.

Hocking, L.M., 1960. "The Theoretical Collision Efficiency of Small Drops," Intern. J. Air Pollution, Vol. 13, p. 154.

Holt, E.C., Jr. and Killmeyer, R.P., Jr., 1984. "Technical/Economic Aspects of Preparing and Delivering Coal-Water Mixtures of Acceptable Quality," Proceedings, First Annual Pittsburgh Coal Conference, September 17-21, Pittsburgh, Pennsylvania.

Honeywell, W.R., 1967. "Column Flotation of Uranium from Elliot Lake," Technical Bulletin TB 96, Mines Branch, E.M.R., p.11.

Hornsby, D. and Leja, J., 1982. in Surface and Colloid Sci., Vol. 12, E. Matijevic (ed.), Plenum Press, New York, p. 217.

Hucko, R.E., 1984. "An Overview of U.S. Department of Energy Coal Preparation Research," SME/AIME Annual Meeting, Preprint No. 84-105, Los Angeles, CA, Febr. 26 - March 1, 1984.

Imaizumi, T. and Inoue, T., 1966. "Kinetic Considerations of Froth Flotation," J. Mining Metall., Inst. Japan., Vol. 293, No. 82., p. 17.

Ingersol-Rand, 1984. "Coal - America's Best Kept Secret," Information Circular, Ingersol-Rand, Mining Machinery Group, 4201 Lee Highway, Bristol, VA, 24201.

Jameson, G.J., Nam, S. and Young, M.M., 1977. "Physical Factors Affecting Recovery Rates in Flotation," Minerals Sci. & Engrg., Vol. 9, No. 3, p. 103.

Jenson, V.G., 1959. "Viscous Flow Round a Sphere at Low Reynolds Numbers (<40)," Proceedings, Royal Society, Section A., Vol. 249, p. 346.

Johnson, N.W., McKee, D.J., and Lynch, A.J., 1974. "Flotation Rates of Nonsulphide Minerals in Chalcopyrite Flotation Processes," Trans. Amer. Inst. Minerals and Metallic Petrol. Engrs., Vol. 256, p. 204.

Joshi, J.B. and Shah, Y.T., 1981. "Hydrodynamic and Mixing Models for Bubble Column Reactors, Chem. Eng. Commun., Vol. 11, p. 165.

Jowett, A., 1980. "Formation and Disruption of Particle-Bubble Aggregates in Flotation," in Fine Particles Processing, Vol. 1, (P. Somasundaran, ed.), Amer. Inst. Mining Engrs., New York, N.Y., p. 720.

Kato, Y., Nishiwaki, A., Fukuda, T. and Tanaka, S., 1972. "The Behavior of Suspended Solid Particles and Liquid in Bubble Columns," J. Chem. Engrg., Inst. Japan, Vol. 5, No. 2, p. 14.

Kawecki, V., et al., 1967. Chem. Engrg. Sci., Vol. 22, p. 1519.

Keller, D.V., 1982. "The Otisca Process: An Anhydrous Heavy-Liquid Separation Process for Cleaning Coal," in Physical Coal Cleaning - Present and Developing Methods, (Y.A. Liu, ed.), Marcel Dekker Publ., New York, N.Y., p. 35.

Kelsall, D.F., 1960. "Application of Probability in the Assessment of Flotation Systems," Trans. Inst. Min. Metall., Vol. 70, p. 191. Discussion, ibid: p. 491, p. 741.

Kelsall, D.F., 1960-61. "Application of Probability in Assessment of Flotation Systems," Trans. Inst. Mining & Metall., Vol. 212, p. 581.

Kelsall, D.F., Stewart, P.S.B. and Trahar, W.J., 1974. "Diagnostic Metallurgy. A Systematic Method of Plant Optimization," Proceedings, Symposium on Optimization and Control of Mineral Processing Plants, Brisbane, July 1974. Australian Mineral Ind. Res. Assoc., Parkville, Victoria, p. 53.

Keyser, P.M., 1986. M.S. Thesis, Dept. Mining & Minerals Engineering, Virginia Polytechnic Institute and State University, Blacksburg, Virginia (in preparation).

Kihlstedt, P.G., 1968. "Particle Size Distribution and Separation Results of Selective Flotation of Complex Sulphide Ores," Proceedings, Intern. Mineral Processing Congress, 8th, Leningrad, p. 425 (in Russian).

King R.P., Hatton, T.A. and Hulbert, D.G., 1974. "Bubble Loading During Flotation," Tech. Note, Trans. Inst. Mining & Metall., Sect. C, March, p. C9.

Kitchener, J.A. and Gochin, R.J., 1980. "The Mechanism of Dissolved Air Flotation for Potable Water," Water Resources, Vol. 15, p. 585.

Klassen, V.I. and Meshcheriakov, 1958. "Flotation of Grains Smaller than 10 Microns by Gas Precipitated from Solution," Proceedings, Acad. Sci., USSR, 121, p. 9.

Klassen, V.I. and Mokrousov, V.A., 1963. An Introduction to the Theory of Flotation, (Translation: J. Leja and G.W. Poling), Butterworths, London (1963).

Klassen, V.I. and Pikkat-Ordynsky, G.A., 1957. "Improving the Flotation of Coal by Spraying the Froth," Coke & Chem., Moscow, No. 1.

Klassen, V.I., Pikkat-Ordynsky, G.A. and Gurevich, R.I., 1956. "Increasing the Effectiveness of Flotation by Spraying the Froth," Non-Ferrous Metals, Moscow, No. 5.

LeClair, B.P., 1970. Ph.D. Thesis, Chem. Engrg, McMaster University, Hamilton, Ontario.

Leja, J., 1982. Surface Chemistry of Froth Flotation, Plenum Publishing Corporation, New York.

Levich, V.G., 1962. Physicochemical Hydrodynamics, Prentice-Hall, Englewood Cliffs, N.J., pp. 700.

Lewis, R.M. and Morris, T.M., 1962. "Operating Data from a Sulfide Flotation Plant," in Froth Flotation, 50th Anniversary Volume, (D.W. Fuerstenau, ed.), Amer. Inst. Mining Engrs., New York, N.Y.

Livshits, A.K. and Dudenkov, S.V., 1957. "The Stabilities of Flotation Froths," Nonferrous Metals, Moscow, No. 1.

Livshits, A.K. and Dudenkov, S.V., 1965. "Some Factors in Flotation Froth Stability," Proceedings, VII International Mineral Processing Congress: New York, Ed. N. Arbiter, Gordon and Breach: New York. p. 367.

Lovell, V.M, 1976. "Froth Characteristics in Phosphate Flotation," in Flotation, A.M. Gaudin Memorial Vol., Vol. 1, (M.C. Fuerstenau, ed.), Amer. Inst. Mining Engrs., New York, N.Y., p. 597.

Lyman, G.J., 1974. "The Gas Bubble in Flotation - A Preliminary Study of the Dorn Effect for Gas Bubbles," M.E. Thesis, McGill University, Montreal, 1974.

Lynch, A.J., Johnson, N.W., Manlapig, E.V. and Thorne, C.G., 1981. Mineral Crushing and Grinding Circuits - Their Simulation and Control, Elsevier, Amsterdam, pp. 291.

Malinovskii, V.A., Matreenko, N.V., Knaus, O.M., Uvarov, Y.P., Teterina, N.N. and Boiko, N.N., 1973. "Technology of Froth Separation and its Industrial Application," Proceedings, 10th Intern. Mineral Processing Congr., London, Paper 43.

Masliyah, J.H., 1970. Ph.D. Dissertation, University of British Columbia, Vancouver.

Masliyah J.H. and Epstein, N., 1972. "Numerical Solution of Heat and Mass Transfer from Spheroids in Steady Axisymmetric Flow," Prog. Heat Mass Transfer, Vol. 6, p. 613.

Mathieu, G.I., 1972. "Comparison of Flotation Column with Conventional Flotation for Concentration of Molybdenum Ore," Canadian Inst. Mining Bulletin., p. 41.

Mathieu, G.I. and Mainwaring, P.R., 1986. "Mineralogy and Deep-Cleaning of Canadian High-Sulfur Coals," Proceedings, AIME-TSM Annual Meeting, New Orleans, Louisianna, March 2-6, 1986.

Maude, A.D., 1961. British J. Appl. Physics, Vol. 12, p. 242.

McCabe, W.L. and Smith, J.C., 1976. Unit Operations of Chemical Engineering, 3rd ed., McGraw-Hill, New York, N.Y., p. 150.

Miagkova, T.M, 1956. "The Effect of Surface-Active Agents on the Dispersion of Air in Flotation Apparatus," Sci. Tech. Information Bulletin, Mekhanobr Inst., No. 3.

Mica, T.S. and Fuerstenau, D.W., 1969. "A Microscopic Model of the Flotation Process," Proceedings, VIII Intern. Mineral Processing Congr., Leningrad, Paper No. 8-4.

Michael, D.H. and Norey, P.W., 1969. "Particle Collision Efficiencies for a Sphere," J. Fluid Mechanics, Vol. 37, Part 3, p. 565.

Miller, F. G., 1969. "The Effect of Froth Sprinkling on Coal Flotation Efficiency," Trans. Amer. Inst. Mining Engrs., Vol. 244, p. 158.

Moon, K.S., 1982. "Counter Current Column Flotation Machine," Canadian Centre for Mineral and Energy Technology, Energy Mines and Resources Canada, Energy Research Program, Mineral Sciences Laboratories Division, Report EPR/MSL 82-55 (IR).

Morris, T.M., 1952. "Measurement and Evaluation of the Rate of Flotation as a Function of Particle Size," Mining Engrg., Vol. 2, p. 794.

Mular, A.L., 1971. "The Selection of Optimization Methods Mineral Processes," Proceedings, 9th International Symposium on Techniques for Decision Making in the Mineral Industry, Montreal 1970, Montreal, Can. Inst. Min. Metall., 1971.

Mular, A.L., 1972. "Empirical Modelling and Optimization of Mineral Processes," Minerals Sci. Engrg., Vol. 4, No. 3, p. 30.

Narasimhan, K.S., Rao, S.B., and Chowdhury, G.S., 1972. "Column Flotation Improves Graphite Recovery," Engrg. Mining J., Vol. 173, No. 5., p. 84.

Nicol, S.K., Engel, M.D. and Teh, K.C., 1986. "Fine-Particle Flotation in an Acoustic Field," Intern. J. Mineral Processing, Vol. 17, p. 143.

Ostwald, W., 1932. "Zur Theorie der Flotation," Kolloid Z. u. Z. Polymere, Vol. 58, p. 179.

Payard, M. and Coutanceau, M., 1974. C. R. Acad. Sci., Series B, Vol. 278, p. 369.

Pearcy, T. and Hill, G.W., 1957. "A Theoretical Estimate of Collection Efficiencies of Small Droplets," J. Royal Metall. Society, Vol. 83, p. 77.

Phillips, P.J. and Cole, R.M., 1980. "Economic Penalties Attributable to Ash Content of Steam Coals," Mining Engrg., March, p. 297.

Platikanov, D., 1964. J. Phys. Chem, Vol. 68, p. 3619.

Pruppacher, H.R., LeClair, B.P. and Hamielec, A.E., 1970. J. Fluid Mech., Vol. 44, p. 781.

Reay, D. and Ratcliff, G.A., 1973. "Removal of Fine Particles from Water by Dispersed Air Flotation," Canadian J. Chem. Engrg., Vol. 51, p. 178.

Reay, D. and Ratcliff, G.A., 1975. "Experimental Testing of the Hydrodynamic Collision Model of Fine Particle Flotation," Can. J. Chem. Engrg., Vol. 53, p. 481.

Reynolds, J.K., 1956. "Mining Methods and Costs at the Morning Mine, American Smelting and Refining Co.," U.S. Bureau of Mines, Information Circular 7743, p. 39.

Reynolds, O., 1886. "On the Theory of Lubrication," Philosophical Trans., Royal Society of London, Vol. 177, p. 157.

Rimon, Y. and Cheng, S.I., 1969. Physics Fluids, Vol. 12, p. 949.

Rose, E.H., 1946. "Controversial Art of Flotation," Trans. Amer. Inst. Mining Engrs., Vol. 169, p. 240.

Rulev, N.N., 1977. "Efficiency of Particle Capture by Bubble in Noninertial Flotation," Colloid Science, Vol. 40, No. 5, p. 747.

Rulev, N.N., Deryagin, B.V. and Dukhin, S.S., 1977. "Kinetics of Flotation of Fine Particles by a Group of Bubbles," Colloid Science, Vol. 39, No. 2, p. 267.

Schuhmann, R., 1942. "Flotation Kinetics I. Methods for Study of Steady-State Problems", J. Phys. Chem., Vol. 46, p. 891.

Schulze, H.J., 1975. "Einige Untersuchungen uber das Zerrissen dunner Flussigkeitsfilme auf Feststoffoberflachen," Colloid & Polymer Sci., Vol. 253, No. 9, p. 730.

Schulze, H.J. and Cichos, Chr., 1972. Z. Phys. Chem., Vol. 251, p. 145.

Schulze, H.J. and Gottschalk, G., 1981. Proceedings, 13th International Mineral Processing Congress, Warsaw, Poland, June, 1979 (J. Laskowski, ed.), Elsevier, New York, Part A, p. 63.

Seeley, L.E., Hummel. R.L. and Simth, J.W., 1975. "Experimental Velocity Profiles in Laminar Flow Around Spheres of Intermediate Reynolds Numbers," J. Fluid Mechanics, Vol. 68, Part 3, p. 591.

Sennett, P. and Young, R.H., 1979. "Current Problems in Beneficiation of Kaolin Clay," in Beneficiation of Mineral Fines - Problems and Research Needs, (P. Somasundaran and N. Arbiter, eds.), Report of Workshop by Columbia University, Sterling Forest, New York, August 27-29, 1978.

Shafrir, U. and Neiburger, N., 1964. "Collision Efficiencies of Two Spheres Falling in a Viscous Medium," J. Geophys. Res., Vol. 68, p. 4141.

Singh, S.P.N., 1982. "Economic Assessment of Selected Coal Beneficiation Methods," in Physical Coal Cleaning - Present and Developing Methods, (Y.A. Liu, ed.), Marcel Dekker Publ., New York, N.Y., p. 451.

Smith, J.M., 1956. Chemical Engineering Kinetics, McGraw-Hill Book Co., New York, N.Y.

Spedden, H.R., and Hanna, W.S., 1948. "Attachment of Mineral Particles to Air Bubbles in Flotation," Tech. Publ. No. 2354, Amer. Inst. Mining Engrs., March, 1948.

Steiner, L, Hunkeler, R. and Hartland, S., 1977. "Behavior of Dynamic Cellular Foams," Trans. Inst. Chem. Engrg., Vol. 55, p. 153.

Sutherland, K.L., 1948. "Kinetics of the Flotation Process," J. Phys. Chem., Vol. 52, p. 394.

Sutherland, K.L. and Wark, I.W., 1955. Principles of Flotation, Australian Inst. of Mining and Metallurgy, Melbourne.

Taylor, G.I., 1925. Quoted by Hardy, W. and Bircumshaw I.

Thiessen, R., 1920. "Occurrence and Origin of Finely Disseminated Sulfur Compounds in Coal," Trans. Amer. Inst. Mining Engrs., Vol. 63, p. 913.

Tomlinson, H.S. and Fleming, M.G., 1963. "Flotation Rate Studies," Proceedings, 6th Intern. Mineral Processing Congr., Cannes, (A. Roberts ed.), Oxford, Pergamon, p. 563.

Trahar, W.J. and Warren, L.J., 1976. "The Floatability of Very Fine Particles - A Review," Intern. J. Mineral Processing, Vol. 3, p. 103.

Trahar, W.J., 1981. "A Rational Interpretation of the Role of Particle Size in Flotation," Intern. J. Mineral Processing, Vol. 8., p. 289.

Tyurnikova, V.I. and Naumov, M.E., 1981. Improving the Effectiveness of Flotation, Published 1981, by Technicopy Ltd., Stonehouse, England.

Van Dyke, M., 1982. An Album of Fluid Motion, Parabolic Press, Stanford, CA, pp. 176.

Waksmundzki, A., Neczaj-Nruzewicz, J. and Planik, M., 1972. "Mechanism of Carryover of Gangue Slimes During Flotation of Sulphur Ore," Trans. Inst. Mining Metall., Vol. 81, Section C., p. C249.

Wark, J.W., 1933. "The Physical Chemistry of Flotation," J. Phys. Chem., Vol. 37, p. 623.

Warren, L.J., 1984. "Ultrafine Particles in Flotation," in Principles of Mineral Flotation, The Wark Symposiu, (M.H. Jones and J.T. Woodcock, eds.), Austr. Instit. Mining & Metall., Symp. Series No. 40, Victoria, Australia, p. 185.

Watson, D. and Grainger-Allen, T.J.N., 1974. "Study of Froth Flotation Using a Steady State Approach," Trans. Amer. Inst. Mining Engrs., Vol. 256, p. 242.

Weber, M.E., 1981. "Collision Efficiencies for Small Particles with a Spherical Collector at Intermediate Reynolds Numbers," J. Separation Process Technol., Vol. 2, p. 29.

Weber, M.E. and Paddock, D., 1983. "Interceptional and Gravitational Collision Efficiencies for Single Collectors at Intermediate Reynolds Numbers," J. Colloid and Interface Sci., Vol. 94, No. 2, p. 328.

Wheeler, D.A., 1966. "Big Flotation Column Mill Tested," Engrg. Mining J., p. 98.

Whelan, P.F. and Brown, D.J., 1956. "Particle-Bubble Attachment in Froth Flotation," Bulletin Inst. Mining & Metall., Vol. 65, No. 591, p. 181.

Woo, S.W., 1971. Ph.D. Dissertation, McMaster University, Hamilton, Ontario

Wright, A.C., 1985. "Collecting Fines for New Markets," Coal Age, January, p. 57.

Yang, D.C., 1984. "Static Tube Flotation for Fine Coal Cleaning," Proceedings, 6th Inter. Symp. on Coal Slurry Combustion and Technology, Orlando, FL, June 25-27, 1984., p. 582.

Yoon, R.H., 1982. "Flotation of Coal Using Micro-Bubbles and Inorganic Salts," Mining Congress Journal, Vol. 68, No. 12, p. 76.

Yoon, R.H., 1984a. "Microbubble Flotation of Fine Coal," Final Report Prepared for the U.S. Department of Energy, Report No. DOE/PC/30234-T3, 182 pp.

Yoon, R.H., 1984b. "Micro-Bubble Flotation," Presentation, Engineering Foundation Conference on Advanced Coal Cleaning: Impact of Coal Quality on Downstream Processes, Santa Barbara, California, January, 1984.

Yoon, R.H. and Luttrell, G.H., 1986. "The Effect of Bubble Size on Fine Coal Flotation," Coal Preparation, An International Journal, Vol. 2, p. 179.

Yoon, R.H., Luttrell, G.H., Adel, G.T. and Trigg, R.D., 1984. "Cleaning of Ultrafine Coal by Microbubble Flotation," Proceedings, 1st Annual Pittsburgh Coal Conference, Pittsburgh, PA, September, 1984, p. 880.

Yoon, R.H. and Miller, K. J., 1982. "A Preliminary Investigation on the Application of Microgas Dispersion for Fine Coal Flotation," Proceedings of the Technical Program, International Powder and Bulk Solids Handling and Processing, Rosemont, Illinois, May, p. 357.

Yordan, J.L. and Yoon, R.H., 1985. "Induction Time Measurements for the Quartz-Amine Flotation System," Presentation, 115th SME-AIME Annual Meeting, New Orleans, Louisiana, March 2-6, 1985.

Young, P., 1982. "Flotation Machines," Mining Magazine, January, 1982, p. 35.

Yousef, A.A., Arafa, M.A. and Boulos, T.R., 1971. "Influence of Manganese Dioxide Slimes on Quartz Flotation," Trans. Inst. Mining & Metall., Sect. C., Vol. 80, p. 223.

Zimmerman, R.E. and Sun, S.C., 1979. "Flotation Theory," in Coal Preparation, 4th Edition, (J.W. Leonard, ed.), Amer. Inst. Mining Engrs., New York, N.Y., 1979, p. 10.

Zipperian, D.E., 1984. "Characteristics of Column Flotation Utilizing Aspirated Aeration," Proceedings, SME-AIME Fall Meeting, Denver, Colorado, October 24-26.

Zipperian, D.E. and Christophersen J.A., 1985. "Plant Operation of the Deister Flotaire Column Flotation Cell," Proceedings, SME-AIME Annual Meeting, New York, New York, February 24-28.

APPENDIX I

PROGRAM FOR CALCULATION OF THE MINIMUM APPROACH DISTANCE BETWEEN A PARTICLE AND BUBBLE

```
1000 ''''''''''''''''''''''''''''''''''''''''''''''''''''''''''''''''''''''''
1010 '                                                                       '
1020 '          CALCULATION OF MINIMUM PARTICLE APPROACH DISTANCE            '
1030 '                                                                       '
1040 '                      INTERMEDIATE FLOW CONDITIONS                     '
1050 '                                                                       '
1060 '          VIRGINIA POLYTECHNIC INSTITUTE & STATE UNIVERSITY            '
1070 '          DEPARTMENT OF MINING & MINERALS ENGINEERING                  '
1080 '          213 HOLDEN HALL, BLACKSBURG, VIRGINIA  24061                 '
1090 '                                                                       '
1100 '          PROGRAMMER:  GERALD H. LUTTRELL                              '
1110 '          DATE:  FEBRUARY 1986                                         '
1120 '                                                                       '
1130 ''''''''''''''''''''''''''''''''''''''''''''''''''''''''''''''''''''''''
1140 '
1150 'PARAMETER LIST:
1160 '
1170 '          FILE$ = DATA STORAGE FILEMANE
1180 '             Q$ = PROGRAM DUMMY VARIABLE
1190 '           DBUP = UPPER BUBBLE DIAMETER LIMIT (UM)
1200 '           DBLO = LOWER BUBBLE DIAMETER LIMIT (UM)
1210 '           DBST = BUBBLE DIAMETER STEP SIZE (UM)
1220 '           PDUP = UPPER PARTICLE DIAMETER LIMIT (UM)
1230 '           PDLO = LOWER PARTICLE DIAMETER LIMIT (UM)
1240 '           PDST = PARTICLE DIAMETER STEP SIZE (UM)
1250 '         PROBUP = UPPER COLLECTION PROBABILITY LIMIT
1260 '         PROBLO = LOWER COLLECTION PROBABILITY LIMIT
1270 '         PROBST = COLLECTION PROBABILITY STEP SIZE
1280 '             PD = LOOP COUNTER PARTICLE DIAMETER (UM)
1290 '             BD = LOOP COUNTER BUBBLE DIAMETER (UM)
1300 '           PROB = LOOP COUNTER COLLECTION PROBABILITY
1310 '             RP = PARTICLE RADIUS (CM)
1320 '             RB = BUBBLE RADIUS (CM)
1330 '             RL = LIMITING DISTANCE DEFINING STREAMLINE (CM)
1340 '             DT = TIME STEP (SEC)
1350 '             PI = PI
```

```
1360 '              UB = BUBBLE RISE VELOCITY (CM/SEC)
1370 '              RE = BUBBLE REYNOLDS NUMBER
1380 '   FNTANG(X,TH) = TANGENTIAL PARTICLE VELOCITY RELATIVE TO THE RISING
1390 '                  BUBBLE AS A FUNCTION OF X AND THETA (CM/SEC)
1400 '   FNRADI(X,TH) = RADIAL PARTICLE VELOCITY RELATIVE TO THE RISING
1410 '                  BUBBLE AS A FUNCTION OF X AND THETA (CM/SEC)
1420 '          R,TH = RADIAL COORDINATES OF THE PARTICLE RELATIVE TO THE
1430 '                  CENTER OF THE RISING BUBBLE
1440 '         START = INITAL ITERATION STARTING DISTANCE AHEAD OF THE
1450 '                  BUBBLE (CM)
1460 '          HMIN = MINIMUM APPROACH DISTANCE BETWEEN THE PARTICLE AND
1470 '                  BUBBLE (CM)
1480 '             T = TIME (SEC)
1490 '          ROLD = PREVIOUS ITERATION VALUE OF R
1500 '       COUNTER = PROGRAM MARKER
1510 '            UR = RADIAL PARTICLE VELOCITY (CM/SEC)
1520 '            UT = TANGENTIAL PARTICLE VELOCITY (CM/SEC)
1530 '             H = DISTANCE AT ANY TIME BETWEEN THE PARTICLE AND BUBBLE
1540 '             B = VALUE OF BETA IN THE HYDRODYNAMIC RESISTANCE TERM
1550 '
1560 'BEGIN PROGRAM EXECUTION
1570 '
1580 CLS
1590 PRINT "INTERMEDIATE FLOW - CALCULATION OF MINIMUM APPROACH DISTANCE"
1600 PRINT:PRINT
1610 INPUT "DATA STORAGE FILENAME";FILE$
1620 PRINT
1630 PRINT "RUN PROGRAM (R) OR PRINT STORED DATA (P)";
1640 '
1650 'RUN PROGRAM OR STORE DATA?
1660 '
1670 Q$=INKEY$
1680 IF Q$="P" THEN GOTO 3190
1690 IF Q$<>"R" THEN GOTO 1670
1700 '
1710 'OPEN DATA STORAGE FILE
1720 '
```

```
1730 OPEN FILE$ FOR OUTPUT AS #1
1740 '
1750 'DEFINE VARIABLE TYPES
1760 '
1770 DEFDBL A-Z
1780 DEFSNG P,B
1790 '
1800 'DEFINE BUBBLE AND PARTICLE SIZES
1810 '
1820 CLS
1830 PRINT "BUBBLE DIAMETER RANGE:"
1840 PRINT
1850 INPUT "   UPPER (UM)";BDUP
1860 INPUT "   LOWER (UM)";BDLO
1870 INPUT "    STEP (UM)";BDST
1880 PRINT:PRINT
1890 PRINT "PARTICLE DIAMETER RANGE:"
1900 PRINT
1910 INPUT "   UPPER (UM)";PDUP
1920 INPUT "   LOWER (UM)";PDLO
1930 INPUT "    STEP (UM)";PDST
1940 PRINT:PRINT
1950 PRINT "COLLECTION PROBABILITY RANGE:"
1960 PRINT
1970 INPUT "   UPPER";PROBUP
1980 INPUT "   LOWER";PROBLO
1990 INPUT "    STEP";PROBST
2000 PRINT:PRINT
2010 INPUT "ITERATION TIME STEP (SEC)";DT
2020 CLS
2030 '
2040 'BEGIN LOOPS FOR PARTICLE SIZE, BUBBLE SIZE AND COLLECTION PROBABILITY
2050 '
2060 FOR PD=PDLO TO PDUP STEP PDST
2070 FOR BD=BDLO TO BDUP STEP BDST
2080 FOR PROB=PROBLO TO PROBUP STEP PROBST
```

```
2090 '
2100 'CONVERT LOOP VARIABLES INTO PROPER UNITS
2110 '
2120 RP=PD*.0001/2
2130 RB=BD*.0001/2
2140 RL=RB*SQR(PROB)
2150 '
2160 'DEFINE FUNCTIONAL CONSTANTS
2170 '
2180 PI=3.1415927#
2190 UB=324.4*RB^1.14
2200 RE=2*RB*UB*.998/.01
2210 '
2220 'TANGENTIAL AND RADIAL VELOCITY FUNCTIONS
2230 '
2240 DEF FNTANG(X,TH)=UB*SIN(TH)*(1-.75/X-.25/X^3+RE^.72/15*(-2/X^4+1/X^3+1/X))
2250 DEF FNRADI(X,TH)=UB*COS(TH)*(1-1.5/X+.5/X^3+2*RE^.72/15*(1/X^4-1/X^3+1/X-1/
X^2))
2260 'CALCULATE INITIAL STARTING CONDITIONS
2270 '
2280 B=1:T=0
2290 START=20*RB
2300 TH=ATN(RL/START)
2310 R=RL/SIN(TH)
2320 HMIN=R-RP-RB
2330 '
2340 'INCREMENT TIME STEP "T" BY "DT"
2350 '
2360 T=T+DT
2370 '
2380 'TERMINATE PROGRAM EXECUTION?
2390 '
2400 Z$=INKEY$
2410 IF Z$="Q" THEN FLAG=1:BEEP:CLS:PRINT "PLEASE WAIT ..."
2420 IF FLAG=1 THEN GOTO 3080
2430 '
2440 'RESET PROGRAM MARKERS
```

```
2450 '
2460 ROLD=R
2470 COUNTER=0
2480 '
2490 'DETERMINE NEW TANGENTIAL PARTICLE VELOCITY AND LOCATION
2500 '
2510 UT=FNTANG(R/RB,TH)
2520 TH=TH+UT*DT/R
2530 '
2540 'DETERMINE NEW RADIAL PARTICLE VELOCITY
2550 '
2560 UR=FNRADI(ROLD/RB,TH)
2570 '
2580 'CALCULATE NEW PARTICLE APPROACH DISTANCE
2590 '
2600 R=ROLD-UR*DT/B
2610 H=R-RP-RB
2620 IF H<0 THEN H=9.999999E-30
2630 '
2640 'CALCULATE NEW RESISTANCE FORCE PARAMETER "B"
2650 '
2660 BOLD=B
2670 B=.37*(RP/H)^.83
2680 IF B<1 THEN B=1
2690 '
2700 'PRINT DYNAMIC DATA TO SCREEN
2710 '
2720 LOCATE 1,1:PRINT "PARTICLE DIAMETER (UM) = ";PD
2730 LOCATE 2,1:PRINT "BUBBLE DIAMETER (UM)   = ";BD
2740 LOCATE 3,1:PRINT "COLLECTION PROBABILITY = ";PROB
2750 LOCATE 4,1:PRINT "TIME (SEC)             = ";T
2760 LOCATE 6,1:PRINT "THETA (DEGREES)        = ";TH*180/PI
2770 LOCATE 7,1:PRINT "R-VALUE (CM)           = ";R
2780 LOCATE 8,1:PRINT "APPROACH DISTANCE (CM) = ";H
2790 LOCATE 10,1:PRINT "MIN DISTANCE (CM)      = ";HMIN
2800 LOCATE 12,1:PRINT "RAD VELOCITY (CM/SEC)  = ";UR
```

```
2810 LOCATE 13,1:PRINT "TAN VELOCITY (CM/SEC)  = ";UT
2820 LOCATE 15,1:PRINT "VALUE OF BETA          = ";B
2830 LOCATE 17,1:PRINT "COUNTER                = ";COUNTER
2840 '
2850 'IF NO CONVERGENCE THEN ...
2860 '
2870 COUNTER=COUNTER+1
2880 IF COUNTER=25 THEN 2960
2890 '
2900 'CONVERGENCE CRITERIA
2910 '
2920 IF ABS((BOLD-B)/BOLD)>.000001 THEN 2600
2930 '
2940 'DETERMINE MINIMUM APPROACH DISTANCE
2950 '
2960 IF H<HMIN THEN HMIN=H
2970 '
2980 'DETERMINE IF PARTICLE HAS SWEPT PAST BUBBLE
2990 '
3000 IF TH<PI/2 THEN 2360
3010 '
3020 'OUTPUT PARAMETERS "RL" AND "HMIN" TO DISK
3030 '
3040 WRITE #1,BD,PD,PROB,HMIN*1E+08
3050 '
3060 'REPEAT PROCESS FOR NEXT STREAMLINE
3070 '
3080 NEXT PROB
3090 '
3100 'REPEAT PROCESS FOR NEXT BUBBLE AND PARTICLE SIZES
3110 '
3120 NEXT BD
3130 NEXT PD
3140 '
3150 'CLOSE DATA STORAGE FILE
3160 '
```

```
3170 CLOSE #1
3180 END
3190 '
3200 'ROUTINE FOR PRINTING STORED DATA
3210 '
3220 CLS
3230 PRINT "  * SWITCH ON PRINTER *  "
3240 PRINT "PRESS ANY KEY TO CONTINUE"
3250 Q$=INKEY$:IF Q$="" THEN 3250
3260 '
3270 'PRINT TITLE BLOCK
3280 '
3290 LPRINT "BUBBLE","PARTICLE","COLLECTION","APPROACH"
3300 LPRINT "DIAMETER","DIAMETER","PROBABILITY","DISTANCE"
3310 LPRINT "(MICRONS)","(MICRONS)","       ","(NANOMETERS)"
3320 LPRINT
3330 '
3340 'OPEN DATA STORAGE FILE
3350 '
3360 OPEN FILE$ FOR INPUT AS #1
3370 '
3380 'READ DATA FROM STORAGE DISK
3390 '
3400 IF EOF (1) THEN GOTO 3530
3410 INPUT #1,BD,PD,PROB,HMIN
3420 '
3430 'SEND DATA TO PRINTER
3440 '
3450 LPRINT BD,PD,PROB,HMIN
3460 '
3470 'MORE DATA TO READ?
3480 '
3490 GOTO 3370
3500 '
3510 'CLOSE DATA FILE & TERMINATE PROGRAM
3520 '
```

```
3530 CLOSE #1
3540 END
```

APPENDIX II

PROGRAM FOR SIMULATING THE FLOTATION OF FINE COAL PARTICLES IN A COLUMN

```
1000 CLS:KEY OFF
1010 PRINT
1020 PRINT
1030 PRINT "          COLUMN FLOTATION POPULATION BALANCE MODEL"
1040 PRINT
1050 PRINT "      VIRGINIA POLYTECHNIC INSTITUTE & STATE UNIVERSITY"
1060 PRINT "         DEPARTMENT OF MINING & MINERALS ENGINEERING"
1070 PRINT "            213 HOLDEN HALL, BLACKSBURG, VA  24061"
1080 PRINT
1090 PRINT
1100 '
1110 ' PROGRAMMER:  GERALD H. LUTTRELL
1120 ' DATE:  APRIL 1986
1130 '
1140 ' DESCRIPTION:  SIMULATION OF A FLOTATION COLUMN USING THE PBM METHOD
1150 '
1160 ' VARIABLE LIST:
1170 '          BD = BUBBLE DIAMETER (UM)
1180 '          DB = BUBBLE DIAMETER (CM)
1190 '          PD = PARTICLE DIAMETER (UM)
1200 '          DP = PARTICLE DIAMETER (CM)
1210 '         CPC = COAL COLLECTION PROBABILITY
1220 '         CPA = ASH COLLECTION PROBABILITY
1230 '          DC = CELL DIAMETER (CM)
1240 '          HZ = ZONE HEIGHT (CM)
1250 '          GF = FEED AIR FLOW RATE (LPM)
1260 '          QG = FEED AIR FLOW RATE (ML/SEC)
1270 '          TF = FROTH FILM THICKNESS (UM)
1280 '          FT = FROTH FILM THICKNESS (CM)
1290 '          PF = PULP FEED RATE (LPM)
1300 '          QF = PULP FEED RATE (ML/SEC)
1310 '           S = FEED PERCENT SOLIDS BY WEIGHT
1320 '          AP = FEED ASH PERCENT BY WEIGHT
1330 '          DT = EULER METHOD TIME STEP (SEC)
1340 '       NUMUP = NUMBER OF UPPER ZONES
1350 '       NUMLO = NUMBER OF LOWER ZONES
```

```
1360 '          PI = PI
1370 '           G = ACCELERATION OF GRAVITY (CM/SEC^2)
1380 '       LDENS = LIQUID DENSITY (GM/CM^3)
1390 '       CDENS = COAL DENSITY (GM/CM^3)
1400 '       ADENS = ASH DENSITY (GM/CM^3)
1410 '          MU = VISCOSITY (GM/SEC.CM)
1420 '          UB = BUBBLE RISE VELOCITY (CM/SEC)
1430 '          RE = BUBBLE REYNOLDS NUMBER
1440 '         UPC = COAL SETTLING VELOCITY (CM/SEC)
1450 '         UPA = ASH SETTLING VELOCITY (CM/SEC)
1460 '          XA = CROSS-SECTIONAL AREA OF COLUMN (CM^2)
1470 '          VZ = ZONE VOLUME (CM^3)
1480 '       PDENS = PULP DENSITY OF FEED (GM/CM^3)
1490 '         CFC = COAL CONCENTRATION OF FEED (GM/CM^3)
1500 '         CFA = ASH CONCENTRATION OF FEED (GM/CM^3)
1510 '          EF = AIR FRACTION IN THE FROTH BY VOLUME
1520 '          EG = AIR FRACTION IN THE FEED AIR SUSPENSION BY VOLUME
1530 '        MBPA = PERCENT AIR IN THE FEED AIR SUSPENSION BY VOLUME
1540 '      NUMTOT = TOTAL NUMBER OF ZONES
1550 '          VW = WAKE VOLUME/BUBBLE VOLUME
1560 '         KAC = RATE CONSTANT OF COAL COLLECTION (1/SEC)
1570 '         KAA = RATE CONSTANT OF ASH COLLECTION (1/SEC)
1580 '           T = TIME (SEC)
1590 '        E(I) = AIR FRACTION IN ZONE I
1600 '       QW(I) = FLOW RATE DUE TO BUBBLE WAKES IN ZONE I (ML/SEC)
1610 '          QT = REJECT FLOW RATE (ML/SEC)
1620 '          LQ = WASH WATER FLOW RATE (L/MIN)
1630 '          QL = WASH WATER FLOW RATE (ML/SEC)
1640 '          QP = PRODUCT FLOW RATE (ML/SEC)
1650 '       QU(I) = INTERNAL FLOW RATE BETWEEN FROTH AND FEED ZONES (LPM)
1660 '       QD(I) = INTERNAL FLOW RATE BETWEEN FEED AND REJECT ZONES (LPM)
1670 '      MFC(I) = COAL MASS FREE IN ZONE I (GM)
1680 '      MFA(I) = ASH MASS FREE IN ZONE I (GM)
1690 '      MAC(I) = COAL MASS ATTACHED IN ZONE I (GM)
1700 '      MAA(I) = ASH MASS ATTACHED IN ZONE I (GM)
1710 '           Z = AIR DUMMY VARIABLE (dE/dT)
```

```
1720 '        YCOAL = FREE COAL DUMMY VARIABLE (dMFC/dT)
1730 '         YASH = FREE ASH DUMMY VARIABLE (dMFA/dT)
1740 '        XCOAL = ATTACHED COAL DUMMY VARIABLE (dMAC/dT)
1750 '         XASH = ATTACHED ASH DUMMY VARIABLE (dMAA/dT)
1760 '            I = PROGRAM COUNTER
1770 '           A$ = PROGRAM BRANCHING DUMMY VARIABLE
1780 '           Q$ = DISPLAY DUMMY VARIABLE
1790 '          PCF = PRODUCT COAL FLOW RATE (GM/MIN)
1800 '          PAF = PRODUCT ASH FLOW RATE (GM/MIN)
1810 '          RCF = REJECT COAL FLOW RATE (GM/MIN)
1820 '          RAF = REJECT ASH FLOW RATE (GM/MIN)
1830 '       PROASH = PRODUCT ASH FRACTION BY WEIGHT
1840 '       REJASH = REJECT ASH FRACTION BY WEIGHT
1850 '           BM = MIXING FACTOR
1860 '
1870 '
1880 ''''''''''''''''''''''''' DEFINE VARIABLE TYPES '''''''''''''''''''''''''
1890 '
1900 DEFDBL A-Z
1910 DEFINT I,N
1920 '
1930 ''''''''''''''''''''''''' DIMENSION ARRAYS '''''''''''''''''''''''''''''''
1940 '
1950 DIM E(50),QW(50)
1960 DIM QD(50),QU(50)
1970 DIM MFC(50),MFA(50)
1980 DIM MAC(50),MAA(50)
1990 '
2000 ''''''''' INPUT OF OPERATIONAL DATA & CONVERSION TO PROPER UNITS '''''''''
2010 '
2020 LOCATE 10,1:PRINT "INPUT DATA:"
2030 LOCATE 12,1:INPUT "BUBBLE DIAMETER (UM)";BD:DB=BD*.0001
2040 IF BD<0 THEN 2030
2050 IF BD>1000 THEN 2030
2060 LOCATE 13,1:INPUT "PARTICLE DIAMETER (UM)";PD:DP=PD*.0001
2070 IF PD<0 THEN 2060
```

```
2080 IF PD>50 THEN 2060
2090 LOCATE 14,1:INPUT "COAL COLLECTION PROBABILITY";CPC
2100 IF CPC<0 THEN 2090
2110 IF CPC>1 THEN 2090
2120 LOCATE 15,1:INPUT "ASH COLLECTION PROBABILITY";CPA
2130 IF CPA<0 THEN 2120
2140 IF CPA>1 THEN 2120
2150 LOCATE 16,1:INPUT "AIR FLOW RATE (LPM)";GF:QG=GF*1000/60
2160 IF GF<0 THEN 2150
2170 LOCATE 17,1:INPUT "PERCENT AIR";MBPA:EG=MBPA/100
2180 IF MBPA<0 THEN 2170
2190 IF MBPA>100 THEN 2170
2200 LOCATE 18,1:INPUT "PULP FEED RATE (LPM)";PF:QF=PF*1000/60
2210 IF PF<0 THEN 2200
2220 LOCATE 19,1:INPUT "WASH WATER FLOW RATE (LPM)";LQ:QL=LQ*1000/60
2230 IF LQ<0 THEN 2220
2240 LOCATE 20,1:INPUT "TIME STEP (SEC)";DT
2250 IF DT<0 THEN 2240
2260 LOCATE 12,40:INPUT "FEED PERCENT SOLIDS";S
2270 IF S<0 THEN 2260
2280 IF S>100 THEN 2260
2290 LOCATE 13,40:INPUT "FEED ASH PERCENT";AP
2300 IF AP<0 THEN 2290
2310 LOCATE 14,40:INPUT "FROTH FILM THICKNESS (UM)";TF:FT=TF*.0001
2320 IF LQ<0 THEN 2310
2330 IF TF<0 THEN 2310
2340 LOCATE 15,40:INPUT "CELL DIAMETER (CM)";DC
2350 IF DC<0 THEN 2340
2360 LOCATE 16,40:INPUT "ZONE HEIGHT (CM)";HZ
2370 IF HZ<0 THEN 2360
2380 IF AP>100 THEN 2360
2390 LOCATE 17,40:INPUT "NUMBER OF UPPER ZONES";NUMUP
2400 IF NUMUP<1 THEN 2390
2410 LOCATE 18,40:INPUT "NUMBER OF LOWER ZONES";NUMLO
2420 IF NUMLO<1 THEN 2410
2430 LOCATE 19,40:INPUT "MIXING FACTOR";BM
```

```
2440 IF BM<0 THEN 2430
2450 CLS
2460 '
2470 '''''''''''''''''''' INPUT VALUES OF PHYSICAL CONSTANTS ''''''''''''''''''''
2480 '
2490 PI=3.1415927#
2500 G=980.6
2510 LDENS=.998
2520 CDENS=1.3
2530 ADENS=2.2
2540 MU=.01
2550 RTIME=1E+30
2560 '
2570 ''''''''''''''''''''' CALCULATE OPERATIONAL CONSTANTS '''''''''''''''''''''
2580 '
2590 'BUBBLE RISE VELOCITY & REYNOLDS NUMBER
2600 '
2610 UB=324.4*(DB/2)^1.14
2620 RE=DB*LDENS*UB/MU
2630 '
2640 'COAL AND ASH PARTICLE SETTLING VELOCITIES
2650 '
2660 UPC=DP^2*G*(CDENS-LDENS)/(18*MU)
2670 UPA=DP^2*G*(ADENS-LDENS)/(18*MU)
2680 '
2690 'COLUMN CROSSECTIONAL AREA & ZONE VOLUME
2700 '
2710 XA=PI*(DC/2)^2
2720 VZ=HZ*XA
2730 '
2740 'PULP DENSITY & COAL AND ASH FEED CONCENTRATIONS
2750 '
2760 PDENS=100^2/(S*(AP/ADENS+(100-AP)/CDENS+100/LDENS*(100/S-1)))
2770 CFC=PDENS*S/100*(1-AP/100)
2780 CFA=PDENS*S/100*AP/100
2790 '
```

```
2800 'AIR FRACTION CONTENT OF FROTH
2810 '
2820 EF=DB^3/(DB^3+6*DB^2*FT+12*DB*FT^2+8*FT^3)
2830 NUMTOT=NUMUP+NUMLO+4
2840 E(NUMTOT)=EF
2850 '
2860 'WAKE VOLUME/BUBBLE VOLUME RATIO
2870 '
2880 VW=.86*LOG(RE)/2.303-1.12:IF VW<0 THEN VW=0
2890 '
2900 'ADJUSTMENT FOR MIXING IN THE COLUMN
2910 '
2920 VW=VW+BM
2930 '
2940 'FLOTATION RATE CONSTANTS FOR COAL AND ASH
2950 '
2960 KAC=6*CPC*QG/(PI*DB*DC^2)
2970 KAA=6*CPA*QG/(PI*DB*DC^2)
2980 '
2990 '''''''''''''''''''''''''''' DISPLAY DATA ON CRT ''''''''''''''''''''''''''''
3000 '
3010 'WHICH DATA TO BE VIEWED?
3020 '
3030 A$=INKEY$
3040 IF A$=CHR$(32) THEN 7460
3050 IF A$=CHR$(9) THEN GOSUB 7770
3060 IF Q$="S" OR Q$="s" THEN LOCATE 1,1:PRINT "TIME = ";T:GOTO 3200
3070 IF Q$="P" OR Q$="p" THEN 6110
3080 IF Q$="G" OR Q$="g" THEN 5860
3090 IF Q$="R" OR Q$="r" THEN 6590
3100 IF Q$="F" OR Q$="f" THEN 5360
3110 IF Q$="T" OR Q$="t" THEN 6950
3120 IF Q$="C" OR Q$="c" THEN 7120
3130 IF Q$="A" OR Q$="a" THEN 7300
3140 IF Q$="L" OR Q$="l" THEN 7710
3150 IF Q$="Q" OR Q$="q" THEN 5220
```

```
3160 GOTO 7460
3170 '
3180 '''''''''''''''''''''''' RUN TIME GREATER THAN DESIRED? ''''''''''''''''''''
3190 '
3200 IF T>RTIME THEN 2980
3210 '
3220 ''''''''''''''''''''''''' CALCULATE REJECT FLOWRATE ''''''''''''''''''''''
3230 '
3240 QT=QG+QF+QL-QP
3250 '
3260 ''''''''''''''''''''''''' REJECT ZONE CALCULATIONS ''''''''''''''''''''''
3270 '
3280 I=1
3290 '
3300 'INTERNAL FLOWRATE
3310 '
3320 QD(I+1)=QT+UB*XA*E(I)-QG
3330 '
3340 'FRACTIONAL AIR CONTENT
3350 '
3360 Z=(QG*EG+QD(I+1)*E(I+1)-(QT+UB*XA)*E(I))/VZ
3370 '
3380 'WAKE VOLUMETRIC FLOW
3390 '
3400 QW(I)=(UB*XA*E(I)-QD(I+1)*E(I+1))*VW
3410 '
3420 'FREE MASS OF COAL AND ASH
3430 '
3440 YCOAL=-KAC*MFC(I)+((QD(I+1)+UPC*XA+QW(I))*MFC(I+1)-(QT+UPC*XA+QW(I))*MFC(I)
)/VZ
3450 YASH=-KAA*MFA(I)+((QD(I+1)+UPA*XA+QW(I))*MFA(I+1)-(QT+UPA*XA+QW(I))*MFA(I))
/VZ
3460 '
3470 'ATTACHED MASS OF COAL AND ASH
3480 '
3490 XCOAL=KAC*MFC(I)+(QD(I+1)*MAC(I+1)-(QT+UB*XA)*MAC(I))/VZ
```

```
3500 XASH=KAA*MFA(I)+(QD(I+1)*MAA(I+1)-(QT+UB*XA)*MAA(I))/VZ
3510 '
3520 'EULER SOLUTION ROUTINE
3530 '
3540 GOSUB 5250
3550 '
3560 '''''''''''''''''''''''''''''''' LOWER ZONE ''''''''''''''''''''''''''''''''
3570 '
3580 FOR I=2 TO (NUMLO+1)
3590 '
3600 'INTERNAL FLOWRATE
3610 '
3620 QD(I+1)=QD(I)+UB*XA*(E(I)-E(I-1))
3630 '
3640 'FRACTIONAL AIR CONTENT
3650 '
3660 Z=(UB*XA*E(I-1)+QD(I+1)*E(I+1)-(QD(I)+UB*XA)*E(I))/VZ
3670 '
3680 'WAKE VOLUMETRIC FLOW
3690 '
3700 QW(I)=(UB*XA*E(I)-QD(I+1)*E(I+1))*VW
3710 '
3720 'FREE MASS OF COAL AND ASH
3730 '
3740 YCOAL=-KAC*MFC(I)+(QW(I-1)*MFC(I-1)+(QD(I+1)+UPC*XA+QW(I))*MFC(I+1)-(QD(I)+
UPC*XA+QW(I-1)+QW(I))*MFC(I))/VZ
3750 YASH=-KAA*MFA(I)+(QW(I-1)*MFA(I-1)+(QD(I+1)+UPA*XA+QW(I))*MFA(I+1)-(QD(I)+U
PA*XA+QW(I-1)+QW(I))*MFA(I))/VZ
3760 '
3770 'ATTACHED MASS OF COAL AND ASH
3780 '
3790 XCOAL=KAC*MFC(I)+(UB*XA*MAC(I-1)+QD(I+1)*MAC(I+1)-(QD(I)+UB*XA)*MAC(I))/VZ
3800 XASH=KAA*MFA(I)+(UB*XA*MAA(I-1)+QD(I+1)*MAA(I+1)-(QD(I)+UB*XA)*MAA(I))/VZ
3810 '
3820 'EULER SOLUTION ROUTINE
3830 '
```

```
3840 GOSUB 5250
3850 '
3860 NEXT I
3870 '
3880 '''''''''''''''''''''''''''''''' FEED ZONE ''''''''''''''''''''''''''''''
3890 '
3900 I=NUMLO+2
3910 '
3920 'INTERNAL FLOWRATE
3930 '
3940 QU(I)=QF-QD(I)+UB*XA*(E(I-1)-E(I))
3950 '
3960 'FRACTIONAL AIR CONTENT
3970 '
3980 Z=(UB*XA*E(I-1)-(QU(I)+QD(I)+UB*XA)*E(I))/VZ
3990 '
4000 'WAKE VOLUMETRIC FLOW
4010 '
4020 QW(I)=(UB*XA+QU(I))*E(I)*VW
4030 '
4040 'FREE MASS OF COAL AND ASH
4050 '
4060 YCOAL=-KAC*MFC(I)+QF*CFC+(QW(I-1)*MFC(I-1)+(QW(I)+UPC*XA)*MFC(I+1)-(QD(I)+Q
U(I)+UPC*XA+QW(I-1)+QW(I))*MFC(I))/VZ
4070 YASH=-KAA*MFA(I)+QF*CFA+(QW(I-1)*MFA(I-1)+(QW(I)+UPA*XA)*MFA(I+1)-(QD(I)+QU
(I)+UPA*XA+QW(I-1)+QW(I))*MFA(I))/VZ
4080 '
4090 'ATTACHED MASS OF COAL AND ASH
4100 '
4110 XCOAL=KAC*MFC(I)+(UB*XA*MAC(I-1)-(QU(I)+QD(I)+UB*XA)*MAC(I))/VZ
4120 XASH=KAA*MFA(I)+(UB*XA*MAA(I-1)-(QU(I)+QD(I)+UB*XA)*MAA(I))/VZ
4130 '
4140 'EULER SOLUTION ROUTINE
4150 '
4160 GOSUB 5250
4170 '
```

```
4180 '''''''''''''''''''''''''''''''' UPPER ZONE ''''''''''''''''''''''''''''''''
4190 '
4200 FOR I=(NUMLO+3) TO (NUMLO+NUMUP+2)
4210 '
4220 'INTERNAL FLOWRATE
4230 '
4240 QU(I)=QU(I-1)+UB*XA*(E(I-1)-E(I))
4250 '
4260 'FRACTIONAL AIR CONTENT
4270 '
4280 Z=((QU(I-1)+UB*XA)*E(I-1)-(QU(I)+UB*XA)*E(I))/VZ
4290 '
4300 'WAKE VOLUMETRIC FLOW
4310 '
4320 QW(I)=(UB*XA+QU(I))*E(I)*VW
4330 '
4340 'FREE MASS OF COAL AND ASH
4350 '
4360 YCOAL=-KAC*MFC(I)+((QU(I-1)+QW(I-1))*MFC(I-1)+(QW(I)+UPC*XA)*MFC(I+1)-(QW(I
-1)+UPC*XA+QU(I)+QW(I))*MFC(I))/VZ
4370 YASH=-KAA*MFA(I)+((QU(I-1)+QW(I-1))*MFA(I-1)+(QW(I)+UPA*XA)*MFA(I+1)-(QW(I-
1)+UPA*XA+QU(I)+QW(I))*MFA(I))/VZ
4380 '
4390 'ATTACHED MASS OF COAL AND ASH
4400 '
4410 XCOAL=KAC*MFC(I)+((QU(I-1)+UB*XA)*MAC(I-1)-(QU(I)+UB*XA)*MAC(I))/VZ
4420 XASH=KAA*MFA(I)+((QU(I-1)+UB*XA)*MAA(I-1)-(QU(I)+UB*XA)*MAA(I))/VZ
4430 '
4440 'EULER SOLUTION ROUTINE
4450 '
4460 GOSUB 5250
4470 '
4480 NEXT I
4490 '
4500 ''''''''''''''''''''''''''''' TRANSITION ZONE '''''''''''''''''''''''''''''
4510 '
```

```
4520 I=NUMLO+NUMUP+3
4530 '
4540 'INTERNAL FLOW
4550 '
4560 QU(I)=QL+QU(I-1)+UB*XA*(E(I-1)-E(I))
4570 '
4580 'FRACTIONAL AIR CONTENT
4590 '
4600 Z=((QU(I-1)+UB*XA)*E(I-1)-(QU(I)+UB*XA)*E(I))/VZ
4610 '
4620 'WAKE VOLUMETRIC FLOW
4630 '
4640 QW(I)=0
4650 '
4660 'FREE MASS OF COAL AND ASH
4670 '
4680 YCOAL=-KAC*MFC(I)+((QU(I-1)+QW(I-1))*MFC(I-1)-(QW(I-1)+UPC*XA+QU(I))*MFC(I)
)/VZ
4690 YASH=-KAA*MFA(I)+((QU(I-1)+QW(I-1))*MFA(I-1)-(QW(I-1)+UPA*XA+QU(I))*MFA(I))
/VZ
4700 '
4710 'ATTACHED MASS OF COAL AND ASH
4720 '
4730 XCOAL=KAC*MFC(I)+((QU(I-1)+UB*XA)*MAC(I-1)-(QU(I)+UB*XA)*MAC(I))/VZ
4740 XASH=KAA*MFA(I)+((QU(I-1)+UB*XA)*MAA(I-1)-(QU(I)+UB*XA)*MAA(I))/VZ
4750 '
4760 'EULER SOLUTION ROUTINE
4770 '
4780 GOSUB 5250
4790 '
4800 '''''''''''''''''''''''''''''' CALCULATE QP ''''''''''''''''''''''''''''''
4810 '
4820 I=NUMLO+NUMUP+4
4830 QP=(UB*XA+QU(I-1))*E(I-1)/EF
4840 '
4850 'QP TOO LARGE?
```

```
4860 '
4870 IF (QP*EF)>(QG*EG) THEN CLS:PRINT "QUANTITY OF AIR LEAVING FROTH IS HIGHER
THAN AIR ENTERING!":GOTO 5230
4880 IF (QP*(1-EF))>(QF+QL+QG*(1-EG)) THEN CLS:PRINT "QUANTITY OF PULP LEAVING F
ROTH IS HIGHER THAN PULP ENTERING!":GOTO 5230
4890 '
4900 '''''''''''''''''''''''''''''''' FROTH ZONE ''''''''''''''''''''''''''''''''
4910 '
4920 I=NUMLO+NUMUP+4
4930 '
4940 'FRACTIONAL AIR CONTENT
4950 '
4960 Z=((QU(I-1)+UB*XA)*E(I-1)-QP*EF)/VZ
4970 '
4980 'WAKE VOLUMETRIC FLOW
4990 '
5000 QW(I)=0
5010 '
5020 'FREE MASS OF COAL AND ASH
5030 '
5040 YCOAL=(QU(I-1)*MFC(I-1)-QP*MFC(I))/VZ
5050 YASH=(QU(I-1)*MFA(I-1)-QP*MFA(I))/VZ
5060 '
5070 'ATTACHED MASS OF COAL AND ASH
5080 '
5090 XCOAL=((QU(I-1)+UB*XA)*MAC(I-1)-QP*MAC(I))/VZ
5100 XASH=((QU(I-1)+UB*XA)*MAA(I-1)-QP*MAA(I))/VZ
5110 '
5120 'EULER SOLUTION ROUTINE
5130 '
5140 GOSUB 5250
5150 '
5160 ''''''''''''' INCREMENT TIME STEP & CONTINUE PROGRAM EXECUTION ''''''''''''
5170 '
5180 T=T+DT
5190 GOTO 2980
```

```
5200 '
5210 ''''''''''''''''''''''''''' PROGRAM TERMINATION '''''''''''''''''''''''''''
5220 CLS
5230 KEY ON
5240 END
5250 '
5260 ''''''''''''''''''''''''''' PROGRAM SUBROUTINES '''''''''''''''''''''''''''
5270 '
5280 'EULER SUBROUTINE
5290 '
5300 E(I)=E(I)+Z*DT:IF E(I)<0 THEN E(I)=0
5310 MFC(I)=MFC(I)+YCOAL*DT:IF MFC(I)<0 THEN MFC(I)=0
5320 MFA(I)=MFA(I)+YASH*DT:IF MFA(I)<0 THEN MFA(I)=0
5330 MAC(I)=MAC(I)+XCOAL*DT:IF MAC(I)<0 THEN MAC(I)=0
5340 MAA(I)=MAA(I)+XASH*DT:IF MAA(I)<0 THEN MAA(I)=0
5350 RETURN
5360 '
5370 ''''''''''''''''''''''''''' CRT DISPLAY ROUTINES '''''''''''''''''''''''''''
5380 '
5390 'COLUMN FLOWRATE DISPLAY
5400 '
5410 LOCATE 1,1:
5420 PRINT "FEED AIR FLOW RATE (LPM)                    = ";
5430 PRINT USING "######.####";GF
5440 PRINT "FEED AIR PERCENT                            = ";
5450 PRINT USING "######.####";MBPA
5460 PRINT "FEED PULP FLOW RATE (LPM)                   = ";
5470 PRINT USING "######.####";PF
5480 PRINT "WASH WATER FLOW RATE (LPM)                  = ";
5490 PRINT USING "######.####";LQ
5500 PRINT "PRODUCT FLOW RATE (LPM)                     = ";
5510 PRINT USING "######.####";QP*60/1000
5520 PRINT "REJECT FLOW RATE (LPM)                      = ";
5530 PRINT USING "######.####";QT*60/1000
5540 PRINT
5550 PRINT "PRODUCT AIR FLOW RATE (LPM)                 = ";
```

```
5560 PRINT USING "######.####";QP*EF*60/1000
5570 PRINT "PRODUCT PULP FLOW RATE (LPM)                    = ";
5580 PRINT USING "######.####";QP*(1-EF)*60/1000
5590 PRINT "PRODUCT FREE SOLIDS FLOW RATE (GM/MIN)      = ";
5600 PRINT USING "######.####";QP*(MFC(NUMTOT)+MFA(NUMTOT))*60/VZ
5610 PRINT "PRODUCT ATTACHED SOLIDS FLOW RATE (GM/MIN) = ";
5620 PRINT USING "######.####";QP*(MAC(NUMTOT)+MAA(NUMTOT))*60/VZ
5630 PRINT
5640 PRINT "REJECT AIR FLOW RATE (LPM)                      = ";
5650 PRINT USING "######.####";QT*E(1)*60/1000
5660 PRINT "REJECT PULP FLOW RATE (LPM)                     = ";
5670 PRINT USING "######.####";QT*(1-E(1))*60/1000
5680 PRINT "REJECT FREE SOLIDS FLOW RATE (GM/MIN)       = ";
5690 PRINT USING "######.####";((UPC*XA+QT)*MFC(1)+(UPA*XA+QT)*MFA(1))*60/VZ
5700 PRINT "REJECT ATTACHED SOLIDS FLOW RATE (GM/MIN)   = ";
5710 PRINT USING "######.####";QT*(MAC(1)+MAA(1))*60/VZ
5720 PRINT
5730 PCF=QP*(MAC(NUMTOT)+MFC(NUMTOT))*60/VZ
5740 PAF=QP*(MAA(NUMTOT)+MFA(NUMTOT))*60/VZ
5750 RCF=((UPC*XA+QT)*MFC(1)+QT*MAC(1))*60/VZ
5760 RAF=((UPA*XA+QT)*MFA(1)+QT*MAA(1))*60/VZ
5770 PRINT "PRODUCT COAL FLOW RATE (GM/MIN)             = ";
5780 PRINT USING "######.####";PCF
5790 PRINT "PRODUCT ASH FLOW RATE (GM/MIN)              = ";
5800 PRINT USING "######.####";PAF
5810 PRINT "REJECT COAL FLOW RATE (GM/MIN)              = ";
5820 PRINT USING "######.####";RCF
5830 PRINT "REJECT ASH FLOW RATE (GM/MIN)               = ";
5840 PRINT USING "######.####";RAF
5850 GOTO 3200
5860 '
5870 'CELL GEOMETRY DISPLAY
5880 '
5890 PRINT "CELL DIAMETER (CM)                              = ";
5900 PRINT USING "##########.####";DC
5910 PRINT "ZONE HEIGHT (CM)                                = ";
```

```
5920 PRINT USING "##########.####";HZ
5930 PRINT
5940 PRINT "NUMBER OF UPPER ZONES                    = ";
5950 PRINT USING "##########.####";NUMUP
5960 PRINT "NUMBER OF LOWER ZONES                    = ";
5970 PRINT USING "##########.####";NUMLO
5980 PRINT "TOTAL NUMBER OF ZONES                    = ";
5990 PRINT USING "##########.####";NUMTOT
6000 PRINT
6010 PRINT "COLUMN CROSS-SECTIONAL AREA (CM^2)       = ";
6020 PRINT USING "##########.####";XA
6030 PRINT "VOLUME OF EACH COLUMN ZONE (CM^3)        = ";
6040 PRINT USING "##########.####";VZ
6050 PRINT "TOTAL CELL VOLUME (CM^3)                 = ";
6060 PRINT USING "##########.####";NUMTOT*VZ
6070 PRINT "TOTAL COLUMN HEIGHT (CM)                 = ";
6080 PRINT USING "##########.####";NUMTOT*HZ
6090 H$=INKEY$:IF H$="" THEN 6090
6100 GOTO 7460
6110 '
6120 'OPERATIONAL PARAMETER DISPLAY
6130 '
6140 LOCATE 1,1:
6150 PRINT "PARTICLE DIAMETER (UM)                   = ";
6160 PRINT USING "######.##########";PD
6170 PRINT "BUBBLE DIAMETER (UM)                     = ";
6180 PRINT USING "######.##########";BD
6190 PRINT "BUBBLE RISE VELOCITY (CM/SEC)            = ";
6200 PRINT USING "######.##########";UB
6210 PRINT "BUBBLE REYNOLDS NUMBER                   = ";
6220 PRINT USING "######.##########";RE
6230 PRINT "DIMENSIONLESS WAKE VOLUME                = ";
6240 PRINT USING "######.##########";VW-BM
6250 PRINT
6260 PRINT "COAL COLLECTION PROBABILITY              = ";
6270 PRINT USING "######.##########";CPC
6280 PRINT "COAL DENSITY (GM/CM^3)                   = ";
```

```
6290 PRINT USING "######.##########";CDENS
6300 PRINT "COAL SETTLING VELOCITY (CM/SEC)            = ";
6310 PRINT USING "######.##########";UPC
6320 PRINT "COAL FLOTATION RATE CONSTANT (1/MIN)       = ";
6330 PRINT USING "######.##########";KAC*60
6340 PRINT
6350 PRINT "ASH COLLECTION PROBABILITY                 = ";
6360 PRINT USING "######.##########";CPA
6370 PRINT "ASH DENSITY (GM/CM^3)                      = ";
6380 PRINT USING "######.##########";ADENS
6390 PRINT "ASH SETTLING VELOCITY (CM/SEC)             = ";
6400 PRINT USING "######.##########";UPA
6410 PRINT "ASH FLOTATION RATE CONSTANT (1/MIN)        = ";
6420 PRINT USING "######.##########";KAA*60
6430 PRINT
6440 PRINT "FEED PULP DENSITY (GM/CM^3)                = ";
6450 PRINT USING "######.##########";PDENS
6460 PRINT "FEED SOLIDS (WT%)                          = ";
6470 PRINT USING "######.##########";S
6480 PRINT "FEED ASH (WT%)                             = ";
6490 PRINT USING "######.##########";AP
6500 PRINT
6510 PRINT "AVERAGE FROTH FILM THICKNESS (UM)          = ";
6520 PRINT USING "######.##########";TF
6530 PRINT "TIME STEP (SEC)                            = ";
6540 PRINT USING "######.##########";DT
6550 PRINT "MIXING FACTOR                              = ";
6560 PRINT USING "######.##########";BM
6570 H$=INKEY$:IF H$="" THEN 6570
6580 GOTO 7460
6590 '
6600 'SIMULATION RESULTS DISPLAY
6610 '
6620 LOCATE 1,1:PRINT "DURATION OF SIMULATION (MIN)";:PRINT USING "########.###"
;T/60
6630 PCF=QP*(MAC(NUMTOT)+MFC(NUMTOT))*60/VZ
```

```
6640 PAF=QP*(MAA(NUMTOT)+MFA(NUMTOT))*60/VZ
6650 RCF=((UPC*XA+QT)*MFC(1)+QT*MAC(1))*60/VZ
6660 RAF=((UPA*XA+QT)*MFA(1)+QT*MAA(1))*60/VZ
6670 PROASH=PAF/(PAF+PCF)
6680 REJASH=RAF/(RAF+RCF)
6690 PRINT
6700 PRINT "PRODUCT ASH PERCENT                    = ";
6710 PRINT USING "######.####";100*PROASH
6720 PRINT "PRODUCT COAL PERCENT                   = ";
6730 PRINT USING "######.####";100*(1-PROASH)
6740 PRINT
6750 PRINT "REJECT ASH PERCENT                     = ";
6760 PRINT USING "######.####";100*REJASH
6770 PRINT "REJECT COAL PERCENT                    = ";
6780 PRINT USING "######.####";100*(1-REJASH)
6790 PRINT
6800 RECPC=PCF/(PCF+RCF)
6810 RECPA=PAF/(PAF+RAF)
6820 RECRC=RCF/(RCF+PCF)
6830 RECRA=RAF/(RAF+PAF)
6840 PRINT "PRODUCT COAL RECOVERY                  = ";
6850 PRINT USING "######.####";100*RECPC
6860 PRINT "PRODUCT ASH RECOVERY                   = ";
6870 PRINT USING "######.####";100*RECPA
6880 PRINT
6890 PRINT "REJECT COAL RECOVERY                   = ";
6900 PRINT USING "######.####";100*RECRC
6910 PRINT "REJECT ASH RECOVERY                    = ";
6920 PRINT USING "######.####";100*RECRA
6930 PRINT
6940 GOTO 3200
6950 '
6960 'TOTAL COLUMN SOLIDS CONTENT DISPLAY
6970 '
6980 LOCATE 1,1:PRINT "ZONE NUMBER"
6990 LOCATE 1,21:PRINT "PERCENT AIR"
```

```
7000 LOCATE 1,41:PRINT "FREE SOLIDS"
7010 LOCATE 1,57:PRINT "ATTACHED SOLIDS"
7020 FOR I=1 TO NUMTOT
7030 LOCATE NUMTOT-I+3,1:PRINT I
7040 LOCATE NUMTOT-I+3,21:PRINT USING "######.####";E(I)*100
7050 LOCATE NUMTOT-I+3,41:PRINT USING "######.####";MFC(I)+MFA(I)
7060 LOCATE NUMTOT-I+3,61:PRINT USING "######.####";MAC(I)+MAA(I)
7070 NEXT I
7080 LOCATE NUMTOT+2,5:PRINT "REJECT"
7090 LOCATE NUMUP+5,5:PRINT "FEED"
7100 LOCATE 3,5:PRINT "FROTH"
7110 GOTO 3200
7120 '
7130 'TOTAL COLUMN COAL CONTENT DISPLAY
7140 '
7150 LOCATE 1,1:PRINT "ZONE NUMBER"
7160 LOCATE 1,21:PRINT "PERCENT AIR"
7170 LOCATE 1,43:PRINT "FREE COAL"
7180 LOCATE 1,59:PRINT "ATTACHED COAL"
7190 FOR I=1 TO NUMTOT
7200 LOCATE NUMTOT-I+3,1:PRINT I
7210 LOCATE NUMTOT-I+3,21:PRINT USING "######.####";E(I)*100
7220 LOCATE NUMTOT-I+3,41:PRINT USING "######.####";MFC(I)
7230 LOCATE NUMTOT-I+3,61:PRINT USING "######.####";MAC(I)
7240 NEXT I
7250 LOCATE NUMTOT+2,5:PRINT "REJECT"
7260 LOCATE NUMUP+5,5:PRINT "FEED"
7270 LOCATE 3,5:PRINT "FROTH"
7280 GOTO 3200
7290 '
7300 'TOTAL COLUMN ASH CONTENT DISPLAY
7310 '
7320 LOCATE 1,1:PRINT "ZONE NUMBER"
7330 LOCATE 1,21:PRINT "PERCENT AIR"
7340 LOCATE 1,44:PRINT "FREE ASH"
7350 LOCATE 1,60:PRINT "ATTACHED ASH"
```

```
7360 FOR I=1 TO NUMTOT
7370 LOCATE NUMTOT-I+3,1:PRINT I
7380 LOCATE NUMTOT-I+3,21:PRINT USING "######.####";E(I)*100
7390 LOCATE NUMTOT-I+3,41:PRINT USING "######.####";MFA(I)
7400 LOCATE NUMTOT-I+3,61:PRINT USING "######.####";MAA(I)
7410 NEXT I
7420 LOCATE NUMTOT+2,5:PRINT "REJECT"
7430 LOCATE NUMUP+5,5:PRINT "FEED"
7440 LOCATE 3,5:PRINT "FROTH"
7450 GOTO 3200
7460 '
7470 'PROGRAM MENU
7480 '
7490 CLS
7500 BEEP
7510 LOCATE 1,1:
7520 PRINT "PLEASE CHOOSE DISPLAY:"
7530 PRINT
7540 PRINT "     P - OPERATING PARAMETERS"
7550 PRINT "     G - CELL GEOMETRY"
7560 PRINT "     R - RECOVERY/ASH RESULTS"
7570 PRINT "     F - FLOW RATES"
7580 PRINT "     T - TOTAL SOLIDS HOLDUP"
7590 PRINT "     C - TOTAL COAL HOLDUP"
7600 PRINT "     A - TOTAL ASH HOLDUP"
7610 PRINT "     L - SET DURATION OF SIMULATION"
7620 PRINT "     S - RUN SIMULATION"
7630 PRINT "     Q - TERMINATE SIMULATION"
7640 PRINT
7650 PRINT "   TAB - SET FEED SLURRY FLOW RATE"
7660 PRINT "SPACE - RETURN TO MAIN MENU"
7670 Q$=INKEY$:IF Q$="" THEN 7670
7680 IF Q$="+" THEN LPRINT CHR$(12):GOTO 7670
7690 CLS
7700 GOTO 2980
7710 '
```

```
7720 'SET DESIRED DURATION OF SIMULATION
7730 '
7740 CLS
7750 INPUT "DESIRED DURATION OF SIMULATION (SEC)";RTIME
7760 GOTO 7460
7770 '
7780 'SET NEW PULP FEEDRATE
7790 '
7800 CLS
7810 INPUT "NEW PULP FEEDRATE (LPM)";PF
7820 QF=PF*1000/60
7830 T=0
7840 CLS
7850 RETURN
7860 LPRINT "T = ";T
7870 LPRINT "BM = ";BM
7880 LPRINT "PC COAL = ";CPC
7890 LPRINT
7900 PCF=QP*(MAC(NUMTOT)+MFC(NUMTOT))*60/VZ
7910 PAF=QP*(MAA(NUMTOT)+MFA(NUMTOT))*60/VZ
7920 RCF=((UPC*XA+QT)*MFC(1)+QT*MAC(1))*60/VZ
7930 RAF=((UPA*XA+QT)*MFA(1)+QT*MAA(1))*60/VZ
7940 PROASH=PAF/(PAF+PCF)
7950 REJASH=RAF/(RAF+RCF)
7960 LPRINT "PRODUCT ASH PERCENT                    = ";
7970 LPRINT USING "######.####";100*PROASH
7980 LPRINT "PRODUCT COAL PERCENT                   = ";
7990 LPRINT USING "######.####";100*(1-PROASH)
8000 LPRINT
8010 LPRINT "REJECT ASH PERCENT                     = ";
8020 LPRINT USING "######.####";100*REJASH
8030 LPRINT "REJECT COAL PERCENT                    = ";
8040 LPRINT USING "######.####";100*(1-REJASH)
8050 LPRINT
8060 RECPC=PCF/(PCF+RCF)
8070 RECPA=PAF/(PAF+RAF)
```

```
8080 RECRC=RCF/(RCF+PCF)
8090 RECRA=RAF/(RAF+PAF)
8100 LPRINT "PRODUCT COAL RECOVERY                    = ";
8110 LPRINT USING "######.####";100*RECPC
8120 LPRINT "PRODUCT ASH RECOVERY                     = ";
8130 LPRINT USING "######.####";100*RECPA
8140 LPRINT
8150 LPRINT "REJECT COAL RECOVERY                     = ";
8160 LPRINT USING "######.####";100*RECRC
8170 LPRINT "REJECT ASH RECOVERY                      = ";
8180 LPRINT USING "######.####";100*RECRA
8190 LPRINT:LPRINT:LPRINT
8200 RETURN
```

APPENDIX III

OPERATING MANUAL AND SAMPLE DATA FOR THE COLUMN FLOTATION SIMULATOR

COLUMN FLOTATION POPULATION BALANCE MODEL

OPERATION PROCEDURE

This article describes the use of a population model developed for the dynamic simulation of coal flotation in a column. The program, which has been entitled COLUMN, is written in compiled IBM BASIC to reduce execution time. The procedure for running the program is outlined in the following steps.

1. Insert program disk containing the compiled version of COLUMN into drive A.

2. Turn the computer power switch to the ON position.

3. After the system promp, type COLUMN and press RETURN.

4. The operational conditions to be simulated are entered as prompted by the program. This data will include:

   a) BUBBLE DIAMETER - Input the average diameter of bubbles generated in the column in units of microns.

   b) PARTICLE DIAMETER - Input the average particle size of the feed pulp in units of microns.

   c) COAL COLLECTION PROBABILITY - Input the overall probability of collection determined to be appropriate for coal particles.

   d) ASH COLLECTION PROBABILITY - Input the overall probability of collection determined to be appropriate for ash particles.

   e) AIR FLOW RATE - Input the total flow rate of the air (or air suspension) entering the column in units of liters per minute.

   f) PERCENT AIR - Input the percentage of air contained in the total air flow suspension (100% for conventional flotation, approximately 5% for dissolved air flotation).

   g) PULP FEED RATE - Input the total volumetric flow

rate at which feed pulp is entering the column in units of liters per minute.

h) WASH WATER RATE - Input the total volumetric flow rate at which clean rinse water is entering the column in units of liters per minute.

i) TIME STEP - Input the time step to be utilized in the EULER technique in units of seconds.

j) FEED PERCENT SOLIDS - Input the percent solids by weight of the feed slurry entering the column.

k) FEED ASH PERCENT - Input the percent ash by weight of the feed slurry on a dry solids basis.

l) FROTH FILM THICKNESS - Input the average thickness of the films surrounding air bubbles contained in the flotation froth in units of microns.

m) CELL DIAMETER - Input the diameter of the flotation cell in units of centimeters.

n) ZONE HEIGHT - Input the desired height to be used in all simulation zones in units of centimeters.

o) NUMBER OF UPPER ZONES - Input the number of upper zones determined to be appropriate in order to obtain the correct length of column between the froth bed and feed inlet (must be an integer value).

p) NUMBER OF LOWER ZONES - Input the number of lower zones determined to be appropriate in order to obtain the correct length of column between the feed inlet and the reject outlet (must be an integer value).

q) MIXING FACTOR - Input the magnitude of the mixing action in the column. A low value more closely approximates plug flow conditions and a high value more closely approximates perfectly mixed conditions.

5. After all of the operational data has been entered, a menu will appear describing the available display screens. The screens are obtained by pressing any of the letters indicated. The options include:

P - OPERATING PARAMETERS - This screen allows the operational constants entered by the user to be reviewed.

G - CELL GEOMETRY - This screen allows the physical dimensions of the column entered by the user to be reviewed. In addition, other characteristics such as total cell volume and height are displayed.

R - RECOVERY/ASH RESULTS - This screen displays the overall recovery and ash reporting to product and reject streams.

F - FLOW RATES - This screen displays the volumetric and mass flow rates entering and exiting the column.

T - TOTAL SOLIDS HOLDUP - This screen displays the total mass of solids in grams held as either free particles or attached to bubbles in each zone of the column. The percentage of air contained in each zone is also given.

C - TOTAL COAL HOLDUP - This screen displays the total mass of coal in grams held as either free particles or attached to bubbles in each zone of the column. The percentage of air contained in each zone is also given.

A - TOTAL ASH HOLDUP - This screen displays the total mass of ash held as either free particles or attached to bubbles in each zone of the column. The percentage of air contained in each zone is also given.

L - SET DURATION OF SIMULATION - This function allows the user to set the period of time in seconds the simulation will run before pausing for examination of the results. Continuation of the run is possible by entering a new time value larger than the current value.

S - RUN SIMULATION - This function clears the display screen and provides only the cumulative run time of the simulation. The major purpose of this function is to speed program execution by eliminating unnecessary program steps.

Q - TERMINATE SIMULATION - This function terminates program execution and returns the user to DOS.

TAB - CHANGE FLOW RATE OF FEED SLURRY - This function allows the user to alter the flow rate of feed slurry at any point during program execution.

SPACE - RETURN TO MAIN MENU - During a simulation, program execution can be interrupted by depressing the space bar. The main menu will appear and any of the previously described functions or displays may be chosen.

6. Printed copies of any of the display screens can be obtained by simultaneously depressing SHIFT and PRTSC.

INPUT DATA DISPLAY:

COLUMN FLOTATION POPULATION BALANCE MODEL

VIRGINIA POLYTECHNIC INSTITUTE & STATE UNIVERSITY
DEPARTMENT OF MINING & MINERALS ENGINEERING
213 HOLDEN HALL, BLACKSBURG, VIRGINIA 24061

INPUT DATA:

BUBBLE DIAMETER (UM)? 240
PARTICLE DIAMETER (UM)? 5.5
COAL COLLECTION PROBABILITY? 0.00028
ASH COLLECTION PROBABILITY? 0.0
AIR FLOW RATE (LPM)? 0.10
PERCENT AIR? 100
PULP FEED RATE (LPM)? 0.078
WASH-WATER RATE (LPM)? 0
TIME STEP (SEC)? 0.05

FEED PERCENT SOLIDS? 5.3
FEED ASH PERCENT? 36.4
FROTH FILM THICKNESS (UM)? 4.9
CELL DIAMETER (CM)? 2.54
ZONE HEIGHT (CM)? 11.428
NUMBER OF UPPER ZONES? 2
NUMBER OF LOWER ZONES? 2
MIXING FACTOR? 0.5

MAIN MENU:

PLEASE CHOOSE DISPLAY:

P - OPERATING PARAMETERS
G - CELL GEOMETRY
R - RECOVERY/ASH RESULTS
F - FLOW RATES
T - TOTAL SOLIDS HOLDUP
C - TOTAL COAL HOLDUP
A - TOTAL ASH HOLDUP
L - SET DURATION OF SIMULATION
S - RUN SIMULATION
Q - TERMINATE SIMULATION

TAB - SET FLOWRATE OF FEED SLURRY
SPACE - RETURN TO MAIN MENU

OPERATING PARAMETER DISPLAY:

PARTICLE DIAMETER (UM)	=	5.500000
BUBBLE DIAMETER (UM)	=	240.000000
BUBBLE RISE VELOCITY (CM/SEC)	=	2.095789
BUBBLE REYNOLDS NUMBER	=	5.019833
DIMENSIONLESS WAKE VOLUME	=	0.000000
COAL COLLECTION PROBABILITY	=	0.000280
COAL DENSITY (GM/CM^3)	=	1.300000
COAL SETTLING VELOCITY (CM/SEC)	=	0.000497
COAL FLOTATION RATE CONSTANT (1/MIN)	=	0.345366
ASH COLLECTION PROBABILITY	=	0.000000
ASH DENSITY (GM/CM^3)	=	2.200000
ASH SETTLING VELOCITY (CM/SEC)	=	0.001981
ASH FLOTATION RATE CONSTANT (1/MIN)	=	0.000000
FEED PULP DENSITY (GM/CM^3)	=	1.016677
FEED SOLIDS (WT%)	=	5.300000
FEED ASH (WT%)	=	36.400000
AVERAGE FROTH FILM THICKNESS (UM)	=	4.900000
MIXING FACTOR	=	0.500000

CELL GEOMETRY DISPLAY:

CELL DIAMETER (CM)	=	2.5400
ZONE HEIGHT (CM)	=	11.4280
NUMBER OF UPPER ZONES	=	2.0000
NUMBER OF LOWER ZONES	=	2.0000
TOTAL NUMBER OF ZONES	=	8.0000
COLUMN CROSS SECTIONAL AREA (CM^2)	=	5.0671
VOLUME OF EACH COLUMN ZONE (CM^3)	=	57.9065
TOTAL CELL VOLUME (CM^3)	=	463.2523
TOTAL COLUMN HEIGHT (CM)	=	91.4240

RECOVERY/ASH DISPLAY:

SIMULATION TIME = 3300 SEC

PRODUCT ASH PERCENT	=	10.78
PRODUCT COAL PERCENT	=	89.22
REJECT ASH PERCENT	=	58.80
REJECT COAL PERCENT	=	41.20
PRODUCT COAL RECOVERY	=	65.44
PRODUCT ASH RECOVERY	=	13.82
REJECT COAL RECOVERY	=	34.56
REJECT ASH RECOVERY	=	86.18

FLOW RATE DISPLAY:

FEED AIR FLOW RATE (LPM)	=	0.1000
AIR FRACTION	=	1.0000
FEED PULP FLOW RATE (LPM)	=	0.0780
WASH-WATER FLOW RATE (LPM)	=	0.0000
PRODUCT FLOW RATE (LPM)	=	0.0987
REJECT FLOW RATE (LPM)		
PRODUCT AIR FLOW RATE (LPM)	=	0.0876
PRODUCT PULP FLOW RATE (LPM)	=	0.0112
PRODUCT FREE SOLIDS FLOW RATE (GMS/MIN)	=	0.2855
PRODUCT ATTACHED SOLIDS FLOW RATE (GMS/MIN)	=	1.6754
REJECT AIR FLOW RATE (LPM)	=	0.0124
REJECT PULP FLOW RATE (LPM)	=	0.0668
REJECT FREE SOLIDS FLOW RATE (GMS/MIN)	=	2.2095
REJECT ATTACHED SOLIDS FLOW RATE (GMS/MIN)	=	0.0326
PRODUCT COAL FLOW RATE (GMS/MIN)	=	1.7494
PRODUCT ASH FLOW RATE (GMS/MIN)	=	0.2115
REJECT COAL FLOW RATE (GMS/MIN)	=	0.9237
REJECT ASH FLOW RATE (GMS/MIN)	=	1.3184

TOTAL SOLIDS DISPLAY:

ZONE NUMBER		PERCENT AIR	FREE SOLIDS	ATTACHED SOLIDS
8	FROTH	88.68	0.1674	0.9826
7		13.47	1.2805	0.1492
6		13.47	1.4085	0.1390
5		13.47	1.6665	0.1252
4	FEED	13.47	2.1135	0.1036
3		15.38	1.8759	0.0825
2		15.65	1.7116	0.0514
1	REJECT	15.69	1.6056	0.0238

TOTAL COAL DISPLAY:

ZONE NUMBER		PERCENT AIR	FREE COAL	ATTACHED COAL
8	FROTH	88.69	0.0434	0.9826
7		13.47	0.3391	0.1492
6		13.47	0.4499	0.1390
5		13.47	0.7000	0.1252
4	FEED	13.47	1.1408	0.1036
3		15.38	0.9176	0.0825
2		15.65	0.7554	0.0514
1	REJECT	15.69	0.6497	0.0238

TOTAL ASH DISPLAY:

ZONE NUMBER		PERCENT AIR	FREE ASH	ATTACHED ASH
8	FROTH	88.68	0.1240	0.0000
7		13.47	0.9485	0.0000
6		13.47	0.9586	0.0000
5		13.47	0.9665	0.0000
4	FEED	13.47	0.9727	0.0000
3		15.38	0.9583	0.0000
2		15.65	0.9562	0.0000
1	REJECT	15.69	0.9559	0.0000

The vita has been removed from the scanned document